Faculty of Engineering

Optimization of E-slot Applicator for Non-Invasive Hyperthermia Breast Cancer Treatment

Bibi Sarpinah bt Sheikh Naimullah

Doctor of Philosophy
2026

Optimization of E-slot Applicator for Non-Invasive Hyperthermia Breast Cancer Treatment

Bibi Sarpinah bt Sheikh Naimullah

A thesis submitted

In fulfillment of the requirements for the degree of Doctor of Philosophy

(Electronic Engineering)

Faculty of Engineering
UNIVERSITI MALAYSIA SARAWAK
2026

DECLARATION

I declare that the work in this thesis was carried out in accordance with the regulations of Universiti Malaysia Sarawak. Except where due acknowledgements have been made, the work is that of the author alone. The thesis has not been accepted for any degree and is not concurrently submitted in candidature of any other degree.

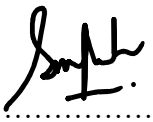

……

Bibi Sarpinah bt Sheikh Naimullah

Matric No.:20010029

Faculty of Engineering

Universiti Malaysia Sarawak

Date : 1.08.2025

ACKNOWLEDGEMENT

In the name of Allah, the Most Gracious, the Most Merciful.

I am deeply thankful to Ir Dr Kasumawati Lias for continuous support, guidance, and encouragement throughout this research journey. I sincerely appreciate my co-supervisors, Professor Dr.Ahmad Tirmizi Jobli, Dato' Ir. Professor Dr. Norlida Buniyamin and Professor Dr Wan Azlan bin Wan Zainal Abidin Tirmizi, for constructive feedback and thoughtful critiques that enhanced the quality of this research. I would also like to thank Dr. Salahuddin bin Mohd Basri from UPM for his technical guidance and support in implementing the Response Surface Method (RSM) in this research.

I also express my gratitude to the Faculty of Engineering, Centre for Graduate Studies, UNIMAS, and the Faculty of Electrical Engineering, UiTM Sarawak, for providing the resources, facilities and research environment to conduct this research. I also sincerely thank the Medical Research and Ethics Committee, Ministry of Health, Malaysia, for providing breast cancer mammogram images from Sarawak General Hospital with reference letter KKM/NIHSEC/P20-578(12).

I want to express my appreciation to my beloved family, especially my husband, my mother, my late father and my son. To my mother, thank you for your endless prayers, love and encouragement. You are my strength in continuing this PhD journey. To my late dad, thank you for your guidance and values, which inspired me to keep studying and improving myself. I dedicated this thesis to you all. Finally, thank you to everyone involved, directly or indirectly, who supported me along the PhD journey.

ABSTRACT

Breast cancer remains one of the leading causes of cancer mortality among women worldwide. Cancer tumors often contain hypoxic cells that are less sensitive to radiotherapy and chemotherapy. Because of this resistance, hyperthermia is used as alternative option to enhance the effectiveness of cancer treatment. Non-invasive hyperthermia breast cancer treatment involves raising the temperature from 40ºC to 45ºC to denature proteins and shrink tumors while minimizing damage to surrounding healthy tissue. However, a major limitation of the hyperthermia applicator is the formation of unwanted hotspots in adjacent healthy tissue and poor electromagnetic (EM) focus on the tumor. Although various applicator structures have been studied to improve EM energy focusing, investigation on the slot applicator for breast cancer hyperthermia remains limited, particularly for the U-slot and E-slot applicators. The study aims to develop and optimize the slot applicator and identify the most effective slot design for focused breast cancer hyperthermia in the Industrial, Scientific and Medical (ISM) frequency band across multiple tumor sizes (T1, T2, and T3). This research used electromagnetic (EM) simulation in SEMCAD X to evaluate SAR distribution in a breast phantom. A comparative analysis between the U-slot and E-slot applicators was conducted. The E-slot applicator was selected based on superior performance in directivity, gain, return loss, SAR distribution and SAR (peak). Response Surface Methodology (RSM) was applied to develop second-order polynomial models relating slot design parameters to the localization SAR distribution, defined by surface and inner depths. ANOVA in Design-Expert software was used to validate and optimize the E-slot parameters. The RSM-based optimization E-slot applicator was further validated with established optimization methods, namely Particle Swarm Optimization (PSO) and Genetic Algorithm (GA). The findings showed that the optimized E-slot applicator performance significantly enhances directivity

(26%: T1, 22.3%: T2, 12%: T3), gain (21%: T1, 8.7%: T2, 24.3%: T3), return loss (36%: T1, 79.8%: T2, 92%: T3) and SAR(peak) (5.6%: T1, 116.5%: T2, 43%: T3) compared to the E-slot applicator. Thus, the optimized E-slot achieved better SAR localization within the tumor and reduced the formation of unwanted hotspots. Unwanted hotspots are areas of excessive heat in surrounding healthy tissue. Less unwanted hotspots indicate reduced excessive heat absorption in healthy tissue. Additionally, it demonstrated a shorter treatment period.

Keywords: Hyperthermia, E-slot applicator, Inner depth, Surface depth, Specific Absorption Rate (SAR), tumor

Pengoptimum Aplikator E-slot bagi Rawatan Hipertermia Kanser Payudara Secara Tidak Invasif

ABSTRAK

Kanser payudara kekal sebagai salah satu punca utama kematian di kalangan wanita di seluruh dunia. Ada di kalangan tumor kanser mengandungi sel hipoksia yang kurang sensitif terhadap radioterapi dan kemoterapi. Disebabkan rintangan ini, hipertermia digunakan sebagai cara alternatif untuk meningkatkan keberkesanan rawatan kanser.Rawatan hipertermia payudara tidak invasif melibatkan peningkatan suhu 40-45°C di kawasan tumor untuk menyahasilkan protein dan mengecilkan tumor sambil meminimumkan kerosakan pada tisu sihat di sekeliling. Walaubagaimanapun, kekangan utama aplikator hipertermia ialah kewujudan hotpsot yang tidak diingini pada tisu sihat serta pemfokusan tenaga electromagnet(EM) yang lemah pada kawasan tumor.Pelbagai struktur aplikator telah dikaji untuk meningkatkan pemfokusan tenaga EM, kajian aplikator berasaskan slot bagi hipertermia kanser payudara masih terhad, khususnya bagi reka bentuk U-slot dan E-slot. Kajian ini bertujuan membangunkan dan mengoptimumkan aplikator slot yang berkesan untuk rawatan hipertermia kanser payudara yang lebih berfokus dalam jalur Industrial, Scientific dan Medical (ISM) bagi pelbagai saiz tumor (T1,T2 dan T3). Kajian ini menggunakan simulasi elektromagnetik (EM) dengan perisian SEMCAD X untuk menilai taburan SAR dalam fantom payudara. Analisis perbandingan antara aplikator U-slot dan E-slot telah dijalankan dan aplikator E-slot dipilih berdasarkan prestasi yang baik dari segi directivity, gain, return loss, taburan SAR dan SAR(peak). Kaedah Response Surface Methodology (RSM) digunakan untuk membangunkan model polynomial tertib kedua yang mengaitkan parameter reka bentuk slot dengan taburan pemfokusan SAR, yang ditakrifkan melalui kedalaman permukaan dan kedalaman dalaman. Pengesahan statistik dan

pengoptimuman E-slot dilakukan dengan ANOVA dengan perisian Design-Expert. Pengoptimum E-slot berasaskan RSM turut disahkan melalui perbandingan dengan kaedah pengoptimum sedia ada, iaitu Particle Swarm Optimization (PSO) dan Generic Algorithm (GA). Dapatan kajian menunjukkan bahawa prestasi E-slot yang telah dioptimumkan meningkat dengan ketara untuk ciri-ciri berikut: dari segi directivity (26%: T1, 22.3%: T2, 12%: T3), gain (21%: T1, 8.7%: T2, 24.3%: T3), return loss (36%: T1, 79.8%: T2, 92%: T3) dan SAR (peak) (5.6%: T1, 116.5%: T2, 43%: T3). Oleh itu, pengoptimum E-slot menawarkan pembaikan dalam pemfokusan SAR serta mengurangkan hotspot yang tidak diingini. Selain itu, ia menunjukkan tempoh rawatan yang lebih singkat.

Kata kunci: *Hipertermia, E-slot aplikator,kedalaman permukaan, kedalaman dalaman , taburan SAR, tumor*

TABLE OF CONTENTS

LIST OF TABLES

LIST OF FIGURES

LIST OF ABBREVIATIONS

ABC	Absorbing Boundary Condition
AGOA	Adaptive Gannet Optimization Algorithm
ANOVA	Analysis of Variance
CMA	Characteristic Mode Analysis
Cor Total	Corrected Total
CST	Computer Simulation Technology
DoE	Design of Experiment
EFS	Effective Field Size
EM	Electromagnetic
FEKO	Field Computation of Electromagnetic waves
GA	Generic Algorithm
HFSS	High Frequency Structure Simulator
HTP	Hyperthermia Treatment Procedure
ID	Inner Depth
IE3D	Integral Equation 3-Dimensional
IEEE	Institute of Electrical and Electronics Engineers
ISM	Industrial, Scientific and Medical
MRI	Magnetic Resonance Imaging
PD	penetration depth
PEC	Perfect Electric Conductor
PI	Prediction Interval
PML	Perfectly Matched Layer
PSO	Particle Swarm Optimization

RL	Return Loss
RSM	Response Surface Methodology
SAR	Specific Absorption Rate
SD	Surface Depth
SEMCAD X	Simulated Electromagnetic Computation and Design X
TEL	Tissue Equivalent Liquid
VSWR	Voltage Standing Wave Ratio
WBH	Whole Body Hyperthermia
WiMAX	Worldwide Interoperability for Microwave Access
WLAN	Wireless Local Network

LIST OF SYMBOLS

f	Frequency
J	Current density
∇E	Electric field
ε_o	Permittivity in free space
ε_r	Relative permittivity
ω	Angular frequency
σ	conductivity of tissue/material
ε'	Real part of complex permittivity
$j\varepsilon''$	Imaginary part of complex permittivity
ρ	Tissue density
C	Specific heat of tissue
T	Temperature of tissue (°C)
K	Thermal conductivity
T	Time duration HTP treatment
Pin	Input power
Pr	Reflected power
S_{11},Ƭ	Reflection coefficient
RL	Return Loss
Zin	Input impedance
Zo	Source impedance (50Ω)
P_{den}	Power density
$\eta_{antenna}$	Antenna radiation efficiency
W	Patch Width

h	Substrate thickness
L	Patch Length
εreff	Effective dielectric constant
Leff	Effective length
$\triangle$L	Fringing effect
Lg	Length of the ground plane
Wg	Width of the ground plane
D	Antenna Slot vertical length
C	Antenna Slot horizontal length
E,F	Antenna Slot thickness
Y	Response(output)
β_0	Intercept coefficient

CHAPTER 1

INTRODUCTION

1.1 Research Background

In 2022, the World Health Organization (WHO) reported that breast cancer was the most frequently diagnosed cancer among women worldwide, accounting for approximately 2.2 million cases or 23.8% of all female cancers (GLOBOCAN, 2022a) , with a mortality rate of 15.4% higher than lung, colorectal, cervical, liver and stomach cancer (GLOBOCAN, 2022c). These numbers are expected to rise annually. In Malaysia, breast cancer has the highest incidence among women with 8371 new cases (31.3%) and the highest cancer-related mortality at 21.4%, making it more common than other cancers such as colorectal, cervical, ovarian, corpus uteri and lung (GLOBOCAN, 2022b). These statistics highlight the urgent need for more effective treatment to enhance survival rates.

Currently, three main treatment procedures depend on tumor size and cancer stage. These include surgery, radiotherapy, chemotherapy and hormone therapy. Surgery is the oldest treatment in which cancer is removed from the body. Meanwhile, radiation therapy uses high-energy particles or waves to kill cancer cells and diminish tumors. Chemotherapy is a cancer treatment that uses drugs to kill cancer cells. Finally, hormone therapy is a treatment that is used to slow or stop the growth of cancer cells (Baskar et al., 2012).

However, the effectiveness of these treatments is limited by the tumor characteristics. In particular, the hypoxia regions within tumor are resistant to radiotherapy and chemotherapy(Dewhirst et al., 2015)(Habash et al., 2006). The hypoxia region in a tumor has low oxygen levels because insufficient oxygen is delivered to poorly organized

blood vessels commonly found in solid tumors. The tumor grows rapidly, potentially increasing its malignancy. Hyperthermia can be introduced as a treatment for this condition. Hyperthermia utilises heat by elevating the temperature to about 42°C to 45°C for a period to denature cancer cells into necrotic tissue with minimal damage to surrounding healthy tissue (Stauffer, 2005; Koo et al., 2014).

Hyperthermia can potentially enhance oxygenation, making the tumor more sensitive to radiation and directly killing cancerous cells (Al Tameemi et al., 2019; Elming et al., 2019; Harris et al., 2022). Hyperthermia increases its effectiveness by combining with radiotherapy (Patrizia Sarogni et al., 2023) .

In addition, hyperthermia has proven clinically effective in enhancing the outcome of chemotherapy and radiotherapy, especially in solid tumors, such as hypoxia. Both pre-clinical and clinical studies demonstrate that hyperthermia improves blood flow and increases perfusion in tumor areas, depending on temperature and duration (Dunne et al., 2020).

There are two methods used in hyperthermia treatment that are non-invasive and invasive (Khan & Singh, 2022; Neagu, 2017). In hyperthermia, various types of non-invasive applicators are used to deliver heat to target tissue, such as microstrip patch applicator, waveguide applicator (Kim et al., 2024), dipole applicator (Yildiz et al., 2023), helical/spiral applicator (Petra et al., 2020) and microstrip slot applicator (Elsaadi & Hamad, 2023).

The microstrip slot applicator has better penetration depth and a small Effective Field Size (EFS), as indicated by (Singh & Singh, 2016). Furthermore, it demonstrates stability in the transmission of electromagnetic waves across different tissue properties. Nonetheless,

designing an efficient antenna remains a significant challenge due to tumor characteristics that vary in size and position. Another crucial factor is to target achieving heat at an appropriate depth within the tissue to ensure effective treatment (Rajebi et al., 2024).

Previous studies have investigated the performance of applicator structures both with and without a slot. As reported by (Elsaadi & Hamad, 2023; Khan, et al., 2023; Khan et al., 2024; Shehata et al., 2021), the microstrip applicator with a slot shows improved return loss, penetration depth (PD) and Specific Absorption Rate(SAR) (Singh & Singh, 2016). The heating region is uniform and focuses on the tumor with slot applicator. Integrating the E-slot into a rectangular patch alters the current density because the E-slot creates an additional path of current distribution (Ramu & Arunachalam, 2023; Shehata et al., 2021; Wu & Chen, 2023).

According to (Rubio, 2016; Szasz, 2024) the amount of heat generated by the applicator is related to the amount of current. The applicator generated more heat as the current increased. For instance, a slot applicator can achieve a therapeutic temperature quickly due to an increment in the current distribution (Elsaadi & Hamad, 2023; Shehata et al., 2021). Therefore, high current density enhances power deposition, resulting in more concentrated heating of the target tissue.

Another critical factor to consider is the duration of hyperthermia treatment. It is related to the effectiveness and safety of the treatment (Yildiz et al., 2023). The tumor should not overheat or underheat. Underheating means the tumor does not reach a sufficient temperature, for example, less than 42°C, leading to ineffective hyperthermia treatment. In contrast, overheating refers to a tumor exposed to >45°C, leading to unwanted hotspots in the surrounding healthy tissue(Dewhirst et al., 2015). Therefore, maintaining the therapeutic

temperature range of 42°C to 45°C for a specified duration is essential to ensure that hyperthermia treatment is safe and effective.

The effects of overheating lead to unwanted hotspots and underheating, which can ineffectively heat tumors (Dewhirst et al., 2015), which causes cancer/tumors not to shrink and damage successfully. Therefore, the efficient treatment time should be considered.

In summary, the effectiveness of hyperthermia depends significantly on the applicator, which is determined by the applicator design. Based on previous studies, the main applicator parameters that affect the SAR distribution towards the targeted tissue to be treated are directivity, gain and return loss. However, a few limitations in the existing applicator need to be addressed to ensure that hyperthermia treatment causes minimal adverse health effects.

1.2 Research Motivation

The increasing mortality rate associated with breast cancer remains a critical global health issue. This issue aligns with the United Nations' 2030 Agenda and Sustainable Development Goal (SDG) 3, which aims to ensure healthy lives and promote well-being at all ages. Specifically, this research is under SDG 3.4, and by 2030, it will contribute to reducing deaths by one-third of premature Non-Communicable Diseases (NCDs) with prevention, treatment and well-being (Walsh et al., 2022).

The success rate of tumor treatment, measured as complete response (tumor no longer detectable), is 38.1% with radiotherapy alone. However, the treatment success rate increases to 60.2% when radiotherapy is combined with hyperthermia (Bakker et al., 2019). In terms of chemotherapy, tumor stabilization (tumor stops progressing), the success rate is 38% with

chemotherapy alone. However, the stabilization rate improved to 60.4% when chemotherapy was combined with hyperthermia (Kaur et al., 2022). This shows the success rate of radiotherapy or chemotherapy increases when combined with hyperthermia.

Hyperthermia improves oxygenation and blood perfusion within tumors, especially in hypoxia regions. Radiotherapy becomes three times more effective at damaging cancer cells by increasing the oxygen level in the blood flow in the tumor. Meanwhile, during chemotherapy, hyperthermia is able to increase blood flow and oxygenation which accelerates drug delivery to tumor and allowing it to work more efficiently(Jha et al., 2016).

The main challenge in hyperthermia treatment is to maintain the heat focus and uniformity within the tumor, especially with varying tumor sizes and depths. A suitable applicator design is required to address the need for various tumor sizes and depths. Additionally, the applicator design must be optimized to ensure effective and safe treatment while minimizing unwanted hotspots (Chishti et al., 2023; Elkayal et al., 2024; Rajebi et al., 2024).In this research, the development of a hyperthermia slot applicator is explored to enhance the effectiveness of hyperthermia treatment

1.3 Problem Statement

Hyperthermia has gained recognition in modern oncology for its proven clinical and research contributions to cancer treatment. Moderate hyperthermia is an elevated temperature of 42° C to 45 °C for 30 to 60 minutes to achieve a therapeutic heating effect. In non-invasive, applicator-deployed externally on the skin surface to deliver electromagnetic (EM) energy to the tumor.

Preclinical studies have demonstrated that controlled heat-enhanced treatment

effectiveness in the tumor by improving tumor oxygenation. These biological effects improve tumor sensitivity and enhance the effectiveness of hyperthermia when combined with radiotherapy or chemotherapy.

In addition, the effectiveness of heat absorption and distribution depends on various hyperthermia applicator parameters such as frequency, size, type of applicator, distance from the applicator to the breast phantom and applicator geometry (Nizam-Uddin et al., 2022). These parameters influenced EM energy focusing and SAR within the tumor region.

However, tumor sizes and location vary among patients, which influence EM penetration depth and SAR distribution. Consequently, determining the most appropriate ISM operating frequency for effective tumor heating remains a critical challenge.

In addition, research on the design of hyperthermia slot applicators remains limited. Therefore, an investigation of a simpler slot-based applicator is required to enhance design simplicity and maintain effective EM energy delivery to the tumor. Furthermore, optimizing the slot dimension to enhance SAR localization while minimizing unwanted hotspots in healthy tissue.

Moreover, the treatment time needs to be explored for the optimized slot applicator across varying tumor sizes. Therefore, the treatment time needs to be determined to minimize unwanted hotspots on surrounding healthy tissue. The following section elaborates on these challenges in detail.

1.3.1 Challenges in Selecting an Appropriate Applicator Frequency Based on Tumor Sizes and Depth

The challenge in non-invasive hyperthermia is determining the appropriate operating frequency to deliver EM energy to tumors of different sizes and depths, as frequency selection is fundamental to applicator hyperthermia. Frequency influences the penetration depth (PD), Specific absorption Rate (SAR) and dielectric properties of biological tissue.

The hyperthermia applicator utilized frequencies within the range designated by the Federal Communications Commission in Industrial, Scientific and Medical (ISM) approved 434MHz, 915MHz and 2450MHz (Altintas et al., 2021 (Zulkefli et al., 2021). The applicator used the ISM frequency to reduce complications and to make device installation more cost-effective in clinic settings (Lyu et al., 2023).

Different frequencies exhibit varying PD and Specific Absorption Rate (SAR) distribution that reflects the amount of heat absorbed within tissue. For instance, 434 MHz has a deeper penetration depth in tissue (Choudhary & Arunachalam, 2022) (Gupta & Singh, 2005) than 915 MHz and 2450 MHz. While 915 MHz has a greater PD than 2450 MHz(Lyu et al., 2023) . Hence, 2450 MHz affects the surface tissue (Li et al., 2021).

Another study investigated an elliptical-shaped applicator operating at 915 MHz and 2450 MHz for spherical tumors with volumes of 1 cm^3 and 2 cm^3. The findings reveal that the 915 MHz applicator shows a large focus point and a deeper PD. In contrast, 2450 MHz has a small focus point and a low PD(Lyu et al., 2023)(Hu et al., 2024) .

The relationship between frequency and wavelength is expressed in the equation $f=c/\lambda$, where f is frequency, c is the speed of light, and λ is wavelength. If the frequency increases, the wavelength decreases, resulting in a shallow PD in tissue. Therefore, 434

MHz is suitable for heating deeply seated tumors but offers less localization; 915 MHz provides intermediate penetration and enables better heat focus on the tumor; and 2450 MHz is more effective for superficial tumors due to its shallow PD and high localization.

Moreover, tissue properties are frequency dependent. Heat absorption differs between fat tissue and tumors due to differences in electrical properties and water content. The electrical properties are tissue conductivity and tissue permittivity. As frequency increases, relative permittivity decreases while electrical conductivity increases (Ramu & Arunachalam, 2023). Meanwhile, tumors have a higher water content than fat tissue. As a result, the tumor has absorbed more heat than fat tissue and keeps healthy tissue safe (Rajput et al., 2021).

1.3.2 Lack of Design in The Slot Hyperthermia Applicator for Breast Cancer Hyperthermia Treatment

In a hyperthermia applicator, parameters such as directivity, gain, and return loss are critical design considerations that influence energy delivery and absorption in the tumor. Directivity refers to the ability of the applicator to concentrate EM energy towards the tumor. Gain is defined as the product of the applicator's directivity and efficiency. Return loss measures the EM energy reflected back due to impedance mismatch between the applicator and the transmission line.

Previous studies demonstrate that slot applicators offer enhanced directivity and gain (Hu et al., 2024; Sethi & Nijhawan, 2016). While the return loss is minimized to enhance the effectiveness of hyperthermia (Sethi & Nijhawan, 2016). In addition, slots integrated with microstrip patches allow localised energy delivery and design flexibility (Hu et al., 2024).

However, there are limitations on the frequency of hyperthermia with the slot applicator. Specifically, 58.82% of applicators operate at 2450 MHz, while only 11.76% use 915 MHz, 17.65% use 434 MHz and 11.76% are designed for dual-frequency operation. This highlights a limited focus on the development of applicator hyperthermia at 915 MHz

Some slot designs for 915 MHz exhibit bidirectional heating, with heat dispersing in multiple directions and low directivity. This leads to reduced focus on the tumor and is less suitable for breast cancer hyperthermia treatment. A previous study by (Kumar et al., 2009) reported that the slot in the patch applicator design improved performance through gain enhancement, resulting in more focused energy delivered to the tumor. However, some slot applicator hyperthermia designs exhibit complex slot structures that integrate into both the patch and the ground. Hence, the development of a single-layer slot applicator at 915MHz with high directivity and low return loss is essential.

E-slot and U-slot single-layer designs offer lower design complexity and exhibit desirable characteristics for use as a slot applicator in breast cancer hyperthermia, such as enhanced directivity, gain and low return loss. These characteristics have been validated in the communication system (Ali et al., 2023; Raja et al., 2023; Umamaheswari et al., 2023).

Specifically, the U-slot design achieves a gain range of 6.95 to 10.6 dBi, a directivity range of 7.49 to 8.11 dBi, and a return loss range of -19dB to -40dB as indicated in Table 2.5. Similarly, the E-slot design offers a gain range of 4.34 to 9.5 dBi, a directivity range of 6.57 to 8.6 dBi and a return loss range of -13.18dB to -47.06dB as depicted in Table 2.8.

The number of slots in the applicator design influences the current density distribution. As reported (Ashyap et al., 2018), the density current distribution increased as the number of slots increased. The slot structure influences the applicator performance, for

instance, as stated in (Parameswari S, 2024),the number of slots contributes to enhancing directivity and minimizing return loss. The U-slot and E-slot applicators have different structures.

However, the application and evaluation of the non-invasive applicator on E-slot and U-slot for breast cancer hyperthermia remain limited in current research. The advantages in directivity, gain, and return loss present a highlighted potential research opportunity for further investigation. In particular, a comparative analysis of E-slot and U-slot applicators for non-invasive breast cancer hyperthermia under different tumor sizes. The comparative analysis contributes to identifying the most effective slot applicator design.

In addition to the type of applicator used in hyperthermia, the distance between the applicator and the breast phantom also influences the energy absorption and SAR distribution (Fiser et al., 2017). However, the distance adjustment results in a reduction in SAR as the distance between the applicator and the breast phantom increases (Kumari et al., 2020; Rajput et al., 2021). Therefore, the optimal distance between the applicator and the breast phantom needs to be determined to enhance the effectiveness of hyperthermia treatment.

Apart from the distance between the applicator and the breast phantom, the slot-applicator geometry also affects the heating distribution. The modification of slot length (horizontal and vertical) and thickness affects the applicator performance, such as return loss, gain, directivity and SAR (Thakur et al., 2024)(Dargar et al., 2022)(Hasan et al., 2012)(Umamaheswari et al., 2023)(Zain et al., 2018). Therefore, identifying the significant slot modification parameters: length horizontal, length vertical, thickness of horizontal, and thickness of vertical is essential before performing slot optimization.

1.3.3 Optimization Slot Applicator

Applicator performance can be improved through slot optimization. The optimization of the slot applicator dimensions aims to enhance applicator performance, including gain, return loss, and directivity. By improving applicator performance, heat concentrates more on the tumor and reduces the unwanted hotspot (Haque et al., 2021; Sivakumar et al., 2019; Tan et al, 2022).

The hyperthermia applicator used optimization techniques such as Particle Swarm Optimization (PSO) (Chishti et al., 2023)(Rajebi et al., 2024) (Yildiz et al., 2023) and Genetic Algorithm (GA), (Aldhaeebi et al., 2014) (G et al., 2025) which focus solely on applicator optimization and do not provide a relationship between dependent and independent variables.

Therefore, Response Surface Model (RSM) was applied in the slot optimization and established a mathematical model for the relationship between slot geometry and penetration depth (Margaret & Manimegalai, 2018)(Koziel & Bandler, 2015)(Ayalew & Asmare, 2022).

Hence, this research aims to evaluate the effectiveness of the selection slot structure by comparing U-slot and E-slot as applicators for breast cancer hyperthermia treatment. Then optimized the selected slot dimension to suit tumors of different sizes.

1.3.4 Improper Time Duration for Hyperthermia Treatment

Before determining the adequate hyperthermia treatment time for tumor sizes T1, T2, and T3, a water bolus is added between the applicator and the breast phantom. The purpose of adding a water bolus is to control surface tissue temperature, prevent skin burn, reduce unwanted hotspots, ensure uniform heat distribution within tumors and reduce patient

discomfort by cooling skin surface (Arunachalam et al., 2010)(Kemal et al.,2020)(Hassan et al., 2025). The time duration is measured after the water bolus is applied.

The time duration of hyperthermia is crucial for its effectiveness and safety. It is to ensure the entire tumor is completely heated. In contrast, the improper time duration management leads to the formation of unwanted hotspots in the surrounding healthy tissue. In addition, the treatment time is associated with SAR and temperature. Time is inversely proportional to SAR (Fiser et al., 2015). Therefore, if SAR decreases, a longer treatment time is needed. A longer time duration generally leads to the accumulation of thermal skin damage (Assi et al., 2022).

The time duration is typically 30 to 60 minutes, within a temperature range of 39 to 45°C (Yildiz et al., 2023)(Rajebi et al., 2020). However, the treatment time is not standardized, as it depends on several factors, such as tumor size (Wong et al., 2021) and applicator (Galal & Ibrahim, 2020). The different structure applicators produce different SAR distribution patterns and different time durations.(Bakker et al., 2020)

Therefore, this research suggests the optimal duration for different tumor sizes.

1.4 Research Objectives

With regard to the problem statement mentioned above, the main objectives for this research are stated as follows:

i. To simulate and evaluate a breast phantom integrated with a non-invasive microstrip applicator under Industrial, Scientific and Medical (ISM) frequency to achieve a desired surface and inner depth within tumor sizes: T1, T2 and T3
ii. To conduct a comparative analysis of E-slot and U-slot applicators based on the applicator's performance and rate of electromagnetic (EM) energy absorbed in

tissue, represented in Specific Absorption Rate (SAR) within tumor sizes: T1, T2 and T3

iii. To validate the optimized E-slot applicator obtained from Response Surface Method (RSM) by comparing its performance with Particle Swarm Optimization (PSO) and Genetic Algorithm (GA)

iv. To generate the optimal hyperthermia treatment time in different tumor sizes : T1, T2 and T3

1.5 Research Scopes and Methodology Framework

The research focuses on hyperthermia treatment for female breast cancer. Figure 1.1 shows the framework of breast phantom development. Breast cancer is represented as a tumor in this research. This research used real clinical data from a breast cancer analysis of mammograms, categorized as T1 (small), T2 (medium), and T3 (large). Meanwhile, T4 is not included in this research because most tumors spread to the chest wall or skin. The electrical properties for the breast phantom, such as fat, tumor, and chest wall, are defined in SEMCAD X.

Figure 1.2 illustrates the framework to address research objective 1. The non-invasive microstrip applicator developed under the Industrial, Scientific and Medical (ISM) standard, which operates at 434 MHz, 915 MHz and 2450 MHz. Figure 1.3 displays the framework of the slot applicator in hyperthermia. The U-slot and E-slot applicator is investigated further in this research, particularly on applicator performance in terms of directivity, gain and return loss. Meanwhile, the heat absorbed in tissue is represented by Specific Absorption Rate (SAR).

The framework in Figure 1.4 is presented to align with research objectives 3 and 4.

It involves slot optimization with Response Surface Method (RSM). The polynomial model was developed and verified using ANOVA in Design-Expert software. The polynomial model shows the relationships between the design parameters and the output response: surface depth and inner depth, which represent the SAR distribution range

The optimized E-slot was verified by repeating the EM simulation process three times. Then, the predicted output value is compared to the EM simulation result. The % error records. After the optimized E-slot was verified, it was validated through a comparative study of optimized methods, namely Particle Swarm Optimization (PSO) and the Genetic Algorithm (GA), which had been used in prior research.

Research objective 4 determines the optimal hyperthermia treatment time for tumors of sizes T1, T2, and T3. A water bolus was added between the applicator and the breast phantom. In the next step, SAR tuning is performed to optimize energy absorption across the entire tumor.

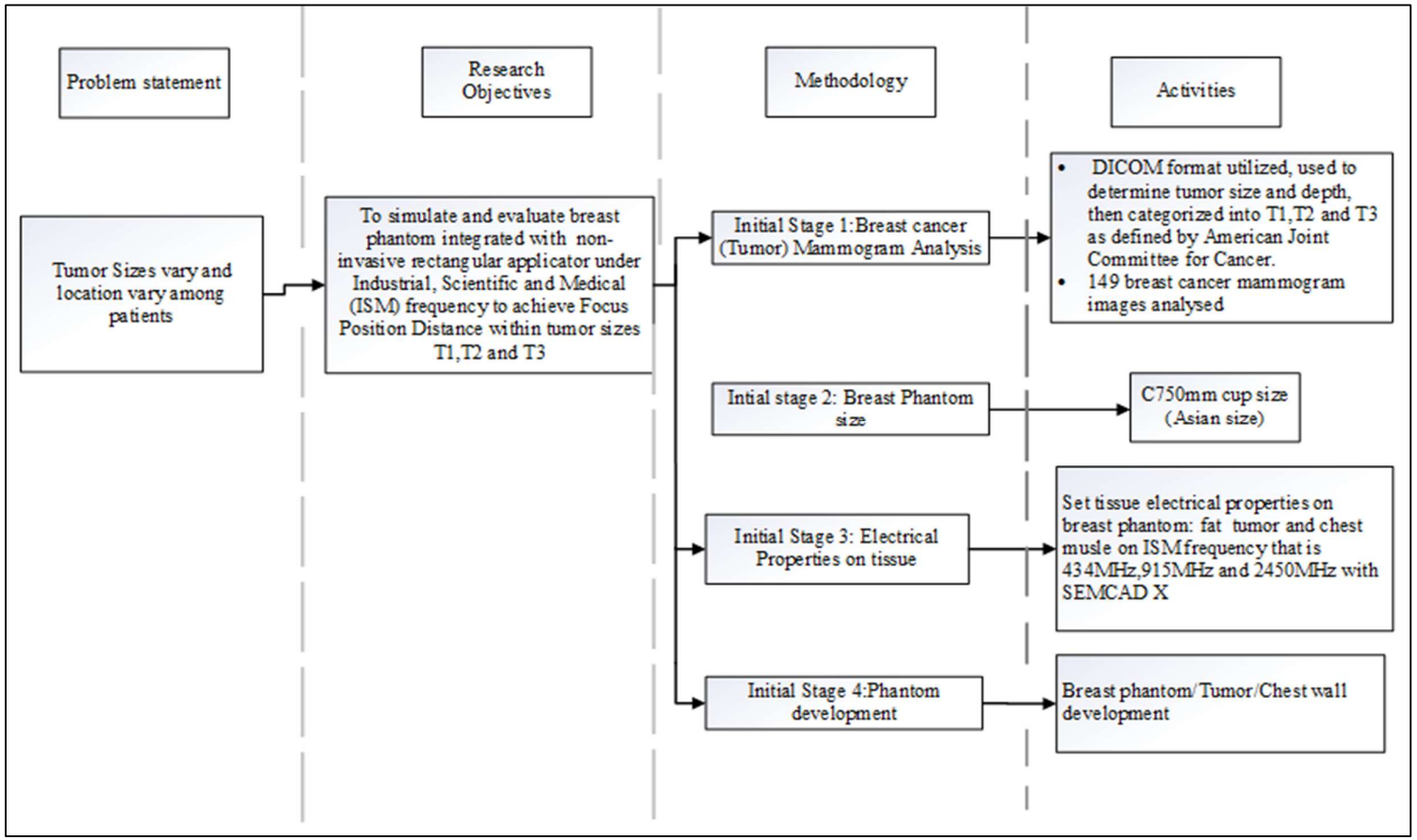

Figure 1.1: Scope of work in research objective 1 (breast phantom)

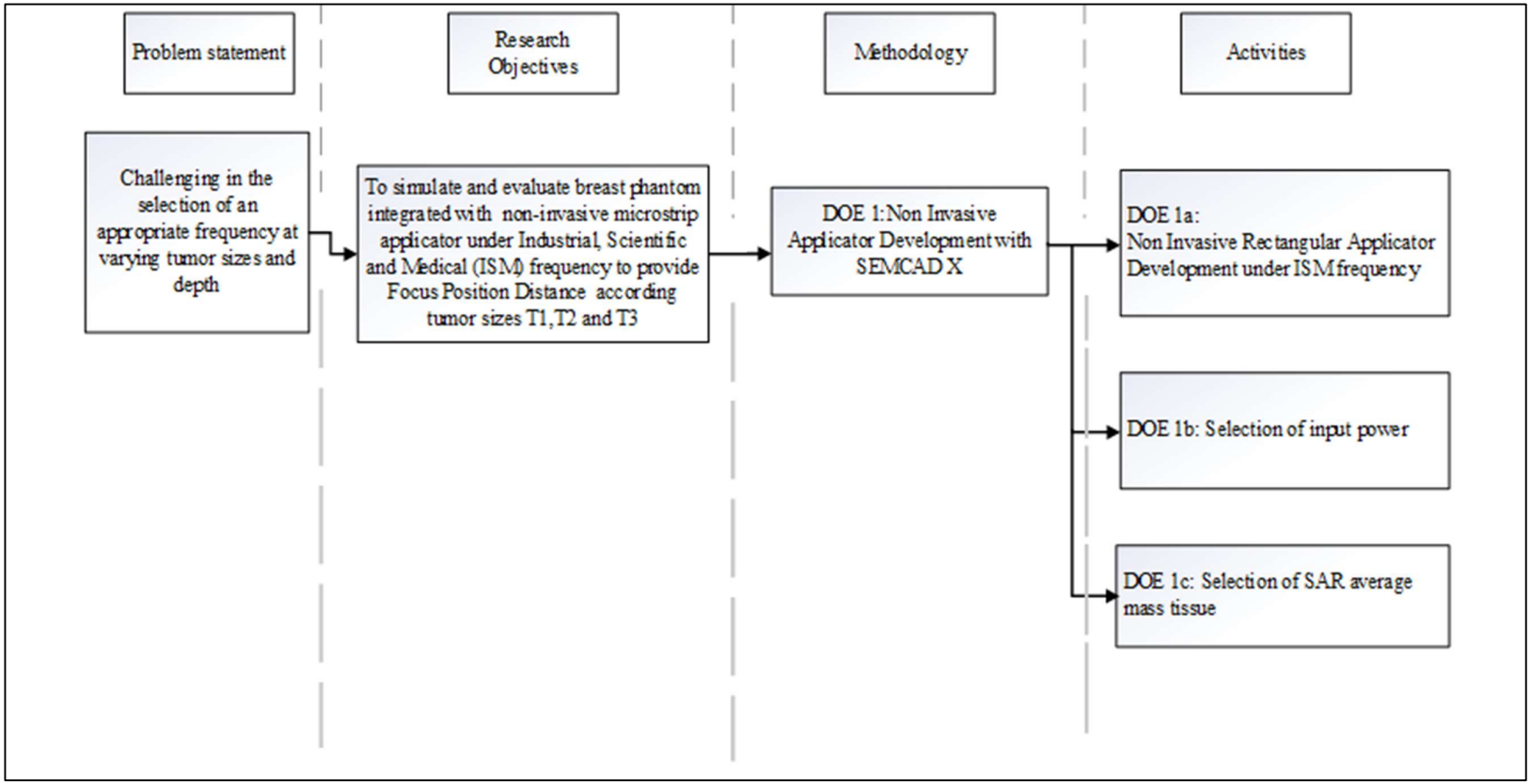

Figure 1.2: Scope of work in research objective 1 (Applicator)

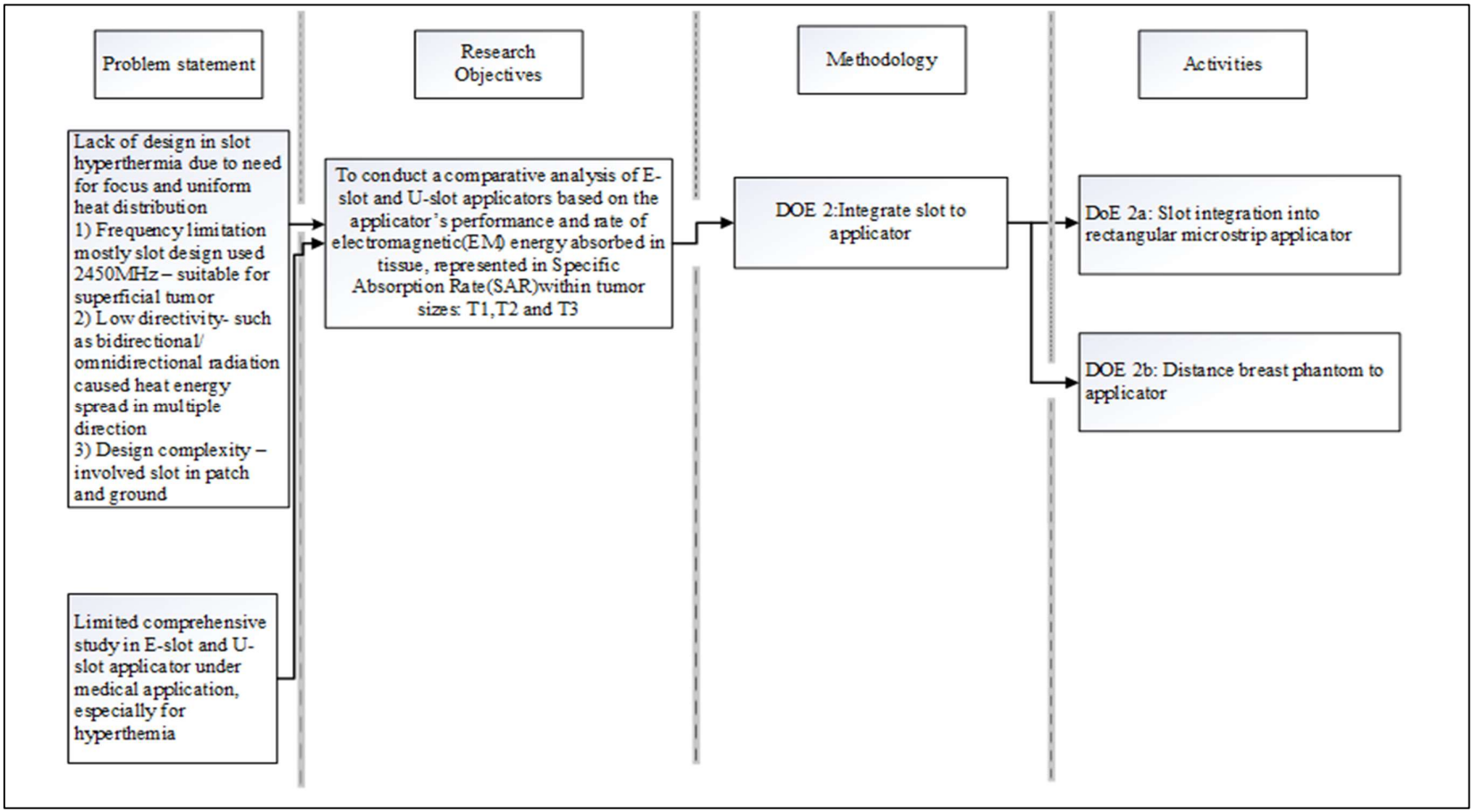

Figure 1.3: Scope of work in research objective 2

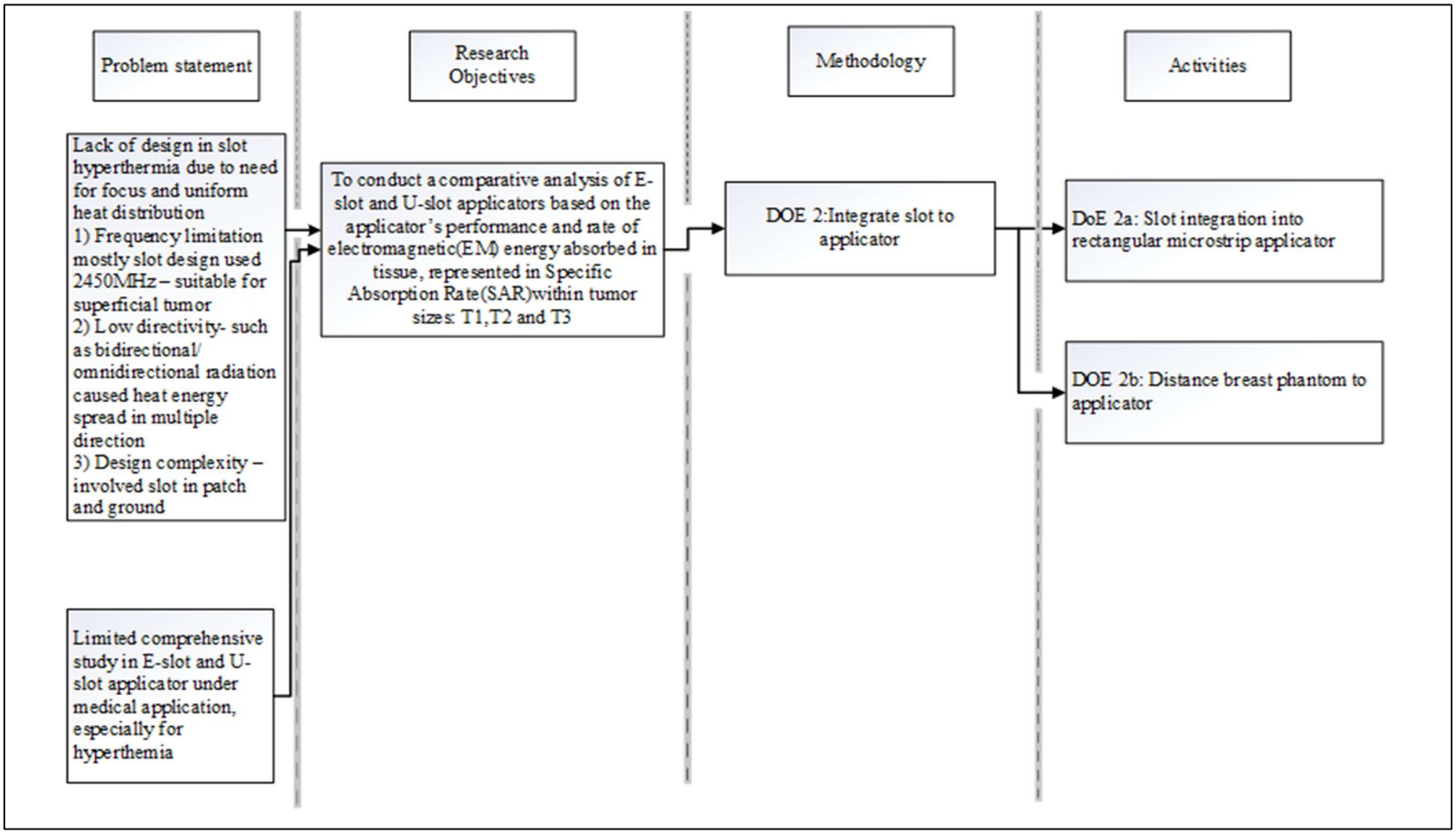

Figure 1.4: Scope of work in research objectives 3 and 4

1.6 Thesis Outline

This thesis is divided into five chapters. The thesis begins with Chapter 1: Introduction. Introduction, which provides the background of the study. It explains hyperthermia treatment for breast cancer and highlights the importance of applicator design for achieving effectiveness and tumor heating.

The problem statement addresses the challenge of ensuring uniform heat distribution on the tumors while minimizing the effect on surrounding healthy tissue. Therefore, the objectives of this research focus on improving the effectiveness of hyperthermia treatment in breast cancer.

In alignment with research objectives, this research focuses on three main elements to overcome the problem of hyperthermia treatment: appropriate frequency, slot integration and efficient time treatment for hyperthermia breast cancer. This chapter also presents the significance of the research, the research scope &methodology framework and thesis outlines.

Chapter 2: This chapter presents a comprehensive literature review of hyperthermia treatment and its application in breast cancer. The chapter begins with an overview of hyperthermia, including treatment types and heating techniques. Then, concepts of human tissue interaction in hyperthermia, dielectric tissue properties and ISM frequency band. Specific absorption Rate (SAR), input power to the microstrip applicator, applicator performance parameters for breast cancer hyperthermia treatment, slot microstrip applicator for hyperthermia and the effect of the distance between the breast phantom and the applicator are also reviewed. Special attention is given to the U-slot and E-slot, which integrate with the applicator due to their suitability for hyperthermia applications. Optimization technique

used to improve SAR distribution, water bolus, breast cancer treatment time and electromagnetic simulation tools used in hyperthermia are outlined.

Chapter 3: This chapter explains the methodology in line with the research objectives. Research activities under methodologies are divided into Design of Experiment (DoE) 1 to DoE 4. Research activities begin with an initial stage, which is breast phantom development. Then DoE 1 is involved in applicator development, followed by DoE 2, which focuses on the integration of the E-slot and U-slot as the applicator and the distance from the breast phantom to the applicator. DoE 3 focuses on the modification of the E-slot, optimization of the E-slot and validation of the E-slot. Finally, DoE 4 is used to determine the hyperthermia treatment time.

Chapter 4: This chapter presents the results of each DoE. Discussion on DoE 1 focuses on a selection of appropriate frequency, suitable input power and selection of the SAR average mass that suits this research. Meanwhile, DoE 2 discussion emphasises the selection of slot integration and the distance between the breast phantom and applicator. Meanwhile, under DoE 3, discuss the modification of the E-slot applicator, slot optimisation, and validation of the optimization of the E-slot applicator. Then, in DoE 3, the hyperthermia treatment time is recommended for T1, T2, and T3.

Chapter 5: Conclusion. This chapter highlights a summary of research findings, contributions to knowledge and future works.

CHAPTER 2

LITERATURE REVIEW

2.1 Introduction

This chapter consists of a comprehensive review of the literature on non-invasive hyperthermia treatment relevant to this research. The literature review is structured in sections 2.2 to 2.22.

2.2 Current Treatment for Breast Cancer

Currently, the treatments for breast cancer are surgery, radiotherapy and chemotherapy. Other therapies, such as hormone therapy and targeted therapy, can be used in conjunction with radiotherapy, chemotherapy and surgery. Table 2.1 summarizes the procedures and side effects of those therapies.

Hyperthermia can be used as a complement to existing cancer therapies. For instance, cells in the hypoxia region are resistant to radiotherapy and chemotherapy (Begg & Tavassoli, 2020). Hypoxia induces an increase in malignancy (Nejad et al., 2021). Therefore, hyperthermia can be combined with radiotherapy and chemotherapy to enhance cancer treatment effectiveness. In addition, hyperthermia a safer option and can be applied independently.

In the following section 2.3, thermal therapy is described before further discussing hyperthermia for cancer treatment.

Table 2.1: Current Cancer Treatment

Breast Cancer Treatment	Procedure	Side Effects and Limitations
Surgery	The surgical removal of cancerous tissue with a margin in healthy tissue is a critical aspect for oncologists (Krontiras et al., 2014). The aim is to remove cancerous tissue and the crucial part is to prevent local recurrence completely.	Severe postoperative pain (pain after surgery) was managed with an analgesic. However, the side effects of this medication are nausea, vomiting, dizziness and vertigo (Alizadeh et al., 2020)
Radiotherapy (RT)	It uses a high-energy X-ray or gamma-ray to kill the cancerous cells. It interrupts DNA in cancer cells by controlling their growth or killing the cancer (Koushik et al., 2013).	Skin changes- dryness, itching, blistering or peeling, Fatigue, long-term side effects: possible development of second cancer(new cancer form and different from the first one) (Dilalla et al., 2020)
Chemotherapy (CT)	It utilizes drugs to destroy cancer cells by interfering with DNA or RNA, preventing cells from growing and dividing (Kaur et al., 2022). It can be given before or after the surgery	Fatigue, Hair Loss, Anemia (low red blood cell count), Nausea and vomiting, Infertility, Appetite changes, Mood change (Katta et al., 2023)

Table 2.1 continued

Hormone therapy	To reduce the size of the primary cancer before surgery or radiotherapy. To minimize the risk of cancer coming back or spreading to another area (Abraham & Staffurth, 2020)	Hot flashes, joint pain, sleep disturbance, osteoporosis, mood swings and depression (Palácová, 2016)
Target therapy	Use drugs to target specific genes and proteins that control the growth and spread of cancer cells. It prevents the formation of new blood vessels in the tumor (Abraham & Staffurth, 2020).	Loss of appetite, diarrhea, nausea, fever, hand-foot syndrome, high blood pressure, difficulty breathing and bleeding (Abraham & Staffurth, 2020).

2.3 Thermal Therapy

Thermal therapy has been introduced into cancer treatment to provide safer, more efficient treatment. It is an ancient treatment that involves increasing the temperature by heating the cancerous cells. A temperature above 41°C can destroy cancerous cells with minimal damage to normal cells. The damage to cells depends on the temperature and the duration of exposure to heat (Righini et al., 2024).

Thermal therapy can be categorized into three types: low-temperature (Diatherma), moderate-temperature (Hyperthermia) and high-temperature (Thermal ablation). Low-temperature hyperthermia or diathermy applies temperature at 40°C-41°C for 6 to 72 hours; moderate hyperthermia or hyperthermia is exposed to 42°C to 45°C within 15 to 60 min;

high temperature is known as thermal ablation with temperature > 46°C for 4 to 6 min (Habash et al., 2006).

The effect of the results on thermal therapy depends on the type of therapy. The hyperthermia mechanism increases blood flow and oxygen levels in tumor/cancerous cells. It is a technique to expose cancerous tissue to EM radiation therapy. Based on previous research, this hyperthermia technique can convert the cancerous tissue into necrotic tissue and destroy the cancerous tissue with minimal side effects (Korkmaz et al., 2013; Sharma et al., 2014; Sim, 1986).

The effectiveness of hyperthermia significantly increases when combined with radiotherapy or chemotherapy. A combination of radiotherapy and hyperthermia enables the radiotherapy to target the oxygenation of outer cells, while hyperthermia acts on the inner cells, particularly those affected by hypoxia. Meanwhile, combining chemotherapy and hyperthermia enhances the effect of drug delivery to the tumor (Fatehi et al., 2009).

The first clinical trial of hyperthermia in cancer patients began in the '70s and '80s (Sim, 1986). Since then, numerous studies have investigated the effects of combining hyperthermia with radiotherapy and chemotherapy in various types of cancers, such as breast, cervical, head, neck, prostate and sarcoma (Rao et al., 2010). In addition, the results generally show improvement in patients' local tumor control and survival rates (Guisasola et al., 2018). The type of hyperthermia treatment depends on the specific cancer types, locations and sizes. The next section elaborates on the types of hyperthermia used in cancer treatment.

2.4 Types of Hyperthermia Cancer Treatment

The hyperthermia approaches under moderate temperatures are whole-body Hyperthermia (WBH), regional and local hyperthermia (Rao et al., 2010). WBH is applied to treat cancerous cells/tumors that have spread to different body parts, melanomas, soft tissue sarcomas or leukemia (Stauffer, 2005).

Regional hyperthermia is a therapeutic approach to treating deep-seated tumors in specific body regions, such as the pelvic or abdominal region. This technique aims to heat a larger body region, typically encompassing the entire tumor volume, to a therapeutic temperature of 40-44ºC (Rao et al., 2010). This non-invasive method involves an external applicator in a ring-shaped position around the patient (Kroeze et al., 2001).

Local hyperthermia with a temperature >40° C enables hyperthermia to cut off the nutrients and oxygen to the tumor cells. This leads to a low potential of hydrogen (PH) and a collapse in tumor vasculature. Local hyperthermia provided non-invasive and invasive treatment (Issels et al., 2002) .

Both invasive and non-invasive microstrip applicators achieved good hyperthermia treatment outcomes, but their procedures differed. A non-invasive hyperthermia applicator was placed on the skin surface with a cancerous cell in the tissue (Ma et al., 2022). In contrast, the invasive hyperthermia applicator procedure involves inserting the applicator inside the skin and directing it to the tumor (Neagu, 2017), which can cause discomfort and pain for patients.

The non-invasive hyperthermia applicator has different designs in size and shape, such as a waveguide applicator (Kim et al., 2024), dipole applicator (Yildiz et al., 2023),

helical/spiral applicator (Kok et al., 2020), microstrip and slot applicator (Babak & Vrba, 2022; Sharma et al., 2018; Khan & Dubey, 2023). The following section highlights hyperthermia heating techniques.

2.5 Hyperthermia Heating Techniques

The heating techniques for EM heating, including capacitive, inductive and radiative, are used to deliver heat to cancerous tissue. Capacitive uses an EM field between 2 electrodes (Szasz, 2021). Inductive uses a magnetic field to induce eddy currents within tissue (Vasilchenko et al., 2022) and radiative (Lim et al., 2015).

Radiative applicator uses EM radiation to generate and concentrate heat in the treated tissue. The radiative technique used in a microstrip as the applicator (Behrouzkia et al., 2016; Chicheł et al., 2007; Habash et al., 2006). It is suitable for heating small cancerous tissues. Non-invasive hyperthermia can be approached using radiative (Choi et al., 2016).

A microstrip radiator applicator has been developed and can operate at low (Dayanc et al., 2008) and high frequencies, 433MHz to 2450MHz (Franckena & Zee, 2010). These applicators are lightweight and flexible, making them more convenient.

2.6 Human Tissue Interaction with the Hyperthermia Applicator

The interactions between EM radiations from the microstrip applicator engaging with the tissue's electrical properties are the beginning of cancer treatment in hyperthermia. The electric field on tissue leads to energy formation. The electrical properties of tissue describe how the tissue responds to an electric field by either conducting or obstructing the flow of electric current (Bevacqua et al., 2018).

Several complex simulation models have been developed for numerical

computational investigation of EM wave propagation within tissues, such as the Finite Difference Time Domain (FDTD) method (Kelley & Luebbers, 1996).

Comprehensive studies have been conducted to determine the dielectric properties of different tissues across a wide range of frequencies (Lazebnik et al., 2007; Sha et al., 2002). The Cole-Cole equation models the electrical behaviour of tissue over a specific frequency range. This model is based on the Gabriel database. By fitting the Cole-Cole model to experimental data, the electrical properties of different tissues can be estimated (Said & Varadan, 2009).

The interaction of an electric field (E-field) with tissue is characterized by tissue complex permittivity, given in Equations 2.1 and 2.2.

$$\varepsilon = \varepsilon' - j\varepsilon'' \qquad \text{Equation 2.1}$$

$$\varepsilon = \varepsilon_r \varepsilon_o - j\frac{\sigma}{\omega} \qquad \text{Equation 2.2}$$

Equations 2.1 and 2.2 consist of the real part and the imaginary part. The real part of permittivity is known as the dielectric constant, which is related to the tissue's ability to store energy. In contrast, the imaginary part is related to energy loss within the tissue due to the conductivity and frequency of the electric field.

2.7 Dielectric Tissue Properties

The dielectric properties, including tissue permittivity and conductivity, are strongly influenced by water content. Tissues with high water content, such as tumors, have higher water content and exhibit high relative permittivity and conductivity compared to low water content, such as fat (Hesabgar et al., 2017)(Bah et al., 2015).

Therefore, tissue such as tumor absorbs more EM energy than normal tissue with low water content (Vaupel & Piazena, 2022). This is due to the high number of polar molecules in water, which interact strongly with the electric field.

The dielectric properties are frequency-dependent (Nguyen, 2016). As the frequency increases, the relative permittivity decreases while the electrical conductivity increases. Similar trends in the electrical properties with frequency are revealed in (Ramu & Arunachalam, 2023).

The dielectric properties determine how tissue interacts with EM energy and influence energy absorption in tissue , which can be evaluated by SAR. Therefore, selecting the appropriate frequency improved PD. The following section explains the Industrial, Scientific and Medical (ISM) frequency band.

2.8 ISM Frequency band

The hyperthermia applicator operates under ISM frequency and is used in various medical applications. The ISM frequency band is 434MHz. 915MHz and 2450MHz. The applicator operates under the ISM band, reduces complications and minimizes the installation cost in the clinic (Baskaran & Arunachalam, 2021; Lyu et al., 2023).

In the context of frequency selection within the ISM band, such as hyperthermia, it is essential to ensure an optimal balance between tissue penetration depth and energy absorption. A previous study reported that the frequency utilized in the applicator design influenced the PD (Choudhary & Arunachalam, 2022; Nguyen et al., 2015), while (Choi et al., 2012; Hand, 1986).

Therefore, frequency is essential to the hyperthermia applicator. The low-frequency applicator penetrates deeper into the tissue (high PD), while the high-frequency applicator, conversely(Sharma et al., 2025). The frequency is selected based on tumor size and position.

2.9 Specific Absorption Rate (SAR)

SAR is the measurement of the rate of energy absorbed per unit mass by the treated tissue in W/Kg or mW/g(Wessapan et al., 2012). The mass density of tissue suggests that 1g and 10g are the standard values in IEEE/IEC62704-1 (IEEE, 2017). SAR also described (Fiser et al., 2015) W/ in the electric field effect as in Equation 2.3

$$SAR = \frac{\sigma}{\rho}|E|^2 = \frac{\sigma_s + \omega\varepsilon''}{\rho}|E|^2 = \frac{\sigma_s + 2\pi f\varepsilon''}{\rho}|E|^2 \quad \text{Equation 2.3}$$

The equivalent of conductivity is σ= $\sigma_s + \omega\varepsilon''$ and σ_s = static (electrical conductivity of tissue at f=0Hz, $\omega\varepsilon''$= alternating current (electrical conductivity varies with frequency), ρ is the tissue density (kg/m^3), E is the field intensity. The relationship between SAR and temperature and time period is given by Equation 2.4.

$$SAR = \frac{C\Delta T}{\Delta t} \quad \text{Equation 2.4}$$

Where C is the specific heat capacity of the exposed tissue in J/kg/°C, T is the change in temperature(°C), and △t is the exposure duration (s). Heat absorption within tissue increases temperature. *C* = the specific heat capacity (J/kg°C). SAR measurement typically averages over a 1g and 10g cubic tissue volume as specified by IEEE and IEC 62704 (Xplore, 2017).

SAR (peak) and SAR distribution are important parameters for describing EM energy

observed by tissue. SAR (peak) refers to the highest localized SAR value measured within a specific volume of tissue. Meanwhile, SAR distribution is the spatial pattern of SAR within the target tissue (SEMCAD X, 2012).

2.10 Hyperthermia Applicator Type: Microstrip Antenna Patch

A microstrip applicator is the simplest configuration, consisting of a radiation patch on a dielectric substrate and a ground plane. Its advantages are lightweight, low volume and a thin profile configuration that can be made conformal. Additionally, feed lines and matching networks can be fabricated simultaneously.

Microstrip applicators have a variety of shapes. Several microstrip applicators are used in practice: square, rectangular, circular, elliptical, equilateral triangle, and ring. The most commonly used patches are rectangular and circular. However, the simplest patch is a rectangular antenna.

A microstrip design proposed with a circular patch applicator for SAR and return loss improvement, as stated by (Elsaadi et al., 2019) and (Sethi & Nijhawan, 2016). However, (Lias et al., 2019) present a modified microstrip applicator with a rectangular patch that performs better than a circular patch. The rectangular patch provides better SAR, penetration depth, focus and minimizes unwanted hotspots on healthy cells.

A slot can be introduced into a microstrip antenna, which can exhibit either bidirectional or unidirectional radiation, depending on its design configuration, such as the slot's geometry. The radiation pattern (SAR) can be determined by the input power level set on the applicator.

2.11 Input Power to Microstrip Applicator

The input power influences the SAR distribution in the microstrip applicator hyperthermia. The input power from the applicator determines the amount of EM energy absorbed in tissue and affects SAR and PD.

Several studies have investigated the effect of varying input power on SAR distribution. For instance, (Lias et al.,, 2019) increase the input power in three levels: 10 W, 100W and 200W in breast cancer hyperthermia treatment. Increasing input power leads to higher SAR and a deeper PD. However, the increase in power also raises the heating region and affects normal tissue.

Another study (Selmi et al., 2020) analyzed microstrip applicator performance under 10W, 45 W and 75W. The results reveal that the input power exceeding 10W caused the formation of an unwanted hotspot in healthy tissue. This finding highlights the importance of restricting input power to prevent excessive heat to healthy tissue.

Additionally, the input power directly affects treatment duration. According to (Naimullah et al., 2023) the operating power of 10 W resulted in shorter treatment time compared to the lower power of 1W, due to increase in energy absorption in the target tissue. This indicated that appropriate power selection can improve time duration without excessive heat affecting healthy tissue.

Overall, it shows that input power enhances SAR distribution and PD; power levels above 10W increase the risk of overheating in healthy tissue.

2.12 Applicator Performance Parameters for Breast Cancer Hyperthermia

The efficiency and safety of EM energy delivered to the target tissue during hyperthermia treatment depend on the performance of the applicator. The parameters such

as return loss, directivity and gain determine how effectively the applicator focuses the EM energy on target tissue while minimizing exposure to healthy tissue. Enhancing these parameters is essential for improving heat on the target tissue and reducing unwanted heat on healthy tissue.

Low return loss in the applicator for hyperthermia is critical for effective heat delivery to the target tissue (Hu et al., 2024). The degree of mismatch between input power, *Pin*, and reflected power, *Pr*, is given in the ratio *Pin/Pr*, return loss expressed in dB (Bird, 2009) defined as:

$$\text{Return Loss, } RL = 10 \log_{10} \left(\frac{Pin}{Pr}\right) \qquad \text{Equation 2.3}$$

Directivity, *D* is the ratio of the power density of the real applicator in its major direction to the power density of the isotropic antenna (Parameters, 1943).

$$D = \frac{Pden}{Pi} \qquad \text{Equation 2.4}$$

Where,

Pden= power density

Pi = isotropic power

Directivity in the applicator used for hyperthermia is important as its ability to concentrate the heat radiation on the target tissue while minimizing unwanted hotspots (Sethi & Nijhawan, 2016; Nitika Sharma et al., 2022).

Gain uses to provide focus on the target tissue in hyperthermia treatment (M. Tayel

et al., 2017). Gain refers to the efficiency with which the applicator directs EM waves in a particular direction.

$$\text{Gain} = \quad \eta . D \qquad \text{Equation 2.5}$$

Where,

η = antenna efficiency

D =directivity of antenna

2.13 Slot Microstrip Applicator in Hyperthermia

Slot microstrip applicators are widely used in cancer hyperthermia treatment. The purpose of adding a slot is to obtain focus and uniform heat toward the tumor, especially for breast cancer hyperthermia treatment.

In most studies, slot integration was added using three methods: present only in the patch, only at the bottom/ground, or in both the patch and the bottom/ground. As reported by (Alex & Chakaravarthi, 2023) slot integrated into the patch and into the ground demonstrated that the applicator effectively heats the superficial and deep tumor at 434MHz. In addition, enabled the design of an applicator with dual frequency (Lyu et al., 2023; Younesiraad et al., 2017).

The microstrip design has various patch shapes, such as an elliptical patch with an annular ring slot, a hexagon patch with an annular ring slot and a pentagon patch with an annular ring slot. However, the slot design is integrated only into the ground plane. Moreover, the studies claimed that return losses improved (Khan & Dubey, 2023; Khan, 2023; Khan et al., 2023)

The majority of the designs focus on integrated slot in the patch since it results in less complication and reported enhancement in return loss (Khan et al., 2024; Hu et al., 2024; Khan & Mishra, 2023; Khan & Singh, 2023; Singh et al., 2019) , while (Hu et al., 2024) addressed increments in PD and SAR with uniform heat distribution. Additionally, the surface current increases due to the integrated slot in the microstrip (Khan & Mishra, 2023; Khan & Singh, 2023) .

Several studies have covered a gain applicator, with a negative value (Khan et al., 2024; Khan & Dubey, 2023; Khan & Singh, 2023). According to (Charan et al., 2020) negative gain is due to the lossy tissue surrounding the microstrip applicator.

The results in (Khan & Dubey, 2023; Khan & Mishra, 2023; Khan & Singh, 2023) show that bi-directional radiation is not suitable for hyperthermia treatment, especially in breast cancer. Bi-directional radiation refers to energy radiating in two opposite directions. It can cause heat in the tumor, but heat can also spread to surrounding healthy tissue, raising safety concerns for the patient (Kok et al., 2015; Smrkovski et al., 2013). Therefore, the preferred approach in breast cancer is the directivity applicator since it is more localized and focuses on specific tissue/tumor (Sethi & Nijhawan, 2016a; Yildiz et al., 2022).

In summary, most of the previous studies focused on an operating frequency of 2450MHz (Elsaadi & Hamad, 2023; Hu et al., 2024; Khan et al., 2024; Khan & Singh, 2023; Shehata et al., 2021; Singh et al., 2019; Singh et al., 2023; Singh & Singh, 2016) which offers limited PD and is suitable for superficial tumors. However, few studies have explored the 915 MHz band, and those that have done so have limitations.

The existing applicator design with 915MHz has several limitations, such as a complicated design (rectangular slots and a slit) (Lim et al., 2015), a dual-frequency

applicator that operates at 915MHz and 2400MHz (Lyu et al., 2023) or 434MHz and 915MHz (Younesiraad et al., 2017) also involved in complex slot configuration, typically requiring slot integration on both the patch and the ground plane. Moreover (Khan & Mishra, 2023), has bidirectional radiation, which is not suitable for breast cancer treatment.

In conjunction with the limited number of studies on slot shape at frequency 915 MHz, a more comprehensive study should be conducted on hyperthermia treatment, especially in breast cancer, which is the actual clinical tumor size. Consequently, another type of slot needs to be proposed with characteristics required in hyperthermia breast cancer treatment, such as enhanced directivity, improved gain and low return loss, to ensure the enhancement of the hyperthermia procedure. In addition, the literature review in sections 2.11 and 2.12 emphasized that U-slot and E-slot microstrip exhibit these required characteristics.

Furthermore, the integration of the E-slot or U-slot only in the patch is less complicated compared to the integration of slots on the bottom only or both sides of the patch and the bottom. The E-slot integration in the patch shows improvements in return loss, SAR uniform heat distribution and an increase in surface current.

The following sections present a matrix of slot antennas for hyperthermia, as shown in Table 2.2.

Table 2.2: Matrix table slot applicator in hyperthermia

Author/ Year	Slot structure	Fed Antenna	Freq	Method	Tissue	Results	Conclusion	Remarks
Khan et al., 2024	T-slot structure. A slot cut into the patch. The slot's impact on the patch is to increase the overall electrical length of the surface current	50Ω coaxial feed	2.45 GHz	Design T - slot with Finite Element Method (FEM) with FR4 substrate. ANSYS HFSS -EM simulation Optimization of T-slot antenna with GA	Single-layer TEL. The measurement of tissue permittivity using a Network Analyzer.	Gain = -5.1 dBi The antenna provides a heating pattern with low energy deposition in surrounding healthy tissue. The SAR(peak) = 230.75W/kg with an input power of 6.93mW. The antenna performance compared to the previous study shows better RL= -33.49dB Radiation =bidirectional	The proposed T-slot antenna is effective in HTP applications - focuses EM energy at 2.45GHz. It is suitable for heating cancerous cells at superficial.	The parameters studied: Gain, RL and surface current.

Table 2.2 continued

Hu et al., 2024	Octagonal patch with four symmetrical-Cross-slots-open metal cavity added to antenna surface. Slot on the patch	50Ω coaxial feed	2.45 GHz	The substrate permittivity is 10.2.EM simulation: COMSOL : Optimization -parameter adjustments-patch length, slot dimension and feed position - manual adjustment. The parameters are	Tissue layer consists of 3 layers: skin =1.5mm, fat=5mm, and muscle 73.5mm. The tumor is inserted into the muscle tissue with a diameter of 20mm. The tissue permittivity is based on a previous study.	RL< - 20dB, enhance directed radiation, increased PD(26mm) Pin =1.4W T= 42-45° C SAR= 56.6W/Kg without tumor SAR= 72.1W/kg (tumor) SAR evaluated at various depths of the tumor, 10mm, 20mm and 30mm, shows uniform distribution and effective focusing of heat.	The proposed applicator demonstrated significant promise in HTP in both superficial and deep-seated cancer.	The parameter studied: RL, SAR, PD

Table 2.2 continued

				systematically varied to study the impact of antenna performance				
Khan & Singh, 2023	A cross slot and L-slots to all four corners. Slot on the patch. – Single-layer antenna design	Feed line	2450 MHz	Antenna substrate is not mentioned. EM simulation: HFSS	Single-layer TEL phantom. Tissue permittivity is determined experimentally using a network analyzer.	RL=-20.08dB (without tissue) RL=-15.91dB with TEL tissue SAR(peak) =404.15W/kg, Pin =3.9mW The current distribution surface concentrates towards the center of the patch	The proposed antenna has omnidirectional radiation, making it suitable for biomedical applications.	The parameter studied: RL, SAR, gain, radiation

Table 2.2 continued

Khan & Mishra, 2023	Antenna with a square patch with a symmetrical L-slot. Eight L-slots at the corner and 8 in the middle of the patch	50Ω coaxial feed	915 MHz	EM Simulation – HFSS. Substrate FR4	3-layer tissue: muscle, fat, and skin. Add a water bolus. The method of determining tissue permittivity is not mentioned	RL= -11.60dB Surface current =372.2A Radiation pattern- bi-directional	The study used tri-layer tissue to demonstrate the effectiveness of hyperthermia applications	The parameter studied: RL, surface current, radiation
Elsaadi & Hamad, 2023	Comparison of typical rectangular patch antenna (non-slot) and rectangular slot	Feed line	2.45 GHz	EM simulation – CST suite Substrate FR4	The tissue layer consists of 3 layers: the breast, breast fat layer, and the skin layer. The skin radius = 70mm, thick 5mm breast fat	Slot design has a better RL compared to non-slot. RL=-10.7dB (Non-slot) RL=-47.7dB (Slot) E field	The design with a slot antenna improved antenna performance, as it ensured better energy	The parameter studied: RL, treatment tie,

Table 2.2 continued

	rectangular at the center of the patch (slot) Both designs – single-layer				radius =65mm, the breast glandular radius =15mm, and the breast glandular and tumor are fibroglandular layer, the spherical in shape with 100mm and 200mm diameters, respectively	15.5dBV/m (Non-slot) 16.7dBV/m (Slot) The tumor is positioned at a different location. The distance of the antenna to the breast phantom =15mm Treatment time is 15 minutes at Tmax=45.6°C.	delivery to the tumor while minimizing reflection. The study did not specify a method for determining tissue permittivity .	SAR, E field

Table 2.2 continued

Alex & Chakara varthi, 2023	The antenna is designed with a circular ring patch with two rectangular slots and 2 meander line slots on the ground	50Ω coaxial feed	434 MHz	Substrate RO3010 εr = 10.20 EM simulation-HFSS	The electrical properties of human tissue from Cole-Cole dielectric model	SAR coverage of 18cm^2. PD=13.67mm. SAR(peak) =115W/Kg(breast model) SAR(peak) =446W/kg (chest wall recurrence model) RL= -15.62dB (breast model) RL=-10.5dB (chest wall recurrence model)	The design effectively heats tumor positions in both superficial and deeper depths.	The parameter studied: RL, SAR, PD
Lyu et al., 2023	Semi-elliptical slot in the ellipse patch.	Feed line	915 MHz 2.45 GHz	Antenna substrate = RT5880 εr = 2.2	The breast model includes a skin layer	The RL=-18dB(915MHz) and -21dB(2.45GHz) The simulation results confirm that thermal	This design provide dual frequency	The parameter studied:RL, SAR

Table 2.2 continued

	Ground plane-symmetrical quarter circle and Intermediate rectangular slot			EM simulation, Ansys HFSS and Fabrication	(1mm thickness), adipose tissue(fat), chest wall, and tumor. The tissue permittivity is based on a literature review. The tumor size is determined based on focal range and PD. Focal range refers to the region in	energy focuses on the tumor . optimization of slot with phase array-used 12 elements, SAR improvement. SAR at 2.45GHz has better focusing effect and small focusing range than 915MHz Radiation -not included		

Table 2.2 continued

					which heat energy is concentrated. Tumor size=1cm^3 (small) used 2450MHz and tumor size = 2cm^3 (big) used 915MHz			
Khan et al., 2023	Elliptical patch with radius 45mm, with elliptical ring slot inner radius 54mm and	50Ω coaxial feed	2.48 GHz	The antenna substrate used RT/droid 5880. The simulation tool is	TEL single-layer phantom. The tissue permittivity is based on	RL= -15.1dB (simulated) RL= -14.9dB (Experimental) SAR = 5.13808W/kg	The study confirms the antenna's effectiveness in HTP treatment while maintaining	The parameter studied: RL, SAR

Table 2.2 continued

	outer radius 60mm Ground plane rectangular orthogonal cross slots with square slot position behind elliptical patch			HFSS, which used Finite Element Method (FEM). The simulation and experimental. No radiation included.	theoretical calculations .		compliance with safety standards	
Khan et al., 2023	The hexagon with an annular ring and two rectangular orthogonal cross slots	50Ω coaxial feed	434 MHz	The FR4 substrate antenna. EM simulation HFSS.	TEL Single-layer Method to determine tissue permittivity,	Without phantom Simulated RL= -15.19dB, Measured RL -31.53dB With phantom	The simulation closely aligns with the experimental results. The gain is negative, and	The parameters studied were SAR, S11 and Gain

Table 2.2 continued

	and square slots at the ground				not mentioned	RL= -21.23dB (simulated) RL=-26.42dB (experiment) Gain =-9.1dB Bidirectional radiation SAR =0.089W/kg (distance phantom to antenna = 3cm)	the radiation pattern is bidirectional, meaning energy is emitted in two opposite directions.	
Khan & Dubey, 2023	The pentagon patch with pentagon ring slot, rectangular orthogonal cross slots and square slots on the ground	50Ω coaxial feed	434 MHz	The FR4 substrate antenna. EM simulation HFSS based on FEM	The single-layer tissue. The method to determine tissue permittivity is not mentioned	Without phantom Simulated RL= -15.19dB, Measured RL= -31.53dB With phantom RL= -21.23dB (simulated)	The simulation closely aligns with the experimental results. The gain is negative, and the radiation pattern is	The parameters studied were SAR, RL and Gain.

Table 2.2 continued

						RL= -26.42dB (experiment) Gain =-9.1 dBi Bidirectional radiation SAR =0.089W/kg (distance phantom to antenna = 3cm)	bidirectional, meaning energy is emitted in two opposite directions.	
Singh & Singh, 2022	Circular ring slot on the circular patch. At ground: two rectangular slots perpendicular to each other, with a circular slot	50Ω coaxial feed	2.45 GHz	The antenna substrate is FR4. EM simulation with FEM based on HFSS	Phantom muscle model: 83.655mm x 83.655mm x 50mm (thick)	SAR=5.2424W/kg for the distance between the phantom and the antenna is 25mm.PD increases as the distance between the antenna and the breast phantom is reduced. The results show that the slot antenna with PD improved to 20mm and	SAR distribution is uniform in specific regions. The PD improved. Antenna design with lightweight and efficient.	The parameters studied: S11, PD, SAR(peak)

Table 2.2 continued

						the conventional antenna =18mm RL=-27.9dB SAR(peak)=5.2424W/kg		
Shehata et al., 2021	A rectangular antenna with 8 small circular slots	Inset feed	2.45 GHz	The antenna substrate is FR4. The EM simulation is CST with FEM method	The breast tissue consists of skin, fat, gland and tumor. Water bolus was used in this paper. The tumor size is spherical, with a radius of	The microstrip patch antenna (MSA) with 8 small circular slots recorded higher electric field and SAR values compared to MSA without slots. As input power increased , SAR increased too. Pin=1W:SAR(non-slot)=0.920W/Kg SAR(slot)=0.957W/Kg	The design and performance of the antenna were validated through simulation and experimentation.	The parameters studied: RL

Table 2.2 continued

					6mm. The location of the tumor is in the middle of the breast phantom.	Pin=4W:SAR(non- slot) =3.685W/Kg SAR(slot)=3.831W/Kg RL= - 25.424dB		
Singh et al.,2019	Microstrip slot antenna with circular corrugated slot patch	50Ω microstrip line	2.45 GHz	Antenna substrate RT5880. EM simulation - CST	Tissue-muscle	The antenna has an impact on the corrugated slot in terms of PD, EFS, and temperature distribution. PD decreases as the circular corrugated radius increases.PD=17.5mm to 17mm RL =-32dB to	The study explores the effect of radius circular corrugated slot in terms of PD, EFS and RL	The parameters studied: PD, EFS, RL and Temperature

Table 2.2 continued

						-50dB(depend on corrugated radius)		
Singh et al., 2019	Corrugated circular slot in multilayer. Water bolus included	50Ω microstrip line	2.45 GHz	Multilayer structure: 1st layer = RT6010, 2nd layer= RO3003 3rd layer = neoprene layer 4th layer = Perfect Electric conductor (PEC)	Tissue – muscle	The larger the radius of the corrugated circular, the greater the PD increases. EFS tends to increase as the corrugated slot radius increases. Temperature distribution – no unwanted hot spots observed in the superficial region of the tissue RL<-24dB for various values of corrugated circular radius	The study explores the effect of radius circular corrugated slot with multilayer in terms of PD, EFS and RL	The parameters studied: PD, EFS, RL and Temperature

Table 2.2 continued

Younesiraad et al., 2017	Square ring slot- patch surface. Cross slot with a small circle in the middle-ground plane	50Ω coaxial feed	Dual freq: 434 MHz and 915 MHz	The antenna substrate=FR 4 EM simulation =HFSS	Tri-layer tissue model: skin, fat, and muscle. Add with water bolus. The tissue permittivity obtained based on the previous study	SAR(peak) =1.32W/Kg (434MHz) SAR(peak) =1.44W/Kg (915MHz) PD 434MHz=6.5cm 915MHz=6cm RL=-16dB(434MHz) RL=-13dB(915MHz)	A dual-frequency antenna obtained with 2 different PD	The parameters studied: SAR(peak) and PD

Table 2.2 continued

Singh & Singh, 2016	Two circular patches are located within the rectangular slot. Ground also has two circular patches within the rectangular slot	50Ω microstrip line	2.45 GHz	The antenna substrate is RT Duroid with εr = 2.2. EM simulation: CST	Tissue - muscle. Tissue permittivity from literature	Conventional patch antenna PD=18mm EFS(mm^2)=39x28 BW=50MHz S11= -21dB Slot Antenna PD=23mm EFS=12x18mm^2 BW=170MHz S11= -24dB	The slot antenna has better characteristics compared to conventional terms of RL, PD and BW. EFS is more focused on the slot antenna	The parameters studied: PD,EFS, BW, RL
Lim et al., 2015	Modified rectangular microstrip patch antenna incorporates of multiple slits on the	Not mention	915 MHz	Antenna substrate FR4 EM simulation: not to mention	The tumor size is 30mm, but it is not explicitly stated how to get it.	RL(with slit only) = -5dB RL(slit + slot)= -24dB T max rise = 9.7ºC	RL improved with a slot added to the antenna	The parameters studied: RL, Tmax

Table 2.2 continued

	front side of the antenna, Two rectangular slots on the ground				The method obtains tissue permittivity, which is not mentioned.	Tmax at the middle of tumor area		

2.14 Effect of Distance Breast Phantom to Applicator on Hyperthermia Treatment

Previous studies have shown that the distance between the applicator and the phantom affects the effectiveness of hyperthermia treatment. The study by (Wong et al., 2021) reported direct contact between the applicator and the breast phantom. This helps deliver heat to the target tissue effectively and localization SAR distribution.

However, according to (Elsaadi & Hamad, 2023) the best distance from the applicator to the phantom is 10 mm. The placement of the applicator at this distance is crucial for the treatment's effectiveness. The delivery of EM waves is optimized at this distance and minimizes the impact on surrounding healthy tissue.

Another study mentioned the relationship between the distance between the applicator and the phantom with return loss. The observed distances are 20 mm and 40 mm. The return loss decreases as the distance between the applicator and the phantom increases. This means the applicator becomes less effective at detecting tumors as the distance between the applicator and the phantom increases. The distance of 20mm is more effective compared to 40 mm in identifying the tumor (Kurt, 2023).

Since the appropriate distance varies and cannot be represented by a fixed value, it was essential to determine the optimal distance, as it significantly affects treatment effectiveness. Therefore, this research examines the distance between the breast phantom and applicator, ranging from 0mm (direct contact with the skin) to 20mm.

2.15 Slot Applicator Modification

The modification of the E-slot applicator impacts its performance and characteristics, including resonance frequency, gain, directivity and return loss. Slot modification can

modify the resonance frequency (Govindarajulu et al., 2023; Haque et al., 2021) by adjusting parameters such as slot width (Ws), slot gap (Wg) and slot position relative to the feed, the antenna achieves optimal performance, enhancing operating bandwidth and resonant frequency (Latha et al., 2022; Tan et al, 2022).

In addition, a slot on the patch also changes the input impedance (Abdelgwad, 2018). The impedance characteristics were evaluated through return loss, where low return loss indicated better impedance matching and efficient power transfer (Kee et al., 2024; Mary et al., 2023; Parameswari et al., 2024). Therefore, the slot modification can enhance the impedance matching (Govindarajulu et al., 2023).

The modification of the dimension of the E-slot (Ahmed & Islam, 2013; Kishore et al., 2014; Sivakumar et al., 2019) and U-slot (Dargar et al., 2022; Hasan et al., 2012) led to improvement of return loss, directivity, and gain, ultimately enhancing overall antenna performance. The subsequent section discusses U-slot microstrip antenna characteristics.

2.16 U-slot Microstrip Antenna Characteristics

U-slot and E-slot microstrip patches have similar characteristics, as both types of slots can enhance antenna performance. The symmetrical U-slot provided a broad bandwidth and stable radiation. In contrast, an asymmetric U-slot offers high bandwidth with increased cross-polarization. Additionally, variations in slot length and feed-point location significantly influence input impedance and resonance frequency (Astuti et al., 2022). According to (Deshmukh & Chavali, 2023; Hasan et al., 2012) gain and directivity improved by integrating a U-slot into the microstrip antenna. In addition by (Dong et al., 2023; Roy et al., 2013) claimed that U-slot significantly improves return loss. In addition, (Borkar & Parlewar, 2024) demonstrated that radiation efficiency improved. Tables 2.3 and

2.4 present the matrix tables of the U-slot microstrip antenna in communication and the U-slot in medical applications, respectively.

Table 2.3: Matrix table U-slot microstrip

References	Structure	Freq	Substrate	Simulation tool	Finding	Limitation	Diagram
(Deshmukh et al., 2024)	U- slot – square patch Coaxial feed	2.4GHz	FR4	IE3D	U-slot – tuning frequency Gain =8.5dBi Radiation pattern – has broadside radiation, indicates a focus beam, and good directivity.	Complexity design – involves gap coupling and the use of multiple slots. No value of directivity and ,RL	

Table 2.3 continued

(Thakur et al., 2024)	A triple U- slot (microstrip feed line)	9.3GHz Band 1 11.65 GHz Band 2	FR4	CST	Length adjustment- determine antenna performance Bandwidth enhancement Gain =6.95dBi (Band 1 and 2) RL -21.47dB(band 1) -20.24dB(Band 2) Directivity 8.11dBi (Band 1 and 2) VSWR 1.18(Band 1) VSWR 1.21(Band 2)	Complexity design – triple U-slot	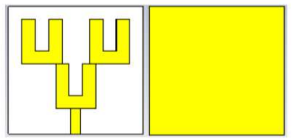 (a) (b) Figure 1: Antenna View (a) Top (b) Bottom

Table 2.3 continued

(Edara et al., 2023)	Horizontal slot and U-slot Inset feeding method	2.6348 GHz	Dielectric constant 4.08, type of material not mentioned	Not mention	Slot: create a specific current path and impact impedance matching of the antenna Gain =7.11dBi RL=-27.47dB (high impedance matching and minimal signal reflection) Directivity – based on radiation pattern – reduces cross polarization – better directivity and symmetrical radiation pattern – due to the position of the U-slot in the symmetric	The antenna efficiency is not stated. No value stated for direction, only based on main lobe only	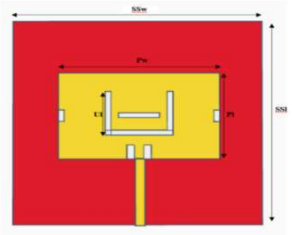

Table 2.3 continued

(Dargar et al., 2022)	U-slot Coaxial feed	2.5GHz 5.27GHz	RT5880	CST	Gain :8.017dBi(2GHz to 4GHz) Return loss = -19.5dB(2.5GHz), -30dB(5.27GHz) Finding: Slot length (horizontal and vertical), slot width and feed location influence the RL value	Directivity and antenna efficiency are not mentioned	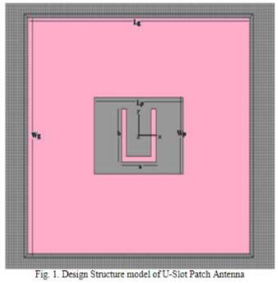 Fig. 1. Design Structure model of U-Slot Patch Antenna
(Naik et al., 2022)	E- patch, U-slot	6.5GHz	Not mention	CST and Altair FEKO	Gain =10.6dBi RL = -40dB Broadside radiation Radiation pattern maintains consistency	Complexity in design-used characteristic mode analysis (CMA)	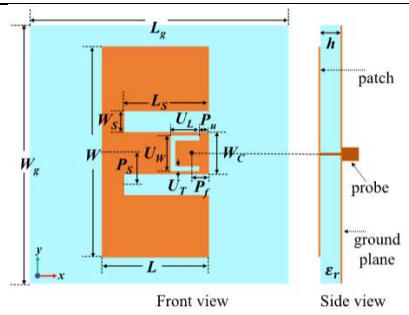 Front view Side view

Table 2.3 continued

						Directivity and antenna efficiency are not stated	
(Astuti et al., 2022)	inverted U- slot and combine two U-slot microstrip line fed	2.47G 3.3GHz	RT5880	HFSS	RL 2.47GHz : -19dB 3.3GHz: -24dB Omnidirectional radiation pattern	Gain and directivity are not provided in detail	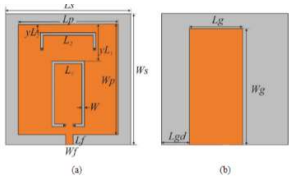 Fig. 1 Schematic figure antenna: (a) top view, (b) bottom view.
(Hasan et al., 2012)	U-slot with a different dielectric constant and a	3.65 GHz(f1) 5.25GHz (f2)	Dielectric constant =2.2	CST	Antenna A and B have the same dielectric constant,2.2. The slot width Antenna A=1.25 and Antenna B=2mm 7.55dBi(f1), 7.49dBi(f2)	Antenna design with two frequencies	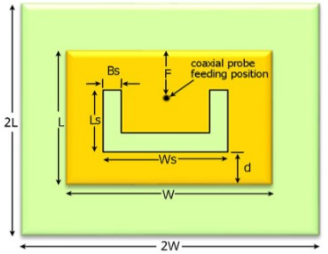 U-slot patch antenna with dimensional variables

Table 2.3 continued

	different slot width Coaxial probe feed				Antenna C has a dielectric constant of 4.3 and slot width = 1.2mm Antenna A RL= -20.34dB (freq 1), -23.37dB (freq 2) Gain .62dB(f1),6.34dB(f2) Directivity 7.55dBi(f1), 7.49dBi(f2) Antenna A RL= -20.34dB(f1) -23.37dB(f2) Gain .62dB(f1),6.34dB(f2) Directivity Antena A and B exhibit better Rl, gain, and directivity compared to Antena C.		

Table 2.3 continued

					It shows that the dimensions of the slot and the slot substrate influence RL, gain and directivity. The substrate with a low dielectric constant shows better RL, gain, and directivity.		

Table 2.4: U-slot in medical

References	Structure	Freq	Substrate	Simulation tool	Finding	Limitation	Diagram
Borkar & Parlewar, 2024	Antipodal Vivaldi (APV) antenna with U - slot	Range 1GHz to 40GHz	FR4	HFSS	Use Adaptive Gannet Optimization Algorithm (AGOA) in parameter Optimization. Directivity noU- slot = 6.3dBi Directivity (with U-slot) = 9dBi Gain no slot = 10dB Gain (with U-slot) = 13.7dB This study also compares the performance of the triangle slot and the U-slot in APV	Complexity in design	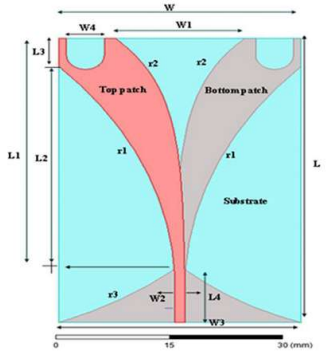

Table 2.4 continued

					RL -17.495dB (APV + triangle slot),-14.818dB (APV) -50.73dB(APV+U-slot) -30.62dB(APV) Gain 6.041dB(APV+triangle slot) 7.477dB(APV) 7.36(APV+U-slot) 8.62dB(APV) Overall, incorporating the U-slot leads to enhanced gain and high directivity.		

Table 2.5 shows the summarized gain, directivity and return loss of the U-slot microstrip antenna. The summarization is based on the matrix table in Tables 2.3 and 2.4.

Table 2.5: Summary Characteristics of the U-slot Microstrip

References	Directivity	Gain	Return Loss
Deshmukh et al., 2024)	NA	8.5dBi	NA
Thakur et al., 2024	8.11dBi	6.95dBi	-21.47dB(band1) -20.24dB(band 2)
Edara et al., 2023	NA	7.11dBi	-27.47dB
Dargar et al., 2022	NA	8.017dBi	-19.5dB(2.5GHz) -30dB(5.27GHz)
Naik et al., 2022	NA	10.6dBi	RL=-40dB
Astuti et al., 2022	NA	NA	-19dB(2.47GHz) 24dB(3.3GHz)
Hasan et al., 2012	7.55dBi(3.65GHz) 7.49dBi(5.25GHz)	6.62dB(3.65GHz) 6.34dB(5.25GHz)	-20.34dB(3.65GHz) -23.37dB(5.25GHz)

2.17 E-slot Microstrip Antenna Characteristics

Slots integrated with microstrip patches allow localized energy delivery and design flexibility(Hu et al., 2024). However, hyperthermia applications have been explored less, especially those involved in E-slot microstrip antennas. An E-slot antenna is widely used in other fields, particularly communications (Ali et al., 2023; Raja et al., 2023; Umamaheswari et al., 2023).

The E-slot and E-shape microstrip aim to improve wireless communication's bandwidth, gain, return loss and directivity. The E-slot is cut inside the patch to improve the antenna's performance (Pragati et al., 2023), whereas the E-shaped antenna is created on the patch antenna (Haque et al., 2021).

E-slot antenna generally exhibits higher gain compared to E-shape antennas. For instance, an E-slot microstrip patch antenna designed for WLAN application achieved a gain of 4.92dBi at 6 GHz. In contrast, a modified E-shaped antenna demonstrates a gain of 3.16 dB in wireless communication (Goyal et al., 2023).

The design and simulation of the E-slot microstrip patch antenna show good performance with a minimum return loss (Ali et al., 2023; Khangarot, 2015; Umamaheswari et al., 2023) and increased directivity(Rani & Malhotra, 2018). The E-slot antenna also exhibits a satisfactory radiation pattern and gain (Nitin et al., 2018).This is due to the E-slot's ability to control the radiation pattern and reduce unwanted hotspots (Charan et al., 2021; Garg & Saini, 2020).

Table 2.6 and Table 2.7 show the matrix of the E-slot microstrip antenna for communications and medical applications, respectively.

Table 2.6: Matrix table for E-slot Microstrip Antenna

Reference	Structure	Freq	Substrate	Simulation tool	Finding	Limitation	Diagram
Iqbal & Zulkifli, 2023	E-slot and two U-slots: Ground-DGS	5.860GHz-6.579GHz	FR4	Not mention	Gain with no slot=4.34dBi Gain with slot=4.92dBi (with slot) Return loss (no slot)=-22.14dB Return loss (slot) -14.60dB Improvement in gain suggests improvement in antenna ability to focus energy Bandwidth enhancement No slot: 277MHz With slot:710MHz WLAN application	Complexity in design Directivity is not mentioned	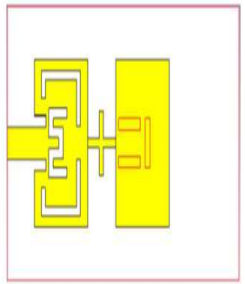

Table 2.6 continued

Umamaheswari et al., 2023	E-slot: Coaxial probe feed	5.9GHz	FR4	Cadfeko	Impact of E-slot: affects the radiation pattern and improves Return loss The radiation pattern is uniform in a specific direction (directivity is good) Gain varies between 8.8 and 9.5dBi By adjusting the length and width of the E-slot antenna, RL decreases Optimal RL= -40dB E-slot – suitable for WLAN – low volume, low weight and ease of fabrication	Antenna less efficient performs on thick and high permittivity surface, causing surface waves (noise)	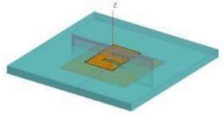

Table 2.6 continued

Pragati et al., 2023	E -slot Inset feed technique	2.70GHz	FR4	ANSOFT HFSS	E-slot enhances antenna performance. It alters the current distribution on the patch and leads to improved radiation characteristics, gain, RL. At frequency 2.70GHz, RL= -24.4701dB indicates good impedance matching and efficient power transfer. VSWR =1.0396 Application in GPS, WiMAX, Wi-Fi, mobile satellite and space communication	The simulation covers return loss, radiation characteristics, and VSWR. It did not cover , specific measurement of gain and directivity.	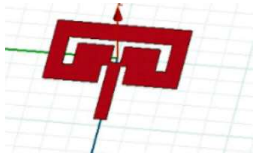 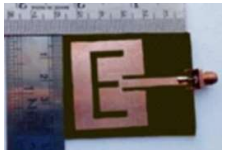

Table 2.6 continued

Raja et al., 2023	E-slot Feed line compared with coaxial feed line	2.5GHz	RT5880	Ansoft HFSS	The E-slot design microstrip patch antenna achieved a return loss of -13.18dB(effective impedance matching and minimal signal reflection) VSWR=1.5615 Gain =7.05dB Coaxial and feed line: provide more directivity. High directivity in the main lobe. WiMAX application	The simulation only covers gain, VSWR, and Return loss, but the directivity antenna only mentions the lobe without providing a specific value.	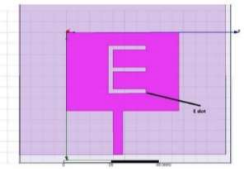 E-Slot Patch of(a) MicroStrip Feed Line

Table 2.6 continued

Latha et al., 2022	E-slot Coaxial probe feed	15GHz and 18GHz	RT5880	HFSS	E-slot- achieve broad bandwidth, Good return loss The radiation pattern exhibits stable and directional (low cross-polarization and broadside) Gain =5.9dBi(15GHz) and 5.3dBi(18GHz) RL=-17dB(15.5GHz) -16dB(17.5GHz) Satellite communication	The study covers gain, radiation pattern, and return loss. But antenna directivity not included	

Table 2.6 continued

Haque et al., 2021	E -slot on the patch Microstrip feed line	13.9GHz 18.8GHz	RT5880	CST and HFSS	HFSS and CST provide similar results Good return loss 15.423GHz:-34.09dBi 17.246GHz:--32.11dBi Gain range:6.1 to 8.6dB - high gain Directivity: range 6.8dBi – 9.6dBi Radiation efficiency:82% to 94% VSWR; 1.045 and 1.065 Satellite communication	Design complexity – there is another slot in the middle of E- shape	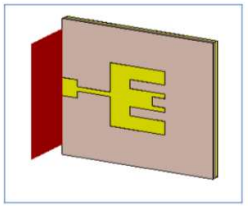

Table 2.6 continued

A. Gupta et al.,2020	Modified E-slot	Multiple frequencies in GHz 1.165 3.665 4.605 5.095 6.01 6.385 8.045 8.816	FR4	HFSS	Subtract thickness affects the frequency and return loss As the subtract thickness increases, the number of frequencies is reduced In return loss , substrate with 0.8mm(the thinnest) achieved maximum return loss (RL= -30dB)	The study covers substrate thickness and frequency only. Details and value of directivity, gain is not stated	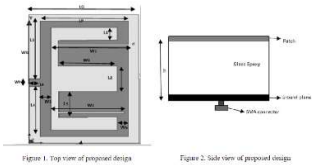

Table 2.6 continued

Haque et al., 2019	H-slot and double E-slot Microstrip inset line feeding	60GHz	RT5880	CST	E-slot compared to U-slot(previous study. E-slot shows better in RL. U-slot shows better in gain RL=-47.06dB(E-slot) RL=-37dB(U-slot) Gain= 6.64dB(E-slot) Gain = 8.2dB (U-slot) Directivity = 7.76dBi(E-slot) No record (U-slot)	The antenna design is complex due to the inclusion of E and U-slots.	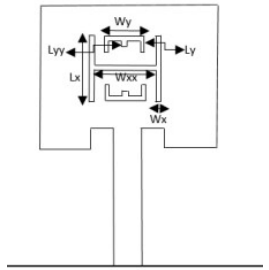

Table 2.6 continued

Agrawal et al., 2018	E-slot with 2 truncated corners upper and lower Inset feeding	4.7GHz 5.7GHz 8.4GHz	FR4	HFSS	This antenna focuses on the ability of the antenna to operate under multiple frequencies. Provide a radiation pattern for gain, directivity in the 3D model. Unidirectional radiation at 4.7GHz and 5.7GHz Broadside radiation at 8.4GHz RL -12.5891dB (4.7GHz) -19.2392dB (5.7GHz) -22.184dB (8.4GHz)	The features like truncated corner increase the complexity of antenna design No gain and no directivity are given.	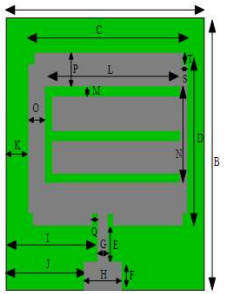

Table 2.6 continued

Rani & Malhotra, 2018	E,L, and U- slot Inset feeding	2.5GHz	FR4	CST	Multiband Return loss improved compared to the slot Gain(non-slot) 2.4GHz= 3.79dB Gain(slot) 2.4GHz=3.31dB RL(non-slot)=-11.75dB RL(slot)=-23.83dB Directivity (non-slot)=6.53dBi Directivity(slot)= 6.47dBi	The antenna design is complex due to the inclusion of E, L and U-slots.	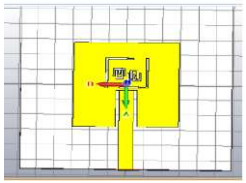

Table 2.6 continued

Khangarot, 2015	E-slot-patch Microstrip line feed	5.39GHz 5.49GJz	GIL GML 1032	HFSS	5.39GHz,5.49GHz (simulated) 5.38GHz and 5.5GHz (fabricated) RL -23.574dB(5.44GHz): simulation -24.007dB(5.43GHz) fabrication The max gain =6.49dBi VSWR =1.419(5.44GHz) After fabrication VSWR=1.1346(5.43GHz) Current distribution, E field observed around the central arm of the E-slot.	The study covers Return loss, Bandwidth, gain and VSWR. No directivity value.	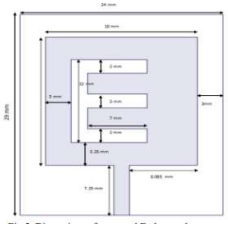 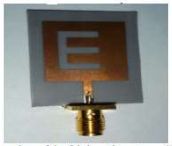 Front view of the fabricated prototype E-slot patch Antenna 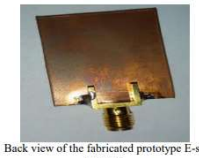 Back view of the fabricated prototype E-slot patch antenna

Table 2.7: E-slot in medical application

References	Structure	Freq	Substrate	Simulation tool	Finding	Limitation	Diagram
Chishti et al., 2023	E-slot with Generic algorithm-probe feed method	400MHz 630MHz 930MHz	FR4	CST	Use Genetic Algorithm (GA) and Particle Swarm Optimization (PSO) as effective methods for optimizing antenna parameters. Gain Original =3dBi PSO=1.94dBi GA= 3.04dBi Directivity Original=7.7dBi PSO=2.51dBi GA=3.8dBi	This paper mention about SAR values but do not specify type of tissue The return loss of antenna after optimization with PSO and GA are lower compared to original design. Antenna efficiency	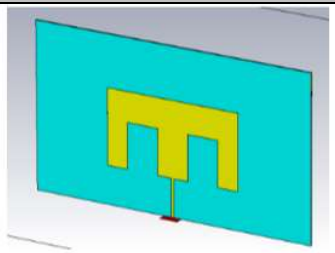

Table 2.7 continued

					Return Loss Original 400MHz= -8dB 650MHz= -16dB GA 357MHz= -36dB 630MHz= -23dB PSO 400MHz= -19dB 550MHz= -16dB GA has better performance in terms of gain and return loss compared to PSO. SAR in GA: 378MHz 2.64W/Kg(1g) 0.82W/Kg(10g)	not stated in detail	

Table 2.7 continued

					617MHz 4.74W/Kg(1g) 1.36W/Kg(10g)		
Ashyap et al., 2018	E-slot -fed by 50Ω microstrip line	2.4GHz	textile	CST microwave studio	Ant 1,RL=-12dB Ant2, RL=-18dB Ant3,RL=-20dB Ant4,RL=-15dB Ant5,RL=-13dB Based on this RL, it shows that the E-slot has the lowest RL, which means less reflected power is directed to the antenna. The maximum current density is concentrated at the E-slot patch. As the	The study focuses on miniaturized medical applications. However, it has not yet been tested with biological tissue. The antenna gain and directivity are not stated in detail.	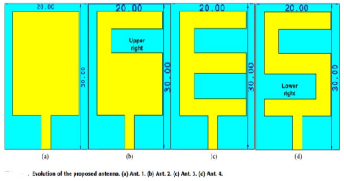 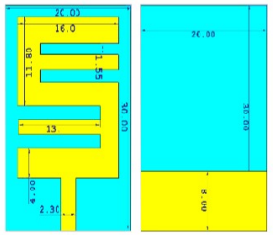 (a) Proposed antenna (Ant.5) (a) Front view (b) Back view

Table 2.7 continued

					number of slots increases, current density increases and improves the antenna radiation efficiency by Ant5,RL=-13dB Based on this RL, it shows that the E-slot has the lowest RL, which means less reflected power is directed to the antenna. The maximum current density is concentrated at the E-slot patch. As the	antennas for wearable medical applications. However, it has not yet been tested with biological tissue. The antenna gain and directivity are not stated in detail. antennas for wearable	

Table 2.7 continued

					number of slots increases, current density increases and improves the antenna radiation efficiency by concentrating EM energy on treated tissue.		
Sethi & Nijhawan, 2016	Rectangular E- shape slot	2.45GHz	FR4 εr=4.3	IE3D software	Rectangular E-shape slot The position of the feed point was tested at points 1(Pos1) and 2(Pos2). Pos 1 is better than Pos 2. Return loss	This study only covers allocating the microstrip line feed No directivity value	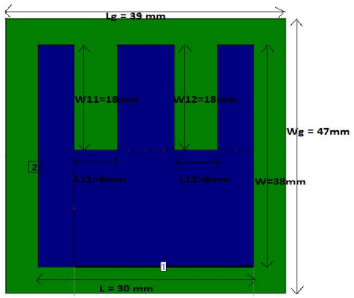

Table 2.7 continued

					Pos 1 = -19.3dB, Pos2= -4dBi and efficiency Pos 1=95% Pos2=92% Gain Pos 1= 6.3dBi Pos 2= 6.1dBi The findings highlight that the antenna is suitable for effective hyperthermia treatment.		

Table 2.8 shows the summarized gain, directivity and return loss of the E-slot microstrip. The summarization is based on the matrix table in Tables 2.6 and 2.7.

Table 2.8: Summary of the characteristics of the E-slot microstrip

References	Directivity	Gain	Return Loss
(Iqbal & Zulkifli, 2023)	NA	Without slot (non-slot) =4.34dBi With slot (slot) =4.92dBi	-14.60dB
(Umamaheswari et al., 2023)	NA	8.8-9.5dBi	-40dB
(Raja et al., 2023)	NA	7.05dB	-13.18dB
(Pragati et al., 2023)	NA	NA	-24.4701dB
(Haque et al., 2021)	6.8-8.6dBi	NA	-34.06dBi (15.4GHz) -32.11dBi (17.25GHz)
(Haque et al., 2019)	7.76dBi	NA	RL=-47.06dB
(Rani & Malhotra, 2018)	6.57dBi11	NA	-11.75dB(non-slot) -23.83dB(with slot)
(Agrawal et al., 2018)	NA	NA	-12.5891dB(4.7GHz) -19.2392dB(5.7GHz) -22.184dB(8.4GHz)
(Shailander Singh Khangarot, 2015)	NA	6.49dBi	NA

In summary, Table 2.3 and Table 2.4 show that the U-slot is widely used in communication and medical applications. Similar to Tables 2.6 and 2.7, the E-slot is also widely used in communication and medical applications. The characteristics of these two slot structures are suitable for hyperthermia applications, such as good performance in terms of directivity, gain and return loss. However, their use in hyperthermia treatment is still limited. Therefore, both slot structures were investigated in this research. The best-performing slot design was selected for further optimization.

2.18 Optimization Techniques used to Improve SAR Distribution

The applicator optimization for hyperthermia involves enhancing design parameters to improve SAR, minimize damage to healthy tissue and achieve effective heating on target tissue (Acar et al., 2024; Rajebi et al., 2024). Optimizing the dimensions of the slot led to improvement of return loss, directivity and gain, ultimately enhancing overall performance (Ahmed & Islam, 2013; Kishore et al., 2014; Sivakumar et al., 2019) .

Several studies have applied optimization techniques such as Particle Swarm Optimization (PSO) (Chishti et al., 2023; Rajebi et al., 2024; Yildiz et al., 2023) and Genetic Optimization (GA) (Aldhaeebi et al., 2014;G et al. 2025) in hyperthermia. However, these two methods focus solely on applicator optimization and do not provide a mathematical model to explain the relationship between the dependent and independent variables.

Response Surface Methodology (RSM) is a statistical, theoretical and mathematical technique for constructing a model representing the relationship between multiple independent and dependent variables. The mathematical equation is usually a second-order polynomial equation. RSM was originally applied in chemical and biochemical engineering (Bezerra et al., 2008; Ghadge & Raheman, 2006). In recent years, numerous studies have

employed RSM techniques for optimizing the design of applicators (Koziel & Bandler, 2015; Koziel & Bekasiewicz, 2015). The optimization applicator used numerical optimization based on this mathematical model (Ayalew & Asmare, 2022).

Although RSM is less commonly used in hyperthermia, it has been widely used in communication systems (Ayalew & Asmare, 2022; Chen et al., 2023; Nahas, 2022). It can predict and optimize applicators, making it suitable for hyperthermia applications.

2.19 Water Bolus Added for Effective and Skin Protection in Hyperthermia Treatment

In clinical practice (Bakker et al., 2020), the water bolus is utilized during the hyperthermia treatment. The purpose of adding a water bolus is to cool the skin (Korkmaz, Isik, & Nassor, 2013). Furthermore, the temperature increase in the breast phantom during hyperthermia treatment can be controlled. Therefore, skin burn problems and unwanted hotspots are reduced (Ebrahimi-Ganjeh & Attari, 2008; Hassan et al., 2025).

The presence of a water bolus also influences the SAR and PD in hyperthermia treatment (Ebrahimi-Ganjeh & Attari, 2008). Normally, in hyperthermia, the water bolus is filled with distilled water (Ebrahimi-Ganjeh & Attari, 2008). The reason is to improve the heat conduction into the tissue (Shehata et al., 2021).

The effectiveness of the water bolus in hyperthermia is affected by water bolus content, geometric dimensions and shape. For instance, the variation in water bolus thickness from 5mm to 40mm affects heat distribution and hot spots during treatment. A thicker water bolus helps to conform the chest wall, but a thickness of less than 10mm ensures better treatment effectiveness (Rodrigues et al., 2015).

Another study reported that the water bolus thickness (less than 10mm) is essential to prevent standing waves. According to (de Bruijne et al., 2006; Rajebi et al., 2024) there is a significant decrease in thermal energy transfer into tissue with an increment of water bolus thickness.

The water bolus has various shapes, such as square, rectangular, cylindrical and breast shapes. The rectangular shape and the square are placed in front of the breast model (Birkelund et al., 2009; Ebrahimi-Ganjeh & Attari, 2008). In contrast to cylindrical shape water bolus with a thickness of 1mm and a breast-shaped shape water bolus with a thickness of 2mm, covering the surrounding breast model. It helps to distribute heat more uniformly throughout the breast tissue during hyperthermia treatment and heat is efficiently absorbed in the target cancer region.

Therefore, a water bolus can enhance the effectiveness of the treatment by ensuring heat transfer to the tumor effectively while protecting surrounding healthy tissues and acting as a cooling element to the tissue (Shehata et al., 2021; Wong et al., 2023). The water bolus

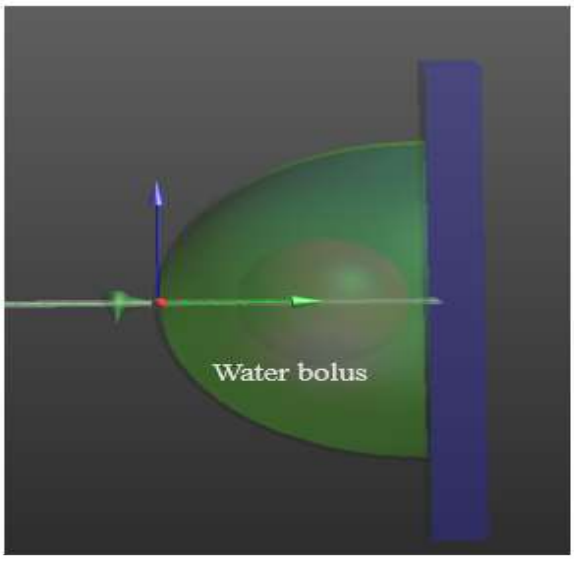

Figure 2.1: Water bolus (green color) in breast shape

is placed between the microstrip applicator and breast phantom, as illustrated in Figure 2.1.

2.20 Breast Cancer Treatment Time in Hyperthermia

The proper time duration to ensure the entire tumor is completely heated, maintain safety and without damage to the surrounding healthy tissue. According to (Stauffer & Paulides, 2014),(Yildiz et al., 2023) the duration time of hyperthermia treatment for temperatures 41ºC to 45ºC is about 30 min to 60 min to avoid damage to healthy tissue and skin burn.

However, the duration of the treatment time for delivering sufficient heat to the tumor depends on the type of applicator used (Firuzalizadeh et al., 2025; Selmi et al., 2022) and tumor size(Wong et al., 2021). The amount of heat absorbed by tumor tissue is associated with the SAR.

Equation 2.4 states that SAR can be used to determine the hyperthermia treatment period. Based on this equation, the relationship between SAR and t is inversely proportional, meaning that the time duration can be shortened by increasing the SAR (SAR optimization). It has been reported in (Cappiello et al., 2017; Nizam-Uddin & Elshafiey, 2017; Wang et al., 2011) SAR optimization aims to maximize heat in the tumor while minimizing hotspots in surrounding healthy tissue.

2.21 Electromagnetic Simulation Tools Used in Hyperthermia

Electromagnetic (EM) simulation tools are essential in the development of breast phantoms and applicators. The EM simulation tool enables the visualization and analysis of SAR within a breast phantom, particularly in a tumor.

In this research, SEMCAD X 14.8.4 is employed to perform full-wave 3D

simulations using the Finite Difference Time Domain (FDTD) method. SEMCAD X is widely recognized for its accuracy and has been validated according to the IEEE/IEC 62704-1 standard (Tu, 2010).

SEMCAD X uses boundary conditions to control EM waves. The Absorbing Boundary Condition (ABC) boundary is used to minimize the reflection of EM waves back into the model. The most effective ABC in SEMCAD X is the Perfectly Matched (PML) layer, where PML absorbs reflected EM waves (Aronsson & Askeroth, 2002).

2.22 Summary of the Chapter

This chapter presents a comprehensive literature review on breast cancer hyperthermia treatment with a non-invasive applicator. The literature review covers two main elements: heat absorption in tissue and the type of applicator. The EM interaction with tissue is mainly determined by the dielectric properties and the operating frequency of the applicator. SAR is a measure of heat absorption in target tissue.

This chapter also examines the appropriate applicator design for these research objectives. The applicator input power and the distance of the applicator influence SAR. The microstrip applicator integrates with a slot (particularly the E-slot and U-slot), which is preferred because it enhances the applicator's performance, including directivity, gain and return loss. These parameters ensure effective heat transfer and tumor absorption while avoiding damage to healthy tissue.

A water bolus is added to hyperthermia treatment to prevent skin burns and make the patient more comfortable. The optimal treatment time is important to ensure the tumor is fully heated. Finally, the EM simulation tool SEMCAD X was used to develop a model of a breast phantom and applicator and to analyze SAR during hyperthermia treatment.

CHAPTER 3

RESEARCH METHODOLOGY

3.1 Introduction

The research methodology is structured using the Design of Experiments (DoE) approach to ensure that each research objective is addressed systematically. This research is divided into four (4) DoEs, each DoE corresponds to a specific research objective. The overall research activity is presented to illustrate the general research workflow, while the detailed implementation under each DoE is explained in Section 3.2.

3.2 Research Activities

Figure 3.1 and 3.2 provide the flowchart of research activities, beginning with the development of a breast phantom embedded with tumor sizes, T1, T2 and T3 at the initial stage. Then followed DoE1, in which the applicator development was conducted at ISM and an appropriate frequency was selected based on the SAR distribution. SAR distribution was evaluated using SD and ID for T1, T2 and T3. Next, input power for the applicator and SAR average mass were selected based on the SAR distribution and the SAR (peak).

Subsequently is DOE 2. The slot integration of U-slot and E-slot to the microstrip applicator. The slot with superior performance in terms of directivity, gain, return loss, SAR (peak) and SAR distribution was selected for further analysis. The process continued with determining the optimal distance between the breast phantom and the applicator based on the SAR distribution that heats the tumor rather than the surrounding healthy tissue.

In the next phase is DoE 3. The slot modification is a parametric process that involves observing the slot segment (horizontal and vertical length and thickness) to influence the

desired SD and ID. Only the significant slot segments were considered in the RSM slot optimization.

The RSM was used to develop a polynomial model and to optimize the slot. The polynomial model was validated using ANOVA. Numerical optimization is performed to obtain the slot dimensions to improve tumor-focused heating. The optimized slot was validated through simulation in SEMCAD X by comparing the predicted and simulated SD and ID. The percentage error is then obtained. The optimized slot applicator further validates with previous studies, such as PSO and GA.

The final stage is DoE 4. The water bolus was added between the breast phantom and the applicator before the hyperthermia time treatment was determined. SAR optimization was performed by adjusting SAR until the entire tumor was heated, ensuring adequate heating in the tumor region. Subsequently, the treatment time is determined based on SAR = CdT/dt. The DoE4 completed the overall research activities.

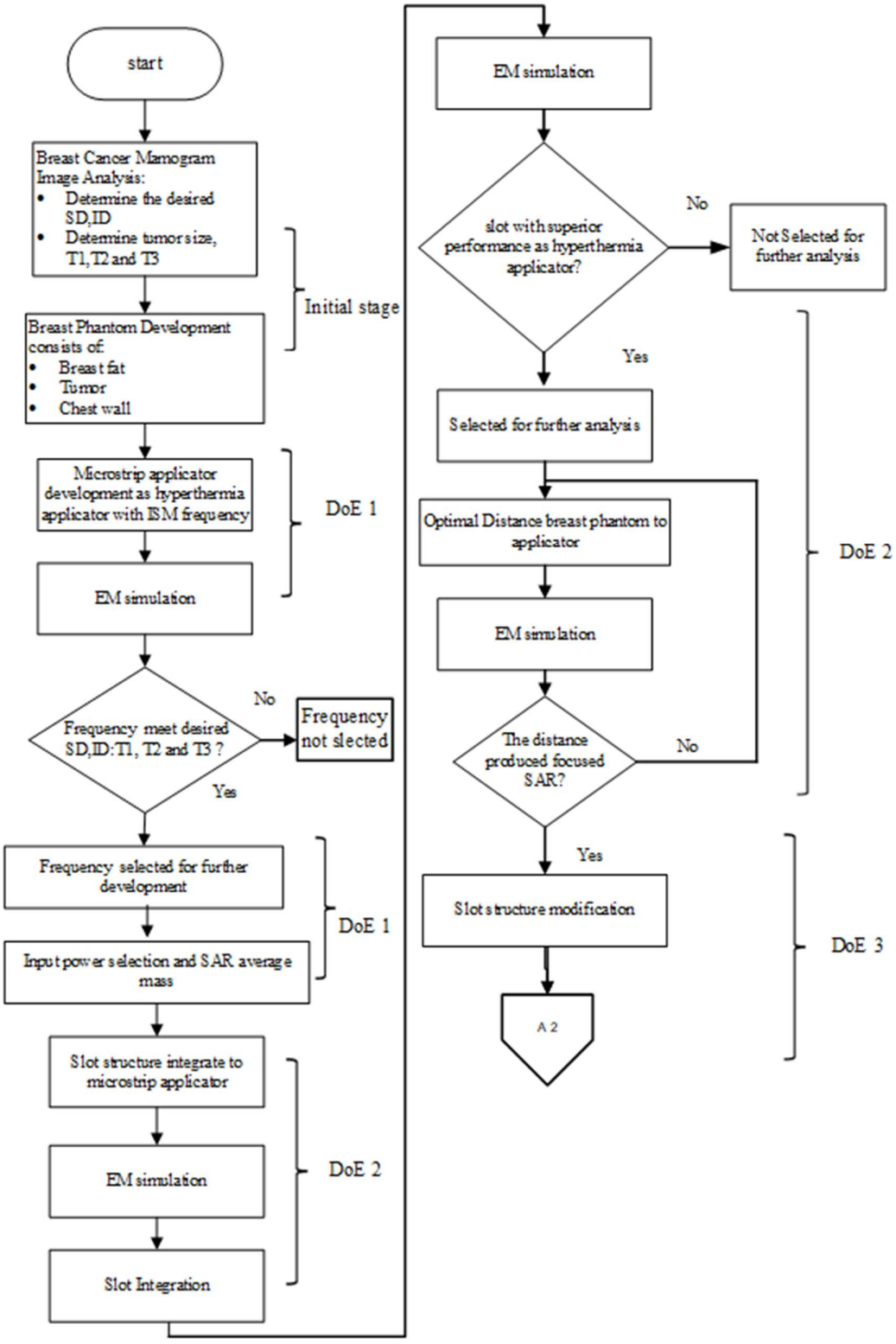

Figure 3.1: Research activities

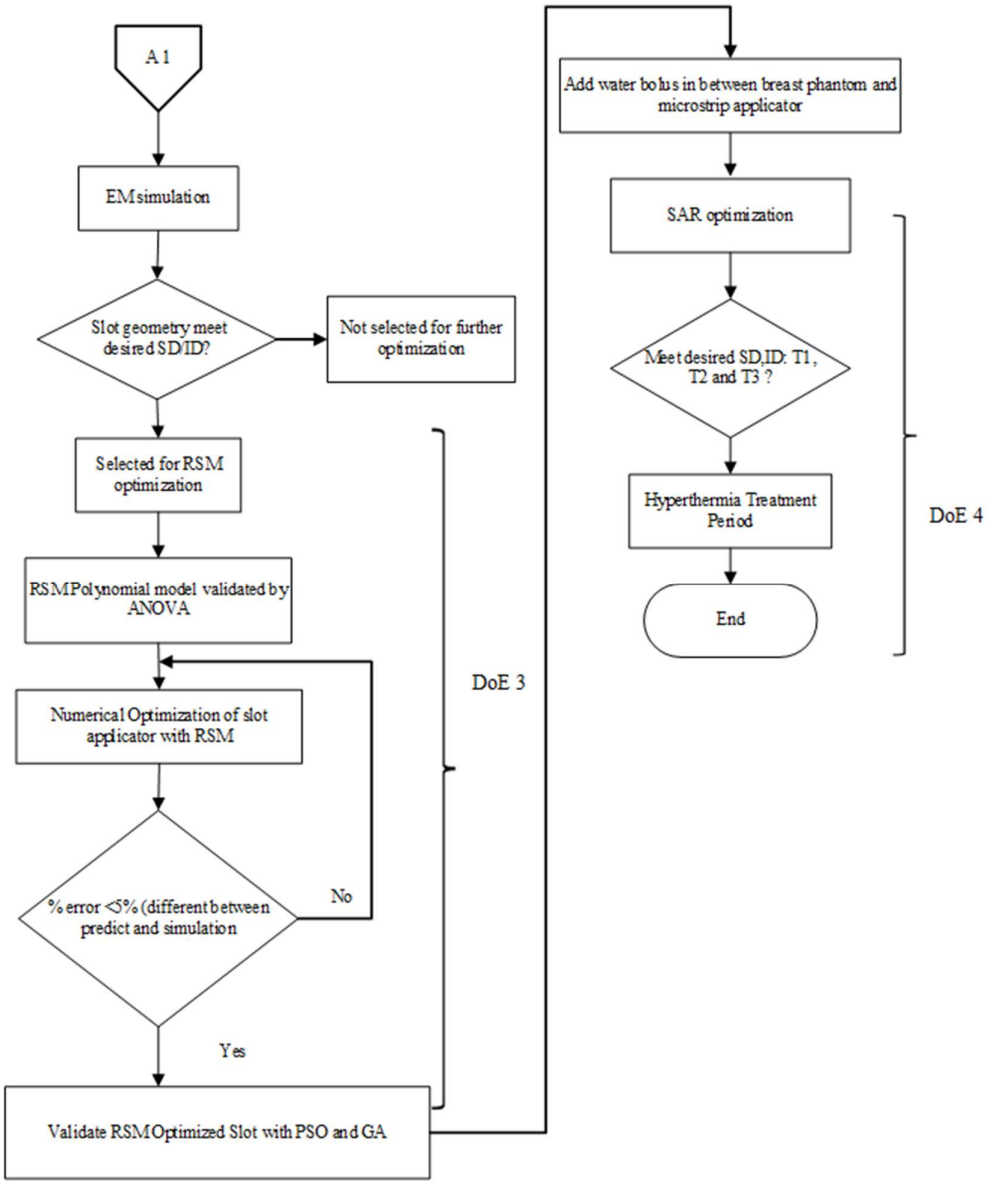

Figure 3.2: Research activities (continued)

Table 3.1 provides the structure mapping between the research methodology and the corresponding research objectives, including the assessment criteria for each Design of Experiment (DoE).

Table 3.1: Research Methodology with objectives, assement and output

Research Methodology	Objectives	Assessment	Output
DoE 1a	Research objective 1	Frequency selection based on ISM frequency:434MHz, 915MHz and 2450MHz. SAR distribution observed under different frequencies. The SAR distribution is accessed by measuring the SD and ID, both expressed in mm.	The SAR distribution covering the tumor region was selected for further development
DoE 1b	Research objective 1	The input power that affects SAR (peak). SAR value influences the treatment time duration, (t α 1/SAR). Therefore, the SAR (peak) is compared between Pin = 1 W and Pin = 10W. The SAR (peak) with the greater value is selected because it shortens treatment time.	The input power was selected based on SAR (peak)

Table 3.1 continued

DoE 1c	Research objective 1	Compare the SAR distribution on the SAR average mass tissue 1g and the SAR average mass tissue 10g. The SAR distribution shows the heat absorption in tissue. Therefore, the SAR of 1g or 10g, which shows more localized heating regions, will be selected. Localized SAR distribution based on the ability to achieve the desired SD and ID.	The SAR 1g or 10g was selected based on the localized SAR distribution
DoE 2a	Research objective 2	Integrate the U and E slots into the microstrip applicator. Comparison of slot applicator characteristics: directivity, gain, and return loss in the U-slot and E-slot applicator. Then the comparison is made in SAR distribution, SD, ID, SAR (peak) and unwanted hotspot formation.	The superior performance will be selected for further analysis.
DoE 2b	Research objective 2	The applicator-to-phantom distance was assessed by analyzing its effect on SAR distribution at the SD, ID and on SAR (peak).	The optimal distance was selected

Table 3.1 continued

DoE 3a	Research Objective 3	Modify slot segment: horizontal and vertical (length and thickness). The parametric study was conducted on the slot arm and evaluated its influence on SAR distribution. The analysis was performed to identify which slot segment significantly contributes to achieving the desired SD and ID.	The significant arm geometry was obtained.
DoE 3b	Research Objective 3	The polynomial model was developed with RSM and statistically validated with ANOVA. The optimization slot dimensions were validated through simulation in SEMCAD X. The percentage error (between predicted output and simulation value) is then used as an assessment criterion.	The RSM polynomial model was developed. Optimized slot dimensions for tumor sizes T1, T2, and T3 were developed. Validated the predicted output with the output from the SEMCAD X simulation, with percentage error.

Table 3.1 continued

DoE 3c	Research Objective 3	Validated RSM slot applicator with PSO and GA based on directivity, gain and return loss.	The validation is based on a comparison of RSM applicator optimization performance with PSO and GA.
DoE 3d	Research Objective 3	The analysis was performed between the optimized slot and the slot compared in terms of directivity, gain, return loss, and SAR (peak).	The output analysis is displayed in a graph. The improvement of optimized slot is presented in percentage.
DoE 4	Research Objective 4	SAR optimization, SAR is adjusted until the heat covers the entire tumor without affecting the surrounding healthy tissue. The treatment time can be determined based on SAR= c dT/dt	The hyperthermia treatment time was determined in T1, T2 and T3.

3.2.1 Tumor Size Analysis- Initial Stage

The research activity begins with an analysis of breast cancer mammograms. Female breast cancer mammogram images were gathered from the hospital in Kuching, Sarawak. Before collecting the data from the hospital, ethical approval was obtained from the National Medical Research Register (NMRR) of the Ministry of Health Malaysia. The ethical approval letter is shown in Appendix A. This is a standard procedure to ensure the patient data is not manipulated or misused. The data is limited to specific geometrical characteristics such as shape, size and tumor position

There are 149 breast cancer mammogram images gathered and used for further investigation. Then, the ground truth with the expert radiologist is carried out to identify abnormal tissue due to cancer before the data analysis is performed. Cancers have different sizes, shapes and locations for each patient. The images consist of the left and right breasts that have been affected by cancer.

Digital Imaging and Communications in Medicine (DICOM) is an international standard imaging format established by the National Electrical Manufacturers Association (NEMA) to distribute and view medical images such as CT, Magnetic Resonance Imaging (MRI), mammograms and ultrasounds. In this research, DICOM was used to aid the analysis of mammographic images.

A mammogram image is the most effective method for screening for abnormalities that could indicate the presence of cancer or other breast diseases. This method has an accuracy rate of 85% in the recommended population (Basurto-hurtado et al., 2022). The mammogram breast images are provided on the left and right sides. Each of the left and right sides of mammogram breast images was divided into two (2) positioning views, medio-

lateral oblique (MLO) and cranio-caudal (CC) (Sasikala, S., Ezhilarasi, M., & Arun Kumar, 2020) as indicated in Figures 3.3 and 3.4.

Medio-Lateral Oblique (MLO)	Cranio-Caudal (CC)
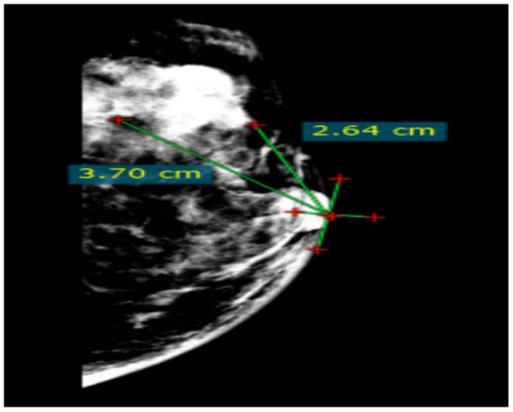	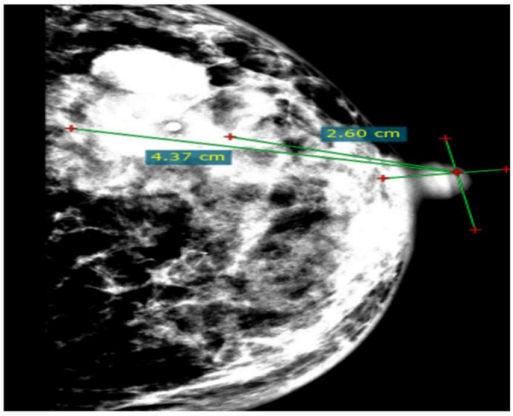
Surface depth:26.4mm Inner Depth : 37mm	Surface depth:26mm Inner Depth : 43.7mm

Figure 3.3: View of MLO and CC

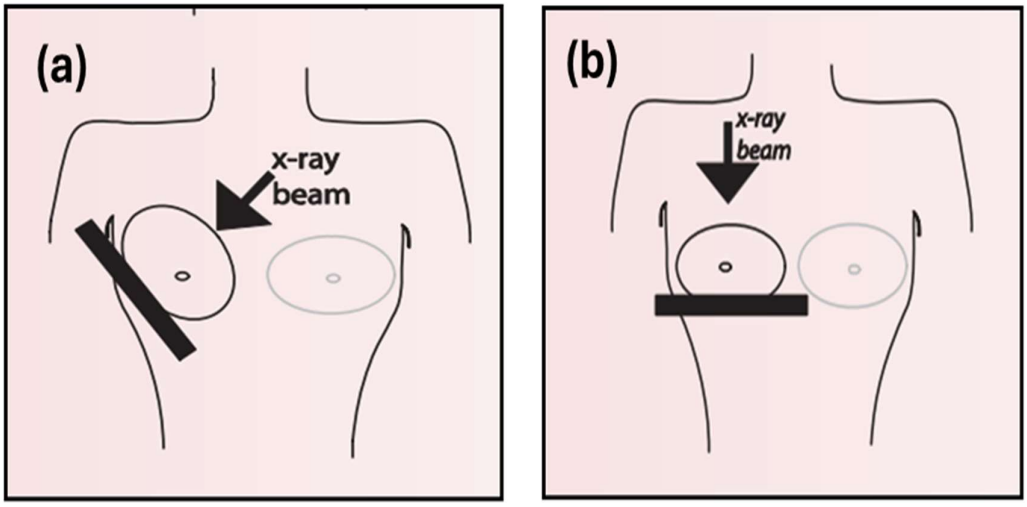

Figure 3.4: (a) MLO and (b) CC angle (Miller, 2016)

Based on 149 breast cancer mammogram images (in Appendix B), the cancer size in a spherical shape is 65.1% and 34.9% in an oval shape. Therefore, a spherical shape is considered cancer tissue/tumor. The data extracted from the analysis were SD and ID. Mamilla is the reference point for measuring SD and ID. The SD denotes the distance from the front part (the mamilla) to the first point where heat reaches the tumor. On the other hand, ID refers to the distance from the mamilla to the farthest point within the tumor that heat reaches

Then, the tumor size is determined based on the diameter of the tumor. The description of T1, T2, T3 and T4 was provided by (Koh & Kim, 2019) and American Joint Committee for Cancer as follows: T1 was defined as tumor size with a diameter of less than or equal to 20 mm (T1 ≤ 20 mm), while 20mm ≤ T2≤ 50mm, and T3 > 50 mm (Giuliano et al., 2017). However, T4 is not included in this study because most tumors in this category spread into the chest wall or the skin. Therefore, immediate treatment, such as surgery, was necessary.

The desired SD and ID were determined using Equations 3.1-3.4. The analysis results are displayed in Figures 3.5 and 3.6, which show the average SD and the ID, respectively. The tumor size is calculated using Equation 3.5. The results are tabulated in Table 3.2. All the measurements are in mm.

$$\text{Average MLO / CC Surface depth, } \overline{SD} = \frac{\sum_{i=1}^{N} x_i}{N} \qquad \text{Equation 3.1}$$

$$\text{Average MLO /CC Inner depth, } \overline{ID} = \frac{\sum_{i=1}^{N} x_i}{N} \qquad \text{Equation 3.2}$$

Where N = number of a set of data

x_i= sum of x value ($\frac{x_{1+}\, x_2+\, x_3\, +x_4\, +\, \ldots\ldots\ldots\ldots\ldots\ldots x_N}{N}$)

i= 1,2,3,4……N

Hence, the SD and ID are determined based on:

$$\text{Surface depth, SD} = \frac{\overline{\text{SD}}\text{MLO}+\overline{\text{SD}}\, CC}{2} \qquad \text{Equation 3.3}$$

$$\text{Inner depth, ID} = \frac{\overline{ID}\text{MLO}+\overline{ID}\text{CC}}{2} \qquad \text{Equation 3.4}$$

$$\text{Diameter} = \text{ID} - \text{SD} \qquad \text{Equation 3.5}$$

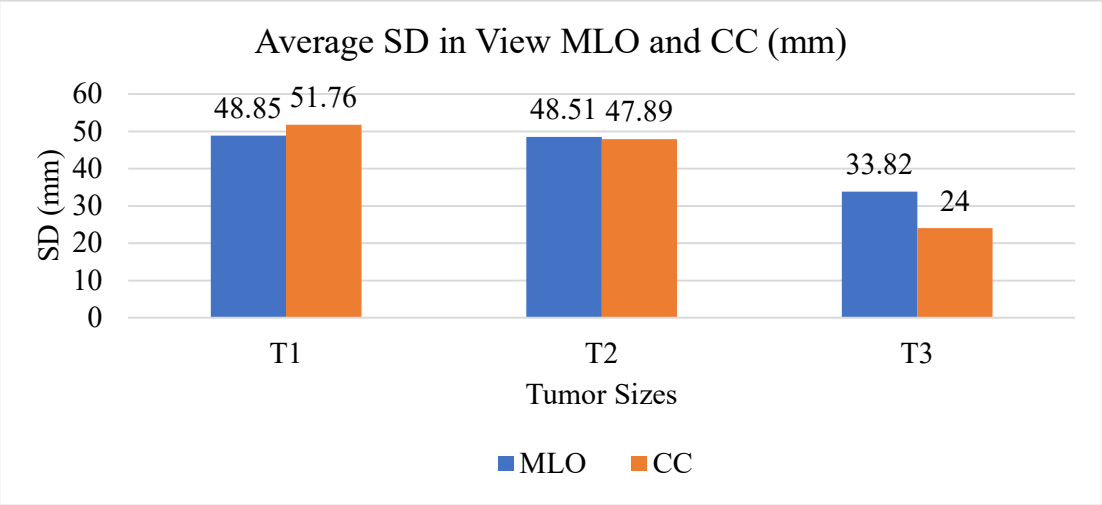

Figure 3.5: SD in MLO and CC (mm)

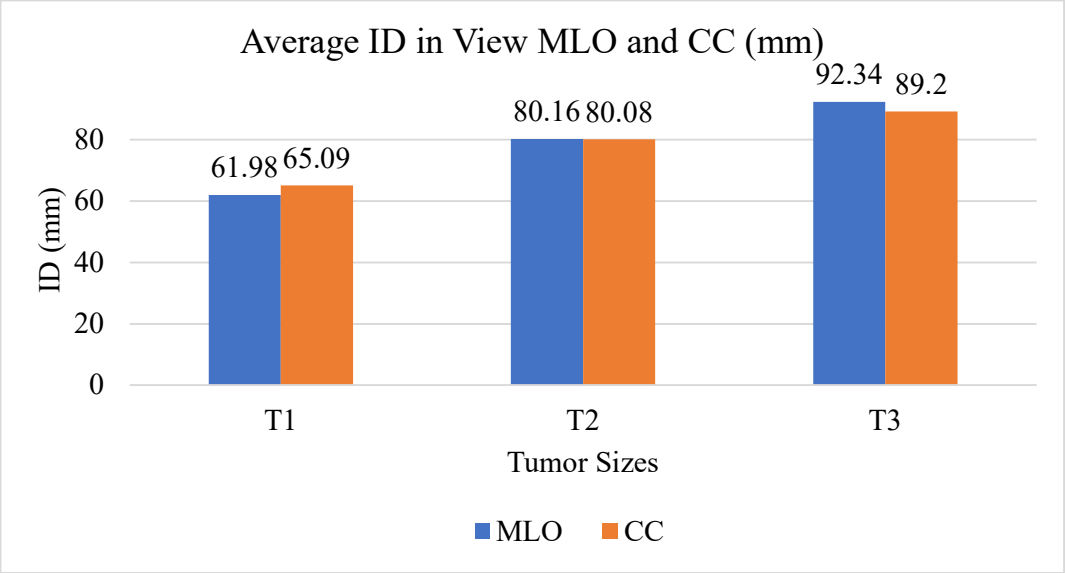

Figure 3.6: ID in MLO and CC (mm)

Table 3.2: Desired SD and ID in both MLO and CC

Tumor size	T1	T2	T3
SD (mm)	50	48	28
ID (mm)	64	80	90
Diameter(mm)	14	32	62

3.2.2 Breast Phantom Size – Initial Stage

Hemispherical breast phantom was considered in breast size. Band size and cup size were parameters used as reference anatomical measurements. The size chart representing under-burst and band size measurements, as presents in Table 3.3, that is adopted based on Triumph measurements. The under-burst measurements range from 680mm to 1020mm. In

this research, under the bust measurement range 730-770mm was selected, and the median value of 750mm was used as a representative dimension. Accordingly, the breast phantom was developed based on C75cm or C750mm.

Table 3.3: Size chart (mm)

Underbust(mm)	Median	Band size
680-720	700	32
730-770	750	34
780-820	800	36
830-870	850	38
880-920	900	40
930-970	950	42
980-1020	1000	44

Subsequently, the band size of 750mm represents the circumference of the chest and back. Hence, the band is divided into the back and front regions. For this reason, the front area = $\frac{\text{band size}}{2} = \frac{750}{2}$ =375mm. The front area consists of the left and right breasts. Therefore, for each breast $\frac{375}{2}$ =187.5mm. Then, the radius of breast fat is determined with $\frac{187.5}{2}$ =93.75mm, which is approximately 95mm. The next section explains the dimensions of the breast phantom and the process of developing it in SEMCAD X.

3.2.3 Tissue Electrical Properties – Initial Stage

SEMCAD X has built in the Gabriel database to fit the electric properties of tissue such as tumor, fat and chest wall. Fat tissue represents normal tissue in this research. The finding of electrical properties on breast fat, tumor and chest wall is illustrated in Table 3.4. The findings showed that both permittivity and conductivity in the tumor are higher than in breast fat due to the high-water content compared to normal tissue.

Table 3.4: Electrical properties of breast fat, tumor and chest wall

Tissue-T1/T2/T3	Frequency (MHz)					
	434		915		2450	
	Relative Permittivity,ε_r	Electrical Conductivity, σ(S/m)	Relative Permittivity,ε_r	Electrical Conductivity, σ(S/m)	Relative Permittivity,ε_r	Electrical Conductivity, σ(S/m)
Breast fat	3.987	0.570	3.413	0.651	3.126	0.892
Tumor	55.224	1.20	43.273	4.738	16.082	33.741
Chest wall	51.887	5.942	28.79	12.883	13.708	35.728

In hyperthermia, both electrical and thermal properties must be considered. Thermal properties of tissue, including density, specific heat capacity and thermal conductivity, are required. Each of these thermal properties plays a significant role in how heat is absorbed, maintained and dissipated within the tissue (Bianchi et al., 2022)(Camilleri et al., 2022). Table 3.5 presents the thermal properties of fat, tumor and chest wall, generated using SEMCAD X.

Table 3.5: Thermal properties of the breast phantom

Tissue	Density, $\rho(kg/m^3)$	Specific Heat Capacity, C(J/Kg/K)	Thermal Conductivity, K(W/m/K)
Breast Fat	950	2493	0.24
T1	1050	3600	0.5
T2	1050	3600	0.5
T3	1050	3600	0.5
Chest wall	1050	3600	0.5

This research primarily focuses on EM simulation, specifically examining the propagation, absorption, reflection and scattering of EM waves in tissue, which is represented as a SAR distribution.

3.2.4 Breast Phantom/Tumor/Chest Wall-Initial Stage

The hemisphere breast phantom has a radius of 95mm with an outer hemisphere diameter of 150mm (Curto et al., 2018), was developed in SEMCAD X. The model incorporates vital tissue layers such as breast fat, tumor and chest wall, as illustrated in Figure 3.7. The tumor size and location are determined by mammogram breast cancer analysis.

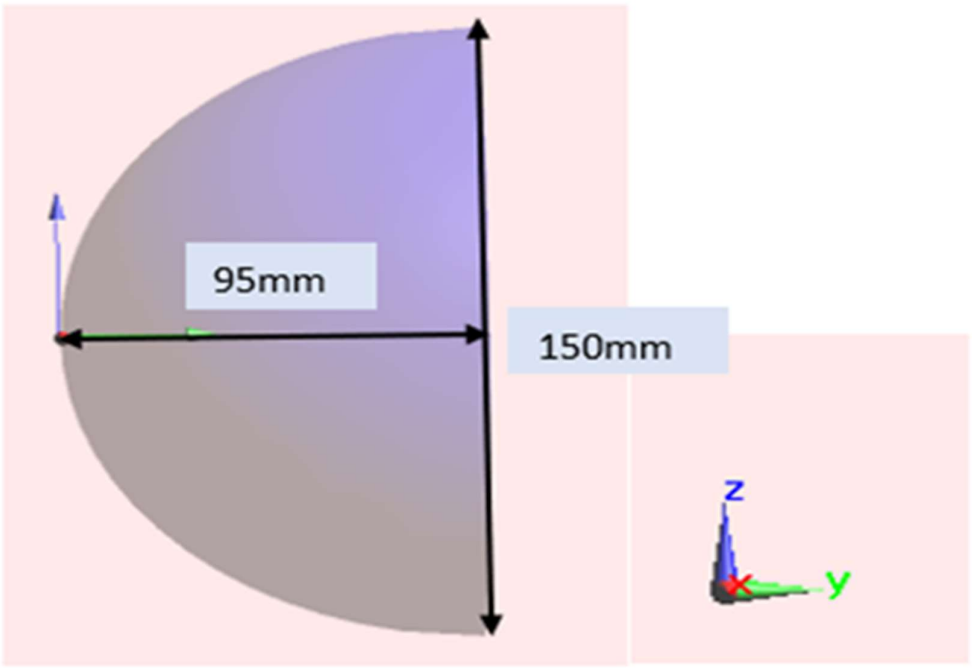

Figure 3.7: Breast phantom development

Breast fat is located within a bounding box defined by the minimum (P1) and maximum (P2) coordinates. The breast fat is situated at P_1 (X_1:-76.18mm, Y_1:0.46mm, Z_1:-76 mm) and coordinate P_2 is (X_2:76.18mm, Y_2:95mm, Z_3:76mm). The tumor is located in the heterogeneous breast phantom model at (T1) coordinates P1 (X1: 7 mm, Y1: 50 mm, Z1: 7 mm) and at P2 (X2: 7 mm, Y2: 64 mm, Z3: 7 mm). For T2, the location is at coordinates P1 (X1: 16 mm, Y1: 48 mm, Z1: 16 mm) and coordinate P2 is (X2: 16 mm, Y2: 80 mm, Z3: 16 mm). Meanwhile, the coordinates for tumor T3 are P1 (X1: 31 mm, Y1: 28 mm, Z1: 31 mm) and P2 (X2: 31 mm, Y2: 90 mm, Z3: 31 mm). The tumor location with coordinates is illustrated in Figure 3.8.

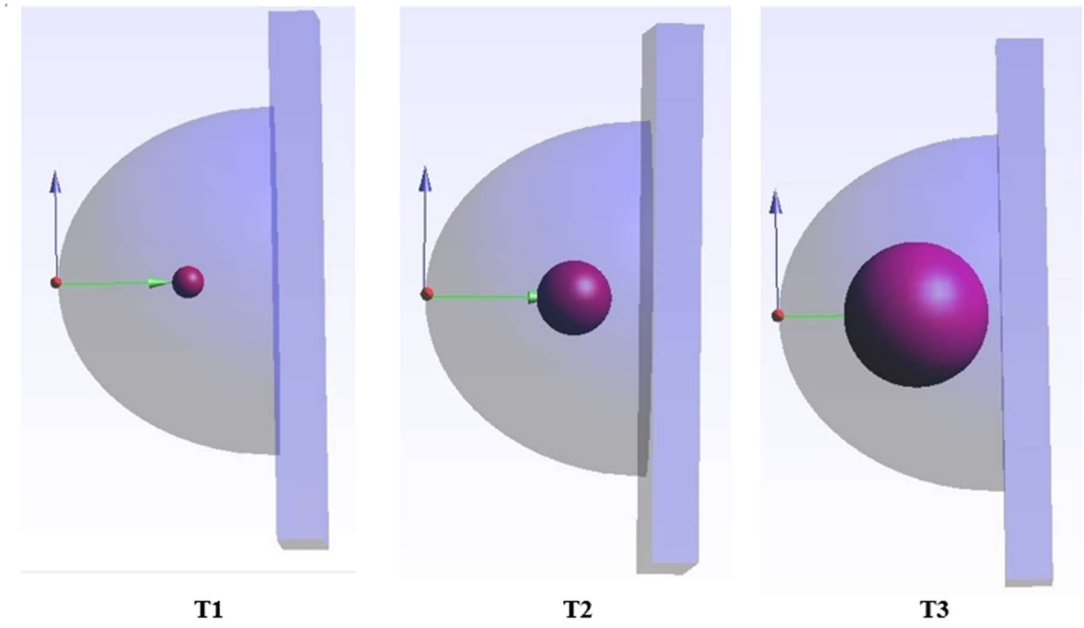

Figure 3.8: Position of T1, T2 and T3 in breast phantom

SD the distance from point a to b, with point a as the reference. ID is measured from points a to c. This measurement is based on mammogram analysis, as shown in Table 3.2, section 3.2.1. The desired SD and ID are shown in Figure 3.9.

T1	T2	T3
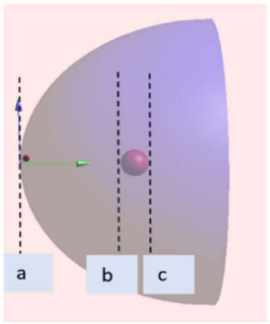	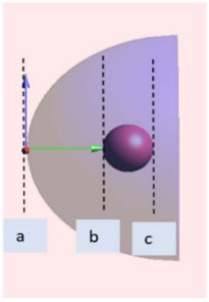	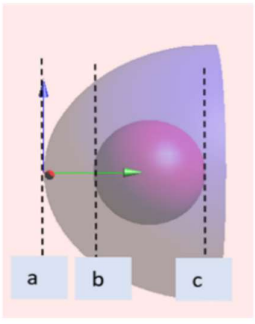
ab = 50mm ac= 64mm	ab = 48mm ac= 80mm	ab = 28mm ac= 90mm

Figure 3.9: Desired SD and ID in T1, T2 and T3

Finally, the chest wall is modelled in a rectangular shape with dimensions 230mm x 230mm. The development of the chest wall is illustrated in Figure 3.10. In this research, a 20-mm-thick chest wall was implemented based on (Curto et al., 2018). The coordinate location of the muscle at P_1 is (X_1:-115mm, Y_1:95mm, Z_1:-115 mm) and the coordinate P_2 is (X_2:115mm, Y_2:115mm, Z_3:115mm).

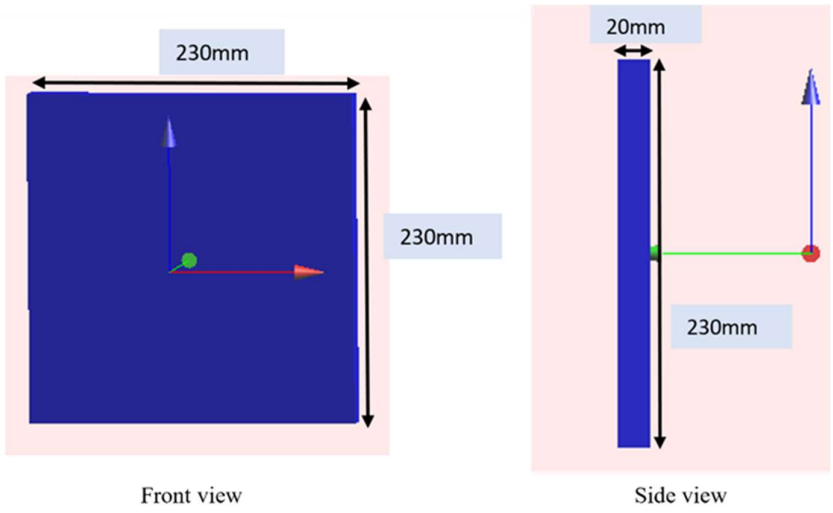

Figure 3.10: Chest wall development

3.2.5 DoE 1a: Rectangular Microstrip Applicator Development based on ISM Frequency

The rectangular microstrip applicator uses RT5880 as the substrate and operates at 10 W input power. The RT5880 substrate has improved several performance aspects, including enhanced return loss, increased gain and improved directivity (Rana et al., 2023).

Additionally, RT5880 has a low tangent and a low dielectric constant, which are essential properties for microstrip applicator. According to the datasheet (Avenue, 2022), the thicknesses of RT5880 and copper are 1.575 mm and 0.035 mm, respectively. It suggests

that the thinner substrate enhances applicator performance in terms of resonance frequency and return loss (Gupta et al., 2020).

The substrate has a dielectric constant, $\varepsilon_r = 2.2$ and loss tangent tanδ=0.0009 (Fang, 2011). The copper has $\varepsilon_r = 1$ and loss tangent near 0. The microstrip line is used as a feeding method and the feed line is $\frac{\lambda}{4}$. The transmission line is 50Ω.

The dimensions length and width used in the rectangular patch microstrip design are based on the governing equations (Balanis, 2016) that are represented in Equations 3.6 to 3.14.

1) The patch width (w) is determined:

$$w=\frac{c}{2fr}\sqrt{\frac{2}{\varepsilon_r+1}} \qquad \text{Equation 3.6}$$

Where f= operational frequency, ε_r= substrate permittivity and c is the speed of EM wave in vacuum = $3x10^8 ms^{-1}$

2) The effective dielectric constant (εreff) is calculated:

$$\varepsilon reff=\frac{\varepsilon_r+1}{2}+\frac{\varepsilon_r-1}{2}\left[\frac{1}{\sqrt{1+\frac{12h}{w}}}\right] \qquad \text{Equation 3.7}$$

Where h = substrate thickness.

3) The effective Length (*Leff*) is computed:

$$Leff=\frac{c}{2fr\sqrt{\varepsilon reff}} \qquad \text{Equation 3.8}$$

4) The patch extension (ΔL) is calculated:

$$\Delta L=0.412h\frac{(\varepsilon reff+0.3)(\frac{w}{h}+0.264)}{(\varepsilon reff-0.258)(\frac{w}{h}+0.8)} \quad \text{Equation 3.9}$$

ΔL is the extension length due to the fringing effect, where the EM waves expand to the outside of the patch.

5) The patch length patch (L) is obtained:

$$Leff=L+2\Delta L \quad \text{Equation 3.10}$$

$$\text{Therefore } L=Leff-2\Delta L \quad \text{Equation 3.11}$$

6) The ground plane dimension is calculated:

Length of the ground plane (Lg) and width of the ground plane (Wg)

$$Lg=L+6h \quad \text{Equation 3.12}$$

$$Wg= W+6h \quad \text{Equation 3.13}$$

The width of the feed line (wo) is computed by :

$$Zo=\frac{120\pi}{\sqrt{\varepsilon reff\left[\frac{Wo}{h}+1.353+0.667\ln(\frac{Wo}{h}+1.444)\right]}}, \quad \text{Zo is set to } 50\Omega. \quad \text{Equation 3.14}$$

Figure 3.11 shows the experiment setup in SEMCAD X. The tumor in the breast phantom is developed based on the diameter of the tumor, which is explained in section 3.2.1.

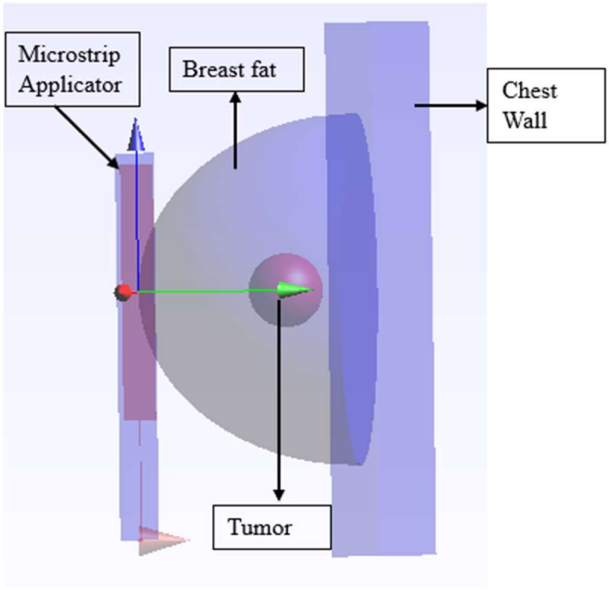

Figure 3.11: Experiment set-up for breast model and applicator

The size of a rectangular microstrip applicator at 915 MHz is 166.68*(l)* x 138.96*(w)* x 1.575*(h)* mm³. The patch dimension is 110.39 *(l)* x 129.51 *(w)* x 0.035 *(h)* mm³. The size of a rectangular microstrip applicator at 2450 MHz is 49.473 *(l)* x 57.819 *(w)* x 1.575 *(h)* mm³. The patch dimension is 40.02*(l)* x 48.37*(w)* x 0.035*(h)* mm³. The dimensions length and width are displayed in Figure 3.12.

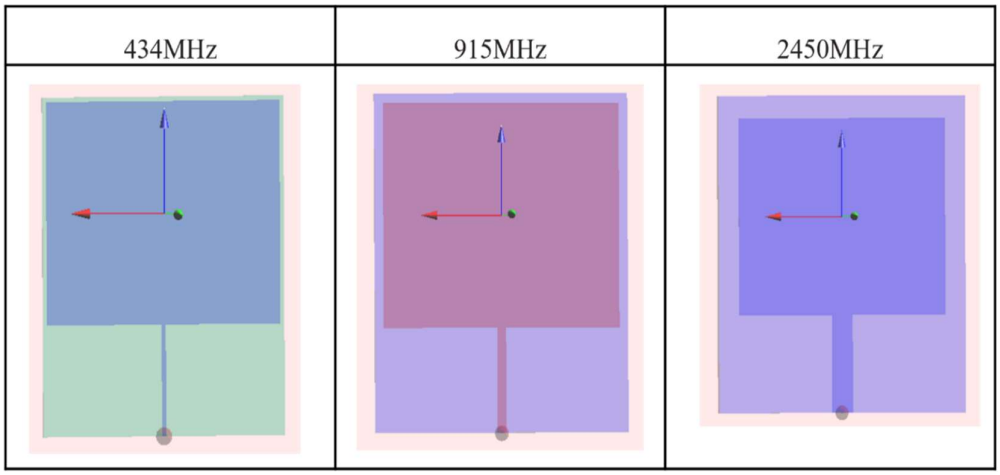

Figure 3.12: The applicator size with ISM frequency

Figure 3.13 presents the detailed steps involved in microstrip applicator development at the selected ISM frequencies, represented by DoE 1a. The microstrip applicator is designed to operate at Industrial, Scientific and Medical (ISM) frequencies of 434 MHz, 915 MHz and 2450 MHz Three applicators were developed for 434 MHz, 915 MHz and 2450 MHz. The breast phantom is embedded with three tumor sizes: T1, T2 and T3.

Electromagnetic simulations (EM) are conducted with SEMCAD X, and each applicator-phantom model is analysed based on SAR distribution within the tumor in the breast phantom. The SAR distribution is used as the indicator of EM energy absorption and focusing within the tumor region.

The effectiveness of the operating frequency is evaluated based on its ability to achieve the desired SD and ID for tumor size: T1: SD = 50 mm, ID = 64 mm; T2: SD = 48mm, ID = 80 mm; and T3: SD = 28mm.ID=90mm.

The SD and ID are determined based on the SAR distribution. The frequency that achieves localization within predefined SD and ID in the tumor is the appropriate operating frequency for this research.

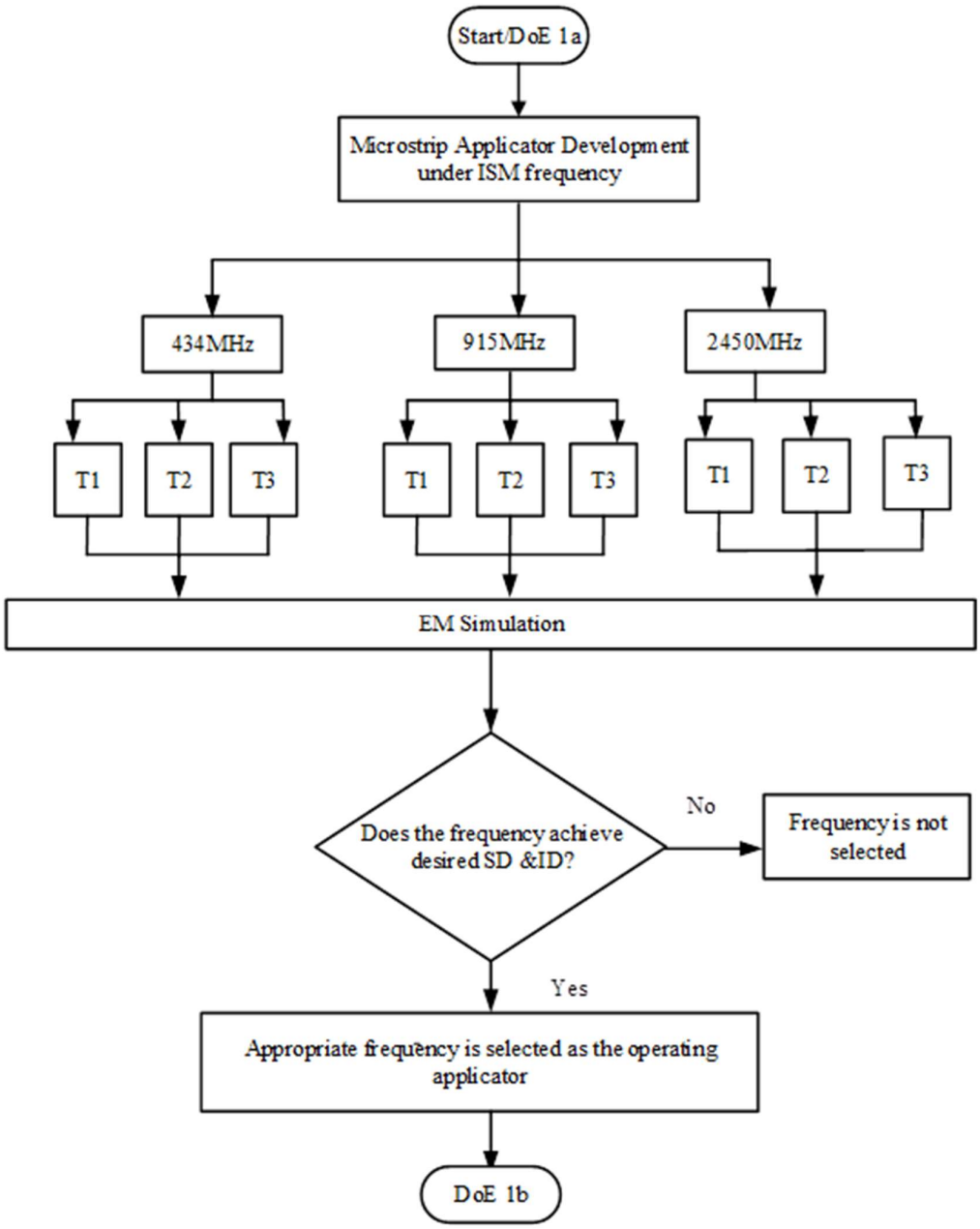

Figure 3.13: DoE 1a: Microstrip Applicator Development based on ISM Frequency

3.2.6 DoE 1b: Selection of Input Power

The operating power of 1W and 10W was investigated in this research. The suitable operating power is selected based on the SAR distribution result. Figure 3.14 shows the process flow in DoE 1b.

After assigning the appropriate frequency to the applicator, the input power is determined. Two input power levels were evaluated: low power (Pin = 1W) and high power (Pin = 10W).

The EM simulation with SEMCAD X was conducted on each power level. The selection of input power was based on the SAR (peak) value, which is inversely proportional to the hyperthermia treatment time.

If the SAR (peak) in the input power is 10 W greater than the input power of 1W, then Pin 10 W was selected, maintaining localized heating within the tumor without unwanted hotspots in the surrounding healthy tissue.

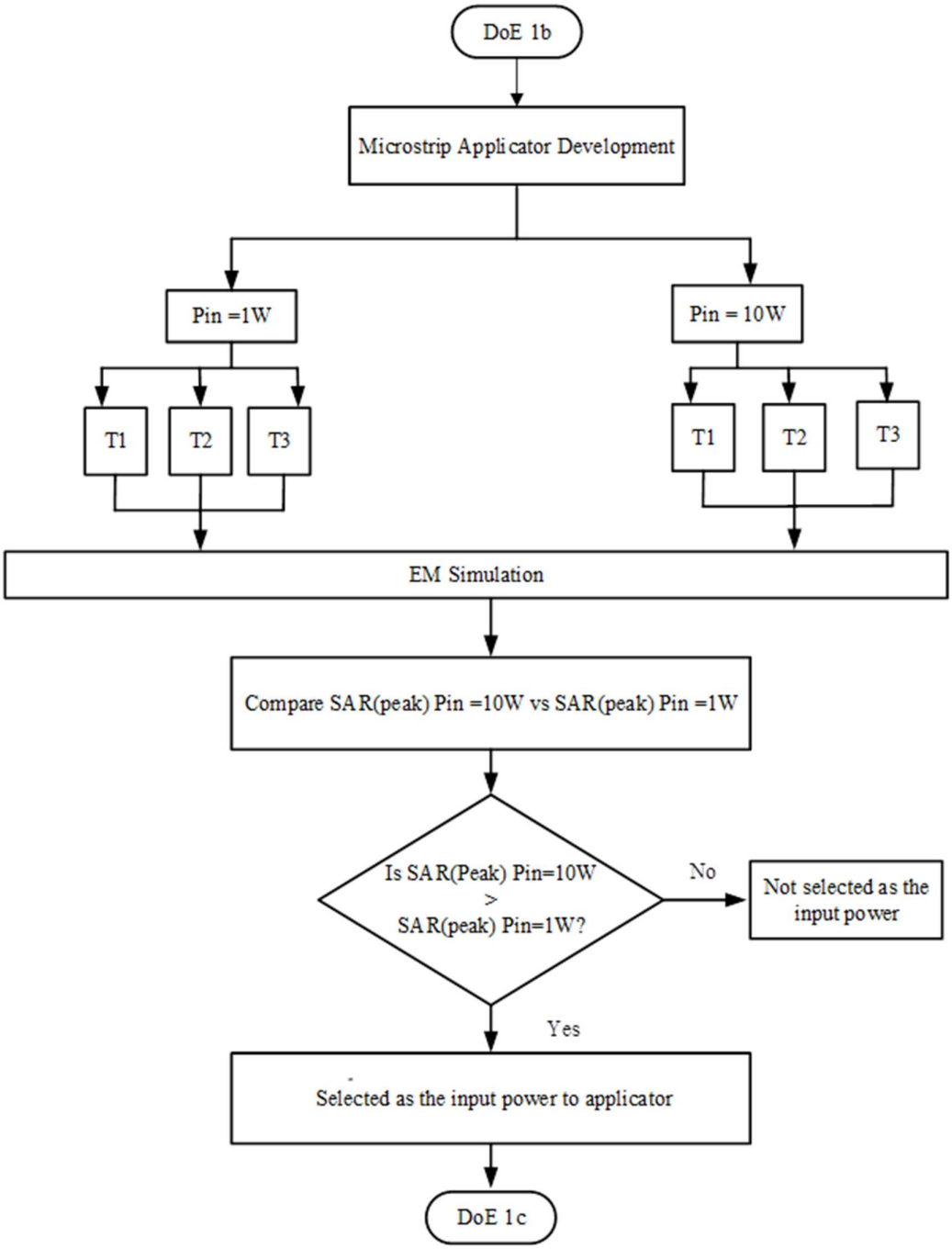

Figure 3.14: DoE 1b: Selection of Input Power

3.2.7 DoE 1c: Selection of SAR Average Tissue Mass

After the input power is selected, the next step is to select the SAR average tissue mass, namely SAR averaged at 1g tissue or SAR averaged at 10g tissue. The flowchart in Figure 3.15 outlines the DOE1c step for evaluating SAR across different tissue masses. The microstrip applicator and the breast phantom embedded with T1, T2 and T3 tumors were simulated for SAR conditions.

EM simulation was conducted to observe the SAR distribution. The selection of SAR average tissue mass was based on the SAR distribution that produces localized heat and meets the desired SD and desired ID for each tumor size. The SAR average tissue mass that demonstrated better localization of heat absorption, while achieving the desired SD and ID was selected for subsequent analysis in DoE 2a.

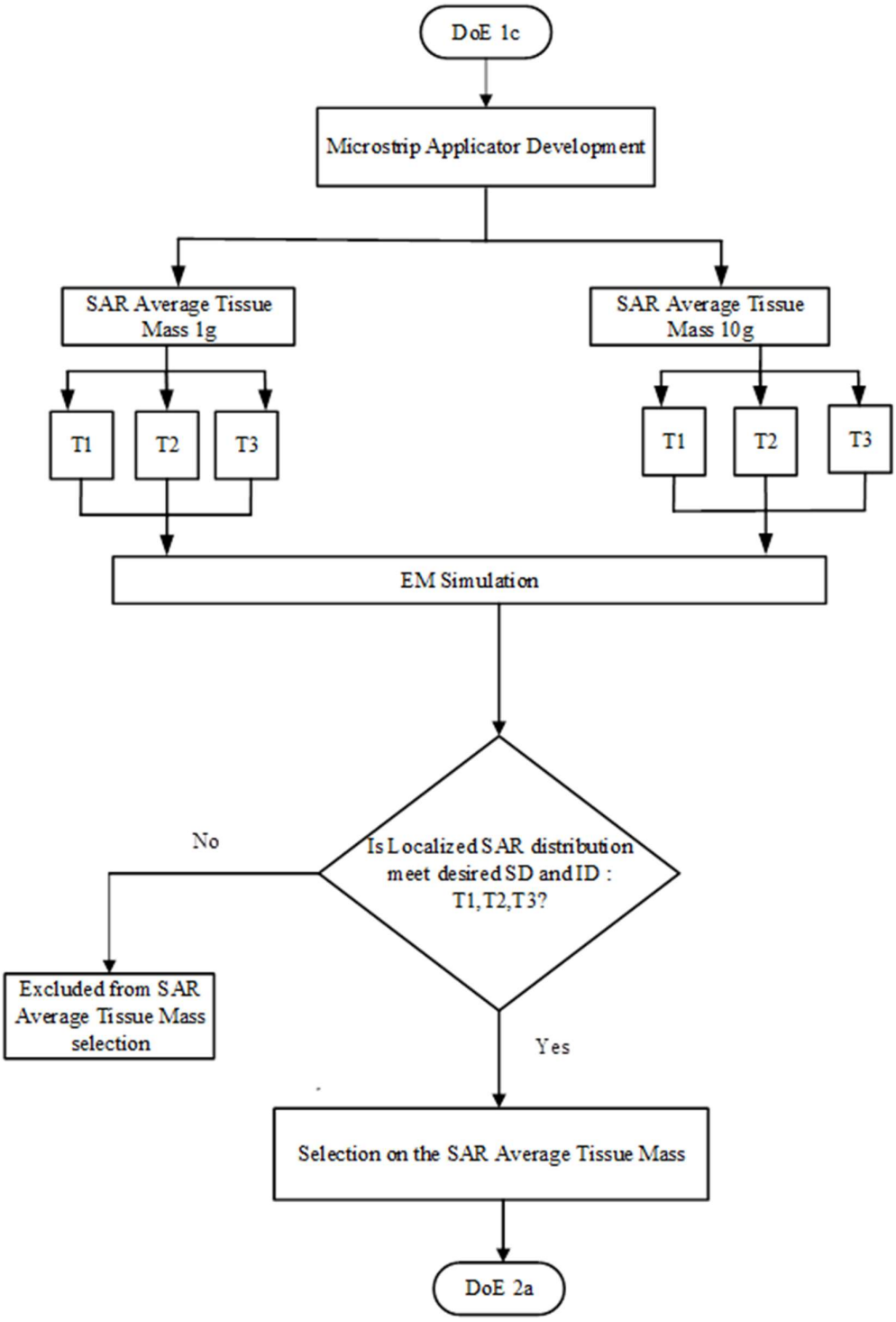

Figure 3.15: DoE 1c: Selection of SAR Average Tissue Mass

3.2.8 DoE 2a: Slot Integration into Rectangular Microstrip Applicator

After the rectangular microstrip applicator was developed, the next step is to integrate the slot into it. The U-slot design can be attained using Equations 3.15 to 3.16 in a design slot (Rani & Dawre, 2010; Roy et al., 2013). The E-slot uses this equation too as a guideline for integrating the E-slot into the microstrip applicator.

Slot Vertical Length, G

$$G = \frac{c}{2flow\sqrt{\varepsilon_{reff}}} - 2(L + 2\Delta L - E) \qquad \text{Equation 3.15}$$

c = speed of light

flow=lower frequency

Slot Horizontal Length, C=D*0.75

$$\text{Slot Thickness, } E = F = \frac{\lambda}{60} \qquad \text{Equation 3.16}$$

Each dimension of the U-slot and E-slot microstrip applicator is depicted in Figure 3.16 and Figure 3.17, respectively. In the U-slot configuration, the horizontal segment consists of two arms: the upper and the bottom. The upper and bottom arm U-slot thickness is indicated as E=F. Meanwhile, the vertical thickness is D. The vertical length is G. The horizontal length of the upper is A and the horizontal length of the bottom is C. The dimensions of H, J, K and L indicate a symmetrical position in the U-slot. The U-slot consists of vertical length (G), horizontal length (A, C) and thickness (D, E, F).

The E-slot includes three (3) horizontal arms: upper, middle and bottom. The thickness of the upper, middle and lower arms is indicated with E=F, vertical thickness is D. In addition, the E-slots are positioned symmetrically. The E-slot is in the symmetric position as indicated in G, H, I, J, and K. The E-slot consists of vertical length (G), horizontal length (A, B, C) and thickness (D, E, F).

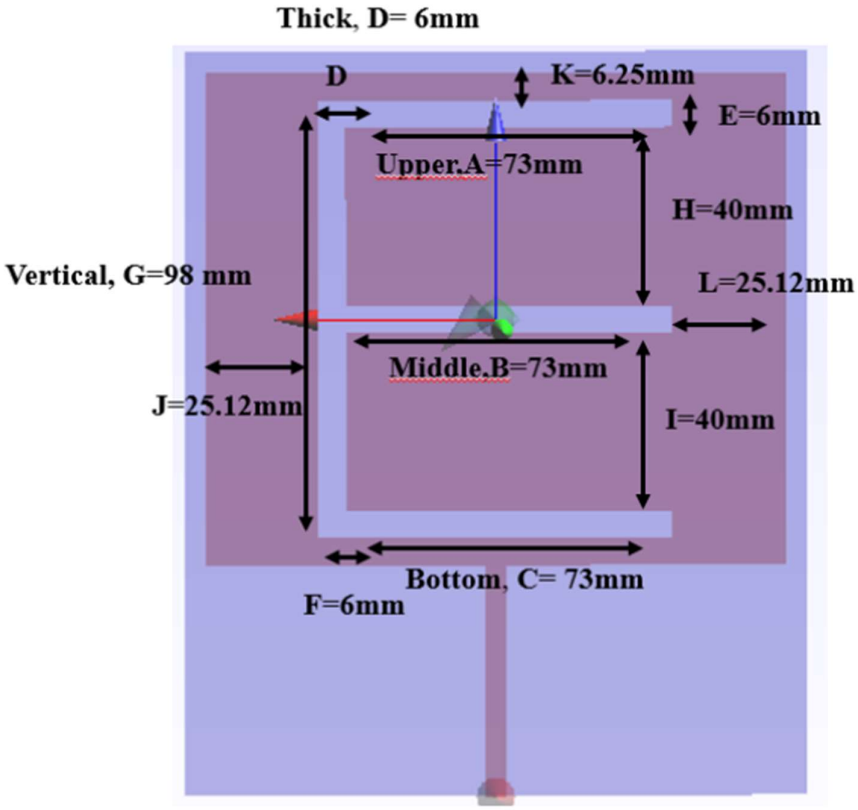

Figure 3.16: E-slot applicator

Figure 3.17 displays the DoE 2a steps. The flowchart illustrates the design process for integrating a slot into a microstrip applicator, followed by a comparison of the two slot structures.

The microstrip applicator was first integrated with a U-slot structure, followed by E-slot structure on each microstrip applicator. EM simulation was then performed for each slot applicator using a breast phantom embedded with tumors of sizes T1, T2 and T3.

EM simulation conducted with SEMCAD X to evaluate the applicator performance. The applicator characteristics, including directivity, gain and return loss, were evaluated based on tumor heating performance, assessed by SAR distribution, SD, ID and SAR (peak).

The comparative analysis was carried out between the U-slot and E-slot applicators in terms of applicator characteristics, SAR distribution, SD, ID and SAR (peak). The slot applicator demonstrates the superior overall performance in applicator characteristics, SAR distribution (more localized), SD, ID near the desired value (T1: SD=50mm, ID =64mm, T2: SD: 48mm ID=80mm, T3: SD: 28mm, ID =90mm) and SAR (peak). It was selected as the slot applicator in this research. The superior slot applicator was selected for further analysis in DOE 2b.

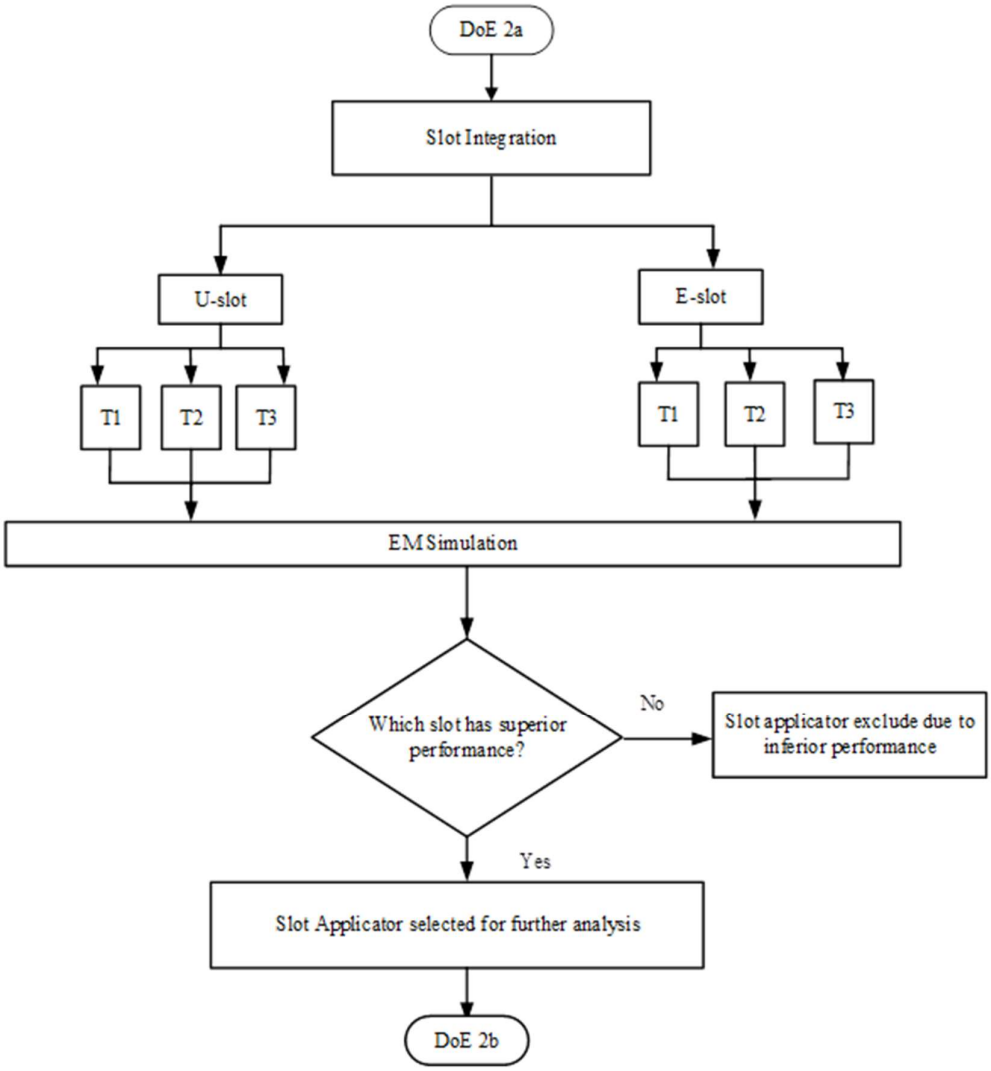

Figure 3.17: DoE 2a: Integration Slot Structure for Microstrip Development

3.2.9 DoE 2b: Distance Breast Phantom to Applicator

The flowchart in Figure 3.18 represents the structured approach for determining the optimal distance between the breast phantom and the applicator. The distance between the breast phantom and the applicator varied from 0mm (direct contact),5mm,10mm,15mm and 20mm. The distance adjustment was performed for each tumor size: T1, T2 and T3. EM was conducted by using SEMCAD X to analyse the SAR distribution within tumor region. The

evaluation focused on localized SAR concentration within the tumor region, while minimizing unwanted hotspots in surrounding healthy tissue.

The distance with localization within SD and ID and less unwanted hotspots in healthy tissue, was selected for the subsequent stage, DoE 3a.

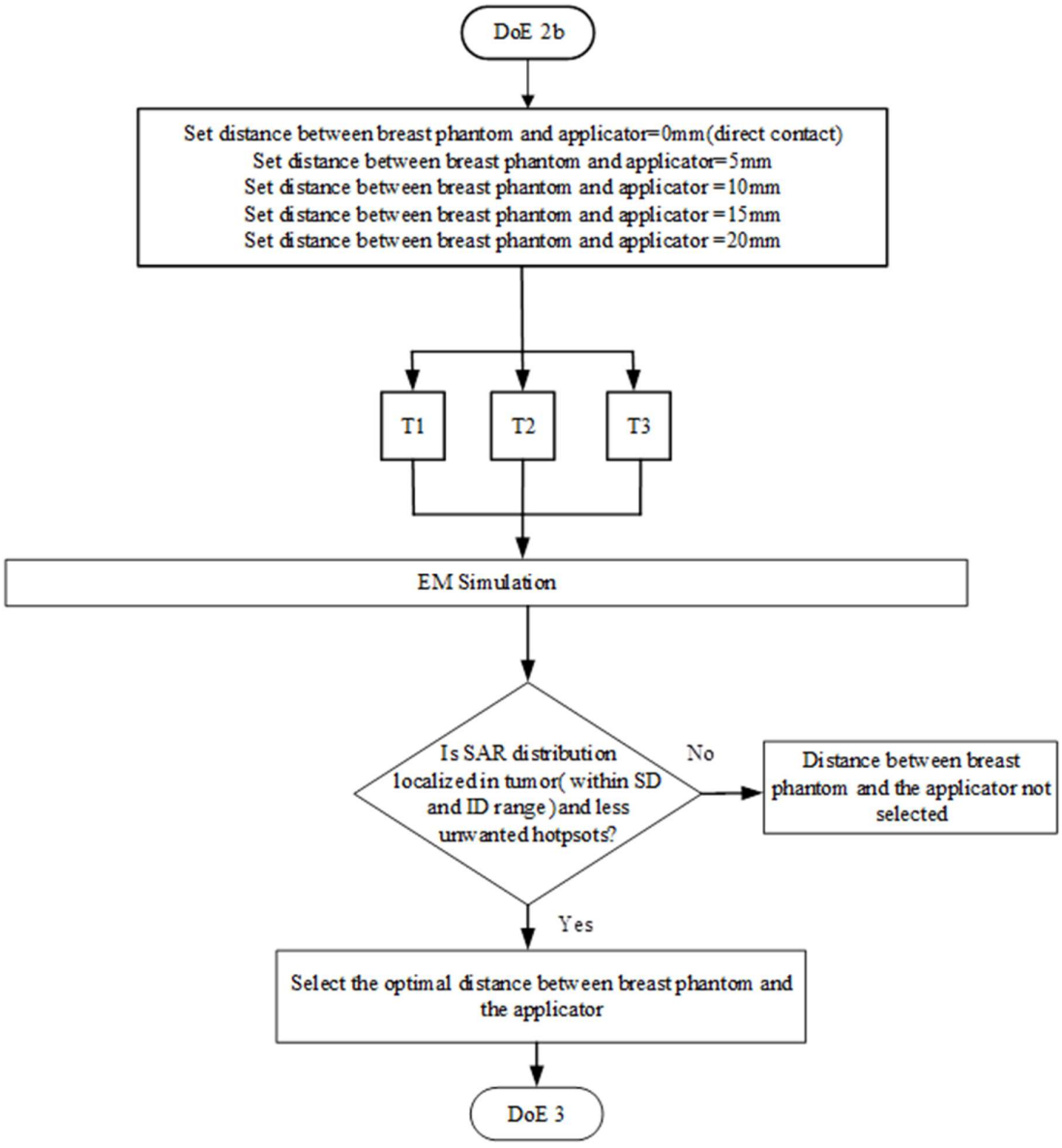

Figure 3.18: DoE 2b: Distance Breast Phantom to Applicator

3.2.10 DoE 3a: Modification of the Selected Slot Applicator

The parametric study involves modifying the selected slot structure, with only one parameter change at a time. The modification encompasses the length and thickness of the slot segment, covering horizontal and vertical dimensions. Figure 3.19 illustrates the DoE 3a process flowchart.

The dimension of horizontal length (upper, middle and bottom) was varied from 93 mm to 3 mm in 10 mm intervals. The vertical length ranged from 98 mm to 18 mm in 10 mm intervals. The horizontal thickness was varied from 6 mm to 46 mm in 4 mm increments at the top and bottom, while the middle thickness was varied from 6 mm to 86 mm in 4 mm increments. The vertical thickness ranged from 6 mm to 78 mm in 6 mm increments.

Each slot modification involves length (horizontal and vertical) and thick (horizontal and vertical), which were evaluated for the breast phantom embedded with T1, T2 and T3 tumors. For each slot modification, EM simulations were performed with SEMCAD X to assess the SAR distribution.

The significant slot segments were identified based on analysis of the desired SD and ID that were required for effective tumor heating in this research. Slot segments that satisfy the desired SD and ID across the tumor sizes were identified as significant and selected for further investigation for optimization of the slot, DoE 3c. The slot segments that did not meet the desired SD and ID requirements were excluded from further analysis.

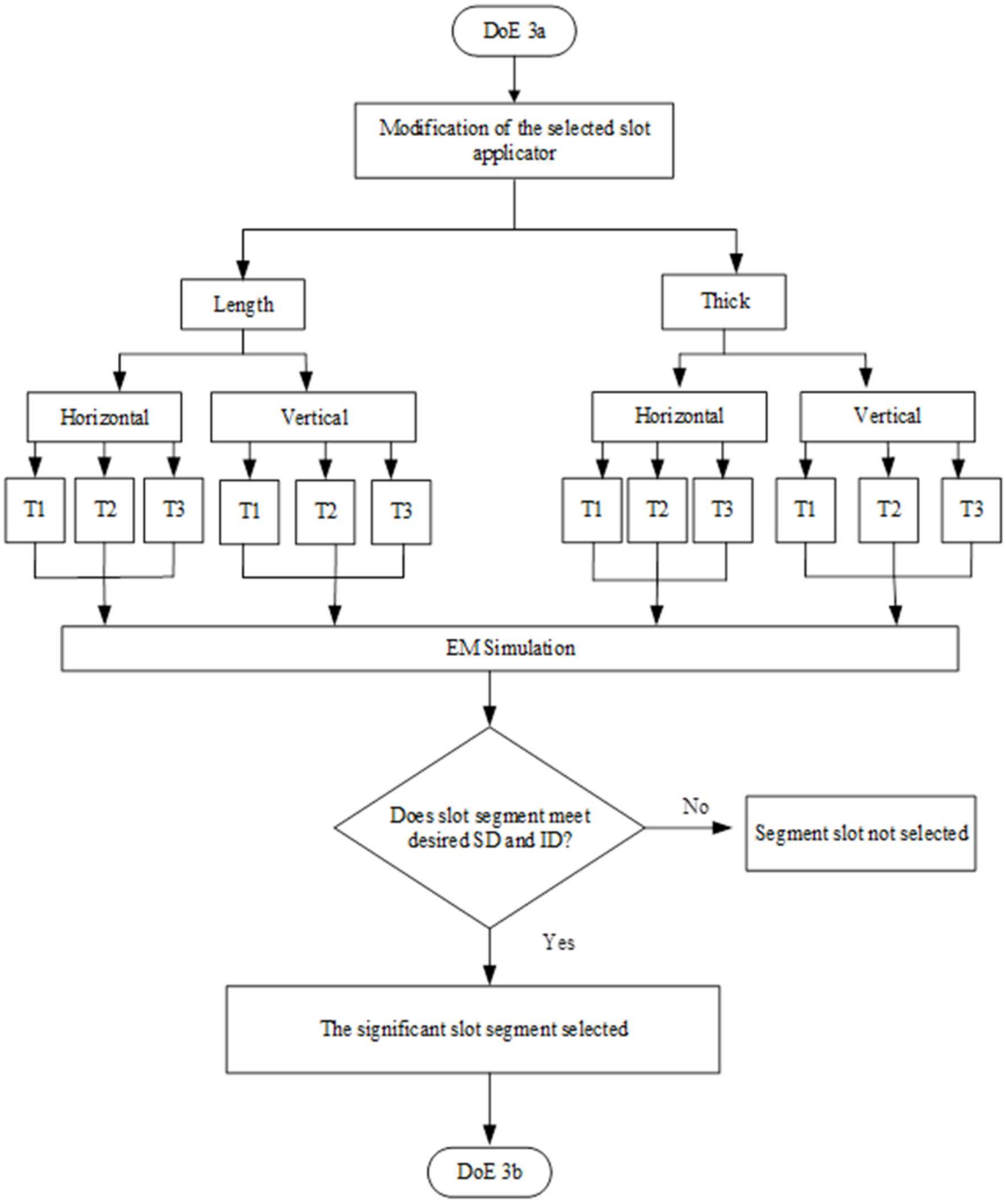

Figure 3.19: DoE 3a: Modification of the Selected Slot Applicator

3.2.11 DoE 3b: Optimization of the Selected Slot with Response Surface Methodology (RSM)

The flowchart in Figure 3.20 represents a systematic approach for optimizing a slot microstrip applicator. The process continued from DoE 3a. These optimized parameters were validated through simulation in SEMCAD X.

The set of Design of Experiment (DoE) runs was generated using Design Expert software based on significant slot segments identified in DoE 3a. Each set of design values (Upper, Middle, Bottom horizontal lengths and vertical thickness) was then evaluated using EM simulation in SEMCAD X, with the breast phantom embedded with T1, T2, and T3 tumor sizes. The SD and ID of the SAR distribution were recorded as response outputs and imported back into Design-Expert software.

The SD and ID were analysed using RSM to develop a polynomial model describing the relationships between the slot dimensions and the output responses (SD and ID). Regression analysis was then performed to estimate the model coefficient and identify significant slot segments that influence SD and ID.

The developed RSM polynomial model was subsequently evaluated using Analysis of Variance (ANOVA) to determine the statistical significance and adequacy (reliability and suitability for representing the predicted output response) of the model. If the model fails to meet the ANOVA requirements, the process returns to the regression analysis stage for model refinement. Once the RSM polynomial model was confirmed to be statistically significant, numerical optimization was performed to determine the optimal slot dimensions.

The optimum values refer to the set of E-slot parameters dimension selected during

the numerical optimization process. This includes the optimal dimensions of the upper, middle and bottom horizontal and vertical thickness.

The optimized design was then validated by comparing the predicted SD and ID values with the EM simulation results. If the mean, SD, and ID values fall within the 95% Prediction Interval (PI)-Low and 95% PI-High, the RSM polynomial model and the optimization were reliable and validated. Otherwise, the optimization process was repeated. Subsequently, the research methodology proceeds to DoE 3c.

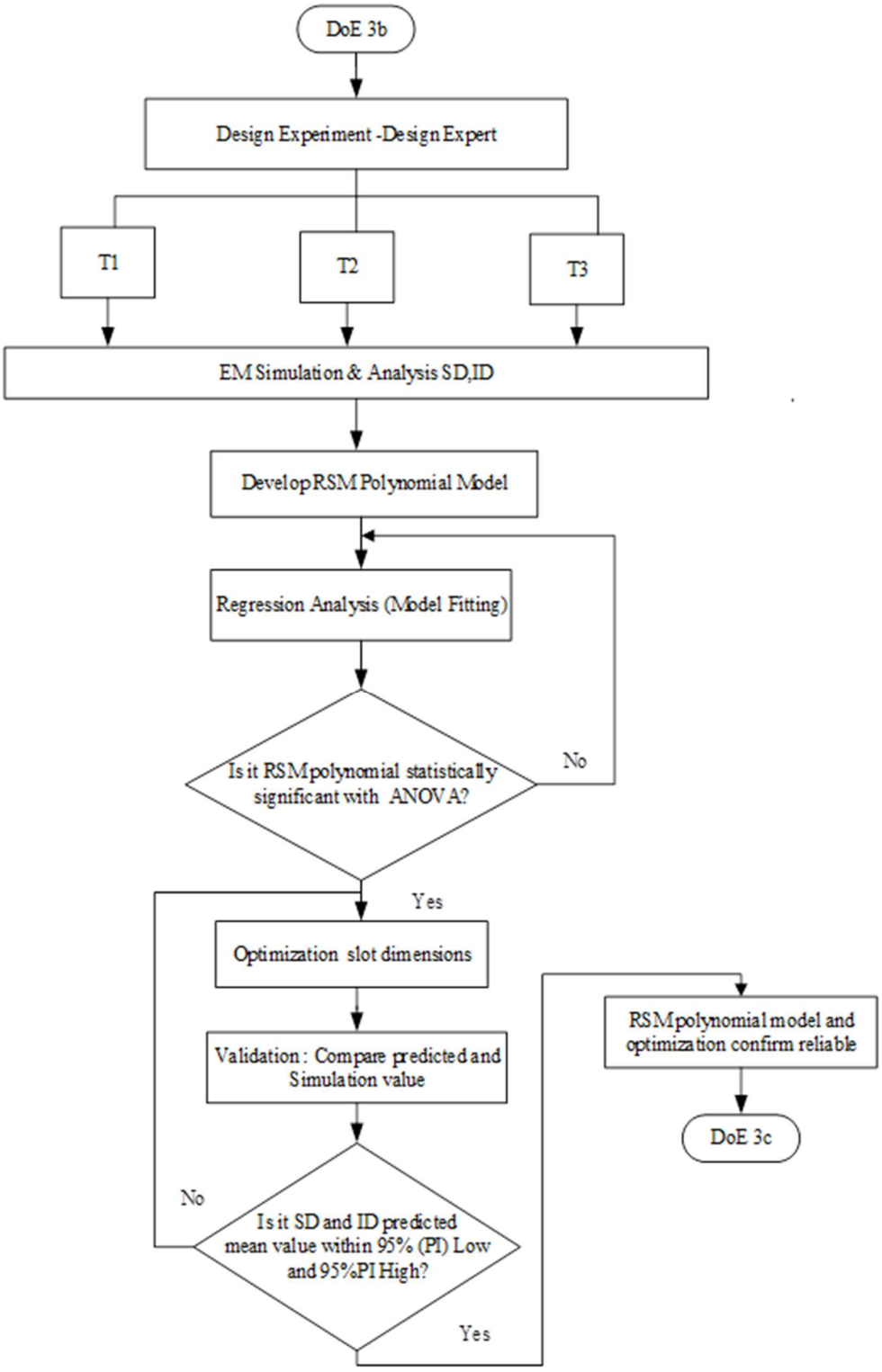

Figure 3.20: DoE 3b: Optimization of the Selected Slot with RSM

DoE 3c, as displayed in Figure 3.21, is initiated after the RSM polynomial model adequacy and optimization reliability have been confirmed in DoE3b. In this DoE3c, the focus was on validation of the optimized slot applicator with the previous optimization approaches that are the Genetic Algorithm (GA) and Particle Swarm Optimization (PSO).

Applicator optimization performance was evaluated based on the applicator's characteristics: directivity, gain, and return loss. The optimized RSM was then validated by comparing its applicator characteristics with those of previous optimization approaches, namely GA and PSO.

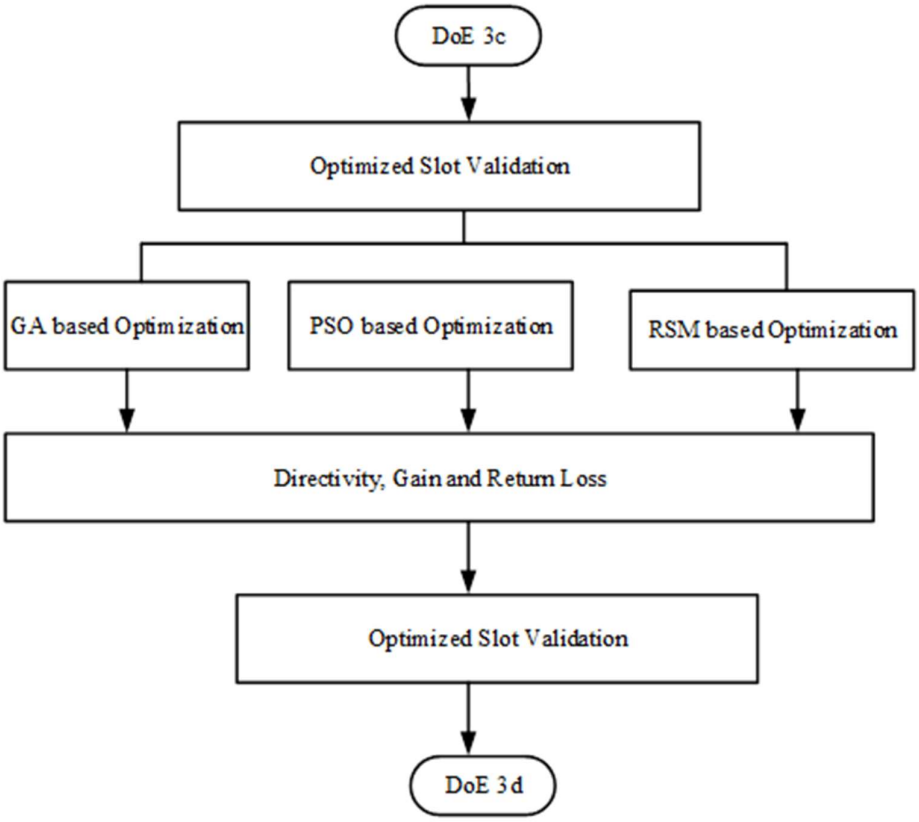

Figure 3.21: DoE 3c: Validation of optimized slot applicator

3.2.12 DoE 3d: Comparison of Slot Applicator: Selected Slot Applicator and Optimized Slot Applicator

The DoE 3d flowchart is illustrated in Figure 3.22. DoE 3d compared the selected slot applicator with the optimized slot applicator for each tumor size: T1, T2 and T3. EM simulations were performed for both designs attached to the breast phantom model. The comparison was conducted based on applicator characteristics and heat absorption within tumor.

The applicator characteristics were evaluated, including directivity, gain, and return loss. Heat absorption in tissue was assessed using SD and ID, which were derived from the SAR distribution and SAR (peak). The applicator demonstrated superior performance in terms of applicator characteristics and localized heat absorption was selected to proceed to DoE4 for SAR optimization and hyperthermia treatment time. Conversely, if performance was unsatisfactory, the applicator was not selected for DoE 4.

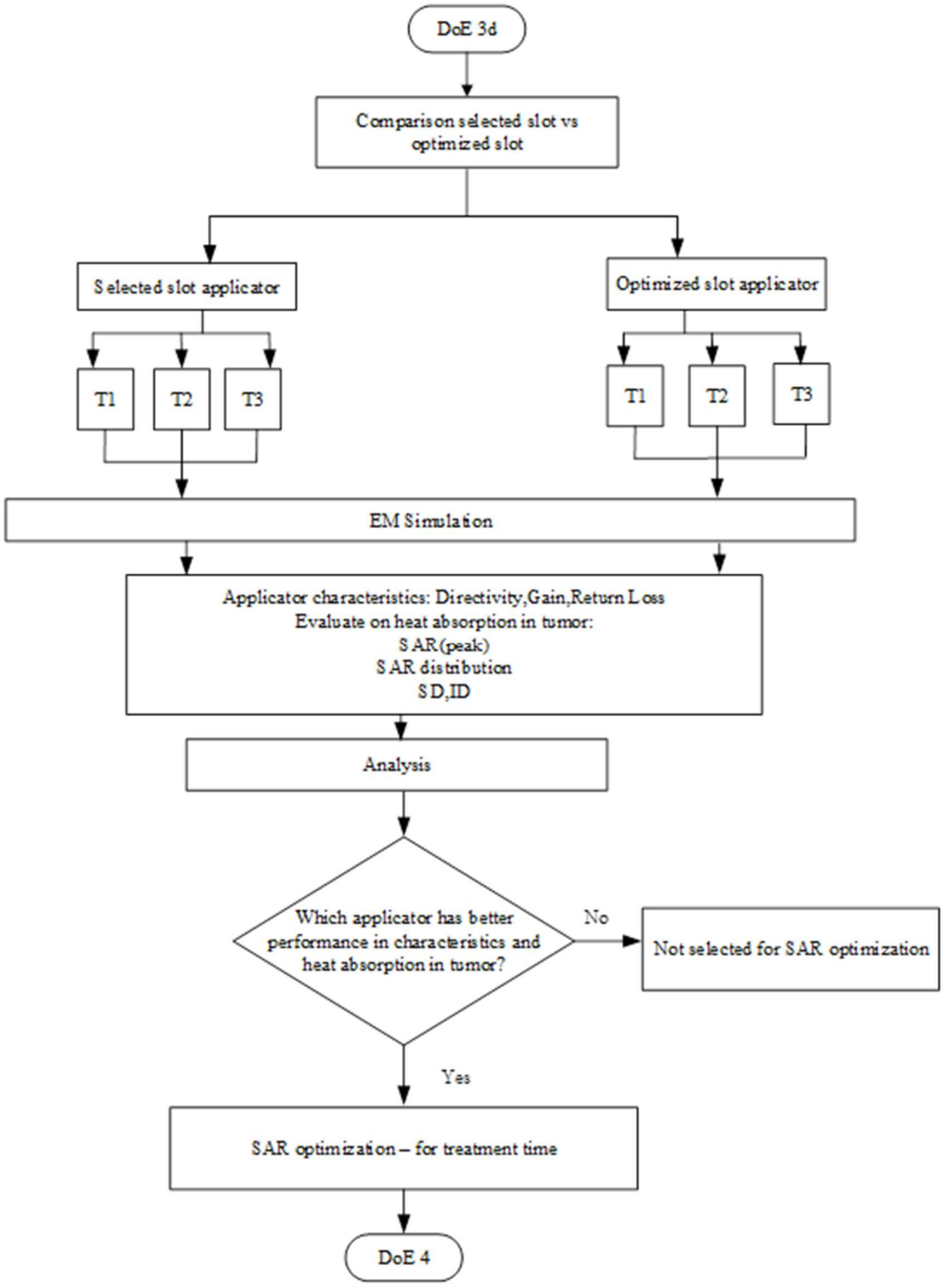

Figure 3.22: DoE 3c: Validation of optimized slot applicator

3.2.13 DoE 4: Hyperthermia Treatment Time: SAR Optimization

Figure 3.23 illustrates the flowchart of the experiment procedure for DoE 3, which aims to determine the optimal hyperthermia treatment time. The optimized slot applicator was integrated with a water bolus to complete the hyperthermia model. Adding a water bolus provides a cooling environment during the treatment. A water bolus with a breast shape and thickness of 2mm was used. Distilled water with relative permittivity.$\varepsilon_r = 74.45$, electrical conductivity, σ =1.88S/m and specific heat capacity = 4.176J/kg/K as in the SEMCAD X database

The experiment was conducted with and without a water bolus. Both with and without a water bolus follow the same procedure. Both models were evaluated using a breast phantom embedded with tumors of T1, T2, and T3 sizes. EM simulations were conducted to compare the SAR optimization between the model with and without a water bolus. SAR was optimized after EM simulation.

SAR optimization was tuned until the SAR distribution adequately covers the entire tumor region for each size. The SAR optimization was repeated until the coverage tumor criteria were satisfied with the desired SD and ID was achieved. The hyperthermia treatment time was subsequently determined only for the water bolus model, as it was required to ensure safety and protect the skin from damage. Finally, the hyperthermia treatment time was determined after the SAR optimization met the desired SD and ID under DoE 4.

.

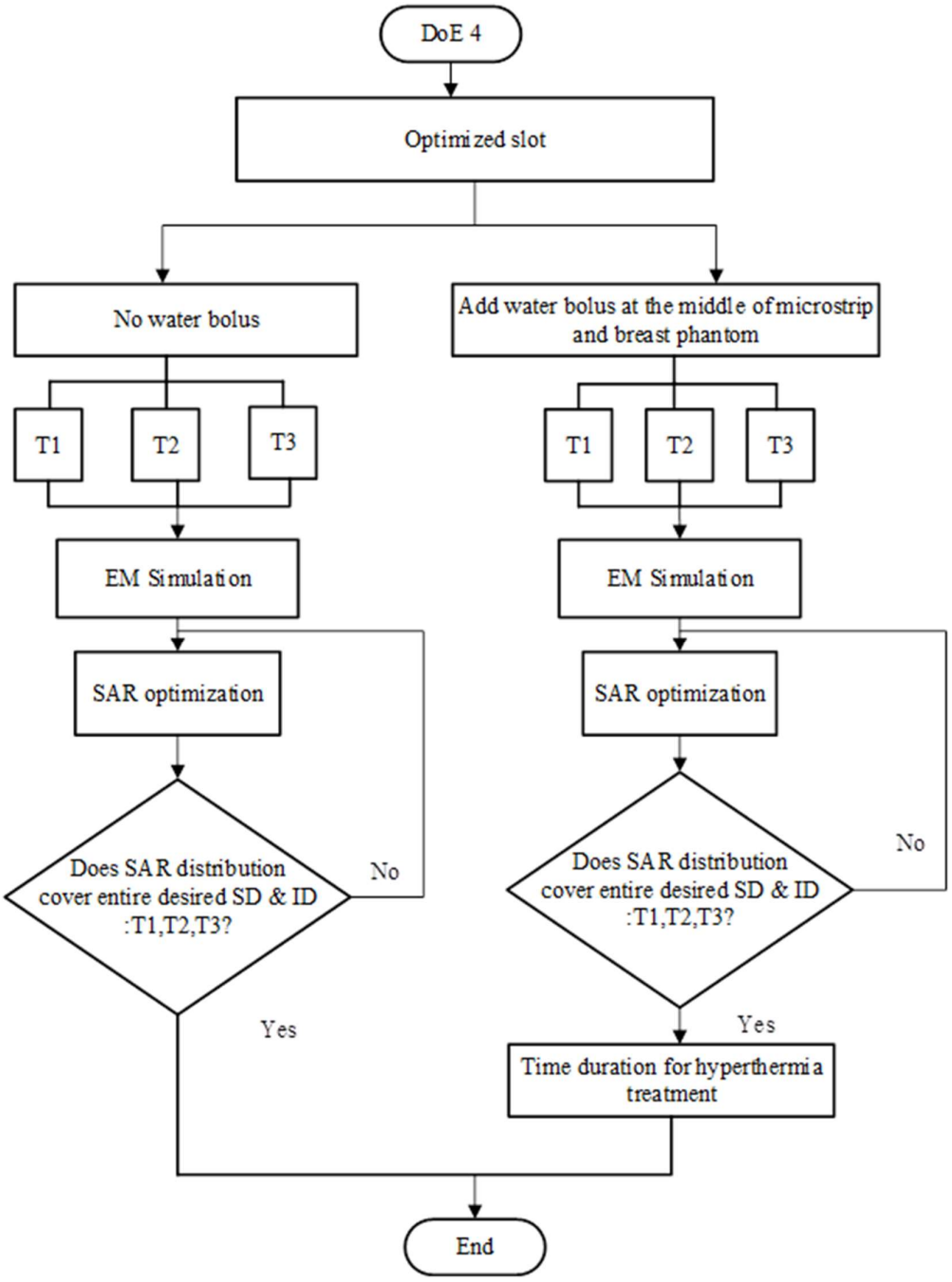

Figure 3.23: DoE 4: Hyperthermia Treatment Time Optimization

3.3 Summary of the Chapter

This chapter presents the overall research methodology used to achieve the research objectives. The methodology was structured using a systematic Design of Experiments (DoE) to investigate a non-invasive microstrip slot applicator for breast cancer hyperthermia treatment. The EM simulation tool, SEMCAD X, was used to evaluate the SAR distribution and SD and ID.

The research commences with DOE 1, which involved developing a breast phantom model with tumor sizes of T1, T2 and T3, followed by the design of a microstrip applicator operating at the ISM frequency. The input power to the applicator and the average SAR in the tissue mass were determined based on the suitability of this research.

Subsequent DoE 2-stage focuses on slot integration and the optimal distance between the breast phantom and the applicator. Next is DOE 3, which highlights slot modification and slot optimization with RSM. Indicators such as SD and ID were used to assess localized tumor heating. Statistical analysis using regression and ANOVA was employed to validate the developed polynomial model and identify significant slot parameters. The next stage was the validation optimization slot, comparing it with the previous optimization approaches, GA and PSO. After that, a comparison of the selected slot structure and the optimized slot in terms of applicator characteristics and heat absorption in the tumor region.

The final stage was the integration of the optimized slot applicator with a water bolus to establish a complete hyperthermia treatment model. SAR optimization was performed iteratively until the tumor region was fully heated. The hyperthermia time was then determined at T1, T2 and T3. The results and discussion are presented in the next chapter.

CHAPTER 4

RESULTS AND DISCUSSION

4.1 Introduction

Chapter 4 presents the findings from the experiments performed in the SEMCAD X simulation. Section 4.2 discusses the outcomes of DoE 1, DoE 2, DoE 3, and DoE 4.

4.2 Results and Discussion

The next section, sections 4.2.1 to 4.2.10, highlights and discusses results from the experiments in Chapter 4. Section 4.2.1 presents a simulation of the performance of a rectangular microstrip applicator at different operating frequencies. Sections 4.2.2 and 4.2.3 discuss the appropriate input power and SAR average mass, respectively. Meanwhile, section 4.2.4 focuses on slot integration on the rectangular microstrip applicator. Section 4.2.5 highlights the distance between the applicator and the breast phantom. Then, slot modifications in sections 4.2.6 and 4.2.7 on slot optimization, are discussed. Subsequently, section 4.2.8 on the validation of the optimized E-slot applicator. The next section, 4.2.9, compares microstrip applicator performance between the E-slot and the optimized E-slot. Finally, section 4.2.10 discusses the treatment time for hyperthermia.

4.2.1 Rectangular Microstrip Applicator Development Based on ISM Frequency

DoE 1a shows that different operating frequencies contributed to different sizes of rectangular microstrip applicator. The dimensions of the microstrip applicator at ISM frequencies 434 MHz, 915 MHz, and 2450 MHz are recorded in Section 3.5.5. Lower operating frequencies result in a larger rectangular applicator than higher ones, based on applicator dimensions.

The simulation model is defined in 3D Cartesian coordinates (x,y,z). In this research, SAR distribution represents the heat distribution within the tissue, ensuring that heat spreads evenly to the tumor and minimizing heat transfer to healthy tissue. The y=0mm is defined as the skin surface and the +y direction increases into the breast phantom. Therefore, SD and ID are measurements along the y-axis that represent the direction of EM propagation in tissue.

Figure 4.1 illustrates the SAR distribution for different tumor sizes: T1,T2 and T3 under ISM frequencies. The SAR distribution varies across regions of the breast phantom at different operating frequencies. EM wave propagation in biological tissue is frequency-dependent and can be described by the wavelength relationship:$\lambda_{tissue} = \frac{c}{f}$, where λ_{tissue} represents the wavelength of the EM wave in tissue, c is the speed of light in free space, and f is the operating frequency.

The SAR distribution at 434 MHz with the applicator covers the middle to near chest wall (from the front to the posterior region). Meanwhile, for the 915MHz applicator, SAR concentrates in the middle region of the breast phantom, while for the 2450MHz applicator, the SAR distribution is near the areola (front region of the breast phantom).

Tumor Size	SAR distribution SAR in breast phantom 434MHz	SD/ID (mm)	SAR distribution SAR in breast phantom 915MHz	SD/ID (mm)	SAR distribution SAR in breast phantom 2450MHz	SD/ID (mm)
T1	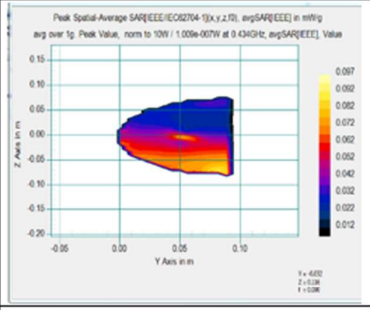	0.65/ 91	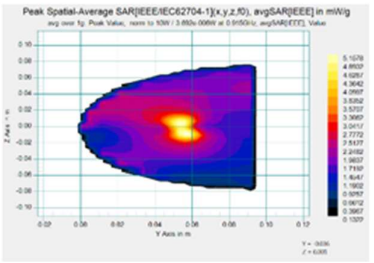	40 /66.8	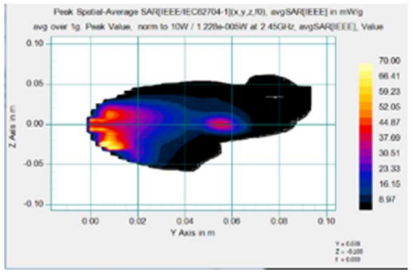	0 / 15
T2	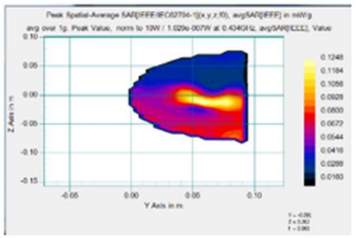	33.4 / 90.5	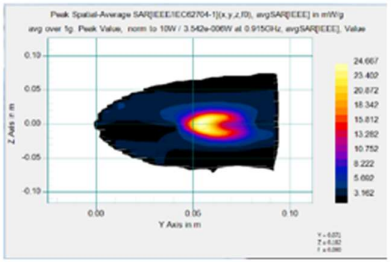	46.5 /71.7	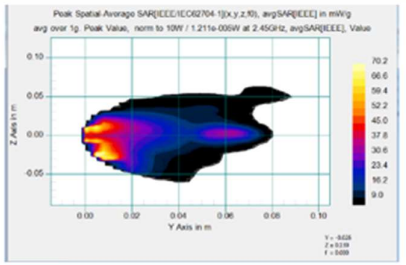	0 /15.4
T3	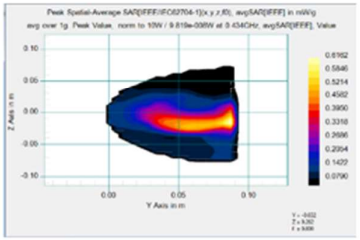	32.1 /90.1	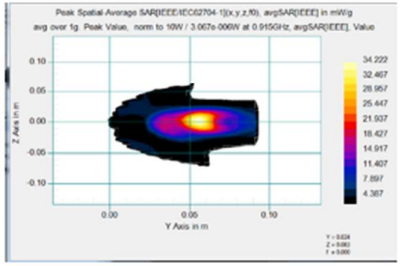	42.6 /67.5	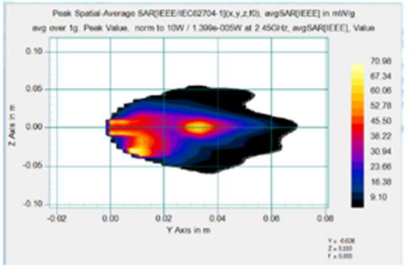	0 / 40

Figure 4.1: SAR distribution of tumor Sizes: T1,T2 and T3 under ISM frequency

The ID obtained from the SAR distribution is presented in Figure 4.2. As the frequency increases, the ID decreases. The trend is similar for all T1, T2 and T3. The deepest ID is at 434 MHz, with 91mm, 90.5mm, and 90.1mm for T1, T2 and T3, respectively. The ID decreases slightly at 915 MHz compared to 434 MHz. The ID at 915 MHz is 66.8mm for T1, 71.7mm for T2 and 67.5mm for T3. The ID decreases at 2450 MHz compared to 915 MHz. The results show that the ID for 2450 MHz is 15mm, 15.2mm and 40mm at T1, T2 and T3, respectively. It indicates that high-frequency signals have a lower ID than low-frequency signals.

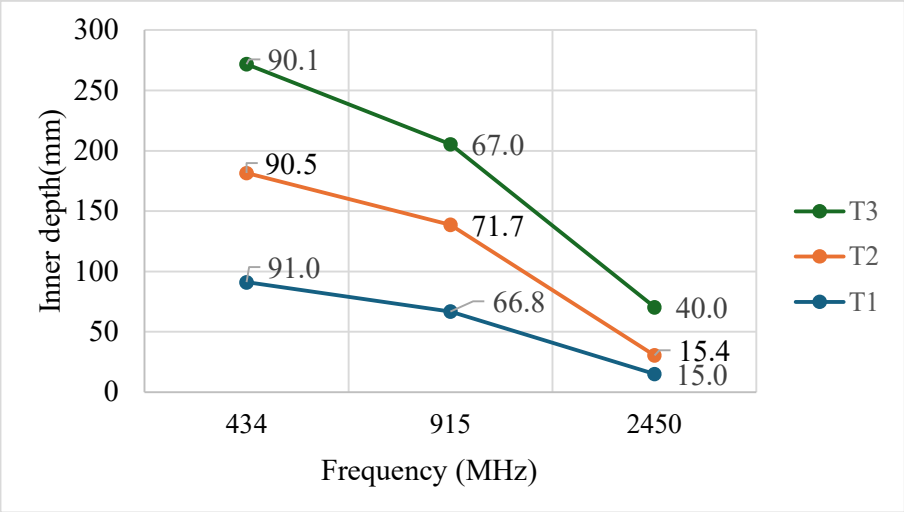

Figure 4.2: ID versus frequency

At low frequencies (434 MHz), EM waves penetrate more deeply into tissue, producing a larger heating region that extends beyond the tumor. According to (Nguyen et al., 2015) if the frequency is too low, the heated area is more expansive than the target area, resulting in damage to healthy cells. For instance, an applicator used 434 MHz to treat locally advanced breast cancer (Choudhary & Arunachalam, 2022), while (Choi et al., 2012; Hand,

1986) demonstrated that 434 MHz provided greater PD than 915 MHz and 2450 MHz (Gupta & Singh, 2005).

Additionally, (Lyu et al., 2023) indicated that the applicator 915 MHz has a more prominent focus point and deeper depth than 2450 MHz. Variation in ID indicates that the efficacy of tumor treatment depends on the applicator's frequency. Conversely, at higher frequencies, EM waves are absorbed near the skin surface, thereby reducing PD. Meanwhile, the 2450 MHz applicator resulted in more focus on target tissue, but with reduced ID (Li et al., 2021). The applicator operates at 2450 MHz, causing the skin adjacent to the applicator to absorb more heat.

The observation and analysis of these results agree with the ID decreases as the frequency increases, as observed by (Gao et al., 2022)(Lyu et al., 2023). The relationship of skin depth (δ) / ID with frequency is stated in this equation, ID= $\sqrt{\frac{1}{\pi\sigma\mu f}}$ (Rodrigues et al., 2022).

The SD measurement is based on the SAR distribution. The findings show SD does not directly relate to frequency, as depicted in Figure 4.3. However, SD varies significantly across operating frequencies. The SD across all frequencies and tumors shows the same trend.

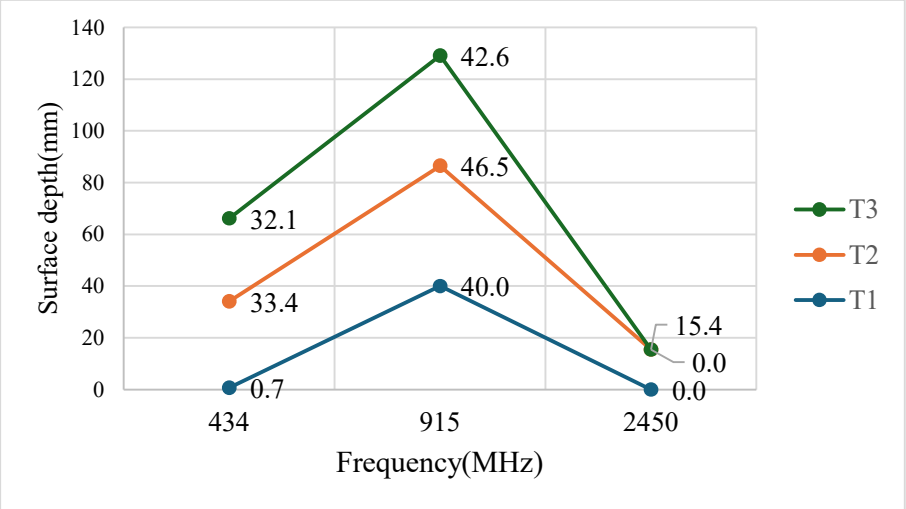

Figure 4.3: SD versus frequency

At 434 MHz, the SD is shallower than at 915 MHz. At 915 MHz, the SD increases sharply across all tumors. Meanwhile, at 2450 MHz, the SD decreases significantly across all tumor sizes. The present findings are consistent with those reported in previous studies.

The results demonstrate that the 915 MHz frequency penetrates deeper into tissue and nearly achieves the desired SD of 50mm and 48mm for T1 and T2, respectively. In contrast, the SD for T3 is closer to the desired value of 28mm at a frequency of 434 MHz. However, the non-uniform SAR distribution at 434 MHz and could impact the effectiveness of hyperthermia treatment. In this research, 915 MHz shows the highest SD and has a significant effect on the frequency.

In summary, ID, SD and SAR distribution are influenced by frequency. In addition to depth characteristics, SAR uniformity is also an important factor in selecting an appropriate frequency for hyperthermia treatment. Based on findings in DOE 1a, a rectangular microstrip applicator operating at 915 MHz was selected as appropriate for this

research. The following section discusses selecting the input power.

4.2.2 Selection of Input Power

The graph in Figure 4.4 illustrates SAR (peak) values for different tumor sizes (T1, T2, and T3) under two input power levels: 1 W and 10 W. At T1, the SAR (peak) is relatively low at 0.5167 mW/g when the input power is 1 W, while the SAR (peak) increases significantly to 5.168 mW/g when the input power is 10 W.

Meanwhile, at T2, the SAR (peak) reaches 2.4667mW/g at input power 1 W and SAR (peak) increase to 24.6670mW/g at input power 10W. For T3, the SAR (peak) is 3.530 mW/g at an input power of 1W and 35.393 mW/g at an input power of 10 W. It demonstrates that in T1 to T3, the ratio of SAR (peak) at input power of 1 W and 10 W is about 1:10.

This finding is supported by (Smitha & Narayanan, 2016)which explores the relationship between SAR and input power; SAR increases with input power. It has been established that when the input power is high, the SAR(peak) increases and the time required to complete the heating of the entire tumor is reduced (Selmi et al., 2020).

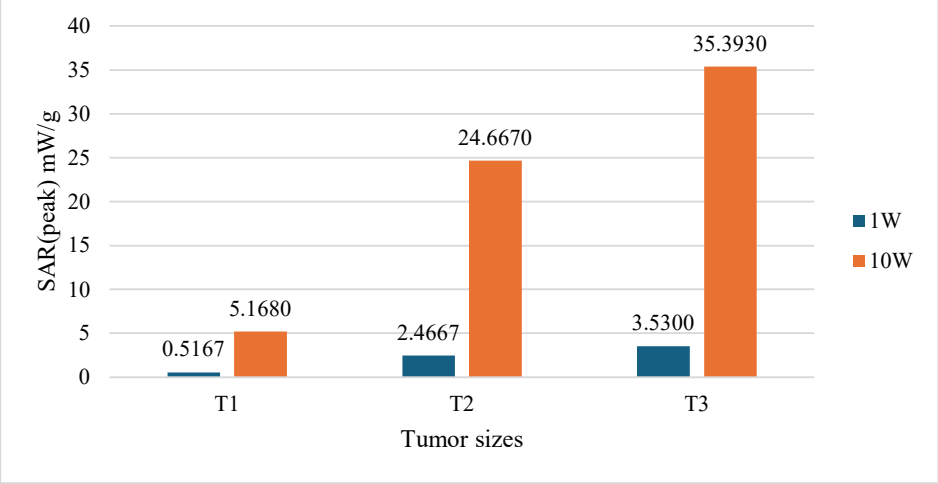

Figure 4.4: SAR(peak) with input power 1W and 10W

Appendix C presents each input power's SAR distribution, SD, ID for T1, T2 and T3. The SAR distribution, SD and ID for both input powers are similar outcomes. The difference results are obviously reflected in the SAR (peak). As stated in Section 2.9, Equation 2.4, the SAR value is associated with the time treatment. SAR (peak) is inversely proportional to time duration. Therefore, input power selection is based on SAR (peak) in this research.

In summary, input power does not significantly affect SAR distribution, SD and ID. However, the SAR (peak) is significantly affected by the input power to the applicator. Therefore, the input power used in this research is 10 W because it shows a high SAR (peak) in all conditions, T1, T2 and T3. The following section discusses the selection of the SAR average mass.

4.2.3 Selection of SAR Average Tissue Mass

Figure 4.5 compares the SAR average mass of 1g and 10g for all T1, T2 and T3. SAR is the measurement of the rate of energy absorbed per unit mass by treated tissue. The mass density of tissue suggests that 1g and 10g are the standard values in IEEE/IEC62704 (IEEE, 2017). The 1 g SAR is used for energy absorption in small tissue volumes, while the 10 g SAR is used for larger tissue volumes (Stuff, 2014).

In the condition of T1, the SAR (peak) for average mass 1g is 5.1578 mW/g, while the SAR (peak) for average mass 10 g is 3.1590 mW/g. The SAR (peak) for average mass 1g is 24.6670 mW/g and for average mass 10g is 15.9900 mW/g in T2. Meanwhile, in T3, the SAR (peak) for average mass 1 g is 34.22 mW/g, and the average mass 10 g is 24.3800mW/g.

The results show that in T1, the SAR average mass of 1 g increased by a factor of 1.6

compared to the average mass of 10g. In T2, the SAR average mass of 1 g increased by 1.5 relative to the average mass of 10 g. Similarly, in T3, the SAR (peak) on average mass of 1 g is 1.4 times that on average mass of 10 g. These findings are supported by previous research, whereby the SAR average mass of 1 g of tissue is higher than the SAR mass average of 10 g of tissue (Bacova & Benova, 2023; Zelinski et al., 2008)(Lias et al., 2016).

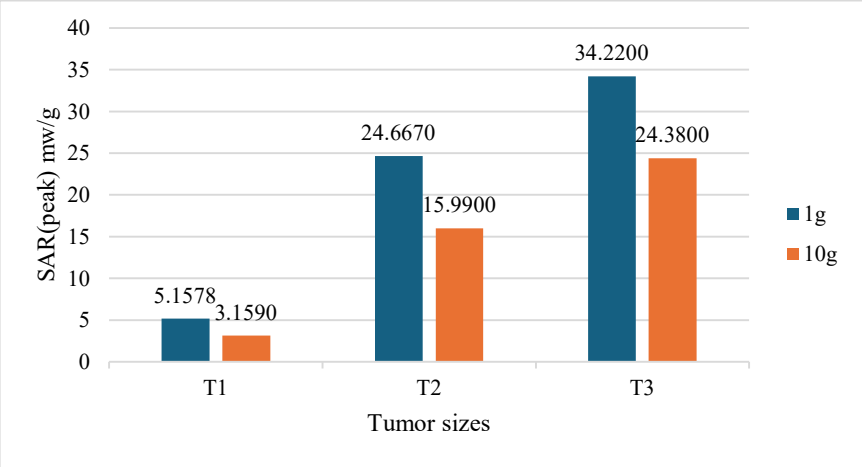

Figure 4.5: Comparison of SAR average mass 1g and 10g

The detailed results of mass averages of 1 g and 10 g are provided in Appendix D. The results indicate that energy absorption in SAR has an average mass of 10 g more than 1g. However, excessive heat is evident in the average SAR distribution, with a mass of 10 g, and can damage healthy tissues, especially in T1.

SAR is a crucial factor in hyperthermia, as it measures the rate of energy absorbed in tumor. The rise in temperature directly affects the SAR value and inversely affects the duration of hyperthermia (Al-Sabti et al., 2023). In summary, the significant differences in SAR(peak) suggest that small average masses experience more localized heating and better energy absorption than large average masses. Therefore, an average SAR mass of 1 g is used

in this research. The next section describes DoE 2a, which involves the integration of E-slot and U-slot designs. Then a comparison was conducted of rectangular, U-slot and E-slot applicators in terms of directivity, gain, return loss, SD, ID and SAR(peak).

4.2.4 Slot Integration into Rectangular Microstrip Applicator

In this research, the impact of slot integration is investigated from two main aspects: heat absorption within the tumor and applicator performance characteristics. Heat absorption within the tumor was evaluated based on SAR distribution and SAR (peak), while applicator performance was assessed in terms of directivity, gain and return loss.

Figure 4.6 compares SAR distribution SD, ID, SAR (peak) for three (3) applicator designs: rectangular, E-slot and U-slot that were evaluated for T1, T2, and T3 tumor sizes. For T1, the E-slot applicator demonstrated reduced unwanted hotspots in the surrounding healthy tissue compared to the U-slot and rectangular applicators. Meanwhile, for T2, the E-slot applicator exhibits more focused heat absorption and localizes within the tumor region than the U-slot and rectangular applicators. For T3, the E-slot applicator produces a broader heat-distribution region than the U-slot and rectangular applicator.

Tumor size	Rectangular applicator	E-slot applicator	U-slot applicator
T1	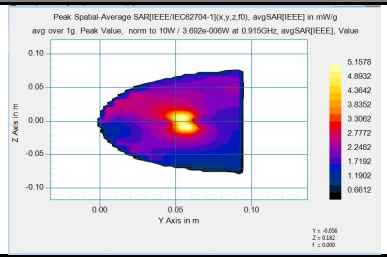	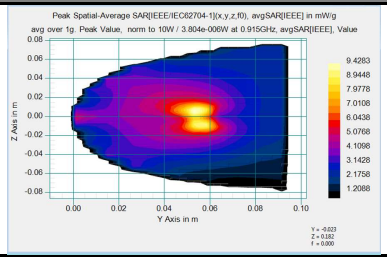	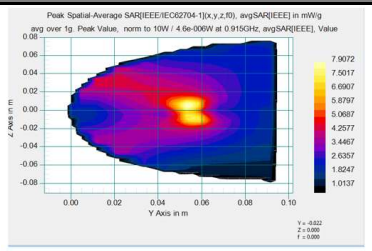
	SD:40mm ID: 66.8mm SAR (peak) = 5.1578 mW/g	SD:40mm ID:64.5mm SAR (peak) =9.4283mW/g	SD:40.2mm ID: 65mm SAR (peak) =7.9072mW/g
T2	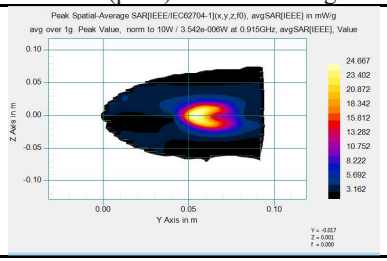	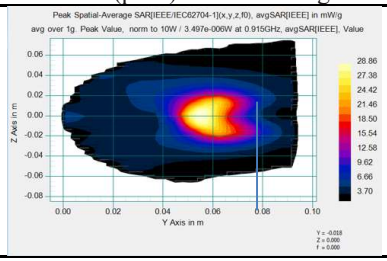	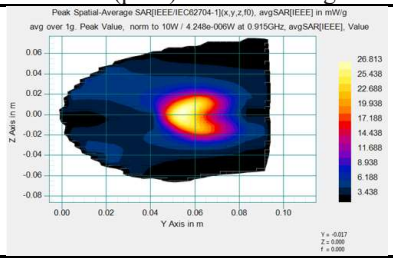
	SD:46.5 mm ID: 71.7mm SAR (peak) = 24.667mW/g	SD:46.7mm ID: 72mm SAR(peak)= 28.86mW/g	SD:46.2mm ID: 70.6mm SAR(peak) = 26.813mW/g
T3	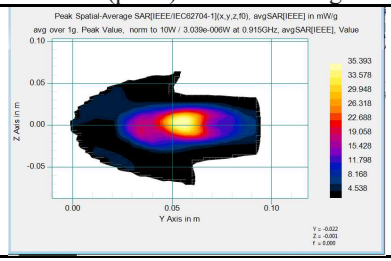	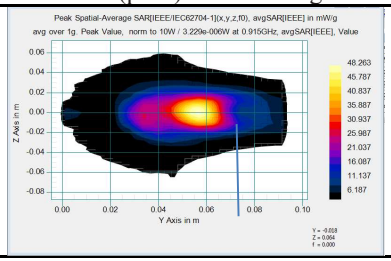	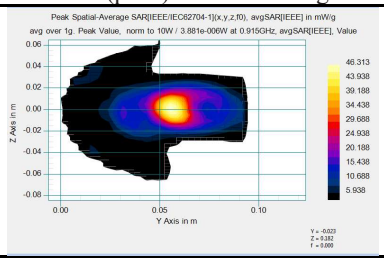
	SD:42.6mm to 67mm SAR(peak) = 35.393mW/g	FPD 40mm to 70 mm SAR(peak) = 48.263mW/g	FPD 46mm-66mm SAR(peak) =46.313mW/g

Figure 4.6: SAR distribution in rectangular, E-slot and U-slot applicator

The SAR (peak) represents the maximum localized heat absorption within the tumor subsequently analysed. Figure 4.7 illustrates the SAR (peak) in the rectangular microstrip, E-slot and U-slot designs under T1, T2 and T3 conditions.

In T1, the rectangular microstrip design, SAR (peak) is 5.1578mW/g; for the U-slot, SAR (peak) is 7.9072 mW/g and for the E-slot, it is 9.4283 mW/g. In T2, rectangular microstrip SAR (peak) is 24.667mW/g, 26.8130 mW/g for the U-slot and 29.3000 mW/g for the E-slot. In T3, the SAR (peak) is 35.3930 mW/g, 40.1700 mW/g and 47.2870 mW/g for rectangular microstrip, U-slot, and E-slot designs, respectively.

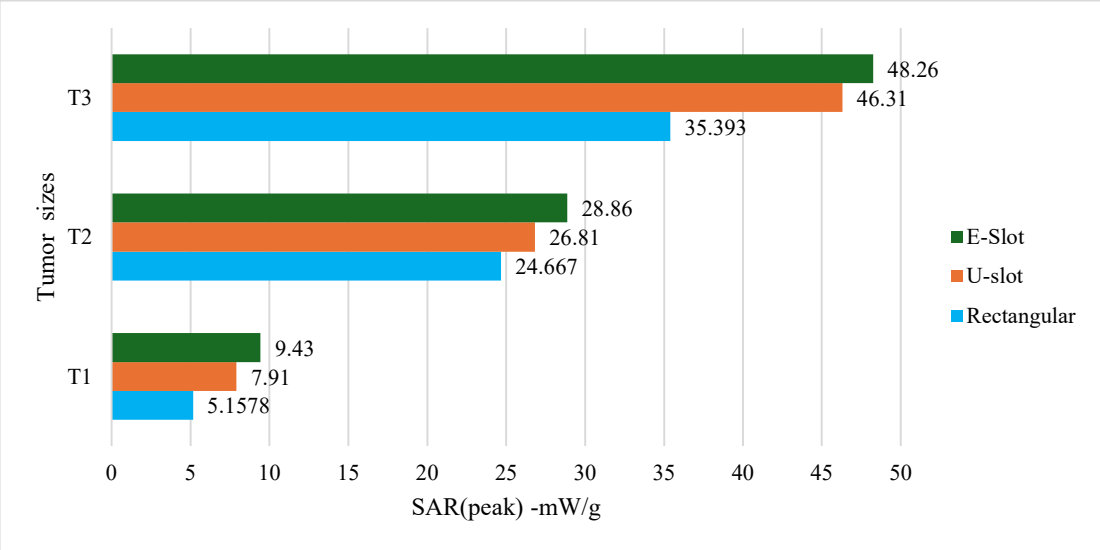

Figure 4.7: SAR(peak) in E-slot, U-slot and rectangular applicator

Overall, the rectangular microstrip design exhibits the lowest SAR(peak) and the highest SAR(peak) is in the E-slot design. As explained before, SAR (peak) influences the time duration of hyperthermia treatment. Therefore, the highest SAR (peak) should be considered to minimize the time duration of hyperthermia treatment.

For further analysis, applicator performance was evaluated in terms of directivity,

gain, and return loss. The directivity performance for three applicator structures: rectangular microstrip, U-slot and E-slot applicator across T1, T2 and T3 is presented in Figure 4.8. Directivity measures radiation intensity, which means radiation power at a specific location expressed in dBi. Higher directivity indicates more efficient transmission in a specific direction, which in this research refers to the transmission of energy to tumors.

In the T1 condition, the directivity of the rectangular microstrip, U-slot and E-slot applicator is 6.1333dBi, 6.9471dBi and 7.1415dBi, respectively. In T2, the rectangular microstrip applicator has a directivity of 6.4594dBi, the U-slot is 7.1456dBi and the E-slot is 7.3110dBi. In T3, the directivity is 6.8055dBi, 7.1672dBi and 7.3408dBi in the rectangular microstrip, U-slot and E-slot, respectively.

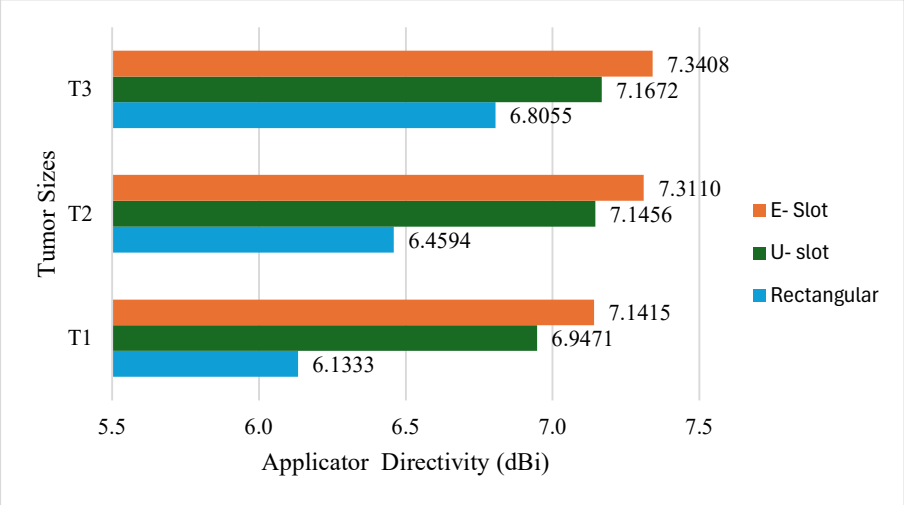

Figure 4.8: Directivity of E-slot, U-slot and rectangular applicator

The E-slot applicator consistently exhibits higher directivity across all the findings. The U-slot also has high directivity, but it is slightly lower than the E-slot. The rectangular microstrip applicator consistently shows the lowest directivity. In this research, the

rectangular microstrip applicator is less desirable because it provides less focused radiation on the tumor. The results show that by integrating E or U-slot into the microstrip applicator, the directivity improves. This finding is supported by (Dargar et al., 2022; Deshmukh & Ray, 2013; Pragati et al., 2023; S. Sharma & Tipathy, 2020).

The directivity improvement for the E-slot is about 16%, whereas the U-slot achieves about 13% in T1 conditions. Meanwhile, in T2, the E-slot demonstrates 13.2% and outperforms the U-slot at 10.6%. Similar to T3, the E-slot records 7.9%, while the U-slot shows 5.31%. These results confirm that the E-slot applicator has better directivity enhancement under T1, T2 and T3 conditions. The percentage is calculated using the rectangular microstrip applicator as the baseline, % directivity improvement (DI) as shown in Equation 4.1.

$$DI = \frac{directivity\ (E-slot) - directivity(rectangular)}{directivity(rectangular)} x100\% \qquad \text{Equation 4.1}$$

The applicator gain is subsequently analyzed. The graph in Figure 4.9 shows the applicator gain on three applicator designs: rectangular microstrip, U-slot and E-slot applicator. The higher gain indicates better applicator performance. In the T1 condition, the applicator gains are 3.8573 dBi, 4.4348 dBi and 4.4925 dBi for rectangular microstrip, U-slot, and E-slot, respectively.

In the T2 condition, the gain in the rectangular microstrip is 4.2976dBi, 4.6686dBi for the U-slot and 4.7318dBi for the E-slot. In the T3 condition, the gain is 4.9801dBi, 5.0955dBi and 5.1360 dBi for the rectangular microstrip, E-slot and U-slot, respectively. The findings show that E-slot and U-slot significantly improve applicator gain compared to a rectangular microstrip design. However, the E-slot design shows a slightly higher gain than

the U- slot design.

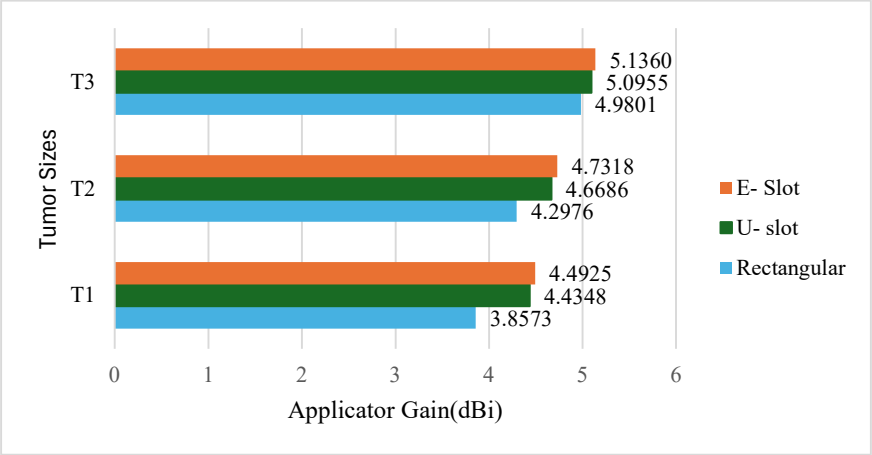

Figure 4.9: Gain of E-slot, U-slot and rectangular microstrip applicator

The E-slot applicator improves by about 16.5%, while the U-slot records 14.9% in T1 conditions. In T2, the E-slot gain attains 10%, outperforming the U-slot gain by 8.6%. Likewise, in T3, the E-slot gain is 3.2%, while the U-slot gain is 2.32%. The gain improvement was evaluated with the rectangular microstrip applicator set as the reference. This finding established that the E-slot has a higher gain than the U-slot.

In addition to improving performance, impedance matching in the applicator was examined from return loss analysis. The graph displayed in Figure 4.10 compares the return loss of rectangular microstrip, U-slot and E-slot designs. Return loss is a critical parameter in applicatora design and performance evaluation. It represents the power reflected back to the source due to impedance mismatches. A lower value indicates better impedance matching and more efficient power transfer.

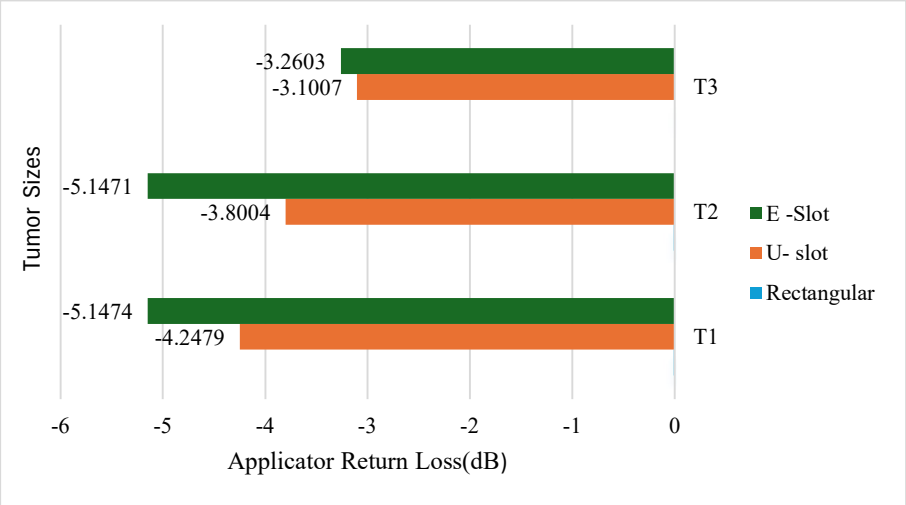

Figure 4.10: Return Loss of E-slot, U-slot and rectangular microstrip applicator

The rectangular microstrip design is not included in this graph because the value is very small: -0.00643dB, -0.00617dB and -0.00529dB for T1, T2 and T3, respectively. The E-slot consistently shows low return loss in all conditions: T1 with -5.1474 dB, T2 with -5.1471 dB and -3.2603 dB for T3. In contrast, the U-slot design demonstrates return loss at -4.2479dB, -3.8004dB and -3.1007dB under T1, T2 and T3, respectively.

Both SD and ID for all applicator designs, rectangular microstrip, E-slot, and U-slot, did not achieve the desired values except for T1 inner depth, as depicted in Figures 4.11 and 4.12. The variations in SD and ID observed across T1 to T3 tumors are due to differences in tumor size.

Although the SD and ID have not yet reached the desired values, the overall applicator performance, including directivity, gain and return loss, has improved. Therefore, further optimization of the E-slot design is considered to enhance PD while maintaining unwanted hotspots in surrounding healthy tissue. The explanation of E-slot optimization is provided in Section 4.2.7.

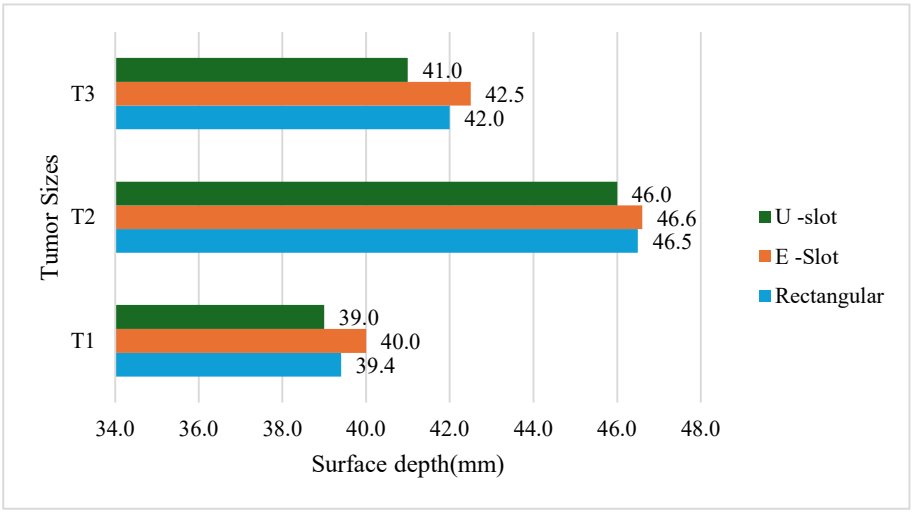

Figure 4.11: Comparison of SD of E-slot, U-slot and rectangular microstrip applicator

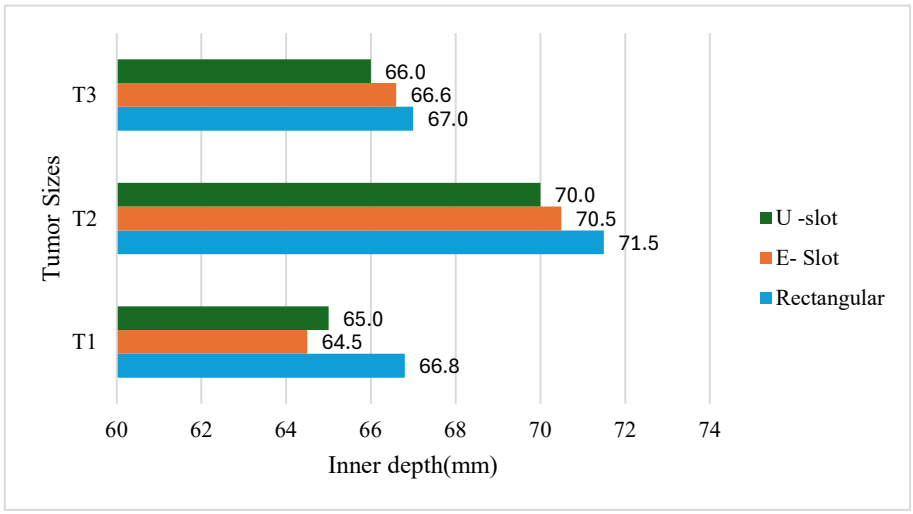

Figure 4.12: Comparison of ID of E-slot, U-slot and rectangular microstrip applicator

Overall, the E-slot and U-slot applicators improve both the SAR distribution localization and the applicator performance. The SAR distribution indicates both E-slot and U-slot achieve more uniform and localized heat within the tumor region compared to the rectangular microstrip applicator. The E-slot and U-slot significantly enhance applicator

performance. However, the E-slot design exhibits a minimum return loss, indicating that it is significantly better than the U-slot for this research.

In addition, E-slot applicator shows superior directivity, gain and return loss. These parameters influence the effectiveness of applicator performance and enhance EM heat delivery to tumor region.

The results are consistent with previous findings, thereby supporting the validity of this research. Previous studies have reported that integrating the E-slot with the applicator improved its performance and effectiveness, especially in directivity, gain and return loss (Deshmukh & Ray, 2013; Pragati et al., 2023; Suganya et al., 2023; Umamaheswari et al., 2023).

Therefore, the E-slot applicator is identified as a suitable design for effective hyperthermia treatment in this research and selected for further enhancement and optimization.

4.2.5 Distance Breast Phantom to E-slot Applicator

The distance from the breast phantom to the applicator varies to find the optimized distance. Appendix E lists the characteristics of the E-slot applicator under T1, T2 and T3 conditions, with distances varying from 0 to 20 mm. The optimized distance is determined by achieving effective tumor heating with minimal unwanted hotspots in healthy tissue, as indicated by SAR distribution. Meanwhile, SD and ID were then extracted from the SAR distribution. The optimal heat region depends on SD and ID, which are close to the desired value of SD and ID.

The SAR distribution is affected as the distance between the applicator and the breast

phantom increases. For instance, in T1, the unwanted hotspot reduces as the distance between the applicator and the breast phantom increases. The heat dissipates to the anterior portion of the breast at a distance of 0-10 mm. However, the findings show that heat focuses more on the tumor at a distance of 15 mm to 20 mm

In T2 and T3 the heat concentrates more on the tumor as the distance increases. The results indicated that 15 mm and 20 mm distances show the optimal heat concentration on the tumor.

The analysis is conducted for SD and ID based on the SAR distribution, as shown in Figures 4.13 and 4.14. The findings show that the distance between the applicator and the breast phantom influences both SD and ID. As the distance increases between the breast phantom and the applicator, the EM wave propagation from the applicator to the tissue becomes longer because it travels in air before interacting with the breast phantom. Consequently, SAR distribution is affected.

For T1, the tumor is small and located at a depth ranging from 50mm (Ymin) to 64mm (Ymax) from the skin surface. As propagation increases, EM penetration limits energy delivery in this tumor region. As a result, the SD and ID are decreasing due to reduced penetration capability.

In contrast, T2 and T3 tumors exhibit an increase in SD and ID with an increased distance between the applicator and breast phantom. The optimal heat region is based on SD, ID and also the localization of heat distribution, with minimal effect on surrounding healthy tissue. The tumors are large, with a depth range of (Ymin to Ymax) 48-80mm for T2 and 28-90mm for T3. In addition, the tumor exhibits higher water content than healthy tissue,

leading to increased dielectric properties and enhanced EM energy absorption as mentioned in (Vaupel & Piazena, 2022).

Therefore, the EM energy absorption increases in the tumor region and contributes to broader SAR distribution. Consequently, both SD and ID increase with increasing breast phantom-to-applicator distance. The distance between the breast phantom and the applicator significantly affects the PD. This finding is supported and validated by (Sarestoniemi et al., 2019).

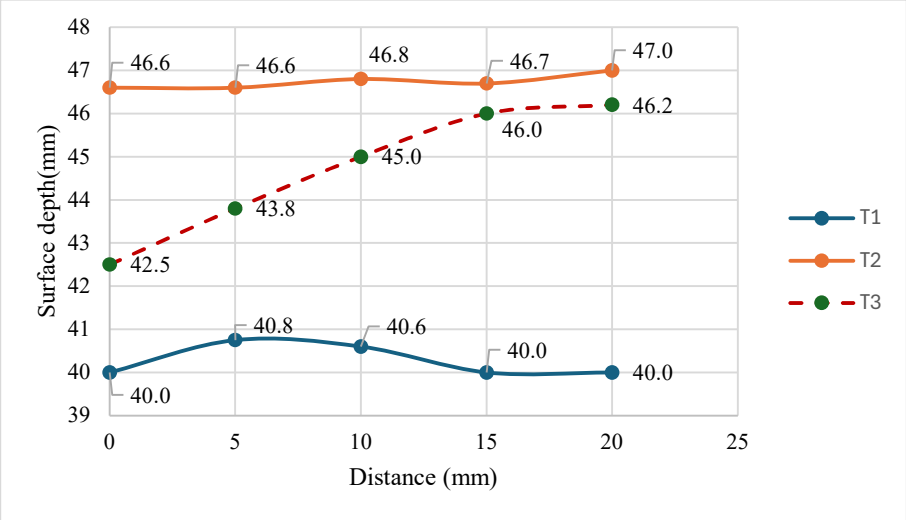

Figure 4.13: Relationship of SD and distance of breast phantom to applicator

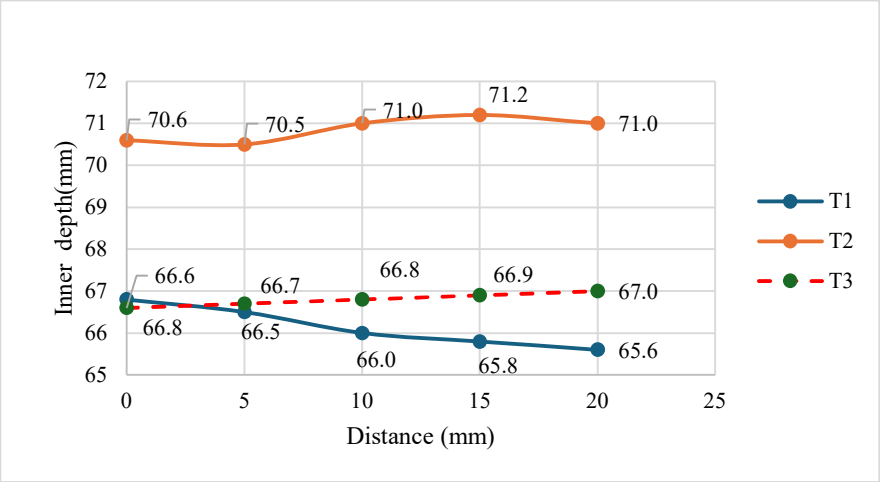

Figure 4.14: Relationship of ID and distances of breast phantom to applicator

Figure 4.15 depicts the relationship between SAR (peak) and the distance between the applicator and the breast phantom. As the distance increases, SAR (peak) decreases. This finding is consistent with a previous study (Luna et al., 2014) (Kumari et al., 2020)(Rajput et al., 2021) which reported that SAR decreases as the distance between the breast phantom and the applicator increases.

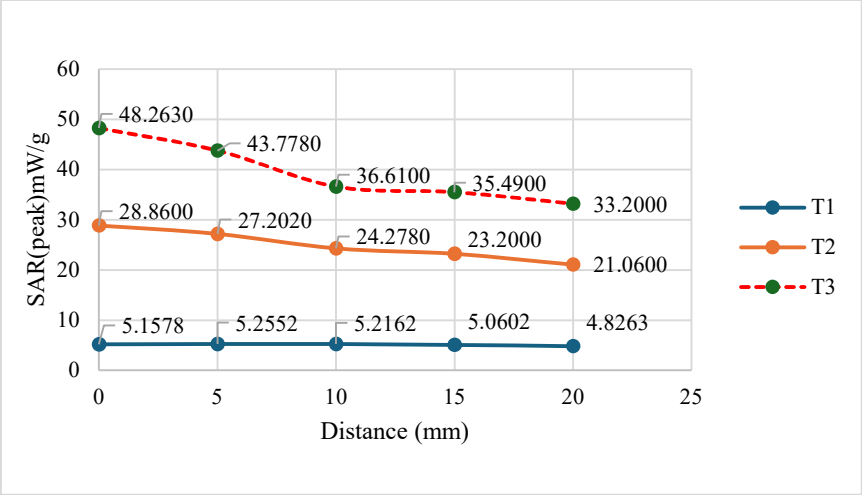

Figure 4.15: SAR (peak) and distance of breast phantom to applicator.

The selection of appropriate distances in this research is based on SAR(peak) and SAR distribution. The findings above indicate that distances of 15 mm and 20 mm are suitable. It shows that heat is focused more on the tumor and the unwanted hotspot is reduced in the healthy tissue.

However, the SAR(peak) of the breast phantom and applicator at 20 mm is smaller than at 15 mm. As mentioned earlier, SAR(peak) is associated with treatment time duration. Therefore, the appropriate distance in this research is 15 mm. The next part elaborates on the effects of modifying horizontal and vertical lengths and thicknesses.

4.2.6 Modification of E-Slot Applicator

The modification is performed to determine the potentially significant segment dimensions of the E-slot applicator: horizontal length, vertical length, horizontal thickness and vertical thickness. The significant segment dimensions are determined based on the analysis findings of the modification segment dimensions, where SD and ID were observed for each tumor size (T1, T2, and T3. The corresponding segments and datasets are summarized in Tables 4.1- 4.6.

Table 4.1: Dataset for horizontal length under T1 condition

Horizontal	Horizontal length (mm)	Remarks
Upper	93 to 43	T1
Middle	93 to 73	
Bottom	93 to 53	

Table 4.2: Dataset for vertical thick under T1 condition

Vertical thick (mm)	Remark
6 to 12	T1

Table 4.3: Dataset for horizontal length under T2 condition

Horizontal	Horizontal length (mm)	Remarks
Upper	93 to 43	T2
Middle	193 to 53	
Bottom	93 to 43	

Table 4.4: Data set for vertical thick under T2 condition

Vertical thick (mm)	Remark
6 to 12	T2

Table 4.5: Data set for horizontal length under T3 condition

Horizontal	Horizontal length (mm)	Remarks
Upper	93 to 43	T3
Middle	93 to 53	
Bottom	93 to 43	

Table 4.6: Data set for vertical thick under T3 condition

Vertical thick (mm)	Remark
30 to 36	T3

The following section explains slot optimization using Design Expert software. The datasets are inserted into the design experiment to perform optimization.

4.2.7 Optimization E-slot Applicator Dimension

RSM is a statistical, theoretical and mathematical technique for constructing a model that represents the relationship between factors and response. It is also a statistical method that effectively optimizes a model (Yang et al., 2022) as explained in section 2.18.

The mathematical model is generated based on experimental design. Design Expert is a statistical software used to execute the experimental design with RSM in this research. Box Behnken design (BBC) is used in RSM (Lee et al., 2016) for further optimization under T1,T2 and T3 conditions.

4.2.7.1 Optimization of E-slot Applicator under T1 condition

The results recorded in section 4.2.6 show that the significant factors for optimization are horizontal length: upper (A), middle (B), bottom (C) and vertical thickness, (D) as these parameters significantly affect SD and ID. The optimization process only considers these significant parameters.

The design experiment is conducted at two levels (low and high) for each significant factor, as stated in (Shinde & Shinde, 2016) Table 4.7 presents a series of experimental

designs, which were analyzed with Design Expert 11 software. Factor 1to factor 4 as design parameters for the responses SD and ID. The experimental design is then simulated using SEMCAD X.

Mathematical equations are used to model and represent the response behaviour. The second-order polynomial response models are mathematically represented as in Equation 4.2 (Chen et al., 2023)

$$Y = \beta_0 + \sum_{i=1}^{k} \beta_i X_i + \sum_{i=1}^{k} \beta_{ii} X_i^2 + \sum_{i=1}^{k-1} \sum_{j>1}^{k} \beta_{ij} X_i X_j \quad \text{Equation 4.2}$$

Where Y is the responses (output), β_0 is the intercept coefficient, β_i is a linear coefficient, β_{ii} is the quadratic coefficient, β_{ij} is the interaction coefficient between X_i and X_j.

Table 4.7: Experimental design: T1

	Factor 1	**Factor 2**	**Factor 3**	**Factor 4**	**Response 1**	**Response 2**
Run	**A:Upper**	**B: middle**	**C: bottom**	**D: Ver Thick**	**SD**	**ID**
	mm	**mm**	**mm**	**mm**	**mm**	**mm**
1	43	83	93	9	38.5	63
2	68	83	53	12	42.2	66.5
3	93	93	73	9	39.5	64
4	43	83	53	9	39.5	66.6
5	43	83	73	12	39	63
6	68	93	73	12	41	63
7	93	83	73	6	39.5	64.2

Table 4.7 continued

8	68	93	93	9	40	63.5
9	68	93	53	9	40.8	66.9
10	68	83	73	9	40.3	64
11	68	83	93	6	41.5	63.5
12	43	83	73	6	41	63.1
13	93	73	73	9	39.2	64.8
14	43	73	73	9	39	63.6
15	68	83	73	9	40.2	64
16	68	73	93	9	40	63.6
17	68	83	53	6	41.5	66
18	68	73	73	12	41	63.5
19	68	83	73	9	40.3	64
20	68	73	53	9	40.7	67
21	93	83	73	12	41	64
22	68	83	93	12	40.6	62.5
23	93	83	53	9	40	67.7
24	43	93	73	9	39	63.5
25	93	83	93	9	39	64
26	68	73	73	6	41.5	63.9
27	68	93	73	6	41.4	63.5

The reduced quadratic model is shown in Equations 4.3 and 4.4. These equations relate the independent variables to the responses (Surface depth-SD and Inner depth-ID).

$$SD=47.1006+0.1462A-0.0130C-2.3594D+0.0117AD+0.0067CD-0.0018A^2+0.0004C^2+0.11162D^2 \quad \text{Equation 4.3}$$

$$ID=74.0310+0.0778A+0.0309B-0.4705C+1.4986D-0.0007AB-0.0063CD+0.0030C^2-0.0605D^2 \quad \text{Equation 4.4}$$

The adequacy of the RSM model is evaluated using analysis of variance (ANOVA) and residual analysis. Statistical parameters such as lack of fit, correlation coefficient (R^2), adjusted R^2 and predicted R^2 were compared to select the best-fitting polynomial, as explained in (Margaret & Manimegalai, 2018).

Tables 4.8 and 4.10 display the ANOVA analysis results for the responses SD and ID, respectively. Meanwhile, Tables 4.9 and 4.11 present the summary of fit statistics for SD and ID, respectively.

Table 4.8: ANOVA for reduced Quadratic model of SD: T1

Source	Sum of Squares	df	Mean Square	F-value	p-value
Model	24.76	8	3.10	257.16	< 0.0001
A-upper	0.4033	1	0.4033	33.51	< 0.0001
C-bottom	2.17	1	2.17	180.07	< 0.0001
D-vertical thick	0.2133	1	0.2133	17.72	0.0005
AD	3.06	1	3.06	254.42	< 0.0001
CD	0.6400	1	0.6400	53.17	< 0.0001
A^2	7.54	1	7.54	626.20	< 0.0001
C^2	0.1204	1	0.1204	10.00	0.0054
D^2	6.05	1	6.05	502.62	< 0.0001
Residual	0.2167	18	0.0120		
Cor Total	24.98	26			

Table 4.9: Summary of fit statistics for reduced Quadratic model of SD: T1

Fit Statistics	Value
R^2	0.9913
Adjusted R^2	0.9875
Predicted R^2	0.9766
Adeq Precision	54.0706

Table 4.10: ANOVA for reduced quadratic model of ID: T1

Source	Sum of Squares	df	Mean Square	F-value	p-value
Model	53.16	8	6.64	351.95	< 0.0001
A-upper	2.90	1	2.90	153.65	< 0.0001
B-middle	0.3333	1	0.3333	17.66	0.0005
C-bottom	35.36	1	35.36	1873.13	< 0.0001
D-vertical thick	0.2408	1	0.2408	12.76	0.0022
AB	0.1225	1	0.1225	6.49	0.0202
CD	0.5625	1	0.5625	29.79	< 0.0001
C^2	9.49	1	9.49	502.67	< 0.0001
D^2	1.90	1	1.90	100.61	< 0.0001
Residual	0.3398	18	0.0189		
Cor Total	53.50	26			

Table 4.11: Summary of fit statistic for reduced Quadratic model of ID :T1

Fit Statistics	Value
R^2	0.9936
Adjusted R^2	0.9908
Predicted R^2	0.9821
Adeq Precision	62.8580

The results show that the experimental data are well represented by a quadratic polynomial model, with coefficient of determination (R^2) values of 0.9913 for SD and 0.9936 for ID. The R^2 measures model accuracy in predicting SD and ID. In addition, the value of R^2 close to 1 indicates that the model fits the data better, as discussed in (Ayalew & Asmare, 2022).

Furthermore, both models show reasonable agreement, as the difference between the predicted R^2 and adjusted R^2 is less than 0.2. The small mean-squared residuals in both models indicate good model fit and high prediction accuracy. Additionally, the precision is 62.858, indicating an adequate signal. The signal-to-noise ratio measures adequate precision; a value greater than 4 is desirable.

ANOVA analysis assesses the statistical significance of the RSM polynomial model describing the relationship between selected input parameters and the response variables (SD and ID). The ANOVA results indicate that the RSM polynomial models for both SD and ID are statistically significant, with p-values <0.05. This confirms that both the SD and ID RSM polynomial models are statistically valid and reliable for prediction and subsequent optimization, as proven by (Pereira et al., 2021).

The next step is residual analysis, which examines the differences between the actual and predicted SD and ID values in the model. Model adequacy is confirmed when residuals follow an approximately normal distribution and are randomly scattered around zero, indicating that prediction errors are normal and random, and the model fits the data well.

Figure 4.16 (a) and (b) display the normal plot of residuals in SD and ID used in residual analysis. Residual analysis is assumed to follow a normal distribution. This assumption is confirmed in both plots, as all points align along a straight line, indicating a

normal distribution of residuals.

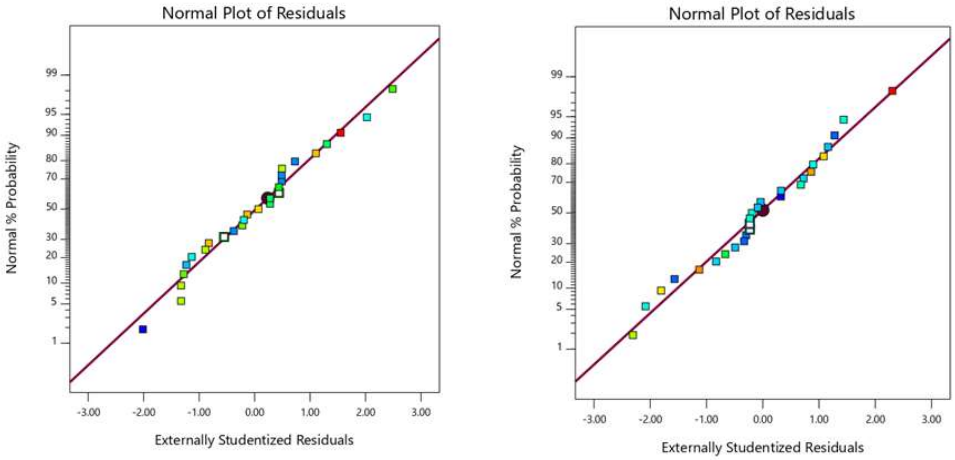

(a) (b)

Figure 4.16: Residual normal probability plot of (a) SD and (b) ID: T1

The other plots in Figure 4.17 (a) and (b) show residual vs run. Both provide information about the model's fitness. The model achieved optimal fit when the residual oscillated randomly around the residual = 0 line, indicating that the model is suitable, as suggested by (Margaret & Manimegalai, 2018). After residual analysis, the next procedure is optimization.

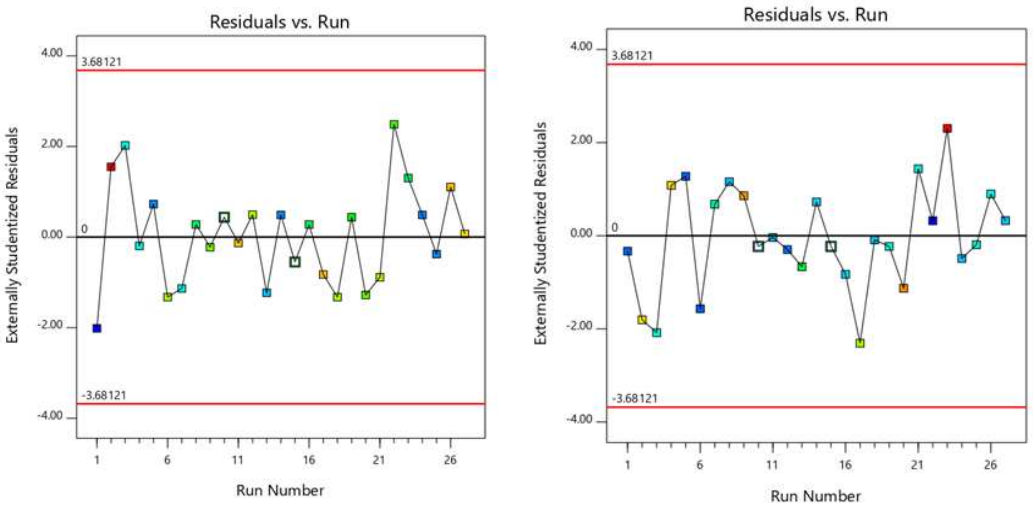

(a) (b)

Figure 4.17: Residual vs Run plot of (a)SD and (b) ID: T1

Numerical optimization was used to optimize the E-slot applicator by setting certain criteria, as listed in Table 4.12.

Table 4.12: Optimization setting criteria:T1

Design parameters/factors	Goal	Lower limit(mm)	Upper limit (mm)
Upper	In range	43	93
Middle	In range	73	93
Bottom	In range	53	93
Vertical thick	In range	6	12
SD	In range	38.5	42.2
ID	In range	62.8	69

Figure 4.18 shows the optimization graph that suggests the optimum values for upper, middle, bottom, vertical thickness, SD and ID. The proposed optimized design for the E-slot is upper (A) =80 mm, middle (B) =93 mm, bottom (C) =71 mm and vertical thickness (D) =6 mm. The predicted SD and ID values are 40.8 mm and 63.8 mm, respectively.

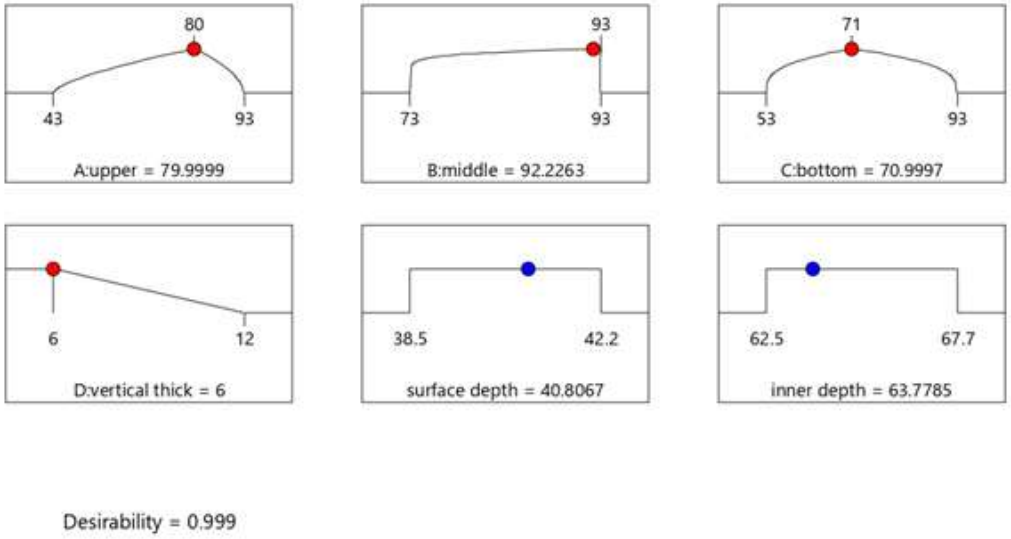

Figure 4.18: Optimization of numerical graph: T1

Design Expert software uses numerical optimization (desirability function), *d* to identify the best (optimize) slot dimension. Simultaneous optimization techniques use the desirability function when multiple responses are considered. The desirability function d is in the range $0 \leq d \leq 1$.

A value of $d=1$, which means the response reaches the desired target, while $d=0$, a response outside the acceptable range. A *d* value is 1, which means the response reaches the desired target, while $d=0$, a response outside the acceptable range (Margaret & Manimegalai, 2018).

The desirability for the E-slot optimization design is 0.999, close to 1, indicating that

all design parameters/factors meet the desired outcome. Finally, all the individual desirability are combined using the geometric mean to optimize the overall desirability, $D.D = (d_1 x d_2 x \ldots . d_m)(d_1 x d_2 x \ldots . d_m)^{\frac{1}{m}}$, where m = number of responses (Li et al., 2008).

Figure 4.19 demonstrates the design of the optimized E-slot applicator validated with SEMCAD X. The horizontal upper length (A) is 80 mm, 93 mm in the middle (B) and 71 mm in the bottom (C), while the vertical thickness (D) is 6mm.

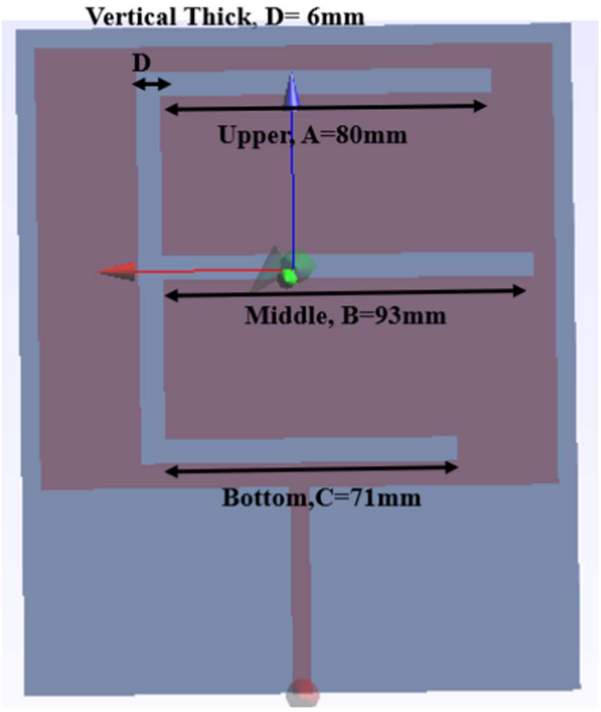

Figure 4.19: Optimized E-slot design: T1

The experimental results are based on simulations and then compared with the predicted values from Equation 4.5. There are 3 experiments run to validate the output. The percentage error for SD is 1.225%, while it is 0.47% for ID. The results are detailed in Table 4.13.

$$\text{Error}(\%) = \left| \frac{predict\ value - Experiment\ value}{predict\ value} \right| \qquad \text{Equation 4.5}$$

Table 4.13: Results validation: T1

No of Exp	SD(mm)			ID (mm)		
	Experiment	**Predict**	**Error (%)**	**Experiment**	**Predict**	**Error (%)**
1	40	40.8	1.961	64	63.8	0.313
2	41	40.8	0.490	64.2	63.8	0.627
3	41.3	40.8	1.225	64.1	63.8	0.470
		% error, E_{avg}	1.225		% error, E_{avg}	0.47

After validating the E-slot optimization results, the next procedure is post-analysis, as shown in Tables 4.14 and 4.15. Table 4.14 provides the results of SD and ID.

Table 4.14: Post analysis: optimization E-slot applicator: T1

Upper(mm)	Middle(mm)	Bottom(mm)	vertical thick(mm)
80	93	71	6
SD(mm)		**ID(mm)**	
40		64	
41		63.5	
41.3		64.1	

Table 4.15 presents a detailed statistical summary of SD and ID obtained from three repeated simulation experiments. Based on three repeated experiments, the mean of SD is 40.7667 mm, closely aligned with the predicted SD value of 40.8067 mm ~40.8 mm. The 95% Prediction Interval (PI) low is 40.6279 mm, and the 95% PI high is 40.9856 mm. The experimental values are near the predicted SD, indicating that the SD model is reliable and well-fitted.

The data mean ID from three (3) repeated experiments is 63.8667mm, compared to the predicted mean of 63.7591 mm to 63.8 mm. The experimental value is close to the predicted ID. In ID, the predicted mean of 63.5211 mm is within 95% PI low and 63.9971 mm is within 95% PI high.

The predicted SD and ID are confirmed to be reliable, as they fall within their respective 95% PI, which means the future measurement is expected to be 95% confident.

Table 4.15: Confirmation of SD and ID: T1

Response	SD	ID
Predicted Mean(mm)	40.8067	63.7591
Predicted Median(mm)	40.8067	63.7591
Std Dev	0.109713	0.137402
n	3	3
Standard Error Pred	0.085132	0.113288
95% Predicted Interval(PI) low(mm)	40.6279	63.5211
Data Mean(mm)	40.7667	63.8667
95% Predicted interval(PI) high(mm)	40.9856	63.9971

The coefficient table in Table 4.16 clearly shows that different factors affect SD and ID, enabling better process control and optimization. Thus, the significant factors that affect SD are upper length (A), bottom length (C), vertical thickness (D), combination of upper length and vertical thick (AD), bottom length and vertical thickness (CD), quadratic term: upper length (A^2), bottom length (C^2) and vertical thickness (D^2).

Meanwhile, the significant factors that affect ID are upper length(A), middle length (B), bottom length (C), vertical thick (D), combination of upper length and middle length (AB), bottom length and vertical thick (CD), quadratic term: upper length (A^2), bottom length (C^2) and vertical thick (D^2)

Table 4.16: Coefficient table: T1

	SD	**p-values**	**ID**	**p-values**
Intercept	40.2556		64.0306	
A	0.183333	<0.0001	0.491667	<0.0001
B			-0.166667	0.0005
C	-0.425	<0.0001	-1.71667	< 0.0001
D	-0.133333	0.0005	-0.141667	0.0022
AB			-0.175	0.0202
AD	0.875	< 0.0001		
CD	-0.4	< 0.0001	-0.375	< 0.0001
A^2	-1.12083	< 0.0001		
C^2	0.141667	0.0054	1.21771	<0.0001
D^2	1.00417	<0.0001	-0.544792	<0.0001

4.2.7.2 Optimization of E-slot Applicator under T2 condition

The E-slot applicator optimization process in T2 follows the same steps as in T1. The experimental design dataset with 2-level factorials listed in Table 4.17 is statistically analysed using Design-Expert 11 software. The experiment design is simulated with SEMCAD X.

Two-level factorial designs mean that each factor (independent variable) is set to two levels: low and high, as presented in Tables 4.3 and 4.4. RSM was implemented in Design-Expert 11, with factors 1 to 4 defined as design parameters and SD and ID as responses.

Table 4.17: Design experiment: T2

Run	Factor 1	Factor 2	Factor 3	Factor 4	Response 1	Response 2
	A:Upper	B:Middle	C:Bottom	D:Ver Thick	SD	ID
	mm	mm	mm	mm	mm	mm
1	68	93	68	12	47.2	69.5
2	68	53	68	12	47.5	69.5
3	43	93	68	9	47	69.4
4	43	73	43	9	47	71
5	43	73	68	6	47.1	69
6	68	73	93	12	47.2	69.5
7	68	93	43	9	46.7	73.3
8	93	73	68	12	47.2	70.2
9	68	73	68	9	47.1	71.5
10	93	53	68	9	48.3	68.2
11	93	93	68	9	47	71.5

Table 4.17 continued

12	68	73	43	6	47	72.1
13	68	53	43	9	47	72
14	68	93	68	6	47.1	70
15	93	73	43	9	47.8	73
16	68	53	68	6	48.1	68.8
17	93	73	68	6	47	70.5
18	68	73	43	12	48.3	73.3
19	68	73	68	9	47.1	71.5
20	93	73	93	9	47	71
21	43	53	68	9	47.2	71
22	43	73	93	9	47	68
23	68	93	93	9	47.2	69
24	68	73	68	9	47.1	71.5
25	68	53	93	9	48	68.2
26	68	73	93	6	47.2	69.2
27	43	73	68	12	48	68.5

A reduced cubic model is used because it includes only significant factors, as shown in Equations 4.5 and 4.6. These equations relate the independent variables to the responses (Surface depth-SD and Inner depth-ID).

$$SD=50.2544 -0.0741A+0.0842B-0.3836C - 4.4629D - 0.0006AB- 0.0003AC+ 0.0347AD-0.0088BC+0.0546BD-0.0043CD- 0.0005B^2+0.162D^2-0.0021AD^2+0.00006B^2C-0.0004B^2D \quad \text{Equation 4.6}$$

$$ID=97.8158-0.5824A–0.9691B–0.066C+2.1167D+0.020AB-0.0014A^2+0.0056B^2-0.1162D^2-0.0001AB^2 \quad \text{Equation 4.7}$$

The reliability of the RSM model is evaluated by Analysis of variance (ANOVA) and residual analysis. Tables 4.18 and 4.20 present the ANOVA analysis for the responses of SD and ID, respectively. Meanwhile, Tables 4.19 and 4.21 present the summary of fit statistics for SD and ID, respectively.

Table 4.18: ANOVA for reduced cubic model of SD: T2

Source	Sum of Squares	df	Mean Square	F-value	p-value
Model	5.12	15	0.3416	30.68	< 0.0001
A-Upper	0.4513	1	0.4513	40.52	< 0.0001
B-Middle	1.27	1	1.27	113.82	< 0.0001
C-Bottom	0.3612	1	0.3612	32.44	0.0001
D-Vertical Thick	0.7200	1	0.7200	64.65	< 0.0001
AB	0.3025	1	0.3025	27.16	0.0003
AC	0.1600	1	0.1600	14.37	0.0030
AD	0.1225	1	0.1225	11.00	0.0069
BC	0.0625	1	0.0625	5.61	0.0372
BD	0.1225	1	0.1225	11.00	0.0069
CD	0.4225	1	0.4225	37.94	< 0.0001
B^2	0.1000	1	0.1000	8.98	0.0122
D^2	0.2560	1	0.2560	22.99	0.0006
AD^2	0.5704	1	0.5704	51.22	< 0.0001

Table 4.18 continued

B^2C	0.9204	1	0.9204	82.65	< 0.0001
B^2D	0.4817	1	0.4817	43.25	< 0.0001
Residual	0.1225	11	0.0111		
Cor Total	5.25	26			

Table 4.19: Summary of fit statistic for reduced cubic model of SD: T2

Fit Statistics	Value
R^2	0.9767
Adjusted R^2	0.9448
Predicted R^2	0.8408
Adeq Precision	18.3108

Table 4.20: ANOVA for reduced cubic model of ID: T2

Source	Sum of Squares	df	Mean Square	F-value	p-value
Model	61.05	9	6.78	25.66	< 0.0001
A-Upper	8.41	1	8.41	31.79	< 0.0001
B-Middle	2.08	1	2.08	7.88	0.0121
C-Bottom	32.67	1	32.67	123.56	< 0.0001
D-Vertical Thick	0.0675	1	0.0675	0.2553	0.6199
AB	6.00	1	6.00	22.70	0.0002
A^2	4.82	1	4.82	18.21	0.0005

Table 4.20 continued

B^2	6.10	1	6.10	23.07	0.0002
D^2	6.56	1	6.56	24.82	0.0001
AB^2	3.84	1	3.84	14.52	0.0014
Residual	4.49	17	0.2644		
Cor Total	65.55	26			

Table 4.21: Summary of fit statistic for reduced cubic model of ID: T2

Fit Statistics	Value
R^2	0.9314
Predicted R^2	0.8064
Adeq Precision	17.5754

It is observed that both experimental data (SD and ID) are significantly represented in a reduced cubic polynomial model. The coefficient of determination, R^2 is 0.9767 for SD and 0.9314 for ID. The R^2 measures model accuracy in predicting SD and ID. Furthermore, the value of R^2 close to 1 indicates that the regression line fits the data perfectly. The fit statistics are in reasonable agreement in both models. This is because the difference between predicted R^2 and adjusted R^2 is less than 0.2.

ANOVA analysis to confirm that both models are significant, which describes the relationship between selected input parameters and the response variable. Consequently, both proposed models have $p<0.05$, considered significant in predicting the output response as reported by (Pereira et al., 2021).

The residual mean squares of 0.0111 for SD and 0.2644 for ID represent the average squared differences between the predicted and simulated responses. The small residual mean square in both models (SD and ID) indicates low predictor error and good model fit.

Subsequently, residual analysis is performed by plotting the residuals against the fitted values. The difference between the response (actual value), Y and the fitted value (predicted value), $\hat{Y}$ is residual that is expressed as e=Y-$\hat{Y}$. The error assumes it follows a normal distribution. If the assumption is valid, the plot exhibits a straight line.

Figure 4.20(a) and (b) display the normal plot of residuals in SD and ID. It shows normal probability plots for both SD and ID. The straight line in the plots indicates that the normality assumption holds for both responses and that the model is good.

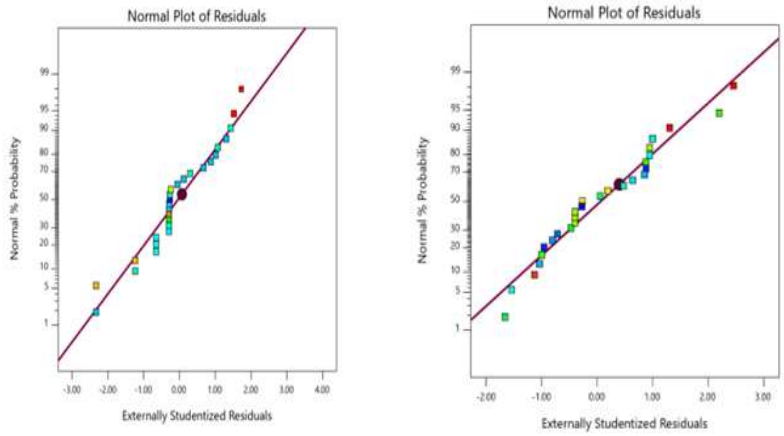

(a) (b)

Figure 4.20: Residual normal probability plot of (a) SD and (b) ID: T2

The other plots in Figure 4.21(a) and (b) show residual vs run. Both provide information about the model's fitness. Both models achieved optimal fit when the residual oscillated randomly around the residual line =0, which indicates that the models have the

best fit, as mentioned by (Margaret & Manimegalai, 2018). Therefore, both models suggest a well-distributed residual. After residual analysis, the next step is to optimize the E-slot applicator.

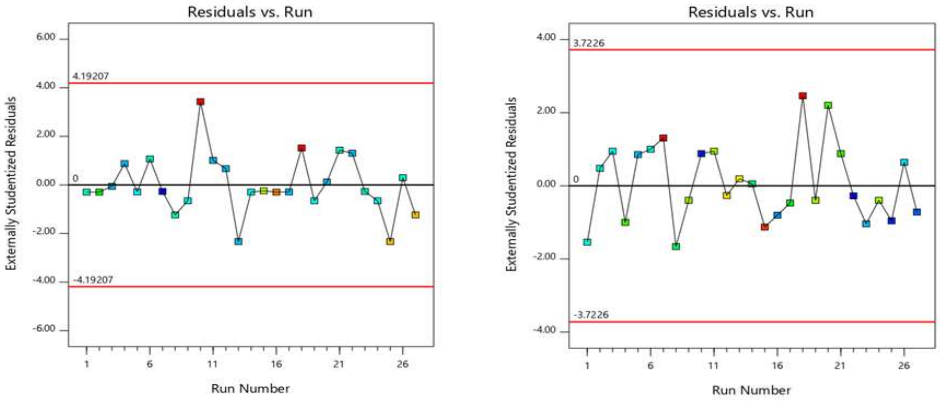

Figure 4.21: Residual vs Run of (a) SD (b) ID

The optimal dimension of the E-slot applicator aims to determine the best design to achieve or nearly achieve SD and ID with focused heating conditions to the tumor. The optimal condition is determined through optimization, thereby maximizing the value of the design parameters. A numerical method is employed for design optimization. The E-slot applicator was optimized numerically by setting the criteria listed in Table 4.22.

Table 4.22: Optimization setting criteria: T2

Design parameters/factors	Goal	Lower limit(mm)	Upper limit (mm)
Upper	In range	43	93
Middle	In range	53	93
Bottom	In range	43	93
Vertical thick	In range	6	12
SD	In range	46.7	48.3
ID	In range	68	72.3

A simultaneous optimization technique uses a desirability function when multiple responses are involved. Each design parameter is converted into an individual desirability function, *d*. The desirability function d is in the range $0 \leq d \leq 1$. A value of $d=1$, which means the response reaches the desired target, while $d=0$, a response outside the acceptable range. Finally, all the individual desirability are combined using the geometric mean to optimize the overall desirability, $D.D = (d_1 x d_2 x \ldots . d_m)(d_1 x d_2 x \ldots . d_m)^{\frac{1}{m}}$, where m = number of responses (Li et al., 2008).

Figure 4.22 shows the optimization graph indicating the optimal values for upper, middle, bottom, vertical thickness, SD and ID. The desirability for the E-slot optimization design is 0.960, which is close to 1, indicating that all the design parameters/factors meet the desired outcome. The proposed optimized design for E-slot is upper = 68 mm, middle = 87 mm, bottom =81 mm, and vertical thick = 9 mm. The predicted SD and ID values are 46.99 ~47 mm and 70.6 mm, respectively.

The optimized E-slot applicator is displayed in Figure 4.23. The horizontal length is upper (A) = 68 mm, middle(B) = 87 mm and bottom (C) =81 mm, while the vertical thickness (D) = 9 mm.

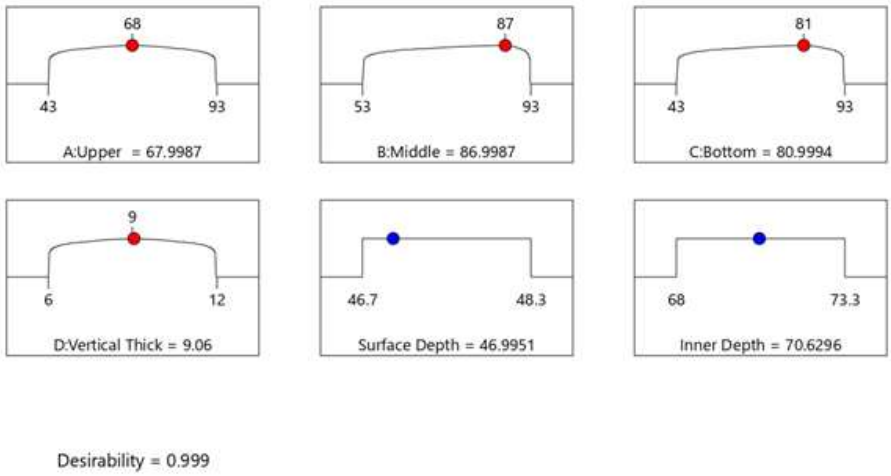

Figure 4.22: Optimization of numerical graph: T2

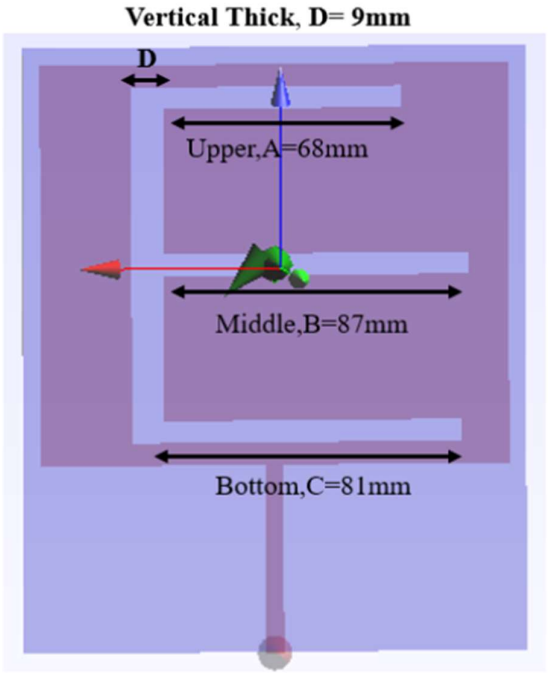

Figure 4.23: Optimize E-slot design: T2

The experimental results are based on simulations compared with the predicted value as expressed in Equation 4.5. Three experiments were run to validate the output. The percentage error for SD is 0.568%, while it is 0.944% for ID. The results are detailed in

Table 4.23.

Table 4.23: Results validation: T2

No of Exp	SD(mm)			ID(mm)		
	Experiment	**Predict**	**Error (%)**	**Experiment**	**Predict**	**Error (%)**
1	46.5	47	1.064	70	70.6	0.850
2	47.2	47	0.426	70	70.6	0.850
3	47.1	47	0.213	69.8	70.6	1.133
		% error,E_{avg}	0.568		% error,E_{avg}	0.944

After validating the E-slot optimization results, the next step is post-analysis, as shown in Tables 4.24 and 4.25.

Table 4.24: Post analysis: optimization of E-slot applicator: T2

Upper(mm)	**Middle(mm)**	**Bottom(mm)**	**vertical thick(mm)**
68	87	81	9
SD(mm)		**ID(mm)**	
46.5		70	
47.2		70	
47.1		69.8	

Table 4.25 provides a detailed statistical summary of SD and ID obtained from three repeated simulation experiments. The data mean of SD based on three repeated experiments

is 46.9333mm, closely aligned with the predicted SD value of 46.9941 mm ~47 mm. The experimental values are close to the predicted SD, indicating that the SD model is reliable and well-fitted.

Table 4.25: Confirmation of SD and ID: T2

Response	SD	ID
Predicted Mean(mm)	46.9941	70.345
Predicted Median(mm)	46.9941	70.345
Standard Deviation	0.105529	0.498121
n	3	3
Standard Error Pred	0.074566	0.395244
95% Predicted Interval(PI) low(mm)	46.83	69.2476
Data Mean (mm)	47.0667	69.9333
95% Predicted interval (PI) high(mm)	47.1582	71.4424

The mean ID across three repeated experiments is 69.9333 mm. This value falls within 95% PI low, which is 69.2476mm, to 95% PI high, which is 71.4424mm. This indicates that the model is reliable and well-fitted. The predicted SD and ID are reliable, as they fall within their respective 95% PI, indicating that the future measurement is expected to be 95% confident.

The coefficient table in Table 4.26 summarizes the significant factors/variables ($p < 0.05$) influencing the output at the SD and ID. The factor in bold indicates that it is statistically significant.

Therefore, the significant factors/variables that affect SD are upper length (A), middle length (B), bottom length (C), vertical thick (D), interaction term: (AB), (AC), (AD), (BC), (BD),(CD), quadratic term :(B^2), (D^2) and quadratic interaction term: (AD^2), (B^2C) and (B^2D).

Subsequently, the significant factors that affect ID are upper length(A), middle length (B), bottom length (C), interaction term (AB), quadratic terms: (A^2),(B^2), (D^2) and quadratic interaction term (AB^2).

Table 4.26: Coefficient table: T2

	SD	**p-values**	**ID**	**p-values**
Intercept	47.1667		71.6889	
A	0.2375	< 0.0001	1.025	< 0.0001
B	-0.325	< 0.0001	0.416667	0.0121
C	-0.2125	0.0001	-1.65	< 0.0001
D	0.3	< 0.0001		
AB	-0.275	0.0003	1.225	0.0002
AC	-0.2	0.003		
AD	-0.175	0.0069		
BC	-0.125	0.0372		
BD	0.175	0.0069		
CD	-0.325	< 0.0001		
A^2			-0.895833	0.0005
B^2	0.125	0.0122	-1.00833	0.0002
D^2	0.2	0.0006	-1.04583	0.0001

Table 4.26 continued

AB^2			-1.2	0.0014
AD^2	-0.4625	< 0.0001		
B^2C	0.5875	< 0.0001		
B^2D	-0.425	< 0.0001		

4.2.7.3 Optimization of E-slot Applicator under T3 condition

The optimization process in T3 follows the same steps as those in T1 and T2. Table 4.27 presents the experimental design for the T3 condition with 2-level factorials, which is statistically analysed with Design Expert 11 software. Factors 1 to 4 are set as design parameters for responses 1 and 2 (SD and ID, respectively). The experimental design is simulated using SEMCAD X.

Table 4.27: Experimental design: T3

	Factor 1	**Factor 2**	**Factor 3**	**Factor 4**	**Response 1**	**Response 2**
Run	**A: Upper**	**B:Middle**	**C: Bottom**	**D:VerThick**	**SD**	**ID**
	mm	**mm**	**mm**	**mm**	**mm**	**mm**
1	68	93	73	36	47.6	72
2	68	33	73	30	46.1	66.6
3	68	63	53	36	45	68
4	93	63	93	33	45.7	65.7
5	43	93	73	33	47.7	72
6	68	63	73	33	45.6	66.7
7	68	33	93	33	46	66.5
8	68	63	53	30	45.3	67.2
9	93	63	73	30	45.7	67
10	93	63	73	36	45.7	67

Table 4.27 continued

11	93	93	73	33	47.2	71
12	43	63	53	33	45.1	67.5
13	68	63	73	33	45.6	66.7
14	68	93	53	33	47.7	75
15	68	63	93	36	45.2	65
16	43	63	93	33	45	66.5
17	43	33	73	33	45.8	66.5
18	93	33	73	33	46.8	67
19	68	93	73	30	47.6	72
20	68	33	53	33	45.4	66
21	68	93	93	33	46.7	68.5
22	68	63	93	30	45.2	66.5
23	68	33	73	36	46	66.6
24	43	63	73	30	45.6	66.5
25	43	63	73	36	45.5	66.7
26	93	63	53	33	45.3	68.3
27	68	63	73	33	45.6	66.7

The reduced quadratic model is applied because it comprises only the significant factors shown in equations 4.8 and 4.9.

$$SD= 3.97841 +0.018917A-0.066375B+ 0.168719C - 0.0005AB - 0.00025AC - 0.000667BC +0.001368B^2-0.000984C^2 \quad \text{Equation 4.8}$$

$$ID=39.6530 - 0.027972B+ 0.444583C + 0.685694D -0.002917BC - 0.009583CD +0.002602B^2 \quad \text{Equation 4.9}$$

The adequacy of the RSM model is evaluated using analysis of variance (ANOVA) and residual analysis. Tables 4.28 and 4.30 display the ANOVA analysis for both response,

SD and ID. Meanwhile, Tables 4.29 and 4.31 present summaries of fit statistics for SD and ID, respectively.

Table 4.28: ANOVA for reduced Quadratic model of SD: T3

Source	Sum of Squares	df	Mean Square	F-value	p-value
Model	19.82	8	2.48	154.88	< 0.0001
A-Upper	0.2408	1	0.2408	15.06	0.0011
B-Middle	5.88	1	5.88	367.61	< 0.0001
C-Bottom	0.0000	1	0.0000	0.0000	1.0000
AB	0.5625	1	0.5625	35.17	< 0.0001
AC	0.0625	1	0.0625	3.91	0.0636
BC	0.6400	1	0.6400	40.01	< 0.0001
B^2	9.70	1	9.70	606.57	< 0.0001
C^2	0.9922	1	0.9922	62.03	< 0.0001
Residual	0.2879	18	0.0160		
Cor Total	20.11	26			

Table 4.29: Summary of fit statistics for reduced Quadratic model of SD: T3

Fit Statistics	Value
R^2	0.9857
Adjusted R^2	0.9793
Predicted R^2	0.9510
Adeq Precision	38.6885

Table 4.30: ANOVA for reduced quadratic model of ID: T3

Source	Sum of Squares	df	Mean Square	F-value	p-value
Model	146.53	6	24.42	151.02	< 0.0001
B-Middle	81.64	1	81.64	504.86	< 0.0001
C-Bottom	14.74	1	14.74	91.16	< 0.0001
D-VerThick	0.0208	1	0.0208	0.1288	0.7234
BC	12.25	1	12.25	75.75	< 0.0001
CD	1.32	1	1.32	8.18	0.0097
B^2	36.56	1	36.56	226.06	< 0.0001
Residual	3.23	20	0.1617		
Cor Total	149.77	26			

Table 4.31: Summary of fit statistics for reduced quadratic model of ID: T3

Fit Statistics	Value
R^2	0.9784
Adjusted R^2	0.9719
Predicted R^2	0.9517
Adeq Precision	46.5598

The results show that the experimental data are represented by a quadratic polynomial model, with coefficient of determination (R^2) values of 0.9857 for SD and 0.9784 for ID. The R^2 is used to assess model accuracy in predicting the SD and ID. In addition, the value of R^2 close to 1 indicates the model fits the data better as reported by (Ayalew & Asmare, 2022).

The adjustable R^2 and predicted R^2 in SD are 0.9793 and 0.9510, respectively. According to the fit statistic in Design-Expert software, both adjusted and predicted R^2 are reasonable because the difference (0.9793-0.9510=0.0283) is less than 0.2.

Similar to ID, the adjusted R^2 =0.9719, while the predicted R^2 =0.9517. The difference is 0.0202, which is less than 2. Therefore, both the adjusted R^2 and predicted R^2 values are reasonable.

Consequently, factors with $p < 0.05$ are considered significant for predicting the output/response. The variables with 95% confidence, where P values, $p<0.05$, imply a significant effect on the response, as demonstrated by (Pereira et al., 2021).

ANOVA analysis to confirm whether this model is significant or not. Based on the ANOVA analysis, both models are significant, as their p-values are <0.05.

Next analysis is residual analysis, where the evaluation is between the response, Y and the fitted value, $\widehat{Y}$ that expressed as e=Y-$\widehat{Y}$. The error assumes it follows a normal distribution. If the assumption is valid, the plot exhibits a straight line.

Figure 4.24 (a) and (b) display the normal plot of residuals in SD and ID used in residual analysis. Residual analysis assumes a normal distribution, which is confirmed in both plots, as all points align along a straight line, indicating a normal distribution of residuals.

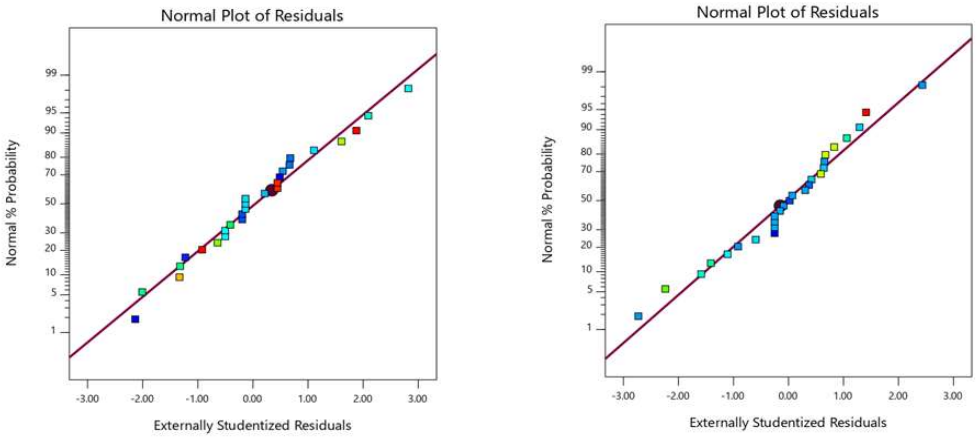

(a) (b)

Figure 4.24: Residual normal probability plot of (a) SD and (b) ID: T3

The other plots in Figure 4.25(a) and (b) show residual vs run. Both provide information about the model's fitness. The model achieved optimal fit when the residual oscillated randomly around the residual = 0 line, which confirms the model has the best fit, as discussed by (Margaret & Manimegalai, 2018).

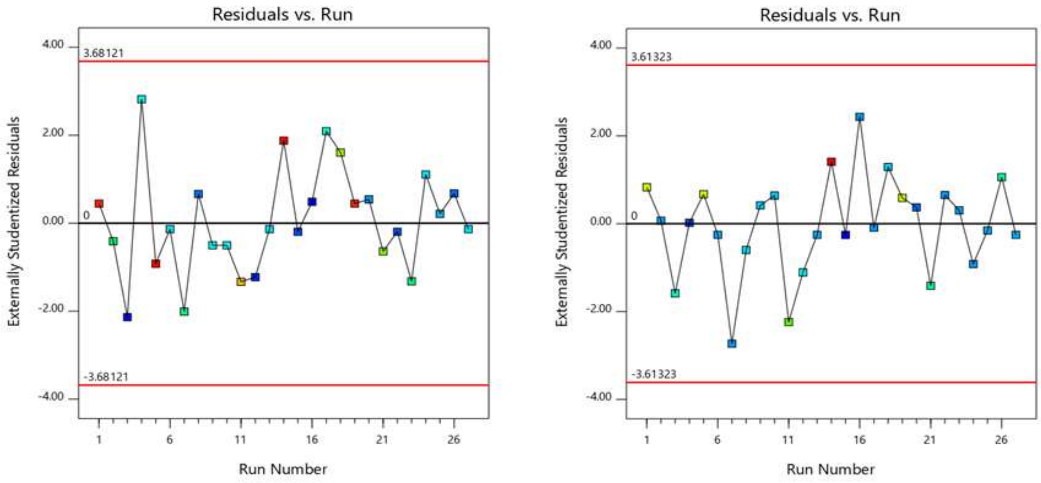

(a) (b)

Figure 4.25: Residual vs Run plot of (a)SD and(b) ID: T3

The E-slot applicator is optimized numerically by setting certain criteria, as listed in Table 4.32.

Table 4.32: Optimization setting criteria: T3

Design parameters/factors	Goal	Lower limit(mm)	Upper limit (mm)
Upper	In range	43	93
Middle	In range	33	93
Bottom	In range	53	93
Vertical thick	In range	30	36
SD	In range	45	47.7
ID	In range	65	75

Figure 4.26 shows the optimization graph indicating the optimal values for upper, middle, bottom, vertical thickness, SD and ID. The desirability for the E-slot optimization design is achieved at maximum desirability 1, indicating that all the design parameters/factors meet the desired outcome.

The proposed optimized design for the E-slot is upper (A)= 68 mm, middle (B) = 63 mm, bottom (C) =73 mm and vertical thickness (D) = 33 mm. The predicted values for SD and ID are 45.6167 mm ~45.6 mm and 66.8 mm, respectively.

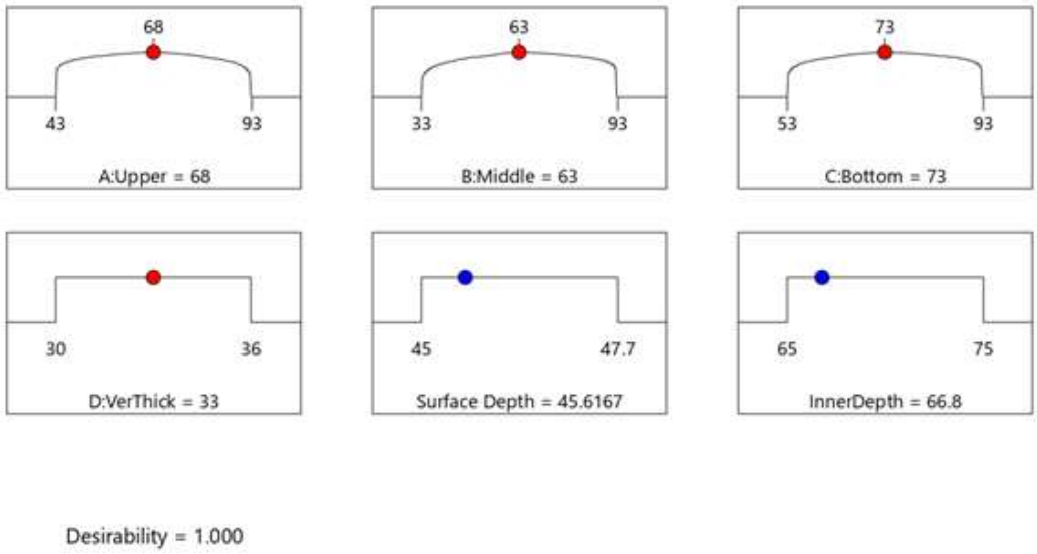

Figure 4.26: Optimization numerical graph: T3

A simultaneous optimization technique uses a desirability function when multiple responses are involved. Each design parameter is converted into an individual desirability function, *d*. The desirability function *d* is in the range $0 \leq d \leq 1$. When the response achieves the goal, $d = 1$, whereas if $d = 0$, it is outside the acceptable range. Finally, all the individual desirabilities are combined using the geometric mean to optimize overall desirability, $D.D = (d_1 x d_2 x \ldots . d_m)(d_1 x d_2 x \ldots . d_m)^{\frac{1}{m}}$, where m = number of response (Li et al., 2008).

Figure 4.27 shows the optimized E-slot applicator design under the T3 condition. The upper horizontal length (A) is 68 mm, middle (B)= 63 mm and bottom (C) =73 mm, while the vertical thickness (D) = 33 mm.

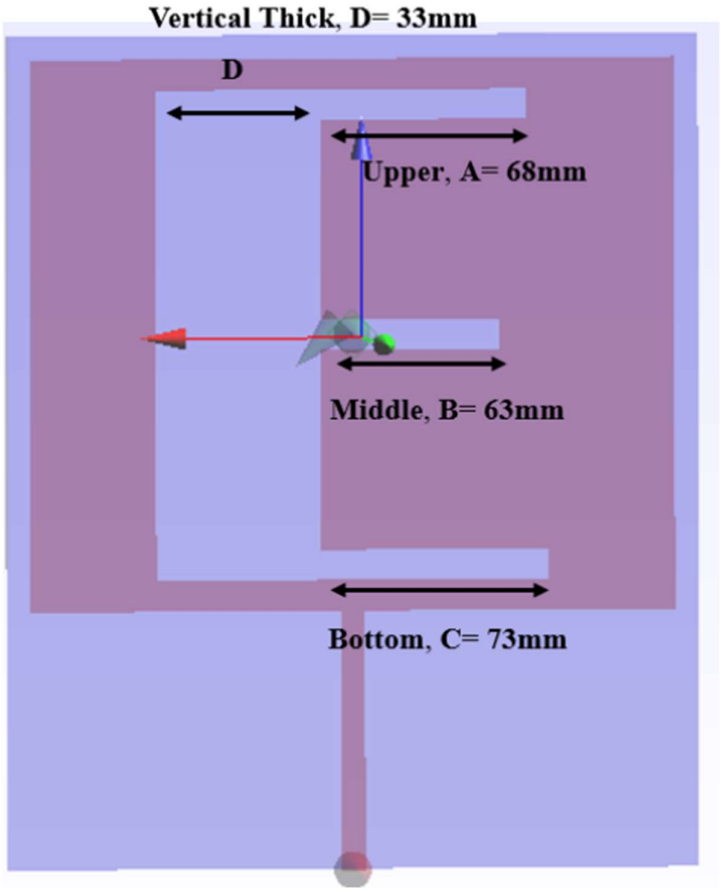

Figure 4.27: Optimize E-slot design :T3

The performance of the optimized E-slot applicator was validated using SEMCAD X. The experimental results are based on simulations compared with the predicted value given in Equation 4.5. There are 3 experiments run to validate the output. The percentage error for surface depth is 0.0731%, while 0.0998% for inner depth. The results are detailed in Table 4.33.

Table 4.33: Results validation: T3

No of Exp	SD(mm)			ID(mm)		
	Experiment	Predict	Error(%)	Experiment	Predict	Error(%)
1	45.6	45.6	0	66.7	66.8	0.1497
2	45.6	45.6	0	66.7	66.8	0.1497
3	45.5	45.6	0.2193	66.8	66.8	0
			0.0731		% error,Eavg	0.0998

After validating the E-slot optimization results, the next step is post-analysis, as shown in Tables 4.34 and 4.35. Table 4.34 provides the results of SD and ID.

Table 4.34: Post analysis: optimization E-slot microstrip antenna: T3

Upper(mm)	Middle(mm)	Bottom(mm)	vertical thick(mm)
68	63	73	33

SD(mm)	ID(mm)
45.6	66.7
45.6	66.7
45.5	66.8

Table 4.35 provides a detailed statistical summary of SD and ID obtained from three repeated simulation experiments. The mean SD from three repeated experiments is 45.5667 mm, which is close to the predicted SD value of 45.6167 mm. The 95% PI low is 45.4395 mm and the 95% PI high is 45.7938 mm. The experimental values are close to the predicted surface depth, indicating that the SD model is reliable and well-fitted.

Table 4.35: Confirmation of surface and inner depth: T3

Response	SD	ID
Predicted Mean(mm)	45.6167	66.8
Predicted Median(mm)	45.6167	66.8
Standard Deviation	0.12647	0.40213
n	3	3
Standard Error Pred	0.08432	0.25433
95% Predicted Interval(PI) low(mm)	45.4395	66.2695
Data Mean (mm)	45.5667	66.7333
95% Predicted interval(PI) high(mm)	45.7938	67.3305

The mean ID from three (3) repeated experiments is 66.7333 mm, compared with the predicted mean of 66.8 mm. The experimental value is close to the predicted ID. In ID, the predicted mean of 66.2695 mm is within 95% PI low, while 67.3305 mm is within 95% PI high. The experimental values are close to the predicted ID, indicating that the Id model is reliable and well-fitted.

The predicted SD and ID are confirmed to be reliable, as they fall within their respective 95% PI, which means the future measurement is expected to be 95% confident.

The coefficient table in Table 4.36 summarizes the significant factors/variables with $p < 0.05$ that influence SD and ID. The significant factors in SD are upper length (A), middle length (B), interaction of upper length and middle length (AB), interaction of middle length and bottom length (BC), quadratic term (B^2) and (C^2).

Meanwhile, middle length (B), bottom length (C), vertical thickness (D), interaction of middle and bottom length (BC), interaction of middle length and vertical thickness (CD) and quadratic term (B^2) significantly affect ID.

Table 4.36: Coefficient Table: T3

	SD	p-values	Inner Depth	p-values
Intercept	45.6167		66.8	
A	0.141667	0.0011		
B	0.7	< 0.0001	2.60833	< 0.0001
C			-1.10833	< 0.0001
D				
AB	-0.375	< 0.0001		
BC	-0.4	< 0.0001	-1.75	< 0.0001
CD			-0.575	0.0097
B^2	1.23125	< 0.0001	2.34167	< 0.0001
C^2	-0.39375	< 0.0001		

4.2.8 Validation of Optimized E-slot Applicator

The optimized E-slot applicator is validated with previous optimization methods, namely the Genetic Algorithm (GA) and Particle Swarm Optimization (PSO), which were applied to the E-slot applicator, as summarized in Table 4.37. The comparison is conducted in terms of performance parameters such as directivity, gain, return loss, operating frequency and the application.

Table 4.37: Validation of the RSM Optimized E-slot Applicator Methods

Slot Optimization	Directivity (dBi)	Gain (dBi)	Return Loss(dB)	Frequency (MHz)	Application
Generic Algorithm (GA)	3.8	3.04	-23	630	Medical
Particle Swarm Optimization (PSO)	2.51	1.94	-16	550	Medical
RSM -T1	20.69	24.06	-9.61	915	Hyperthermia
RSM-T2	12.73	9.14	-11.30	915	Hyperthermia
RSM-T3	7.67	5.89	-16.01	915	Hyperthermia

The GA and PSO operate at frequency (550-0630MHz) and exhibit low directivity (2.5-3.8dBI) and low gain (1.94-3.04 dBi) compared to the RSM optimized E-slot applicator. The optimized E-slot applicator demonstrates higher directivity and gain, particularly for tumor sizes T1 and T2 (20.6 dBi and 12.73 dBi, respectively).

Although the GA and PSO show lower RL than RSM, the values remain within an acceptable impedance-matching range (return loss < -10 dB), which is suitable for hyperthermia applications, thereby improving the ability to focus EM energy on the tumor.

The RSM-optimized E-slot applicator was developed under ISM frequency of 915 MHz for non-invasive hyperthermia treatment, whereas the GA and PSO approaches were primarily developed for general medical applications.

Furthermore, the variation in applicator performance with tumor size demonstrates the adaptability of the optimized E-slot. This indicates that RSM not only improves applicator characteristics but also enables EM energy to be focused on the tumor, a capability not explicitly addressed in GA and PSO.

Therefore, the comparative results validate the effectiveness of the RSM-optimized E-slot applicator, which outperforms GA and PSO, particularly in directivity and gain. The return loss is acceptable for impedance matching and suitable for non-invasive hyperthermia treatment.

4.2.9 Comparison of slot Applicator: E-slot and Optimization E-slot

This section compares the performance of E-slot and optimized E-slot in terms of heat absorption and applicator performance (directivity, gain and return loss). Heat absorption was evaluated using SAR distribution, with SD and ID measured as shown in Figure 4.28.

Tumor size	E-slot applicator	Optimized E-slot applicator
T1	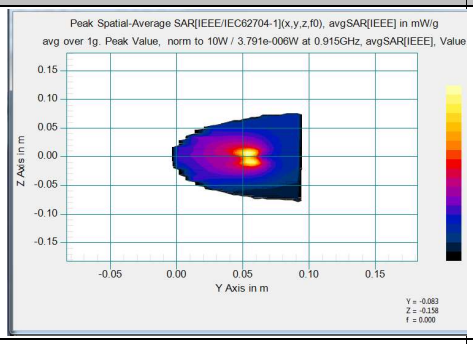	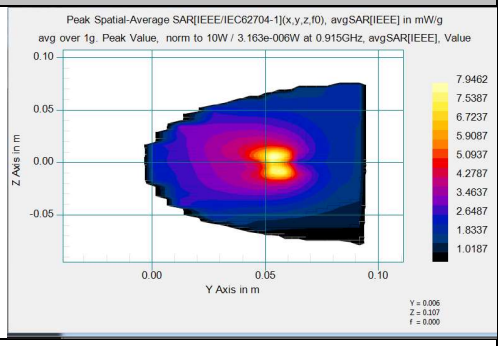
	SD: 40mm ID:64.5mm SAR(peak) =7.8mW/g	SD:40.2mm ID: 65mm SAR =7.9072mW/g
T2	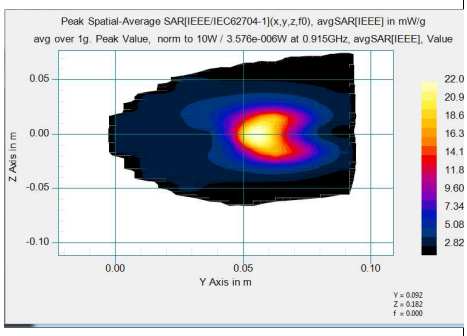	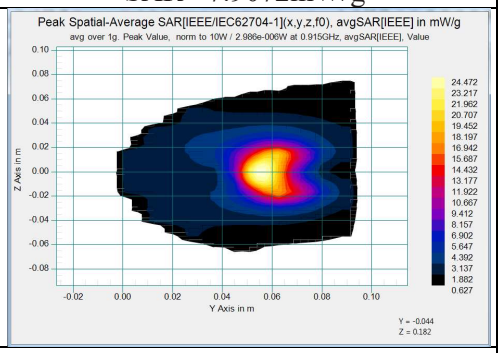
	SD: 46.7mm ID:71.2mm SAR(peak)= 22.03mW/g	SD: 47.1mmID: 69.8mm SAR(peak)= 24.472mW/g
T3	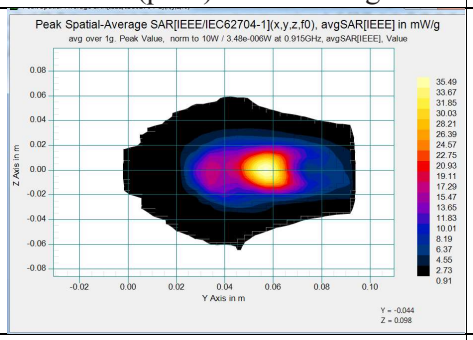	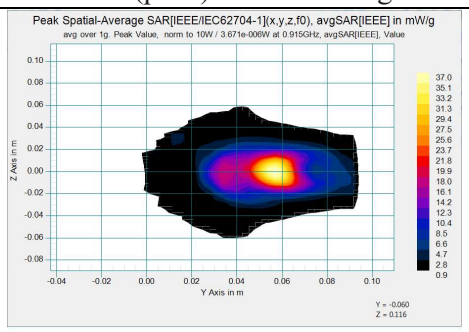
	SD: 46mm ID:66.6mm SAR(peak) = 35.49mW/g	SD :45.6mm ID: 66.7mm SAR(peak)= 37mW/g

Figure 4.28: SAR distribution comparison in E-slot and Optimized E-slot Applicator

The graph in Figure 4.29 illustrates the SAR(peak) for the E-slot and the optimized E-slot applicator for T1, T2 and T3. The optimized E-slot exhibits improvement of 5.6% for T1, 116.5% for T2 and 43% for T3.

In particular, the findings of this research show that the optimized E-slot has the highest SAR (peak) compared to the E-slot applicator. This indicates that the optimized E-slot provides a shorter treatment time than the E-slot applicator.

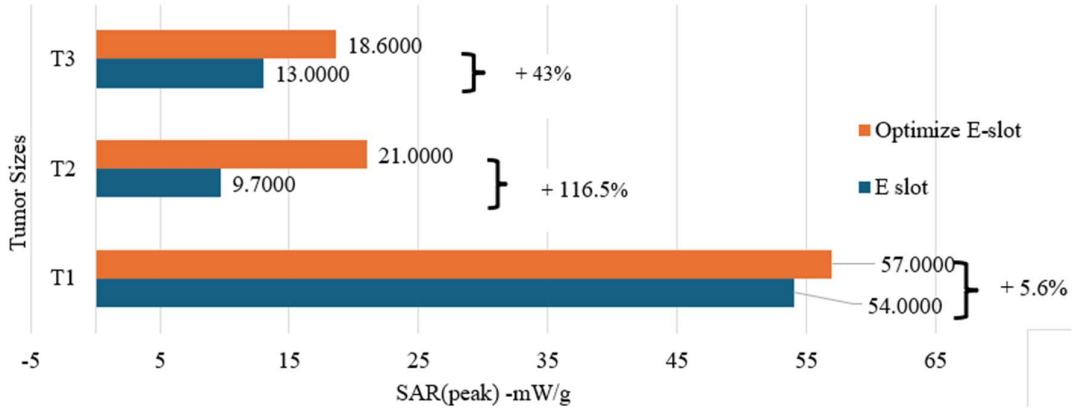

Figure 4.29 : SAR(peak) improvement in Optimized E-slot Applicator

The optimized E-slot applicator shows an improvement of applicator directivity of 26% for T1, 22.3% for T2 and 12% for T3 compared to the E-slot microstrip applicator, as presented in Figure 4.30. The improvement in directivity indicates that the optimized E-slot focuses EM energy more locally while minimizing the effect on surrounding healthy tissue (Abdulhussain et al., 2023; Rajebi et al., 2024).

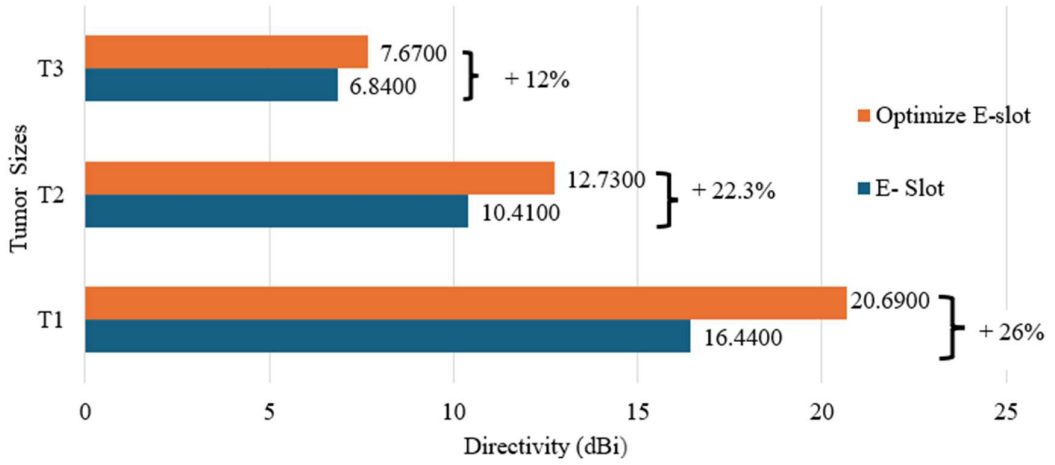

Figure 4.30: Directivity improvement in optimized E-slot applicator

The results in Figure 4.31 indicate that the optimized E-slot showed gain improved by 21%,8.6% and 24.3% for T1, T2 and T3, respectively. The high gain reflects the applicator's improved ability to radiate more power in a specific region and contribute to more efficient energy delivery, which is essential for ensuring sufficient tumor heating (Tayel et al., 2017).

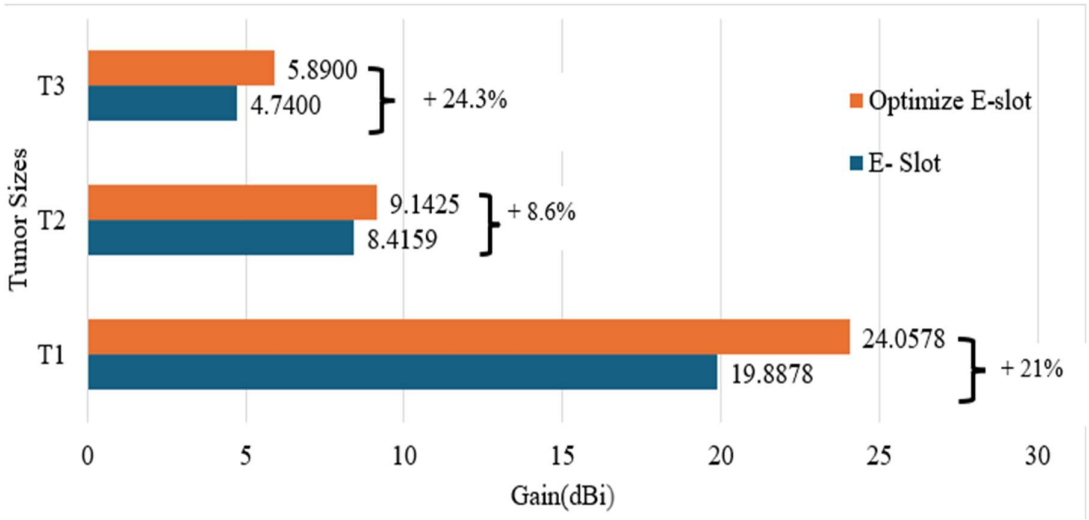

Figure 4.31: Gain improvement in optimized E-slot applicator

Figure 4.32 compares the return loss of the E-slot and the optimized E-slot in T1, T2 and T3 conditions. The optimized E-slot applicator demonstrated lower return loss than the E-slot applicator under all conditions (T1, T2 and T3). Hence, the optimized E-slot applicator has better impedance matching and reduces signal reflection. Moreover, a minimum return loss is required to ensure minimal signal reflection and maximize power toward the target tissue (Hojjatollah, 2018).

Return loss for T1: E-slot (-7.6648dB) and optimized E-slot (-9.6095dB), return loss T2: E-slot (-4.3578dB) and optimized E-slot (-11.2981dB), return loss T3: E-slot (-5.0425dB) and optimized E-slot (-16.009dB). The improvement of the optimized E-slot compared to the E-slot in terms of return loss is 25.4%, 159.2 % and 217.5% on T1, T2 and T3, respectively.

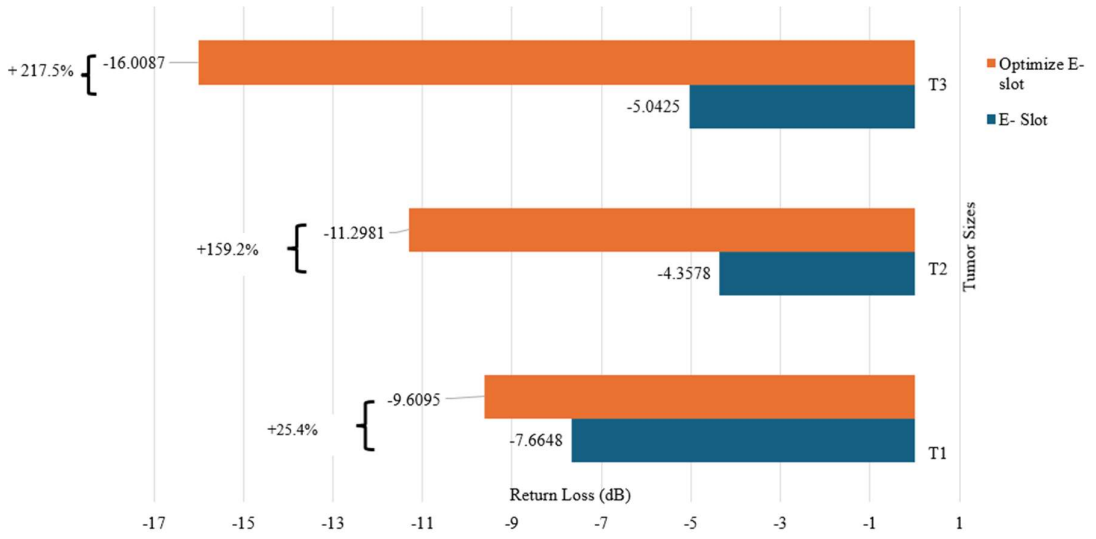

Figure 4.32: Return loss (dB) improvement in optimized E-slot applicator

The findings in Figures 4.33 and 4.34 indicate that both SD and ID obtained do not reaches the desired values. Nevertheless, the optimized E-slot exhibits improved SAR distribution and is more localized, as indicated in Figure 4.28 across all tumor sizes: T1, T2

and T3. In addition, the results indicate that optimized E-slot improves performance in terms of directivity, gain, return loss and SAR (peak).

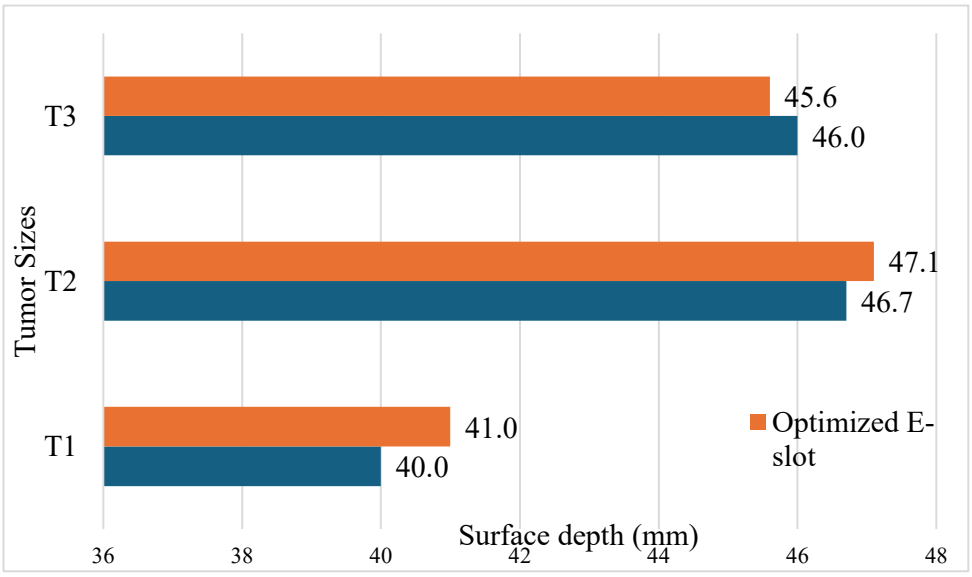

Figure 4.33: SD in E-slot and optimized E-slot Applicator

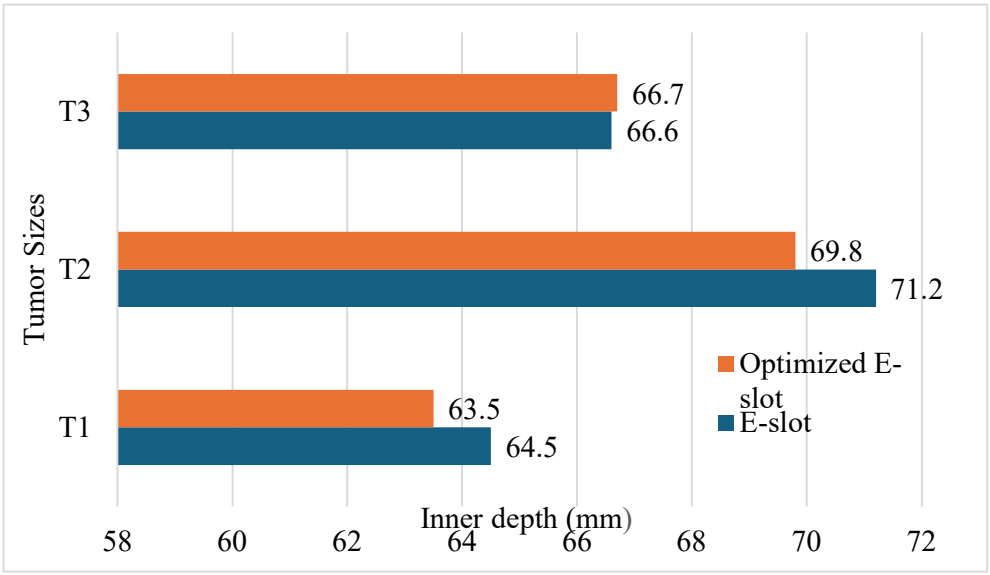

Figure 4.34: ID in E-slot and optimized E-slot Applicator

Since the SD and ID do not reach the desired value, SAR optimization is conducted in DoE 4. This is to ensure that the entire tumor is heated sufficiently and uniformly. The duration of the hyperthermia treatment is then determined based on SAR optimization. The duration of hyperthermia treatment is elaborated on in the next section.

4.2.10 Hyperthermia Treatment Time

SAR optimization is used to determine the treatment time for hyperthermia. SAR optimization can be obtained based on a numerical approach or software (Kok, Kotte, et al., 2017; Nizam-Uddin & Elshafiey, 2017). SEMCAD X includes hyperthermia treatment plan tools, such as SAR (peak) optimization, to deliver adequate heat to the tumor.

In this research, SAR is associated with SAR (peak). A high SAR (peak) indicates a shorter time to reach T_{max}. This indicates that EM energy rapidly increases in the tumor, leading to a more rapid rise in temperature. Consequently, the hyperthermia treatment time can be reduced. As described in (Hunt et al., 1991) suggests that shorter treatments provide significant improvement in hyperthermia treatment. It also proved that rapid heating yields a more uniform heat distribution across the treated tissue.

The SAR optimization included the simulation for the breast phantom without and with water bolus. As mentioned in section 2.19, the thickness of the water bolus influences the SAR distribution pattern. Also, mention in (Rajebi et al., 2024) (Ebrahimi-Ganjeh & Attari, 2008), the increment thickness of the water bolus significantly decreases thermal energy transfer into tissue and results in lower SAR(peak). Therefore, this research uses a water bolus thickness of 2mm to reduce skin burn effects during hyperthermia treatment and improve the energy focusing (Wong et al., 2023).

The summary of SAR optimization is included in Appendix F for T1, T2 and T3. Figures 4.35, 4.36 and 4.37 show a clear trend of decreasing ID when water bolus is applied compared to when it is not.

Figure 4.35 demonstrates the SAR optimization range from 8 mw/g to 5 mW/g for ID in T1 without water bolus and with water bolus. SAR (peak) value was adjusted from 8 mW/g to 5 mW/g. The SAR (peak) was initially set to 8 mW/g as the baseline, based on the first SAR (peak) value generated in SEMCAD X.

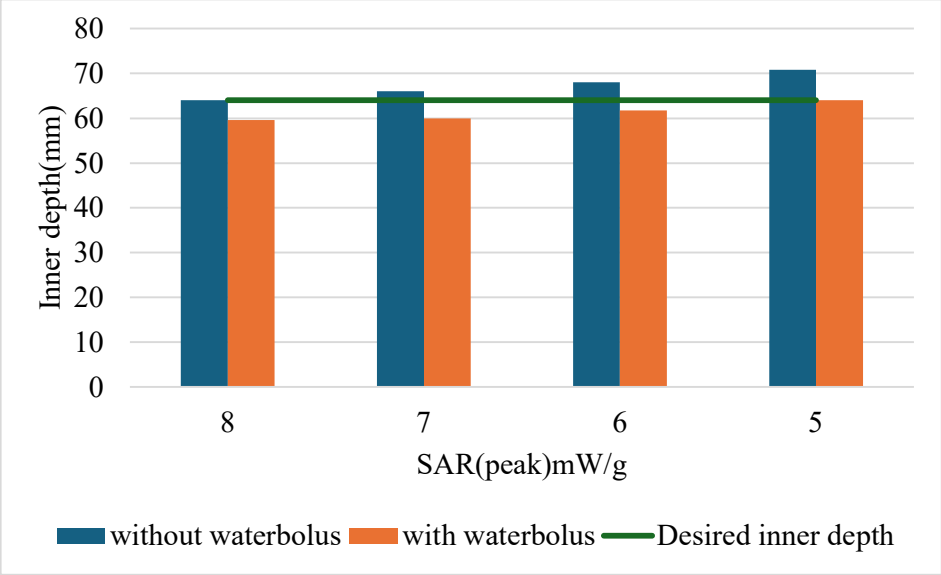

Figure 4.35: SAR optimization in ID, T1

The SAR optimization selection depends on achieving the desired ID of 64 mm. It demonstrated that SAR (peak)= 8 mW/g (without water bolus), whereas SAR (peak) =5 mW/g (with water bolus) attained ID of 64mm.

In T2 ID, the SAR (peak) value is adjusted from 28 mW/g to 4 mW/g. The SAR (peak) is initially established at 28mW/g as the baseline, derived from the first SAR (peak)

generated in SEMCAD X. Figure 4.36 presents SAR optimization ID for T2 with and without water bolus. The SAR optimization is 12 mW/g without water bolus and 8mW/g with water bolus. It is selected based on the desired ID of 80 mm.

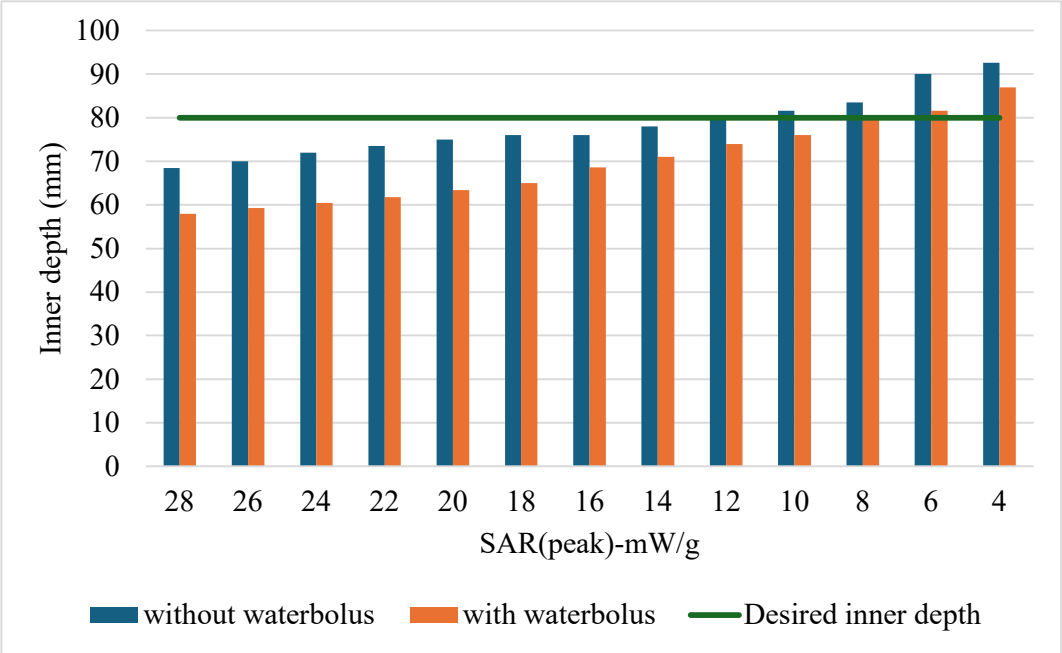

Figure 4.36: SAR optimization in ID, T2

The SAR (peak) value is adjusted from 38 mW/g to 4 mW/g for ID in T3. The SAR (peak) is initially set to 38 mW/g as the baseline. This baseline value is based on the first value of SAR (peak) generated in SEMCAD X. Figure 4.37 displays the SAR optimization range from 38 mw/g to 4 mW/g for ID in T3 without water bolus and with water bolus. The SAR optimization is 9 mW/g for both without water bolus and with water bolus. The SAR optimization is selected based on the desired ID, which is 90 mm.

Table 4.38 presents a summary of SAR optimization for ID for T1, T2 and T3 conditions without water bolus and with water bolus. The SAR (peak), SAR distribution and ID are significantly affected by the water bolus.

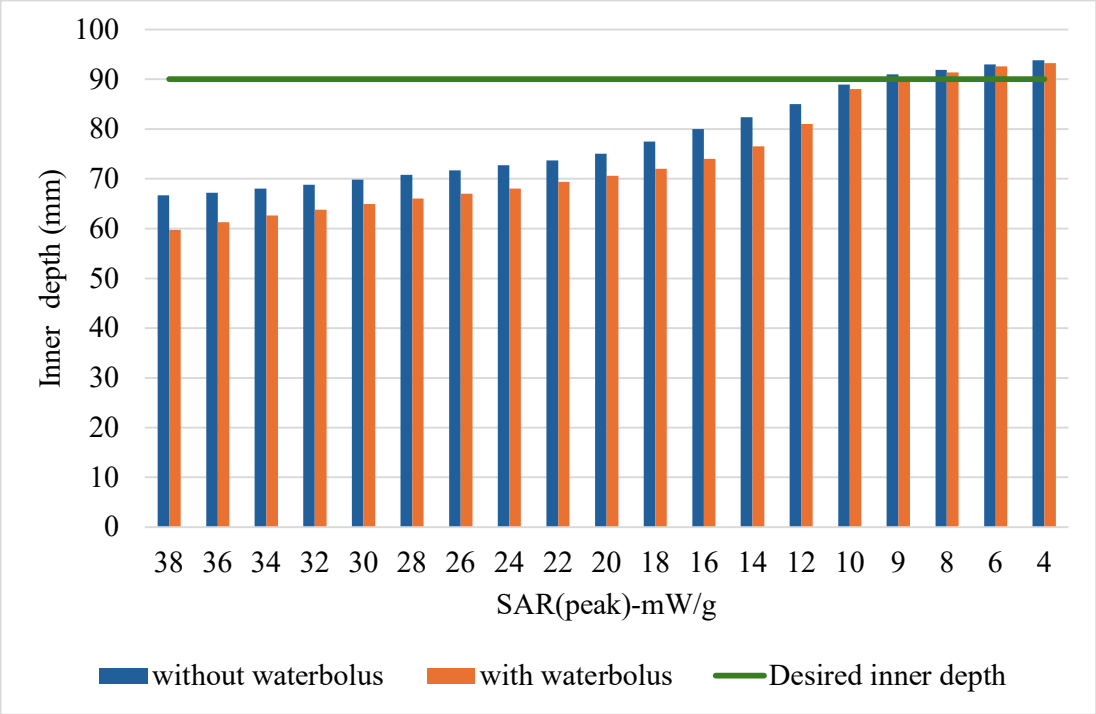

Figure 4.37: SAR optimization in ID, T3

Table 4.38: SAR optimization summary – ID

	SAR optimization Without water bolus			**SAR optimization With water bolus**		
Tumor size	**SAR optimization (mW/g)**	**ID (mm)**	**SAR (peak) mW/g**	**SAR optimization (mW/g)**	**ID (mm)**	**SAR (peak) mW/g**
T1	8	64.2	7.8	6	64	5.8
T2	12	80	11.7	8	80	7.8
T3	9	91	8.77	9	90	8.77

The findings show that water bolus reduces the effect of unwanted hotspots and concentrates heat more on the treated tissue. Furthermore, water bolus is a cooling technique that can cool the skin surface, avoid overheating, avoid skin burn and enhance patient comfort (Arunachalam et al., 2009). Therefore, in this research, the time duration of hyperthermia treatment is considered only with water bolus.

Table 4.39 presents the time duration required in ID for T1, T2 and T3. This reflects that the heating process in T3 and T2 is more efficient than in T1. It also observes that the SAR (peak) corresponds to shorter treatment. T_{max} is 45 °C, remaining below the safety limit for hyperthermia treatment. T_{min} is 37ºC. The initial time (t_0) is 0s. The equation can be represented as stated in Equation 4.10:

$$\Delta t = \frac{C\Delta T}{SAR(peak)} = \frac{T_{max} - T_{min}}{t_1 - t_0} \qquad \text{Equation 4.10}$$

The $\Delta T = 45°C - 37°C = 8°C$, the initial time = 0s and C is specific heat capacity = 3600J/kg°C.

Table 4.39: Recommended time duration in inner depth for T1, T2 and T3

T size	ID (mm)	SAR(peak)mW/g	Time		
			sec	min	hour
T1	64	5.8	4965.5	82.76	1 hr 23min
T2	80	7.8	3692.31	61.54	1 hr 1 min 32 sec
T3	90	8.77	3283.93	54min 44sec	

The large tumors (T3 and T2) maintain high temperatures for a shorter period due to their low surface area to volume ratio and poor blood perfusion. In addition, the large tumors have disorganized and less efficient blood vessels than the small tumors (Babbs & DeWitt, 1981). The ratio of spherical tumor in surface area to volume is represented in Equation 4.11 (Babbs & DeWitt, 1981) :

$$\frac{A}{V} = \frac{4\pi r^2}{\frac{4}{3}\pi r^3} \text{ in simplifying form } \frac{A}{V} = \frac{3}{r} \qquad \text{Equation 4.11}$$

The A/V is inversely proportional to radius, r. This means that large tumors (T3) and medium tumors (T2) have a lower A:V ratio than small tumors (T1). This can be demonstrated in Table 4.40 in ID.

Table 4.40: ID ratio surface area to volume

ID				
T size	**Radius (mm)**	**Surface area,A(mm^2)**	**Volume,V(mm^3)**	**A/V**
T1	10.8	1465.74	5276.67	0.278
T2	18.9	4488.83	28279.65	0.159
T3	32.5	13273.23	143793.31	0.092

The medium tumor (T2) and large tumor (T3) have a lower surface area to volume ratio than T1. This indicates that large and medium tumors retain heat more effectively and sustain high temperatures because less heat escapes to the surrounding area. In addition, according to Pennes' bioheat equation, heat transfer in biological tissue is influenced by blood perfusion, which acts as a cooling mechanism. The blood perfusion in T2 and T3 is

lower, leading to reduced convective heat removal and slower cooling rates (Babbs & DeWitt, 1981).

In contrast to T1, the small tumor has a high surface area to volume ratio, which allows heat to escape quickly to the surrounding area, resulting in a faster cooling effect on the tumor itself. Additionally, blood perfusion is more efficient in small tumors and the blood flow helps to carry the heat away more effectively (Babbs & DeWitt, 1981).

These difference in heat retention and cooling behaviour explains why the treatment time in T1 is longer than in T2 and T3. Furthermore, in terms of location, T1 is farther from the front skin than T2 and T3.

Moreover, as highlighted by (Wong et al., 2021) the duration of tumors of small size is longer than that of tumors of large size. This research categorized the size of the tumors as Stage 1 (small size), Stage 2 (medium size) and Stage 3 (large size). Frequencies of 915 MHz and 2450 MHz were used with rectangular microstrip applicator and an input power of 1W. However, Table 4.41 compares the time duration when using only 915 MHz.The results also reveal that the optimized E-slot applicator performs more efficiently than in the previous study.

Table 4.41: Comparison of time duration with the previous study

Previous study (Wong et al., 2021)			**This research (Optimized E-slot)**		
Stage	Inner depth (mm)	Time duration	Tumor Size	Inner depth (mm)	Time duration
Stage 1	63	6hr 27min	T1	64	1 hr 23min
Stage 2	61	2hr 40min	T2	80	1 hr 1min 32 sec
Stage 3	51	2 hr 22 min	T3	90	54min 44sec

4.3 Summary of the Chapter

This chapter presents the analysis results and discussion based on DoE 1, DoE 2, DoE 3 and DoE 4. The main finding in DoE 1 is that the appropriate frequency is 915 MHz. The frequency related to ID and SAR distribution.

The main finding under DoE 2 concerns selecting the best-performing U-slot or E-slot applicator for this research. The E-slot applicator has better performance and a more localized SAR distribution. In addition, the E-slot has better directivity, gain, return loss and SAR (peak) than the U-slot applicator, which allows heat to focus more on the tumor than the surrounding healthy tissue. Therefore, hyperthermia's effectiveness improved.

The main finding under DOE 3 concerns the modification, optimization, validation and comparison of the E-slot with the optimized E-slot in terms of applicator performance and SAR.

Lastly, in DoE 4, the hyperthermia treatment time is established based on SAR optimization, with SD and ID values that closely match the desired value. Then, the recommended time durations for T1, T2, and T3 are provided.

CHAPTER 5

CONCLUSION AND RECOMMENDATIONS

5.1 Introduction

This chapter presents the summary of research findings, contribution to knowledge and future work.

5.2 Summary of Research Findings

Research objective 1 was addressed through DoE 1. The most significant finding was that 915 MHz is the most appropriate frequency, as the tumor is located in the middle of the breast phantom. The location of tumor is determined based on the analysis in section 3.2.1.

Research objective 2 was achieved through DoE 2, comprising DoE 2a and DoE 2b, which focused on the integration of the U-slot and E-slot. The performance of both slots is then compared. The results showed that E-slot is superior to U-slot in terms of gain, directivity and return loss. Therefore, the E-slot was selected for integration in this research. DoE 2b concerns determining the distance of the applicator relative to the breast phantom. The optimal distance is 15mm and the unwanted hotspot at the surrounding healthy tissue is minimized.

Research objective 3 was achieved by DoE3, which comprises DoE3a, 3b, 3c and 3d. DoE 3a, which emphasized the effects of slot modification on the E-slot applicator. The significant parameters identified were the horizontal lengths of the upper, middle and bottom, as well as the vertical thickness for tumor sizes T1, T2, and T3. DoE 3b specifically concentrated on slot optimization. The Polymodal model was established to predict SD and

ID in the SAR distribution. The results also demonstrated that slot optimization significantly enhances antenna performance, particularly in gain, directivity, return loss and SAR (peak) observed under tumor sizes T1,T2 and T3.

DoE3c is the validation of optimization of the E-slot applicator with previous optimization methods, such as GA and PSO. The RSM-optimized E-slot was validated using PSO and GA, as reported in previous research. The directivity and gain of the RSM-optimized E-slot are better than those of GA and PSO. DoE 3d comparison of optimized E-slot and E-slot applicator. The directivity, gain, return loss and SAR (peak) improved in the optimized E-slot applicator.

DOE 4 was conducted to determine the hyperthermia treatment time that addresses Research objective 4. The treatment time was 1 hour 23 minutes for T1, 1 hour 1 minute 32 seconds for T2 and 54 minutes 44 seconds for T3. The research findings are summarized in Table 5.1.

Table 5.1: Research findings in relation to research objectives and methodology

No	Research Objectives	Methodology		Results
1	To simulate and evaluate a breast phantom integrated with a non-invasive microstrip applicator under Industrial, Scientific and Medical (ISM) frequency to achieve a desired surface and inner depth within tumor sizes: T1, T2 and T3	DoE 1a	Microstrip Applicator Development Based on ISM Frequency	915MHz selected as the appropriate frequency
		DoE 1b	Selection of input power	The input power =10W selected
		DoE 1c	Selection of SAR average mass	The average SAR mass selected =1g
2	To conduct a comparative analysis of E-slot and U-slot applicators based on the applicator's performance and rate of electromagnetic (EM) energy absorbed in tissue, represented in Specific Absorption Rate (SAR) within tumor sizes: T1,T2 and T3	DoE 2a	Slot integration into the microstrip applicator	The E-slot was selected due to its higher gain, better directivity and lower return loss compared to U-slot
		DoE 2b	Distance between the applicator and the breast phantom	At a distance of 0 to 10mm, the unwanted hotspot spreads to the front part of the breast. At 15mm, the unwanted hotspots were reduced and heat was concentrated more at tumor

Table 5.1 continued

3	To validate the optimized E-slot applicator obtained from Response Surface Method (RSM) by comparing its performance with Particle Swarm Optimization (PSO) and Genetic Algorithm (GA)	DoE 3a	Modified Slot Structure	The significant parameters identified: horizontal length upper, horizontal length middle, horizontal length bottom, and vertical thickness for tumor sizes T1, T2, and T3. These data/parameters are used as inputs in Design Expert Software for polynomial model development and slot dimension optimization.
		DoE 3b	Slot Optimization Dimension	T1 and T3: Quadratic polynomial model formulated, T2: Cubic polynomial model formulated. E-slot optimized design developed for T1,T2 and T3 The percentage improvement of the optimized E-slot antenna compared to the E-slot only was observed as follows: Directivity: T1=26%, T2 =22.3%,T3=12% Gain : T1=21%,T2=8.7%, T3=24.3% Return Loss: T1=20%, T2=55%, T3 = 71.7%

Table 5.1 continued

				SAR(peak) : T1=5.6%, T2=116.5% ,T3=43%
		DoE 3c	Validation of Optimized Slot Applicator	GA: Directivity =3.8dBi, Gain=3.04dBi, Retrun Loss = - 23dB, Application: Medical PSO: Directivity=2.51dBi,Gain=1.94dBi,Return Loss= -16dB, Application:Medical RSM -T1: Directivity =20.69dBi, Gain=24.06dBi, Return Loss= -9.16dB RSM-T2: Directivty =12.73dBi, Gain = 9.14dBi, Return Loss = - 11.30dB RSM-T3:Directivity = 7.67dBi, Gain =5.89dBi, Return Loss = -16.01dB Application T1,T2 and T3: Hyperthermia

Table 5.1 continued

		DoE 3d	Comparison of slot Applicator: E-slot and Optimized E-slot Applicator	SAR(peak) : T1 = 5.6%, T2 = 116.5% ,T3 = 43% Directivity: T1 = 26%, T2 = 22.3%,T3 = 12% Gain : T1 = 21%,T2 = 8.7%, T3 = 24.3% Return Loss: T1 = 25.4%, T2 = 159.2%, T3 = 217.5%
4	To generate the optimal hyperthermia treatment time in different tumor sizes : T1, T2 and T3	DoE 4	Hyperthermia treatment time	The optimized E-slot time duration improved compared to the previous study. The treatment time: 1 hour 23 minutes for T1, 1 hour 1 minute 32 seconds for T2 and 54 minutes 44 seconds for T3.

5.3 Contribution to Knowledge

This research provides several contributions to knowledge. First, the operating frequency of 915MHz is selected based on the position of tumor derived from the breast cancer mammogram analysis. The tumor is classified as T1, T2 and T3. The frequency selection is aligned with the frequency-dependent dielectric properties of breast fat, tumor, and chest wall.

Secondly, the research develops a second-order polynomial model to accurately predict the SD and ID of tumor sizes T1, T2 and T3 for hyperthermia treatment by using RSM. The SD and ID prediction models include constant, linear, interaction, quadratic term and higher order terms. The complete fitted equations are presented in Equations 4.3 and 4.4 for T1, Equations 4.5 and 4.6 for T2, and Equations 4.8 and 4.9 for T3.

Thirdly, statistically significant slot design parameters influencing SD and ID are identified for each tumor size by using ANOVA. The significant factors include a combination of upper, middle and bottom horizontal slot length and vertical thickness. These parameters provided structural guidance for optimization of the E-slot applicator.

Fourthly, optimized E-slot applicator design is proposed for T1, T2 and T3 tumors. The optimized E-slot applicator demonstrates improvement in applicator performance in terms of directivity, gain, return loss and SAR (peak)

Finally, the time durations required for hyperthermia treatment with the optimized E-slot are recommended as T1: 1 hour 38min, T2: 1 hour 1min, and T3: 54min 44sec. The treatment time was significantly reduced with the optimized E-slot, which was shorter than in the previous study.

5.4 Future Works

For future work, fabrication of the E-slot optimization is recommended to enable validation and comparison between simulation and measured results. A network analyzer is used to measure and verify gain and return loss under real operating conditions.

In addition, the development of a more realistic breast phantom embedded with a tumor is recommended. The phantom tissue is composed of tissue-equivalent materials and other synthetic substances that simulate fat and tumor to improve experimental reliability.

Future research could also extend to developing a polynomial model for the applicator's directivity, return loss and gain of the optimized E-slot applicator. Consequently, the analysis of the relationship between input parameters and output performance is used to improve predictions of applicator performance.

REFERENCES

Abdel-Haleem, M. R., Abouelnaga, T., Ahmed, S. M., & Abo-Zahhad, M. (2018). Convex lenses, horn antenna, microwave hyperthermia scheme. *IET Conference Publications*, *2018*(CP741), 13–17.

Abdelgwad, A. H. (2018). Microstrip patch antenna enhancement techniques. *Medicine (United Kingdom)*, *12*(10), 703–710.

Abdulhussain, Z. N., Qasim, H. B., Al-Ghanimi, H., Shather, A., Sabah, H. A., & Alchilibi, H. (2023). Antenna Microstrip Patch Antenna Design of T Shape and Rectangular Shape for Improved Directivity. In *Proceedings of 3rd International Conference on Advancement in Electronics and Communication Engineering, AECE 2023*, 833–836. https://doi.org/10.1109/AECE59614.2023.10428647

Abdulkawi, W. M., Elshafiey, I., Sheta, A. F. A., & Al-Bawri, S. S. (2024). A 3D wideband electromagnetic horn antenna applicator for biomedical applications. *Engineering Research Express*, *6*(4), 99–110. https://doi.org/10.1088/2631-8695/ad81ae

Abhijeet Singh, Pushpendra Singh, S. P. S. (2022). Design of a circular ring slot patch antenna at 2.45GHZ for hypertehrmia applications. *Mathematical,Computational Intelligiene and Engineering Approaches for Tourism,Agriculture and Healthcare*, *214,* 67–78. https://link.springer.com/10.1007/978-981-16-3807-7

Abouelnaga, T. G., & Abdel-Haleem, M. R. (2023). An Ultra-small heated area masked microwave hyperthermia therapy scheme in fresnel region. *Applied Computational Electromagnetics Society Journal*, *38*(4), 277–285. https://doi.org/10.13052/2023.ACES.J.380407

Abraham, J., & Staffurth, J. (2020). Hormonal therapy for cancer. *Medicine (United Kingdom)*, *48*(2), 103–107. https://doi.org/10.1016/j.mpmed.2019.11.007

Acar, B., Yilmaz, T., & Yapar, A. (2024). Advanced hyperthermia treatment: optimizing microwave energy focus for breast cancer therapy. *Turkish Journal of Electrical Engineering and Computer Sciences*, *32*(2), 268–284. https://doi.org/10.55730/1300-0632.4068

Adela, B. B., Mestrom, R. M. C., Paulides, M. M., & Smolders, A. B. (2013). An MR-compatible printed Yagi-Uda antenna for a phased array hyperthemia applicator.In *proceedings of 2013 7th European Conference on Antennas and Propagation, EuCAP 2013*, 1142–1146.

Adji, R. P. H., Kurniadi, D. P., Taufiqqurrachman, Santiko, A. B., Mandasari, R. D., Pristianto, E. J., Darwis, F., Rahman, A. N., Adi, P. D. P., Kurnia, D., Pratindy, R., & Fathnan, A. A. (2024). Low-cost 9.4 GHz microstrip patch antenna design with PLA and copper tape. In *Proceeding - 2024 International Conference on Radar, Antenna, Microwave, Electronics, and Telecommunications, ICRAMET 2024*, 94–99. https://doi.org/10.1109/ICRAMET62801.2024.10809233

Agrawal, N., Ansari, J. A., Nitin, N., Siddiqui, M. G., & Sayeed, S. S. (2018). Design and analysis of E-slot microstrip antenna. *2018 Recent Advances on Engineering, Technology and Computational Sciences (RAETCS) Design*, *524*(6), 85–94. https://doi.org/10.1007/978-981-13-2685-1_10

Ahmed, R., & Fokhrul Islam, M. (2013). E-shaped microstrip patch antenna for Ku band. *International Journal of Computer Applications*, *80*(6), 15–19. https://doi.org/10.5120/13864-1719

Al-Sabti, S. M. B., Hamdi, M. M., Abdulateef, A. N., Hmad, S. S., Samir, A. S., & Ali, M. D. (2023). The hyperthermia calculating in head blood by the specific absorption rate (SAR) influence in novel vision. in *proceedings of isas 2023 - 7th international symposium on innovative approaches in smart technologies, proceedings*, *january*, 1–6. https://doi.org/10.1109/isas60782.2023.10391759

al taan, l., & ado, m. s. m. w. (2022). effect of three different dielectric substrates on the performance of rectangular microstrip antenna designed for 2.4 ghz using cst. *rafidain journal of science*, *31*(3), 42–54. https://doi.org/10.33899/rjs.2022.175392

al tameemi, w., dale, t. p., al-jumaily, r. m. k., & forsyth, n. r. (2019). hypoxia-modified cancer cell metabolism. *Frontiers in Cell and Developmental Biology*, *7*(1), 1–15. https://doi.org/10.3389/fcell.2019.00004

Aldhaeebi, M., Alzabidi, M., & Elshafiey, I. (2014). Genetic algorithm optimization of SAR distribution in hyperthermia treatment of human head. In *Proceedings - 1st International Conference on Artificial Intelligence, Modelling and Simulation, AIMS 2013*, *March 2017*, 92–97. https://doi.org/10.1109/AIMS.2013.22

Alex, M., & Chakaravarthi, G. (2023). Circular ring microwave applicator for superficial hyperthermia treatment. In *proceedings of 2023 IEEE Microwaves, Antennas, and Propagation Conference, MAPCON 2023*, 1–4. https://doi.org/10.1109/MAPCON58678.2023.10463788

Ali, A. N. S., Gaid, A. G. S. A., Saeed, M. M., Saeed, R. A., & Hawash, B. (2023). High gain, E-shaped microstrip antenna with two identical slits for 5G applications in the 60 GHz band. In *Proceedings of 2023 3rd International Conference on Emerging Smart Technologies and Applications, ESmarTA 2023*, 1–7.

https://doi.org/10.1109/eSmarTA59349.2023.10293412

Alizadeh, R., Aghsaeifard, Z., Alavi, N., Abbasvandi, F., & Khanigarabadi, A. (2020). A cross-sectional study on the postoperative analgesic-associated side effects and clinical parameters following partial mastectomy. *International Journal of Surgery Open*, *27*(2), 114–118. https://doi.org/10.1016/j.ijso.2020.10.018

Alon, L., Lattanzi, R., Lakshmanan, K., Brown, R., Deniz, C. M., Sodickson, D. K., & Collins, C. M. (2018). Transverse slot antennas for high field MRI. *Magnetic Resonance in Medicine*, *80*(3), 1233–1242. https://doi.org/10.1002/mrm.27095

Altintas, G., Akduman, I., Janjic, A., & Yilmaz, T. (2021). A novel approach on microwave hyperthermia. *Diagnostics*, *11*(3), 1–10. https://doi.org/10.3390/diagnostics11030493

Aronsson, N., & Askeroth, D. (2002). *A Comparative Study of Electromagnetic Dosimetric Simulations and Measurements Master of Science Thesis Department of Electroscience*. *April*.

Arunachalam, K., MacCarini, P. F., Schlorff, J. L., Birkelund, Y., Jacobsen, S., & Stauffer, P. R. (2009). Design of a water coupling bolus with improved flow distribution for multi-element superficial hyperthermia applicators. *International Journal of Hyperthermia*, *25*(7), 554–565. https://doi.org/10.3109/02656730903124506

Ashyap, A. Y. I., Zainal Abidin, Z., Dahlan, S. H., Majid, H. A., Waddah, A. M. A., Kamarudin, M. R., Oguntala, G. A., Abd-Alhameed, R. A., & Noras, J. M. (2018). Inverted e-shaped wearable textile antenna for medical applications. *IEEE Access*, *6*(6), 35214–35222. https://doi.org/10.1109/ACCESS.2018.2847280

Astuti, D. W., Patrakomala, A., Muslim, M., Attamimi, S., & Cahyasiwi, D. A. (2022). A Microstrip antenna with Two U-slots for Wi-Fi and 5G applications. *Heliyon*, *11*(4),

274–280.

Ayalew, L. G., & Asmare, F. M. (2022). Design and optimization of pi-slotted dual-band rectangular microstrip patch antenna using surface response methodology for 5G applications. *Heliyon*, *8*(12), e12030. https://doi.org/10.1016/j.heliyon.2022.e12030

Azharuddin Khan, Satya Kesh Dubey, A. K. S. (2023). An elliptical shaped rectangular slot antenn at 2.48GHz for hyperthermia application. *Microwave Opt Tehnology Letter, 2*(4), 554–565.

Azharuddin Khan, A. K. S. (2023). SAR analysis of hexagonal shaped slot loaded patch antenna for hyperthemia application at 434MHz. *Progress In Electromagnetics Research Letters*, *109*, 119–125. https://doi.org/10.1007/s12647-023-00668-4

Babak, M., & Vrba, J. (2022). Waveguide array applicator for microwave medical imaging. In *Proceedings of 52nd European Microwave Conference, EuMC 2022*, 187–190. https://doi.org/10.23919/EuMC54642.2022.9924394

Babbs, C. F., & DeWitt, D. P. (1981). Physical principles of local heat therapy for cancer. *Medical Instrumentation*, *15*(6), 367–373.

Bacova, F., & Benova, M. (2023). The Specific Absorption Rate of 10g and 1g methods comparison for a child and an adult in a shielded space of railway compartment. *2023 24th International Conference on Computational Problems of Electrical Engineering, CPEE 2023*, 1–4. https://doi.org/10.1109/CPEE59623.2023.10285319

Bah, M. ., Hong, J. ., & Jamro, D. . (2015). Study of breast tissues dielectric properties in uwb range for microwave breast cancer imaging. *Proceedings of the International Conference on Computer Information Systems and Industrial Applications*, *18*(2), 473–475. https://doi.org/10.2991/cisia-15.2015.129

Bakker, A., Zweije, R., Kok, H. P., Kolff, M. W., Desiree van den Bongard, H. J. G., Schmidt, M., van Tienhoven, G., & Crezee, H. (2020). Clinical feasibility of a high-resolution thermal monitoring sheet for superficial hyperthermia in breast cancer patients. *Cancers*, *12*(12), 1–18. https://doi.org/10.3390/cancers12123644

Balanis, C. A. (2016). *Antenna Theory Analysis and Design* (4th ed.). Wiley.

Basavaraju, D. R., & Sukumar, R. (2024). Design and analysis of microstrip patch antennas for sub-6ghz 5g: a comparative study of substrates and feeding techniques. *SSRG International Journal of Electronics and Communication Engineering*, *11*(12), 206–218. https://doi.org/10.14445/23488549/IJECE-V11I12P119

Baskar, R., Lee, K. A., Yeo, R., & Yeoh, K. W. (2012). Cancer and radiation therapy: Current advances and future directions. *International Journal of Medical Sciences*, *9*(3), 193–199. https://doi.org/10.7150/ijms.3635

Baskaran, D., & Arunachalam, K. (2021). Design and experimental verification of 434 MHz phased array applicator for hyperthermia treatment of locally advanced breast cancer. *IEEE Transactions on Antennas and Propagation*, *69*(3), 1706–1715. https://doi.org/10.1109/TAP.2020.3016462

Basurto-hurtado, J. A., Cruz-albarran, I. A., Toledano-ayala, M., Ibarra-manzano, M. A., Morales-hernandez, L. A., & Perez-ramirez, C. A. (2022). Diagnostic strategies for breast cancer detection : from image intelligence algorithms. *International Journal of Medical Sciences*, 1–24.

Begg, K., & Tavassoli, M. (2020). Inside the hypoxic tumour: reprogramming of the DDR and radioresistance. *Cell Death Discovery*, *6*(1), 77–88. https://doi.org/10.1038/s41420-020-00311-0

Behrouzkia, Z., Joveini, Z., Keshavarzi, B., Eyvazzadeh, N., & Aghdam, R. Z. (2016). Hyperthermia: How can it be used? *Oman Medical Journal*, *31*(2), 89–97. https://doi.org/10.5001/omj.2016.19

Bevacqua, M. T., Bellizzi, G. G., Crocco, L., & Isernia, T. (2018). Permittivity and conductivity estimation for hyperthermia treatment planning. *IEEE Antennas and Propagation Society International Symposium and USNC/URSI National Radio Science Meeting, APSURSI 2018 - Proceedings*, *3*(2), 591–592. https://doi.org/10.1109/APUSNCURSINRSM.2018.8608545

Bezerra, M. A., Santelli, R. E., Oliveira, E. P., Villar, L. S., & Escaleira, L. A. (2008). Response surface methodology (RSM) as a tool for optimization in analytical chemistry. *Talanta*, *76*(5), 965–977. https://doi.org/10.1016/j.talanta.2008.05.019

Bianchi, L., Asadi, S., De Landro, M., Korganbayev, S., & Saccomandi, P. (2022). Measurement of thermal properties of biological tissues and tissue-mimicking phantom with a dual-needle sensor. In *Proceedings of IEEE International Symposium on Medical Measurements and Applications, MeMeA 2022 - Conference Proceedings*, 0–5. https://doi.org/10.1109/MeMeA54994.2022.9856408

Bird, T. S. (2009). Definition and misuse of return loss. *IEEE Antennas and Propagation Magazine*, *51*(2), 166–167. https://doi.org/10.1109/MAP.2009.5162049

Birkelund, Y., Jacobsen, S., Arunachalam, K., MacCarini, P., & Stauffer, P. R. (2009). Flow patterns and heat convection in a rectangular water bolus for use in superficial hyperthermia. *Physics in Medicine and Biology*, *54*(13), 3937–3953. https://doi.org/10.1088/0031-9155/54/13/001

Borkar, N. M., & Parlewar, P. K. (2024). Designing an ultra-wideband directional antipodal

Vivaldi antenna with U-slots for biomedical applications using an optimized attention network. *Frequenz*, *5*(2), 1–15. https://doi.org/10.1515/freq-2024-0063

Calderwood, S. K., Theriault, J. R., & Gong, J. (2005). How is the immune response affected by hyperthermia and heat shock proteins? *International Journal of Hyperthermia*, *21*(8), 713–716. https://doi.org/10.1080/02656730500340794

Camilleri, J. S., Farhat, I., Farrugia, L., Bonello, J., & Sammut, C. V. (2021). Preliminary investigations on microwave hyperthermia for breast cancer using a dipole antenna. In *Proceedings of 34th General Assembly and Scientific Symposium of the International Union of Radio Science, URSI GASS 2021*, *September*, 1–4. https://doi.org/10.23919/URSIGASS51995.2021.9560617

Camilleri, J. S., Farrugia, L., Curto, S., Rodrigues, D. B., Farina, L., Dingli, G. C., Bonello, J., Farhat, I., & Sammut, C. V. (2022). Review of thermal and physiological properties of human breast tissue. *Sensors*, *22*(10), 1–29. https://doi.org/10.3390/s22103894

Cappiello, G., McGinley, B., Elahi, M. A., Drizdal, T., Paulides, M. M., Glavin, M., O'Halloran, M., & Jones, E. (2017). Differential evolution optimization of the SAR distribution for head and neck hyperthermia. *IEEE Transactions on Biomedical Engineering*, *64*(8), 1875–1885. https://doi.org/10.1109/TBME.2016.2627941

Chakraborty, A., Neogi, K., Banerjee, A., & Sadhu, P. K. (2016). Switching frequency optimization in hyperthermia treatment using BSD 2000. In *Proceedings of International Conference on Energy, Power and Environment: Towards Sustainable Growth, ICEPE 2015*. https://doi.org/10.1109/EPETSG.2015.7510061

Charan, D. R., Akhil, B., Dinesh, S., Sivani, J. N. V, & Upadhyayula, R. K. (2021). Improvement of slotted patch antenna performance for biomedical applications. *IEEE*

Transactions on Biomedical Engineering, *16*(3), 34–40. https://doi.org/10.9790/2834-1603013440

Charan, L., T.V.Rama, K., & K.Kumar, N. (2020). A compact UWB microstrip antenna with hexagonal circular patch and asymmetric cpw-fed for on-body applications. *International Journal of Emerging Trends in Engineering Research*, *8*(2), 4–10. https://doi.org//doi.org/10.30534/ijeter/2020/49822020

Chen, J. H., Cheng, C. Y., Chien, C. M., Yuangyai, C., Chen, T. H., & Chen, S. T. (2023). Multiple performance optimization for microstrip patch antenna improvement. *Sensors*, *23*(9), 34–40. https://doi.org/10.3390/s23094278

Chicheł, A., Skowronek, J., Kubaszewska, M., & Kanikowski, M. (2007). Hyperthermia - Description of a method and a review of clinical applications. *Reports of Practical Oncology and Radiotherapy*, *12*(5), 267–275. https://doi.org/10.1016/S1507-1367(10)60065-X

Chishti, A. R., Abbasi, M. N., Abbasi, D., Khan, M. U. A., Masud, M. J., & Aziz, A. (2023). E-shaped antenna sensor optimization with improved bandwidth using genetic algorithm for biomedical applications. In *Proceedings - 2023 IEEE International Conference on Emerging Trends in Engineering, Sciences and Technology, ICES and T 2023*, 1–6. https://doi.org/10.1109/ICEST56843.2023.10138806

Choi, W. C., Kim, K. J., Park, H. S., & Yoon, Y. J. (2012). Frequency reconfigurable applicator for superficial hyperthermia system. *IEEE Antennas and Propagation Society, AP-S International Symposium (Digest)*, 26–29.

Choi, W. C., Lim, S., & Yoon, Y. J. (2016). Design of noninvasive hyperthermia system using transmit-array lens antenna configuration. *IEEE Antennas and Wireless*

Propagation Letters, *15*(4), 857–860. https://doi.org/10.1109/LAWP.2015.2477428

Choma, W. C. (2001). *Feedback Networks: Theory And Circuit Applications - Wai-kai Chen, John Choma - Google Books*. World Sientific. Retrieved October 2, 2020, from https://books.google.com.my/books?id=yfo7DQAAQBAJ&printsec=copyright&redir_esc=y#v=onepage&q&f=false

Choudhary, R., & Arunachalam, K. (2022). Design and comparison of semi-ellipsoidal and conical phased array applicators operating at 434 MHz for hyperthermia treatment of locally advanced breast cancer. *2022 IEEE Region 10 Symposium, TENSYMP 2022*, 1–3. https://doi.org/10.1109/TENSYMP54529.2022.9864401

Cole, K. S., & Cole, R. H. (1942). Dispersion and absorption in dielectrics: II. Direct current characteristics. *The Journal of Chemical Physics*, *10*(2), 98–105. https://doi.org/10.1063/1.1723677

Creswell, J. W. (2014). *Qualitative, Quantitative and Research Design* (4th ed.). SAGE Publications Inc.

Curto, S., Garcia-Miquel, A., Suh, M., Vidal, N., Lopez-Villegas, J. M., & Prakash, P. (2018). Design and characterisation of a phased antenna array for intact breast hyperthermia. *International Journal of Hyperthermia*, *34*(3), 250–260. https://doi.org/10.1080/02656736.2017.1337935

Dargar, S. K., Gupta, A., Sabir, M., & Lakshmi, A. (2022a). Design of U-slot microstrip patch antenna for wireless applications. *2022 2nd International Conference on Advances in Electrical, Computing, Communication and Sustainable Technologies, ICAECT 2022*, *12*. https://doi.org/10.1109/ICAECT54875.2022.9807838

Dayanc, B. E., Beachy, S. H., Ostberg, J. R., & Repasky, E. A. (2008). Dissecting the role

of hyperthermia in natural killer cell mediated anti-tumor responses. *International Journal of Hyperthermia*, *24*(1), 41–56. https://doi.org/10.1080/02656730701858297

de Bruijne, M., Samaras, T., Bakker, J. F., & van Rhoon, G. C. (2006). Effects of waterbolus size, shape and configuration on the SAR distribution pattern of the Lucite cone applicator. *International Journal of Hyperthermia*, *22*(1), 15–28. https://doi.org/10.1080/02656730500384297

Deshmukh, A. A., Ambekar, A. G., & Chavali, V. A. P. (2024). Circularly polarized gap-coupled variations of square microstrip antennas employing U-slot for WLAN and bluetooth applications. *Electromagnetics*, *44*(1), 1–17. https://doi.org/10.1080/02726343.2024.2316118

Deshmukh, A. A., & Chavali, V. A. P. (2023). Variations of square microstrip antenna loaded with u-slot and pair of rectangular slots for circular polarized response. *Sadhana - Academy Proceedings in Engineering Sciences*, *48*(3), 534–540. https://doi.org/10.1007/s12046-023-02190-4

Deshmukh, A. A., & Ray, K. P. (2013). Analysis of broadband E-shaped microstrip antennas. *IEEE Antennas and Propagation Magazine*, *55*(2), 107–123. https://doi.org/10.1109/MAP.2013.6529321

Dewhirst, M., Stauffer, P. R., Das, S., Craciunescu, O. I., & Vujaskovic, Z. (2015). Hyperthermia. In *Clinical Radiation Oncology* (Fourth Edi). Elsevier Inc. https://doi.org/10.1016/B978-0-323-24098-7.00021-6

Dilalla, V., Chaput, G., Williams, T., & Sultanem, K. (2020). Radiotherapy side effects: Integrating a survivorship clinical lens to better serve patients. *Current Oncology*, *27*(2), 107–112. https://doi.org/10.3747/co.27.6233

Dong, H., Xiao, Y., Tan, S., Hu, J., & Chen, Z. (2023). Dual-broadband circularly polarized reconfigurable antenna based on asymmetric U-slot patch. *IEEE Antennas and Wireless Propagation Letters*, *22*(12), 3052–3056. https://doi.org/10.1109/LAWP.2023.3309504

Du, Yang Xing, Xi, X. L., & Qin, L. (2010). The design of four-arm spiral antenna for microwave hyperthermia. *2010 4th International Conference on Bioinformatics and Biomedical Engineering, ICBBE 2010*, *6*(5), 1–3. https://doi.org/10.1109/ICBBE.2010.5515123

Du, Yong Xin, Xi, X. L., & Guo, W. (2011). The design and simulation of two-armed spiral antenna for microwave hyperthermia. In *Proceedings of 5th International Conference on Bioinformatics and Biomedical Engineering, ICBBE 2011*, 1–4. https://doi.org/10.1109/icbbe.2011.5780310

Dunne, M., Regenold, M., & Allen, C. (2020). Hyperthermia can alter tumor physiology and improve chemo- and radio-therapy efficacy. *Advanced Drug Delivery Reviews*, *163–164*, 98–124. https://doi.org/10.1016/j.addr.2020.07.007

Ebrahimi-Ganjeh, M. A., & Attari, A. R. (2008). Study of water bolus effect on sar penetration depth and effective field size for local hyperthermia. *Progress In Electromagnetics Research B*, *4*(6), 273–283. https://doi.org/10.2528/pierb08011403

Edara, B. L. T., Aishwarya, T. G. N., Manisha, K., Pandey, S. D., & Saida, A. (2023). Design of a combined horizontal and U slot patch antenna with reduced cross-polarization and increased sustainability. *E3S Web of Conferences*, *430*. https://doi.org/10.1051/e3sconf/202343001015

Elkayal, H. A., Aly, M. H., & Ismail, N. E. (2024). Optimization of antenna excitations for

non-invasive microwave hyperthermia for breast cancer treatment. *Journal of Advanced Research in Applied Sciences and Engineering Technology*, *39*(2), 258–269. https://doi.org/10.37934/araset.39.2.258269

Elming, P. B., Sørensen, B. S., Oei, A. L., Franken, N. A. P., Crezee, J., Overgaard, J., & Horsman, M. R. (2019). Hyperthermia: The optimal treatment to overcome radiation resistant hypoxia. *Cancers*, *11*(1), 1–20. https://doi.org/10.3390/cancers11010060

Elsaadi, M., Aid, Y., Abbas, M., Embarek, A., & Salih, K. (2019). Hyperthermia for breast cancer treatment using slotted circular patch antenna. *Circuits and Systems*, *10*(3), 37–44. https://doi.org/10.4236/cs.2019.103003

Elsaadi, M., & Hamad, R. (2023). Breast cancer hyperthermia treatment based on slotted patch antenna at 2.45 GHz. *Circuits and Systems*, *14*(5), 10–18. https://doi.org/10.4236/cs.2023.145002

Elshafiey, I., Sheta, A. F., Nizam Uddin, M. A., Abdulkawi, W. M., & Malik, W. A. (2019). Adaptive energy concentration in hyperthermia treatment of cancer. *APACE 2019 - 2019 IEEE Asia-Pacific Conference on Applied Electromagnetics, Proceedings*, *November*, 1–5. https://doi.org/10.1109/APACE47377.2019.9021009

Emami Nejad, A., Najafgholian, S., Rostami, A., Sistani, A., Shojaeifar, S., Esparvarinha, M., Nedaeinia, R., Haghjooy Javanmard, S., Taherian, M., Ahmadlou, M., Salehi, R., Sadeghi, B., & Manian, M. (2021). The role of hypoxia in the tumor microenvironment and development of cancer stem cell: a novel approach to developing treatment. *Cancer Cell International*, *21*(1), 1–26. https://doi.org/10.1186/s12935-020-01719-5

Fallahi Hojjatollah, P. P. (2018). Antenna designs for microwave tissue ablation. *Critical Reviews in Biomedical Engineering*, *5*(2), 495–521.

https://doi.org/10.1615/CritRevBiomedEng.2018028554. Antenna

Fang, D. G. (2011). Arrays and array synthesis. In *Antenna Theory and Microstrip Antennas*. CRC Press,Taylor & Francis Group. https://doi.org/10.1201/b10302-2

Fatehi, D., van der Zee, J., & van Rhoon, G. C. (2009). Thermoradiotheraphy of cancer: An effective approach. *Australasian Medical Journal*, *2*(14), 224–234. https://doi.org/10.4066/AMJ.2009.136

Firuzalizadeh, M., Gaffoglio, R., Giordanengo, G., Righero, M., Zucchi, M., Musacchio Adorisio, G., Bellone, A., Vallan, A., Perrone, G., & Vecchi, G. (2025). Joint optimization of antenna system matching and specific absorption rate focusing in microwave hyperthermia cancer treatment. *Cancers*, *17*(3), 1–16. https://doi.org/10.3390/cancers17030386

Fiser, O., Merunka, I., & Vrba, J. (2015). Design, evaluation and validation of planar antenna array for breast hyperthermia treatment. *Australasian Medical Journal*, *1*(2), 1–4. https://doi.org/10.1109/COMITE.2015.7120228

Florez, H., Leon, M., Diaz-Nafria, J. M., & Belli, S. (2019). *Hyperthermia study in breast cancer treatment using three applicators*. https://doi.org/10.1007/978-3-030-32475-9_39

Franckena, M., & van der Zee, J. (2010). Use of combined radiation and hyperthermia for gynecological cancer. *Current Opinion in Obstetrics & Gynecology*, *22*(1), 9–14. https://doi.org/10.1097/gco.0b013e328333d1e2

Gabriel, A., A, A. (2025). A multi-objective optimization framework through genetic algorithm for hyperthermia-mediated drug delivery. *Computers in Biology and Medicine*, *189*(2), 109895. https://doi.org/10.1016/j.compbiomed.2025.109895

Gabriel, C., Gabriel, S., & Corthout, E. (1996). The dielectric properties of biological tissues: I. Literature survey. *Physics in Medicine and Biology*, *41*(11), 2231–2249. https://doi.org/10.1088/0031-9155/41/11/001

Gabriel, S., Lau, R. W., & Gabriel, C. (1996). The dielectric properties of biological tissues: III. Parametric models for the dielectric spectrum of tissues. *Physics in Medicine and Biology*, *41*(11), 2271–2293. https://doi.org/10.1088/0031-9155/41/11/003

Gao, B., Ru, G., Ma, Q., & Li, H. (2022). Electromagnetic Multiphysics Sensing Nondestructive Testing. In *Encyclopedia of Sensors and Biosensors: Volume 1-4, First Edition* (Vols. 1–4). Elsevier. https://doi.org/10.1016/B978-0-12-822548-6.00115-1

Garg, M. K., & Saini, J. (2020). Dual frequency electronically controlled radiation beam reconfigurable slotted antenna for detection of a stationary or nonstationary target. *Defence Science Journal*, *70*(5), 486–492. https://doi.org/10.14429/DSJ.70.15155

Ghadge, S. V., & Raheman, H. (2006). Process optimization for biodiesel production from mahua (Madhuca indica) oil using response surface methodology. *Bioresource Technology*, *97*(3), 379–384. https://doi.org/10.1016/j.biortech.2005.03.014

Ghasemlouy, A., & Rajebi, S. (2019). Investigation and evaluation of the effect of silicon layer and its comparison with water bolus in designing microstrip antenna for hyperthermia applications. *Journal of Communications Technology and Electronics*, *64*(11), 1307–1317. https://doi.org/10.1134/S1064226919110093

Giuliano, A. E., Connolly, J. L., Edge, S. B., Mittendorf, E. A., Rugo, H. S., Solin, L. J., Weaver, D. L., Winchester, D. J., & Hortobagyi, G. N. (2017). Breast cancer-major changes in the american joint committee on cancer eighth edition cancer staging manual. *CA: A Cancer Journal for Clinicians*, *67*(4), 290–303.

https://doi.org/10.3322/caac.21393

GLOBOCAN. (2022a). *Globocan 2022-Incidence World*.

GLOBOCAN. (2022b). *Globocan 2022-Mortality Malaysia*.

GLOBOCAN. (2022c). *Globocan 2022-Mortality World*.

Govindarajulu, S. R., Tarek, M. N. A., Guerra, M. R., Hassan, A., & Alwan, E. (2023). Modified U Slot Patch Antenna with Large Frequency Ratio for Vehicle-to-Vehicle Communication. *Sensors*, *23*(13), 34–40. https://doi.org/10.3390/s23136108

Goyal, P., Singhal, P. K., Sahoo, P., & Parsediya, D. K. (2023). Modified E-Shape Rectangular Microstrip Patch Antenna with DGS for Wireless Communication. *International Journal of Electrical and Electronics Research*, *11*(3), 814–818. https://doi.org/10.37391/ijeer.110327

Guisasola, E., Baeza, A., Asín, L., Fuente, J. M. D., & Vallet-Regí, M. (2018). Heating at the Nanoscale through Drug-Delivery Devices: Fabrication and Synergic Effects in Cancer Treatment with Nanoparticles. *Small Methods*, *2*(9), 31–42. https://doi.org/10.1002/SMTD.201800007

Gun, L., Ning, D., & Liang, Z. (2017). Effective Permittivity of Biological Tissue: Comparison of Theoretical Model and Experiment. *Mathematical Problems in Engineering*, *2017*. https://doi.org/10.1155/2017/7249672

Gupta, A., Srivastava, D. K., & Saini, J. P. (2020). Modified e-slotted patch antenna for WLAN/Wi-Max satellite applications. *Telkomnika (Telecommunication Computing Electronics and Control)*, *18*(1), 258–263. https://doi.org/10.12928/TELKOMNIKA.v18i1.12959

Gupta, R. C., & Singh, S. P. (2005). Analysis of the SAR distributions in three-layered bio-media in direct contact with a water-loaded modified box-horn applicator. *IEEE Transactions on Microwave Theory and Techniques*, *53*(9), 2665–2671. https://doi.org/10.1109/TMTT.2005.854209

Habash, R. W., Bansal, R., Krewski, D., & Alhafid, H. T. (2006). Thermal therapy, Part 1: An introduction to thermal therapy. *Critical Reviews in Biomedical Engineering*, *34*(6), 459–489. https://doi.org/10.1615/CritRevBiomedEng.v34.i6.20

Habash, R. W. Y., Bansal, R., Krewski, D., & Alhafid, H. T. (2006). Thermal therapy, Part 2: Hyperthermia techniques. *Critical Reviews in Biomedical Engineering*, *34*(6), 491–542. https://doi.org/10.1615/CritRevBiomedEng.v34.i6.30

Halheit, H., Vander Vorst, A., Tedjini, S., & Touhami, R. (2012). Flexible dual-frequency applicator for local hyperthermia. *International Journal of Antennas and Propagation*, *2*(2), 37–46. https://doi.org/10.1155/2012/389214

Hand, J. L. C. and A. J. H. (1986). Absorbed Power Distribution from Coherent Microwave Arrays for Localized Hyperthermia. *IEE Transction on Microwave Theory and Techniques*, *M*(5), 484–489.

Haque, M. A., Zakariya, M. A., Paul, L. C., Nath, D., Biswas, P., & Azim, R. (2021). Analysis of Slotted E-shaped Microstrip Patch Antenna for Ku Band Applications. *15th IEEE Malaysia International Conference on Communications: Emerging Technologies in IoT and 5G, MICC 2021 - Proceedings*, 98–101. https://doi.org/10.1109/MICC53484.2021.9642100

Haque, M., Datto, S., & Hossain, M. A. (2019). Optimization of Performance Parameter of Microstrip Patch Antenna in Millimeter Wave Region. *3rd International Conference*

on Electrical, Computer and Telecommunication Engineering, ICECTE 2019, 157–160. https://doi.org/10.1109/ICECTE48615.2019.9303581

Harris, B., Saleem, S., Cook, N., & Searle, E. (2022). Targeting hypoxia in solid and haematological malignancies. *Journal of Experimental and Clinical Cancer Research*, *41*(1), 1–16. https://doi.org/10.1186/s13046-022-02522-y

Hasan, M. N., Shah, S. W., Babar, M. I., & Sabir, Z. (2012). Design and simulation based studies of a dual band u-slot patch antenna for WLAN application. *International Conference on Advanced Communication Technology, ICACT*, *April 2018*, 997–1001.

Hassan, M. M., Lias, K., Buniyamin, N., Ahmad, M. Z., Sarpinah, B., Naimullah, S., Basri, H. M., & Alam, S. (2025). *SAR Distribution with Different Water Bolus Shapes for Hyperthermia Breast Cancer Treatment*. *1*(1), 32–47.

Hesabgar, S. M., Sadeghi-Naini, A., Czarnota, G., & Samani, A. (2017). Dielectric properties of the normal and malignant breast tissues in xenograft mice at low frequencies (100 Hz–1 MHz). *Measurement: Journal of the International Measurement Confederation*, *105*(5), 56–65. https://doi.org/10.1016/j.measurement.2017.04.004

Hu, K., Xiao, Q., & Huang, K. (2024). Compact Slot Microstrip Patch Antenna Loaded with Open Metal Cavity for Microwave Hyperthermia. *International Journal of RF and Microwave Computer-Aided Engineering*, *2024*(1), 36–49. https://doi.org/10.1155/2024/9422872

Hunt, J. W., Lalonde, R., Ginsberg, H., Urchuk, S., & Worthington, A. (1991). Rapid heating: Critical theoretical assessment of thermal gradients found in hyperthermia treatments. *International Journal of Hyperthermia*, *7*(5), 703–718.

https://doi.org/10.3109/02656739109056440

Iero, D. A. M., Crocco, L., Isernia, T., & Korkmaz, E. (2016). Optimal focused electromagnetic hyperthermia treatment of breast cancer. *2016 10th European Conference on Antennas and Propagation, EuCAP 2016*. https://doi.org/10.1109/EuCAP.2016.7481515

Iigusa, K., Sawada, H., Miura, A., & Tsuji, H. (2024). Input Impedance of Radiation Efficiency Deterioration State. In *Proceedings of 18th European Conference on Antennas and Propagation, EuCAP 2024*, 1–5. https://doi.org/10.23919/EuCAP60739.2024.10500917

Iqbal, M. W., & Zulkifli, F. Y. (2023). Microstrip Leaky-Wave Antenna Design with E-Slot and Double U-Slot for Bandwidth Enhancement. *International Seminar on Intelligent Technology and Its Applications: Leveraging Intelligent Systems to Achieve Sustainable Development Goals, ISITIA 2023 - Proceeding*, 160–163. https://doi.org/10.1109/ISITIA59021.2023.10221092

Issels, R. D., Nössner, E., & Wust, P. (2002). Hyperthermia in oncology. In *Onkologe, 6*(8), 34–40. https://doi.org/10.1007/s00761-002-0382-0

Jaffar, N. A., Lias, K. B., Madzhi, N. K., & Buniyamin, N. (2018). An overview of metamaterials used in applicators in hyperthermia cancer treatment procedure. *2017 International Conference on Electrical, Electronics and System Engineering, ICEESE 2017*, *2018-Janua*, 32–36. https://doi.org/10.1109/ICEESE.2017.8298389

Jamali, A. A., Amirzada, M. R., Anjum, M. R., & Kanwar, K. (2018). Implementation of Periodic Boundary Conditions in FDTD Algorithm. *Journal of Information Communication Technologies and Robotic Applications*, *9*(2), 28–36.

John W. Creswell, J. D. C. (2018). Research Design Qualitative, Quantitative and Mix Method Approaches. In *JSAGE Publications,Inc* (5th ed.). https://doi.org/10.1017/CBO9781107415324.004

Arunachalam, K. P, Maccarini, T. Juang, P. R. S. (2008). Performance evaluation of a conformal thermal monitoring sheet (TMS) sensor array for measurement of surface temeprature distributions during superficial hyperthermia treatments. *International Journal Hyperthemia*, *24*(4), 313–325. https://doi.org/10.1080/02656730701881133.Performance

Kashyap, P. A., Sarmah, K., Dakua, I., & Baruah, S. (2023). Gain and bandwidth enhancement of slotted microstrip antenna using metallic nanofilms for WLAN applications. *Journal of King Saud University - Science*, *35*(1), 102374. https://doi.org/10.1016/j.jksus.2022.102374

Katta, B., Vijayakumar, C., Dutta, S., Dubashi, B., & Nelamangala Ramakrishnaiah, V. P. (2023). The Incidence and Severity of Patient-Reported Side Effects of Chemotherapy in Routine Clinical Care: A Prospective Observational Study. *Cureus*, *15*(4). https://doi.org/10.7759/cureus.38301

Kaur, K., & Kaur, A. (2022). Archimedes Spiral Antenna for the Microwave Hyperthermia Application. *3rd International Conference on Smart Electronics and Communication, ICOSEC 2022 - Proceedings*, *1*(Icosec), 590–594. https://doi.org/10.1109/ICOSEC54921.2022.9952156

Kaur, S., Mayanglambam, P., Bajwan, D., & Thakur, N. (2022). Chemotherapy and its Adverse Effects – A Systematic Review. *International Journal of Nursing Education and Research*, *January 2023*, 399–402. https://doi.org/10.52711/2454-

2660.2022.00090

Kee, J., Mokayef, M., Summakieh, M. A., Khan, M. K. A. A., & Tiang, S. S. (2024). A Slot-Integrated Microstrip Antenna Design for High-Performance Communication Systems, and Wireless Sensing Application. *Advances in Transdisciplinary Engineering*, *46*(2), 571–576. https://doi.org/10.3233/ATDE231151

Kelley, D. F., & Luebbers, R. I. (1996). Piecewise linear recursive convolution for dispersive media using FDTD. *IEEE Transactions on Antennas and Propagation*, *44*(1), 792–797. https://doi.org/10.1109/8.509882

Khan, A., Dubey, S. K., & Singh, A. K. (2024). Corner T-slot antenna at 2.45 GHz for hyperthermia application. *Journal of Electromagnetic Waves and Applications*, *38*(4), 508–521. https://doi.org/10.1080/09205071.2024.2320742

Khan, A., Dubey, S. K., & Singh, A. K. et. a. (2023). Slot-Loaded Pentagon Microstrip Patch Antenna for Hyperthermia Application at 434 MHz. *Mapan - Journal of Metrology Society of India*, *38*(4), 913–921. https://doi.org/10.1007/s12647-023-00668-4

Khan, A., Mishra, A., Dubey, S. K., & Singh, A. K. (2023). Square patch with symmetrical L-slots resonating at 915 MHz for Hyperthermia application. In *Proceedings of 2nd International Conference on Wireless, Antenna and Microwave Symposium, WAMS 2023*, 1–4. https://doi.org/10.1109/WAMS57261.2023.10242987

Khan, A., & Singh, A. K. (2022). Pentagon-shaped Microstrip Patch Antenna in ISM band for Hyperthermia Application. *2022 IEEE Microwaves, Antennas, and Propagation Conference, MAPCON 2022*, *1*, 460–464. https://doi.org/10.1109/MAPCON56011.2022.10047667

Khan, A., Singh, A. K., & Singh, A. K. et. a. (2023). Analysis of Cross-Slot Antenna at ISM

band for Hyperthermia application. *2nd International Conference on Microwave, Optical and Communication Engineering, ICMOCE 2023*, 1–4. https://doi.org/10.1109/ICMOCE57812.2023.10167190

Kim, I., Lee, D. M., Shin, J. W., Lee, G. J., Kim, E. S., & Kim, N. Y. (2024). Radio frequency hyperthermia system for skin tightening effect by filled waveguide aperture antenna with compact metamaterials. *Frontiers in Bioengineering and Biotechnology*, *12*(March), 1–9. https://doi.org/10.3389/fbioe.2024.1378084

Kirthi, K. A. S., Harish, K., & Avinash, H. U. (2013). Principles of Radiation Oncology: A Beams Eye View for a Surgeon. *Indian Journal of Surgical Oncology*, *4*(3), 255–262. https://doi.org/10.1007/s13193-013-0231-1

Kishore, M. R., Kumar, V. J., & Kumar, G. S. (2014). Design & Simulation of E-Shaped Micro Strip Patch Antenna for GPS Application. *Sensors, 4*(8), 94–100.

Koh, J., & Kim, M. J. (2019). Introduction of a new staging system of breast cancer for radiologists: An emphasis on the prognostic stage. In *Korean Journal of Radiology* (Vol. 20, Issue 1, pp. 69–82). Korean Radiological Society. https://doi.org/10.3348/kjr.2018.0231

Kok, H. P., Bakker, A., Kolff, M. W., Van Tienhoven, G., Hulshof, M. C. C. M., Van Stam, G., & Crezee, J. (2016). A 70 MHz double waveguide set-up for hyperthermia of deep superficial tumors. *European Microwave Week 2016: "Microwaves Everywhere", EuMW 2016 - Conference Proceedings; 46th European Microwave Conference, EuMC 2016*, 1219–1222. https://doi.org/10.1109/EuMC.2016.7824569

Kok, H. P., Kotte, A. N. T. J., & Crezee, J. (2017). Planning, optimisation and evaluation of hyperthermia treatments. *International Journal of Hyperthermia*, *33*(6), 593–607.

https://doi.org/10.1080/02656736.2017.1295323

Kok, H. P., Van Stam, G., Sijbrands, J., Bakker, A., Kolff, M. W., Van Tienhoven, G., Hulshof, M. C. C. M., & Crezee, J. (2017). Clinical use of a waveguide hyperthermia system for superficial tumors with deep infiltration. *European Microwave Week 2017: "A Prime Year for a Prime Event", EuMW 2017 - Conference Proceedings; 47th European Microwave Conference, EuMC 2017*, *2017-Janua*, 868–871. https://doi.org/10.23919/EuMC.2017.8230982

Kok, H. P., Wust, P., Stauffer, P. R., Bardati, F., van Rhoon, G. C., & Crezee, J. (2015). Current state of the art of regional hyperthermia treatment planning: A review. *Radiation Oncology*, *10*(1), 1–14. https://doi.org/10.1186/s13014-015-0503-8

Koo, Y. S., Kazemi, R., Liu, Q., Phillips, J. C., & Fathy, A. E. (2014). Development of a high SAR conformal antenna for hyperthermia tumors treatment. *IEEE Transactions on Antennas and Propagation*, *62*(11), 5830–5840. https://doi.org/10.1109/TAP.2014.2357419

Korkmaz, E., Isik, O., & Kara, S. (2013). Electromagnetic modeling of a female breast hyperthermia applicator. *IEEE Antennas and Propagation Society, AP-S International Symposium (Digest)*, *April 2015*, 2048–2049. https://doi.org/10.1109/APS.2013.6711682

Korkmaz, E., Isik, O., & Nassor, M. A. (2013). A compact microstrip spiral antenna embedded in water bolus for hyperthermia applications. *International Journal of Antennas and Propagation*, *2013*. https://doi.org/10.1155/2013/954986

Korkmaz, E., Isik, O., & Sagkol, H. (2015). A directive antenna array applicator for focused electromagnetic hyperthermia treatment of breast cancer. *2015 9th European*

Conference on Antennas and Propagation, EuCAP 2015, *1*(April).

Kothari, C. R. (2015). Research methodology: Methods and technics. In *Syria Studies, 7*(1), 107–119.

Koziel, S., & Bandler, J. W. (2015). Rapid yield estimation and optimization of microwave structures exploiting feature-based statistical analysis. *IEEE Transactions on Microwave Theory and Techniques*, *63*(1), 107–114. https://doi.org/10.1109/TMTT.2014.2373365

Koziel, S., & Bekasiewicz, A. (2015). Fast multiobjective optimization of narrowband antennas using RSA models and design space reduction. *IEEE Antennas and Wireless Propagation Letters*, *14*, 450–453. https://doi.org/10.1109/LAWP.2014.2367128

Kroeze, H., Van de Kamer, J. B., De Leeaw, A. A. C., & Lagendijk, J. J. W. (2001). Regional hyperthermia applicator design using FDTD modelling. *Physics in Medicine and Biology*, *46*(7), 1919–1935. https://doi.org/10.1088/0031-9155/46/7/313

Krontiras, H., Lancaster, R. B., & Urist, M. M. (2014). What is a clear margin in breast conserving cancer surgery? *Current Treatment Options in Oncology*, *15*(1), 79–85. https://doi.org/10.1007/s11864-013-0270-4

Kumari, V., Sheoran, G., & Kanumuri, T. (2020). SAR analysis of directive antenna on anatomically real breast phantoms for microwave holography. *Microwave and Optical Technology Letters*, *62*(1), 466–473. https://doi.org/10.1002/mop.32037

Kurt, O. (2023). Distance dependent performance of microstrip patch antenna for breast tumor detection. International Congress of New Horizons In Sciences, *November 2022*.

Latha, T., Ram, G., Arun Kumar, G., & Chakravarthy, M. (2022). Compact wideband e-slotted e-shaped patch antenna for ku-band phased array applications. *IEEE*

Transactions on Aerospace and Electronic Systems, *3*(1), 1–11. https://doi.org/10.1109/TAES.2024.3374275

Lazebnik, M., Popovic, D., McCartney, L., Watkins, C. B., Lindstrom, M. J., Harter, J., Sewall, S., Ogilvie, T., Magliocco, A., Breslin, T. M., Temple, W., Mew, D., Booske, J. H., Okoniewski, M., & Hagness, S. C. (2007). A large-scale study of the ultrawideband microwave dielectric properties of normal, benign and malignant breast tissues obtained from cancer surgeries. *Physics in Medicine and Biology*, *52*(20), 6093–6115. https://doi.org/10.1088/0031-9155/52/20/002

Lee, S. H., Kim, Y. J., Lee, K. S., & Kim, S. J. (2016). Multiobjective optimization design of small-scale wind power generator with outer rotor based on box-behnken design. *IEEE Transactions on Applied Superconductivity*, *26*(4), 1–5. https://doi.org/10.1109/TASC.2016.2524620

Li, J., Wang, B., Zhang, D., Li, C., Zhu, Y., Zou, Y., Chen, B., Wu, T., & Wang, X. (2021). A preclinical system prototype for focused microwave breast hyperthermia guided by compressive thermoacoustic tomography. *IEEE Transactions on Biomedical Engineering*, *68*(7), 2289–2300. https://doi.org/10.1109/TBME.2021.3059869

Li, J., & Wang, X. (2019). Comparison of two small circularly polarized antennas for focused microwave hyperthermia. *13th European Conference on Antennas and Propagation, EuCAP 2019*, *January*.

Li, Y., Li, Y. L., & Yu, S. M. (2008). Design optimization of a current mirror amplifier integrated circuit using a computational statistics technique. *Mathematics and Computers in Simulation*, *79*(4), 1165–1177. https://doi.org/10.1016/j.matcom.2007.11.002

Lias, K., Buniyamin, N., & Ahmad Narihan, M. Z. (2016). Specific absorption rate investigation of different EBG-M applicator structures for non-invasive hyperthermia cancer treatment procedure. *International Conference for Innovation in Biomedical Engineering and Life Sciences*, *56*(1), 103–106. https://doi.org/10.1007/978-981-10-0266-3_21

Lias, K., & Buniyamin, N. (2017). FDTD computational simulation for SAR observation towards breast hyperthermia cancer procedure. *Pertanika Journal of Science and Technology*, *25*(S), 221–230.

Lias, K., Buniyamin, N., & Narihan, M. Z. A. (2016). Simulation study of an EBG-M applicator towards non-invasive breast hyperthermia cancer procedure. *Jurnal Teknologi*, *78*(5–6), 75–81. https://doi.org/10.11113/jt.v78.8641

Lias, K., Jaffar, N. A., Buniyamin, N., Basri, H. M., Abidin, W. A. W. Z., Kipli, K., & Mohtadzar, N. A. A. (2019). Simulation study of a modified rectangular microstrip for the hyperthermia breast cancer procedure with SEMCAD X solver. *Journal of Physics: Conference Series*, *1372*(1), 0–8. https://doi.org/10.1088/1742-6596/1372/1/012005

Lim, L. Y., Ho, P. J., Liu, J., Chay, W. Y., Tan, M. H., Hartman, M., & Li, J. (2018). Determinants of breast size in Asian women. *Scientific Reports*, *8*(1), 1–9. https://doi.org/10.1038/s41598-018-19437-4

Lim, S., Choi, W. C., Yoon, Y. J., & Kim, H. (2015a). Modified rectangular patch antenna for improving heating uniformity in hyperthermia application. *IEEE Antennas and Propagation Society, AP-S International Symposium (Digest)*, *2015-Octob*(c), 734–735. https://doi.org/10.1109/APS.2015.7304754

Lim, S., Choi, W. C., Yoon, Y. J., & Kim, H. (2015b). Modified rectangular patch antenna

for improving heating uniformity in hyperthermia application. *IEEE Antennas and Propagation Society, AP-S International Symposium (Digest)*, *2015-Octob*(c), 734–735. https://doi.org/10.1109/APS.2015.7304754

Louise C.Miller. (2016). Mammographic Positioning. *Mammographic Positioning Basics and Advanced*, *7*(3), 100–159.

Luna, A., ni, R., & Marwaha, A. (2014). Hyperthermia applicator for electromagnetic interaction with human tissue at 434 MHz. *IOSR Journal of Electrical and Electronics Engineering*, *9*(4), 32–36. https://doi.org/10.9790/1676-09413236

Lyu, C., Li, W., Li, S., Mao, Y., & Yang, B. (2023). Design of ultra-wideband phased array applicator for breast cancer hyperthermia therapy. *Sensors*, *23*(3). https://doi.org/10.3390/s23031051

Ma, M. L., Zhao, D., Wang, Y., Liang, F., Deng, J., Yan, D., & Wang, B. Z. (2022). A non-invasive tumor hyperthermia method based on microwave field shaping. *2022 International Conference on Microwave and Millimeter Wave Technology, ICMMT 2022 - Proceedings*, 1–3. https://doi.org/10.1109/ICMMT55580.2022.10022843

Margaret, D. H., & Manimegalai, B. (2018). Modeling and optimization of EBG structure using response surface methodology for antenna applications. *AEU - International Journal of Electronics and Communications*, *89*(7), 34–41. https://doi.org/10.1016/j.aeue.2018.03.017

Mario Francisco Jesús Cepeda Rubio, A. V. H. and L. L. S. (2016). High temperature hyperthermia in breast cancer treatment. *Intech*, *11*(2), 13.

Mary, M. J., Marshiana, D., Sabarivani, A., Krishnamoorthy, N. R., Vinothkumar, C., & Harikrishnan, R. (2023). Design and analysis of reflection coefficient with slot

microstrip patch antenna in s-band application. *7th International Conference on Trends in Electronics and Informatics, ICOEI 2023 - Proceedings*, *February 2024*, 162–166. https://doi.org/10.1109/ICOEI56765.2023.10126009

Mendez, H. F. G., Arango, M. A. P., Rico, F. C., & Pardo, I. E. D. (2019a). Microwave hyperthermia study in breast cancer treatment. *2019 Congreso Internacional de Innovacion y Tendencias En Ingenieria, CONIITI 2019 - Conference Proceedings*. https://doi.org/10.1109/CONIITI48476.2019.8960873

Mendez, H. F. G., Arango, M. A. P., Rico, F. C., & Pardo, I. E. D. (2019b). Microwave hyperthermia study in breast cancer treatment. *2019 Congreso Internacional de Innovacion y Tendencias En Ingenieria, CONIITI 2019 - Conference Proceedings*, *1*, 256–267. https://doi.org/10.1109/CONIITI48476.2019.8960873

Miaskowski, A., Gas, P., & Szczygieł, M. (2018). Optimization of SAR coefficient for dipole antennas array with regard to local hyperthermia. *2018 Applications of Electromagnetics in Modern Techniques and Medicine, PTZE 2018*, *2*, 163–166. https://doi.org/10.1109/PTZE.2018.8503175

Microstrip Antenna Design Handbook (Artech House Antennas and Propagation Library) (p. 875). (2001). http://www.amazon.com/Microstrip-Antenna-Handbook-Antennas-Propagation/dp/0890065136

Nahas, M. (2022). Design of a high-gain dual-band LI-slotted microstrip patch antenna for 5G mobile communication systems. *Journal of Radiation Research and Applied Sciences*, *15*(4), 100483. https://doi.org/10.1016/j.jrras.2022.100483

Naik, D. K., Sahu, A. K., Parida, R. K., Raiguru, P., Panda, D. C., & Mishra, R. K. (2022). Design of a broadband U-slot loaded E-shaped patch antenna using characteristic mode

analysis. *AEU - International Journal of Electronics and Communications*, *154*(March), 154310. https://doi.org/10.1016/j.aeue.2022.154310

Naimullah, B. S. S., Lias, K., Jobli, A. T., Ispawie, D. I., & Hassan, M. M. (2023). Specific absorption rate and input power on 915MHz microstrip applicator with hyperthermia treatment. *IEEE 21st Student Conference on Research and Development, SCOReD 2023*, *M*, 214–218. https://doi.org/10.1109/SCOReD60679.2023.10563423

Neagu, V. (2017). A study of the effects of geometry on the efficiency of single slot microwave ablation antennas used in hepatic tumor hyperthermia. *IFMBE Proceedings*, *59*(6), 131–136. https://doi.org/10.1007/978-3-319-52875-5_30

Nguyen, P. T. (2016). *Focusing microwave hyperthermia in realistic environment for breast cancer treatment*. 156. https://espace.library.uq.edu.au/view/UQ:396580

Nguyen, P. T., Abbosh, A., & Crozier, S. (2015). Microwave hyperthermia for breast cancer treatment using electromagnetic and thermal focusing tested on realistic breast models and antenna arrays. *IEEE Transactions on Antennas and Propagation*, *63*(10), 4426–4434. https://doi.org/10.1109/TAP.2015.2463681

Nitin, N., Agrawal, N., Siddiqui, M. G., & Ansari, J. A. (2018). Design and analysis of e-slot microstrip antenna. *IEEE International Conference on 2018 Recent Advances on Engineering, Technology and Computational Sciences, RAETCS 2018*, 1–5. https://doi.org/10.1109/RAETCS.2018.8443948

Nizam-Uddin, N., & Elshafiey, I. (2017). SAR optimization for wideband hyperthermia treatment system. *ICIT 2017 - 8th International Conference on Information Technology, Proceedings*, 956–959. https://doi.org/10.1109/ICITECH.2017.8079974

Obot, A. B., Igwue, G. A., & Udofia, K. M. (2019). Design and simulation of rectangular

microstrip antenna arrays for improved gain performance. *International Journal of Networks and Communications*, *2*(2), 73–81. https://doi.org/10.5923/j.ijnc.20190902.02

Orna Pisconte, R. del P., & Yarleque Medina, M. A. (2017). Development of a prototype of applicator based on 16 antennas for hyperthermia treatments in the head and neck region. *Progress in Electromagnetics Research Symposium*, 1670–1676. https://doi.org/10.1109/PIERS.2017.8262017

Palácová, M. (2016). Ovarian ablation in breast cancer patients and the possibility of influencing treatment side effects [Ovariální ablace u pacientek s karcinomem prsu a možnosti ovlivnění vedlejších účinků léčby]. *Klinicka Onkologie*, *29*(3), 3S29-3S38.

Pang, C. L. K. (2015). Categories and methods of hyperthermia in oncology. In Kaiman Lee (Ed.), *Hyperthermia in Oncology* (pp. 17–26). Taylor & Francis Group, LLC. https://doi.org/10.1201/b18487-2

Panich, S. (2012). Design and Simulation of hypethermia antenna. *Journal of Medical Research*, *12*(3), 30–40.

Parameswari S, Dinesh M, Vignesh G, D. K. M. (2024). MUlti slotted microstrip patch. *2024 International Conference on Communication, Computing and Internet of Things*, 1–4.

Parameters, A. (1943). *3.3. Directivity and Gain*. *64*(Terman), 98–109.

Patel, A. (2020). Benign vs Malignant Tumors. *JAMA Oncology*, *6*(9), 1488. https://doi.org/10.1001/jamaoncol.2020.2592

Patrizia Sarogni, et. a. (2023). Advanced biology - 2023 - sarogni - hyperthermia reduces irradiation-induced tumor repopulation in an in vivo pancreatic. *Advanced Biology, 5*(7), 1831–1849.

Paulides, M. M., Dobsicek Trefna, H., Curto, S., & Rodrigues, D. B. (2020). Recent technological advancements in radiofrequency- andmicrowave-mediated hyperthermia for enhancing drug delivery. *Advanced Drug Delivery Reviews*. https://doi.org/10.1016/j.addr.2020.03.004

Paulides, M. M., Mestrom, R. M. C., Salim, G., Adela, B. B., Numan, W. C. M., Drizdal, T., Yeo, D. T. B., & Smolders, A. B. (2017). A printed Yagi-Uda antenna for application in magnetic resonance thermometry guided microwave hyperthermia applicators. *Physics in Medicine and Biology*, *62*(5), 1831–1847. https://doi.org/10.1088/1361-6560/aa56b3

Pereira, L. M. S., Milan, T. M., & Tapia-Blácido, D. R. (2021). Using response surface methodology (rsm) to optimize 2g bioethanol production: a review. *Biomass and Bioenergy*, *151*(6), 1831–1839. https://doi.org/10.1016/j.biombioe.2021.106166

Petra Kok, H., Groen, J., Bakker, A., & Crezee, J. (2020). Modelling curved contact flexible microstrip applicators for patient-specific superficial hyperthermia treatment planning. *Cancers*, *12*(3), 1841–1854. https://doi.org/10.3390/cancers12030656

Pragati, T., Akshaya, M., Madhavi, T., & Shreya, D. (2023). Design of rectangular microstrip patch antenna with E-slot. *I-Manager's Journal on Digital Signal Processing*, *11*(1), 22-33. https://doi.org/10.26634/jdp.11.1.19784

Raja, M. T., Ece, A. /, Deepthi, S. L., Jansi, P., Jhansirani, K., & Pavithra, M. (2023). Design and analaysis of e-slot patch antenna for wimax lower band. *International Research Journal of Engineering and Technology*, *May*, 364–368. www.irjet.net

Rajebi, S., Ghobadi, C., Nourinia, J., & Mostafapour, E. (2020). SAR enhancement of slot microstrip antenna by using silicon layer in hyperthermia applications. *Wireless*

Personal Communications, *111*(3), 1761–1774. https://doi.org/10.1007/s11277-019-06955-1

Rajebi, S., Pedrammehr, S., Al-Abdullah, K. I. A. L., Asadi, H., & Lim, C. P. (2024a). An optimized microstrip antenna to generate intense localized heating at target sites for maximum effect. *Discover Applied Sciences*, *6*(5), 99-110. https://doi.org/10.1007/s42452-024-05905-2

Rajebi, S., Pedrammehr, S., Al-Abdullah, K. I. A. L., Asadi, H., & Lim, C. P. (2024b). An optimized microstrip antenna to generate intense localized heating at target sites for maximum effect. *Discover Applied Sciences*, *6*(5), 89-101. https://doi.org/10.1007/s42452-024-05905-2

Rajput, J. L., Nandgaonkar, A. B., Nalbalwar, S. L., Wagh, A. E., & Huilgol, N. G. (2021). Performance evaluation of compact rectangular microstrip antenna for breast hyperthermia. *International Journal on Technical and Physical Problems of Engineering*, *13*(3), 87–94.

Ramu, M. R. S., & Arunachalam, K. (2023). Miniaturized 434 MHz cavity encapsulated patch antenna for superficial hyperthermia treatment. *IEEE Journal of Electromagnetics, RF and Microwaves in Medicine and Biology*, *7*(4), 392–399. https://doi.org/10.1109/JERM.2023.3307220

Rana, M. S., Sen, B. K., Mamun, M. T. Al, Mahmud, M. S., & Rahman, M. M. (2023). A 2.45 GHz microstrip patch antenna design, simulation, and anlaysis for wireless applications. *Bulletin of Electrical Engineering and Informatics*, *12*(4), 2173–2184. https://doi.org/10.11591/eei.v12i4.4770

Rani, A., & Dawre, R. K. (2010). Design and analysis of rectangular and u slotted patch for

satellite communication. *International Journal of Computer Applications*, *12*(7), 36–40. https://doi.org/10.5120/1688-1845

Rani, K., & Malhotra, S. (2018). Design and analysis of E, L & U-slotted patch antenna for multiband operation. *International Journal of Applied Engineering Research*, *13*(10), 8648–8653.

Rao, W., Deng, Z. S., & Liu, J. (2010). A review of hyperthermia combined with radiotherapy/chemotherapy on malignant tumors. *Critical Reviews in Biomedical Engineering*, *38*(1), 101–116. https://doi.org/10.1615/CritRevBiomedEng.v38.i1.80

Righini, M. F., Durham, A., & Tsoutsou, P. G. (2024). Hyperthermia and radiotherapy: physiological basis for a synergistic effect. *Frontiers in Oncology*, *14*(8), 1–8. https://doi.org/10.3389/fonc.2024.1428065

Rodrigues, D. B., Dobsicek-trefna, H., Curto, S., Winter, L., Molitoris, J. K., Vrba, J., Vrba, D., Sumser, K., & Paulides, M. M. (2022). Radiofrequency and microwave hyperthermia in cancer treatment. *International Journal of Applied Engineering Research*, *13*(10), 8648–8653.

Rodrigues, D. B., Hurwitz, M. D., Maccarini, P. F., & Stauffer, P. R. (2015). Optimization of chest wall hyperthermia treatment using a virtual human chest model. *2015 9th European Conference on Antennas and Propagation, EuCAP 2015*.

Roy, S., Bhattacharjee, P., & Hanumante, V. (2013). Design of U-slot rectangular patch antenna for wireless LAN at 2.45GHz. *9th International Conference on Microwaves, Antenna, Propagation and Remote Sensing ICMARS-2013, 11th – 14th December*, 132–135.

Said, T., & Varadan, V. V. (2009). Variation of Cole-Cole model parameters with the

complex permittivity of biological tissues. *IEEE MTT-S International Microwave Symposium Digest*, *7*, 1445–1448. https://doi.org/10.1109/MWSYM.2009.5165979

Samal, P. B., Chen, S. J., Tung, T. T., Losic, D., & Fumeaux, C. (2023). Efficiency-Driven Design for Planar Antennas With Lossy Materials. *IEEE Open Journal of Antennas and Propagation*, *4*(10), 23–33. https://doi.org/10.1109/OJAP.2022.3227903

Sarestoniemi, M., Kissi, C., Raez, C. P., Hamalainen, M., & Iinatti, J. (2019). Impact of the antenna-body distance on the wban channel characteristics. *International Symposium on Medical Information and Communication Technology, ISMICT*, *2019-May*. https://doi.org/10.1109/ISMICT.2019.8743894

Sasikala, S., Ezhilarasi, M., & Arun Kumar, S. (2020). *Detection of breast cancer using fusion of MLO and CC view features through a hybrid technique based on binary firefly algorithm and optimum-path forest classifier* (A. S. A. Nilanjan Dey, Siddhartha Bhattacharyya (Ed.); 2020th ed.). In Applied Nature-Inspired Computing: Algorithms and Case Studies. https://doi.org/https://doi.org/10.1007/978-981-13-9263-4

Selmi, M., Dukhyil, A. A. Bin, & Belmabrouk, H. (2020). Numerical analysis of human cancer therapy using microwave ablation. *Applied Sciences (Switzerland)*, *10*(1), 110-119. https://doi.org/10.3390/app10010211

Selmi, M., Iqbal, A., Smida, A., Waly, M. I., & Belmabrouk, H. (2022). Modeling of heat transfer distribution in tumor breast cancer during microwave ablation therapy. *Microwave and Optical Technology Letters*, *64*(8), 1364–1375. https://doi.org/10.1002/mop.33290

SEMCAD X. (2012). Reference Guide. In *Schmid & Partner Engineering AG*

Sethi, M., & Nijhawan, G. (2016a). A Two Slotted Circular Microwave Antenna Design for

Hyperthermia System Applicators. *International Journal of Computer Applications*, *148*(6), 35–39. https://doi.org/10.5120/ijca2016911160

Sethi, M., & Nijhawan, G. (2016b). Design of microwave antenna for hyperthermia system. *International Journal of Wireless and Microwave Technologies*, *6*(4), 39–47. https://doi.org/10.5815/ijwmt.2016.04.04

Sha, L., Ward, E. R., & Stroy, B. (2002). A Review of Dielectric Properties of Normal and Malignant Breast Tissue. *Proceedings IEEE SoutheastCon 2002 (Cat. No. 02CH37283)*, 457-462.

Shailander Singh Khangarot. (2015). Design and fabrication of E-shaped microstrip patch antenna for WLAN application. *Design and Fabrication of E-SLOT Microstrip Patch Antenna for WLAN Application*, *4*(6), 113-119. https://doi.org/10.17148/IJARCCE.2015.4633

Sharma, Nikita, Jain, B., Singla, P., & Prasad, R. R. (2014). Rectangular patch microstrip antenna: a survey. *International Advanced Research Journal in Science, Engineering and Technology*, *1*(3), 144–147.

Sharma, Nitika, Kaur, A., Khanna, R., Singh, H. S., & Agarwal, M. (2022). Design and development of a double spiral antenna with an artificial magnetic conductor structure for hyperthermia treatment. *International Journal of RF and Microwave Computer-Aided Engineering*, *32*(12), 1–17. https://doi.org/10.1002/mmce.23470

Sharma, S., Dimri, T., Kumar, M., & Singh, A. (2018). Microstrip E-Shaped patch antenna for ISM Band at 5.3GHz frequency application. *Proceedings - 2nd International Conference on Micro-Electronics and Telecommunication Engineering, ICMETE 2018*, 219–223. https://doi.org/10.1109/ICMETE.2018.00056

Sharma, S., & Tipathy, M. R. (2020). U slotted wide band wearable patch antenna for wban applications. *Proceedings of the 4th International Conference on IoT in Social, Mobile, Analytics and Cloud, ISMAC 2020*, 252–257. https://doi.org/10.1109/I-SMAC49090.2020.9243463

Shehata, R., Badawi, M., & Ismail, N. E. (2021). Hyperthermia for breast cancer treatment using a slotted microstrip patch antenna array. *Journal of Al-Azhar University Engineering Sector*, *16*(61), 1135–1155. https://doi.org/10.21608/auej.2021.207671

Shinde, J. P., & Shinde, P. N. (2016). M-shape electromagnetic-bandgap structures for enhancement in antenna performance. *AEU - International Journal of Electronics and Communications*, *70*(6), 842–849. https://doi.org/10.1016/j.aeue.2016.03.012

Sim, M. W. D. and D. . (1986). *Estimation of therapeutic gain in clinical trials involving hyperthermia and radiotherapy? 2*(2), 165–178.

Singh, S., Singh, D., & Singh, S. P. (2019a). Compact conformal multilayer slot antenna for hyperthermia. *2019 URSI Asia Pacific Radio Science Conference (AP-RASC)*, *1*(3), 130–132. https://doi.org/10.1109/ICSC45622.2019.8938390

Singh, S., & Singh, S. P. (2016a). Microstrip slot antenna for hyperthermia applications. *2015 IEEE Applied Electromagnetics Conference, AEMC 2015*, *2*, 1–2. https://doi.org/10.1109/AEMC.2015.7509173

Singh, S., & Singh, S. P. (2016b). Microstrip slot antenna for hyperthermia applications. *IEEE Applied Electromagnetics Conference, AEMC 2015*, *2*, 15–16. https://doi.org/10.1109/AEMC.2015.7509173

Singh, S., Singh, S. P., & Singh, D. (2023). Compact conformal metasurface antenna for hyperthermia applications. *Journal of Electromagnetic Waves and Applications*,

37(10–12), 950–965. https://doi.org/10.1080/09205071.2023.2216394

Singh, S., Singh, S. P., & Singh, D. (2019b). Compact conformal slot antenna for hyperthemia applications. *2019 International Conference on Signal Processing and Communication (ICSC)*, *37*(10–12), 130–132. https://doi.org/10.1080/09205071.2023.2216394

Sivakumar, P., Arunadevi, P., Revathi, T., Balaji Vignesh, L. ., & Shanmurgaraja, C. (2019). Design of E shaped microstrip patch antenna for S band applications. *International Journal of Innovative Technology and Exploring Engineering*, *8*(9), 692–695. https://doi.org/10.35940/ijitee.I1111.0789S19

Smitha, C. K., & Narayanan, N. K. (2016). Increase in specific absorption rate (SAR) of mobile phone - a threat to human. *International Research Journal of Electronics and Computer Engineering*, *2*(2), 1-9. https://doi.org/10.24178/irjece.2016.2.2.01

Smrkovski, O. A., Koo, Y., Kazemi, R., Lembcke, L. M., Fathy, A., Liu, Q., & Phillips, J. C. (2013). Performance characteristics of a conformal ultra-wideband multilayer applicator (CUMLA) for hyperthermia in veterinary patients: A pilot evaluation of its use in the adjuvant treatment of non-resectable tumours. *Veterinary and Comparative Oncology*, *11*(1), 14–29. https://doi.org/10.1111/j.1476-5829.2011.00297.x

Stauffer, P. R. (2005). Evolving technology for thermal therapy of cancer. *International Journal of Hyperthermia*, *2*(8), 731–744. https://doi.org/10.1080/02656730500331868

Stauffer, P. R., & Paulides, M. M. (2014). Hyperthermia Therapy for Cancer. In *Comprehensive Biomedical Physics, 8*(10), 99-110. https://doi.org/10.1016/B978-0-444-53632-7.01009-1

Stauffer, Paul R. (2019). Designing effective microwave antennas for clinical applications

in thermal medicine. *Proceedings of European Microwave Conference in Central Europe, EuMCE 2019*, *May*, 403–408.

Stuff, O. R. (2014). 1G VS 10G SAR AVERAGE MASS *ICNIRP/ACEBR/ARPANSA Wollongong Workshop, 11th Nov 2014*

Suganya, E., Chowdary, P. S., Reddy, Y. L. M., & Sree, P. T. (2023). Comparative study of E, H, and T shaped slot in patch antenna for 5G applications. *IEEE International Conference on Advances in Electronics, Communication, Computing and Intelligent Information Systems, ICAECIS 2023 - Proceedings*, 303–308. https://doi.org/10.1109/ICAECIS58353.2023.10170394

Szasz, A. (2021). The capacitive coupling modalities for oncological hyperthermia. *Open Journal of Biophysics*, *11*(03), 252–313. https://doi.org/10.4236/ojbiphy.2021.113010

Szasz, A. (2024). On the thermal distribution in oncological hyperthermia treatments. *Open Journal of Biophysics*, *14*(02), 239–263. https://doi.org/10.4236/ojbiphy.2024.142010

Takook, P., Trefná, H. D., & Persson, M. (2017). Performance evaluation of 2 hyperthermia applicators for deep-seated brain tumors. *2017 1st IEEE MTT-S International Microwave Bio Conference, IMBioC 2017*, *December*, 2–5. https://doi.org/10.1109/IMBIOC.2017.7965790

Tan DGuo CZhai H et al. (2022). E shaped patch to reduction of higher mode H plane radiaton and low cross polarization. *Microwave and Optical Technology Letters*, 7(3), 2222–2229.

Tangwachirapan, S., Thaiwirot, W., & Akkaraekthalin, P. (2022). Design and analysis of antipodal vivaldi antennas for breast cancer detection. *Computers, Materials and Continua*, *73*(1), 411–431. https://doi.org/10.32604/cmc.2022.028294

Tayel, M., Abouelnaga, T., & Elnagar, A. (2017). Pencil beam grid antenna array for hyperthermia breast cancer treatment system. *Circuits and Systems*, *08*(05), 122–133. https://doi.org/10.4236/cs.2017.85008

Tayel, M. B., Abouelnaga, T. G., & Elnagar, A. (2018). Dielectric loaded Yagi fed dual band pyramidal horn antenna for breast hyperthermia treatment. In *Proceedings of the 5th International Conference on Electrical and Electronics Engineering, ICEEE 2018*, 323–328. https://doi.org/10.1109/ICEEE2.2018.8391355

Teksin, M., Aydinalp, C., & Yildiz, G. (2024). Comparison of antennas operating at 2.4 GHz for microwave hyperthermia treatment of breast cancer. In *Proceedings 32nd Telecommunications Forum, TELFOR 2024 - Proceedings of Papers*, 1–4. https://doi.org/10.1109/TELFOR63250.2024.10819167

Thakur, R. K., Rai, R. K., Dholvan, M., & Kumar, A. (2024). A novel triple U-slot microstrip patch antenna design for multiband applications. *2024 IEEE International Students' Conference on Electrical, Electronics and Computer Science, SCEECS 2024*, 1–6. https://doi.org/10.1109/SCEECS61402.2024.10482045

Tu, D. (2010). *Semcad X*. Zurich, Switzerland: Schmid & Partner Engineering AG (SPEAG). Retrieved from https://speag.swiss/products/semcad/solutions/antenna-solution

Umamaheswari, S., Akshaya, V. S., Vijaya Dharshani, R., Rohini, R., & Francis Ajay, M. (2023). E-slot microstrip patch antenna for WLAN applications. In *Proccedings 9th International Conference on Advanced Computing and Communication Systems, ICACCS 2023*, *1*, 584–588. https://doi.org/10.1109/ICACCS57279.2023.10112735

Vallejo, M., Recas, J., del Valle, P. G., & Ayala, J. L. (2013). Accurate human tissue characterization for energy-efficient wireless on-body communications. *Sensors*

(Switzerland), *13*(6), 7546–7569. https://doi.org/10.3390/s130607546

Vasilchenko, I. L., Braginsky, V. I., Rynk, V. V., & Osintsev, A. M. (2022). Use of hyperthermal heating and intraoperatively administered applicator for the treatment of local malignant tumors. *Archive of Oncology*, *28*(2), 21–24. https://doi.org/10.2298/AOO210518004V

Vaupel, P., & Piazena, H. (2022). Strong correlation between specific heat capacity and water content in human tissues suggests preferred heat deposition in malignant tumors upon electromagnetic irradiation. *International Journal of Hyperthermia*, *39*(1), 987–997. https://doi.org/10.1080/02656736.2022.2067596

Whand, J. S. (2020). Physics of electromagnetic energy sources. In Eduardo G.Moros (Ed.), *Physics of Thermal Therapy* (pp. 74–91). CRC Press,Taylor & Francis Group. https://doi.org/10.1201/b13679-9

Walsh, P. P., Banerjee, A., & Murphy, E. (2022). The UN 2030 agenda for sustainable development. *Sustainable Development Goals Series*, *Part F2740*, 1–12. https://doi.org/10.1007/978-3-031-07461-5_1

Wang, M., Lin, L., Chen, J., Jackson, D., Kainz, W., Qi, Y., & Jarmuszewski, P. (2011). Evaluation and optimization of the specific absorption rate for multiantenna systems. *IEEE Transactions on Electromagnetic Compatibility*, *53*(3), 628–637. https://doi.org/10.1109/TEMC.2011.2109005

Wessapan, T., Srisawatdhisukul, S., & Rattanadecho, P. (2012). Specific absorption rate and temperature distributions in human head subjected to mobile phone radiation at different frequencies. *International Journal of Heat and Mass Transfer*, *55*(1–3), 347–359. https://doi.org/10.1016/j.ijheatmasstransfer.2011.09.027

Wong, V. L., Lias, K. bt, Basri, H. M., & Buniyamin, N. (2023). Heat distribution improvement with the implementation of polyethylene-covered water bolus into breast cancer hyperthermia. *Journal of Physics: Conference Series*, *2622*(1), 88-99. https://doi.org/10.1088/1742-6596/2622/1/012005

Wong, V. L., Lias, K., Buniyamin, N., Basri, H. M., & Ahmad Narihan, M. Z. (2021). SAR distribution of non-invasive hyperthermia with microstrip applicators on different breast cancer stages. *Indonesian Journal of Electrical Engineering and Computer Science*, *22*(1), 232–240. https://doi.org/10.11591/ijeecs.v22.i1.pp232-240

Wu, S., & Chen, J. (2023). A near-field focused conformal antenna array for focused microwave head hyperthermia. In *Proceedings of the International Applied Computational Electromagnetics Society Symposium, ACES-China 2023*, *61971340*, 1–3. https://doi.org/10.23919/ACES-China60289.2023.10250053

Xplore, I. (2017). *International Standard IEC/IEEE 62704-1* (Edition 1.)IEC, Geneva, Switzerland

Yang, Z., Jiao, J. L., Han, L., Gao, C., & Liu, Z. (2022). Adaptive Response Surface Method for Antenna Gain Optimization of Large Platforms. *International Conference on Communication Technology Proceedings, ICCT*, *2022-Novem*, 712–716. https://doi.org/10.1109/ICCT56141.2022.10072719

Yildiz, G., Farhat, I., Aydinalp, C., Farrugia, L., Adami, K. Z., Yilmaz, T., & Akduman, I. (2023). Performance evaluation of two particle swarm optimization adaptations for microwave breast hyperthermia focusing. In *Proceedings of the International Applied Computational Electromagnetics Society Symposium, ACES-Monterey 2023*, *May*, 1–3. https://doi.org/10.23919/ACES57841.2023.10114722

Yildiz, G., Farhat, I., Farrugia, L., Bonello, J., Zarb-Adami, K., Sammut, C. V., Yilmaz, T., & Akduman, I. (2023). Comparison of microwave hyperthermia applicator designs with fora dipole and connected array. *Sensors*, *23*(14), 1–22. https://doi.org/10.3390/s23146592

Yildiz, G., Yasar, H., Uslu, I. E., Demirel, Y., Akinci, M. N., Yilmaz, T., & Akduman, I. (2022). Antenna excitation optimization with deep learning for microwave breast cancer hyperthermia. *Sensors*, *22*(17), 1–15. https://doi.org/10.3390/s22176343

Younesiraad, H., Bemani, M., & Nikmehr, S. (2017a). A dual-band slotted square ring patch antenna for local hyperthermia applications. *Progress in Electromagnetics Research Letters*, *71*(1), 97–102. https://doi.org/10.2528/pierl17090503

Younesiraad, H., Bemani, M., & Nikmehr, S. (2017b). A dual-band slotted square ring patch antenna for local hyperthermia applications. *Progress in Electromagnetics Research Letters*, *71*(11), 97–102. https://doi.org/10.2528/PIERL17090503

Zelinski, A. C., Angelone, L. M., Goyal, V. K., Bonmassar, G., Adalsteinsson, E., & Wald, L. L. (2008). Specific absorption rate studies of the parallel transmission of inner-volume excitations at 7T. *Journal of Magnetic Resonance Imaging*, *28*(4), 1005–1018. https://doi.org/10.1002/jmri.21548

Zhang, B., & Chen, J. (2024). A conformal antenna array with adjustable and small-size focal spot for head hyperthermia. *2024 International Applied Computational Electromagnetics Society Symposium, ACES-China 2024 - Proceedings*, 1–3. https://doi.org/10.1109/ACES-China62474.2024.10699492

APPENDICES

Appendix A: Ethical approval from the National Medical Research Register (NMRR) of the Ministry of Health Malaysia.

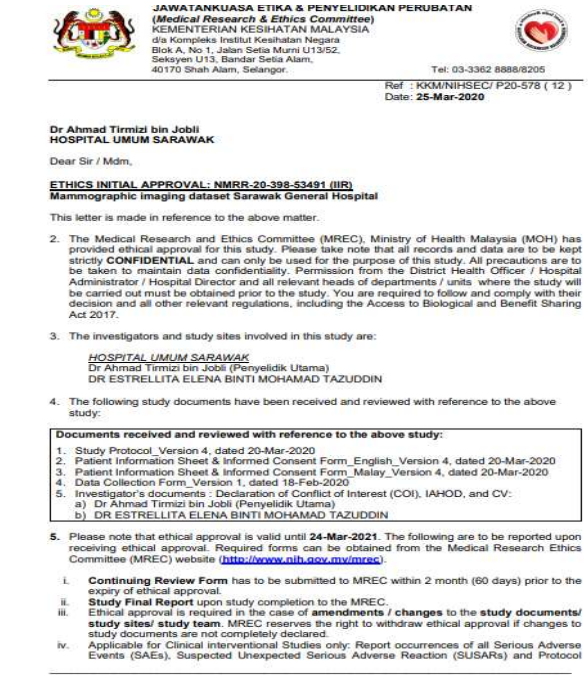

JAWATANKUASA ETIKA & PENYELIDIKAN PERUBATAN
(*Medical Research & Ethics Committee*)
KEMENTERIAN KESIHATAN MALAYSIA
d/a Kompleks Institut Kesihatan Negara
Blok A, No 1, Jalan Setia Murni U13/52,
Seksyen U13, Bandar Setia Alam,
40170 Shah Alam, Selangor.
Tel: 03-3362 8888/8205

Ref : KKM/NIHSEC/ P20-578 (12)
Date: **25-Mar-2020**

Dr Ahmad Tirmizi bin Jobli
HOSPITAL UMUM SARAWAK

Dear Sir / Mdm,

ETHICS INITIAL APPROVAL: NMRR-20-398-53491 (IIR)
Mammographic imaging dataset Sarawak General Hospital

This letter is made in reference to the above matter.

2. The Medical Research and Ethics Committee (MREC), Ministry of Health Malaysia (MOH) has provided ethical approval for this study. Please take note that all records and data are to be kept strictly **CONFIDENTIAL** and can only be used for the purpose of this study. All precautions are to be taken to maintain data confidentiality. Permission from the District Health Officer / Hospital Administrator / Hospital Director and all relevant heads of departments / units where the study will be carried out must be obtained prior to the study. You are required to follow and comply with their decision and all other relevant regulations, including the Access to Biological and Benefit Sharing Act 2017.

3. The investigators and study sites involved in this study are:

HOSPITAL UMUM SARAWAK
Dr Ahmad Tirmizi bin Jobli (Penyelidik Utama)
DR ESTRELLITA ELENA BINTI MOHAMAD TAZUDDIN

4. The following study documents have been received and reviewed with reference to the above study:

Documents received and reviewed with reference to the above study:
1. Study Protocol_Version 4, dated 20-Mar-2020
2. Patient Information Sheet & Informed Consent Form_English_Version 4, dated 20-Mar-2020
3. Patient Information Sheet & Informed Consent Form_Malay_Version 4, dated 20-Mar-2020
4. Data Collection Form_Version 1, dated 18-Feb-2020
5. Investigator's documents : Declaration of Conflict of Interest (COI), IAHOD, and CV:
   a) Dr Ahmad Tirmizi bin Jobli (Penyelidik Utama)
   b) DR ESTRELLITA ELENA BINTI MOHAMAD TAZUDDIN

5. Please note that ethical approval is valid until **24-Mar-2021**. The following are to be reported upon receiving ethical approval. Required forms can be obtained from the Medical Research Ethics Committee (MREC) website (http://www.nih.gov.my/mrec).

i. **Continuing Review Form** has to be submitted to MREC within 2 month (60 days) prior to the expiry of ethical approval.
ii. **Study Final Report** upon study completion to the MREC.
iii. Ethical approval is required in the case of **amendments / changes** to the **study documents/ study sites/ study team**. MREC reserves the right to withdraw ethical approval if changes to study documents are not completely declared.
iv. Applicable for Clinical interventional Studies only: Report occurrences of all Serious Adverse Events (SAEs), Suspected Unexpected Serious Adverse Reaction (SUSARs) and Protocol

Ref : KKM/NIHSEC/ P20-578 (12)

Deviation/Violation at all MREC approved sites to MREC. SAEs are to be reported within 15 calendar days from awareness of event by investigator. Initial report of SUSARs are to be reported as soon as possible but not later than 7 calendar days from awareness of event by investigator, followed by a complete report within 8 additional calendar days.

6. There will be **200 subjects/ patients/ respondents** targeted to be enrolled in this study within Malaysia.

7. Please take note that the reference number for this letter must be stated in all correspondence related to this study to facilitate the process.

Comments (if any): NIL

Project Sites:
HOSPITAL UMUM SARAWAK

Decision by Medical Research & Ethics Committee:
(√) Approved
( ) Disapproved

Date of Approval : **25-Mar-2020**

DR HJH SALINA ABDUL AZIZ
Chairperson
Medical Research & Ethics Committee
Ministry of Health Malaysia
MMC No: 27117

\MREC_Share\Approval 2020\Expedited by Primary Reviewer\March 2020\53491

Appendix B: Breast Cancer mammogram image on T1,T2 and T3

<table>
<tr><td colspan="4">T1</td></tr>
<tr><td>1</td><td> 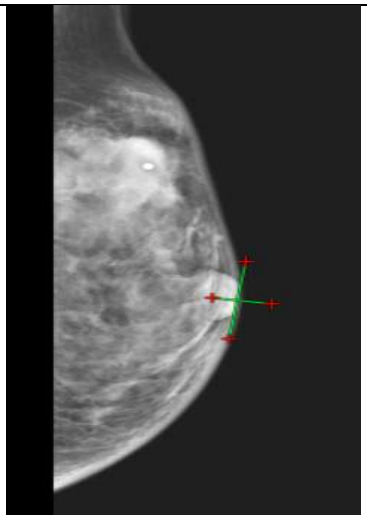 </td><td> 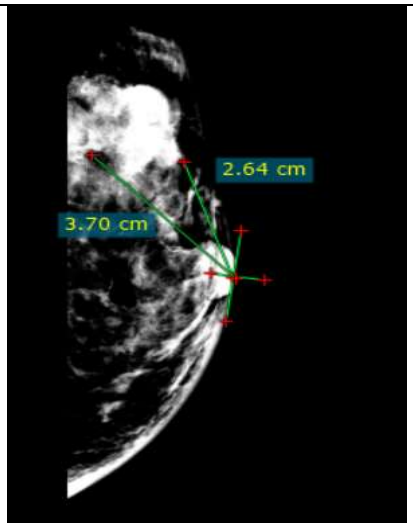
</td><td>
<table>
<tr><td colspan="2">Left</td></tr>
<tr><td>Surface Depth (mm)</td><td>Inner Depth (mm)</td></tr>
<tr><td>MLO</td><td>MLO</td></tr>
<tr><td>26.4</td><td>37.0</td></tr>
<tr><td colspan="2">Diameter (mm)</td></tr>
<tr><td colspan="2">MLO</td></tr>
<tr><td colspan="2">10.6</td></tr>
</table>
</td></tr>
<tr><td>2</td><td> 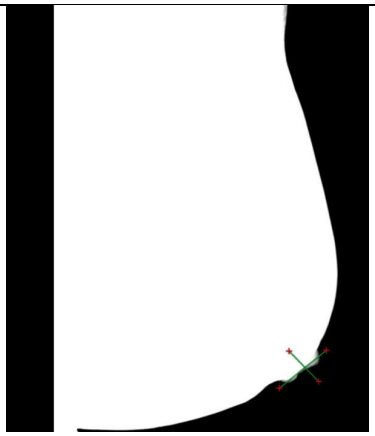 </td><td> 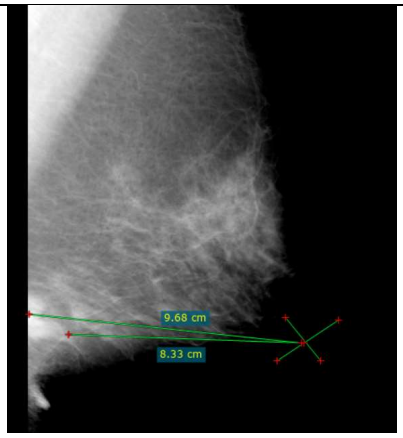
</td><td>
<table>
<tr><td colspan="2">Left</td></tr>
<tr><td>Surface Depth (mm)</td><td>Inner Depth (mm)</td></tr>
<tr><td>MLO</td><td>MLO</td></tr>
<tr><td>83.3</td><td>96.8</td></tr>
<tr><td colspan="2">Diameter (mm)</td></tr>
<tr><td colspan="2">MLO</td></tr>
<tr><td colspan="2">13.5</td></tr>
</table>
</td></tr>
</table>

T1

3	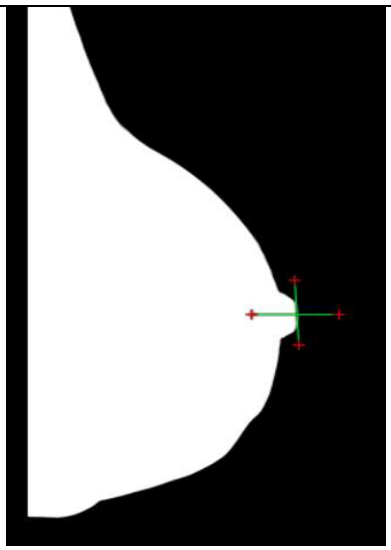	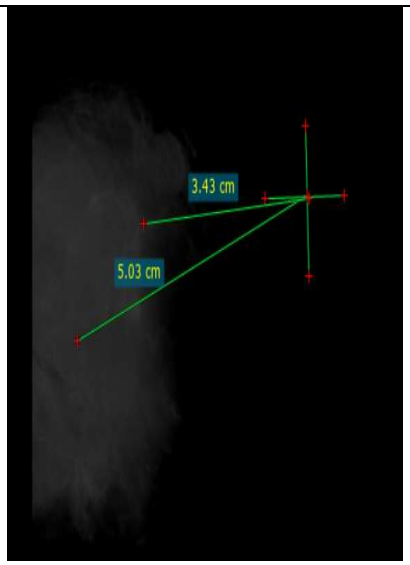	Left Surface Depth (mm) / Inner Depth (mm) MLO / MLO 34.3 / 50.3 Diameter (mm) MLO 16
4	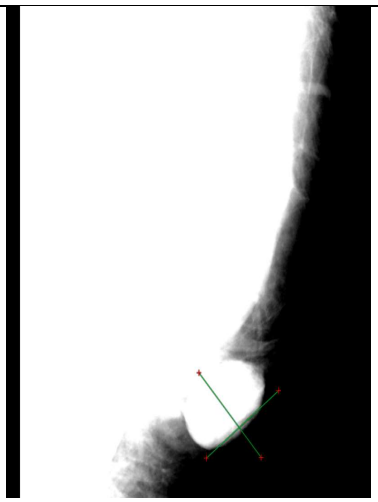	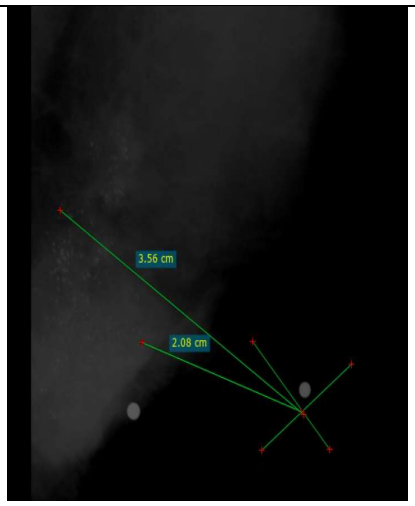	Left Surface Depth (mm) / Inner Depth (mm) MLO / MLO 20.8 / 35.6 Diameter (mm) MLO 14.8

T2

1

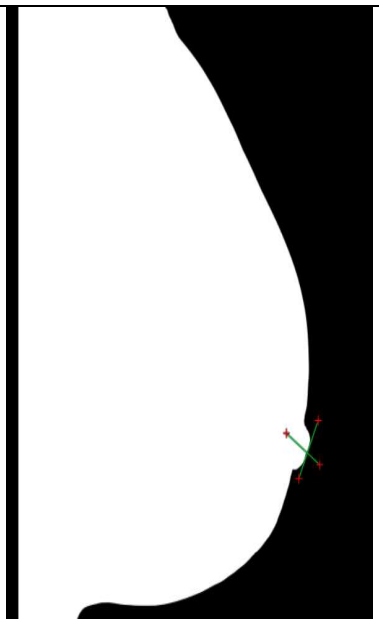

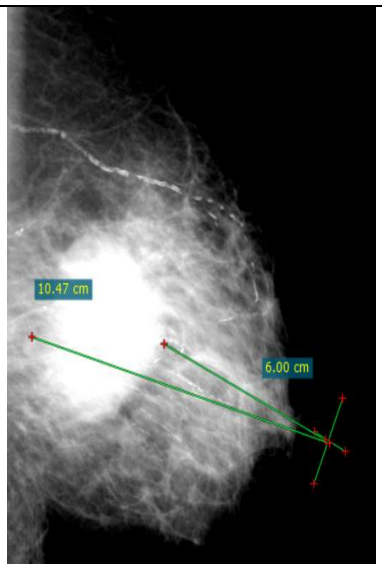

Left	
Surface Depth (mm)	Inner Depth (mm)
MLO	MLO
60	104.7
Diameter (mm)	
MLO	
44.7	

2

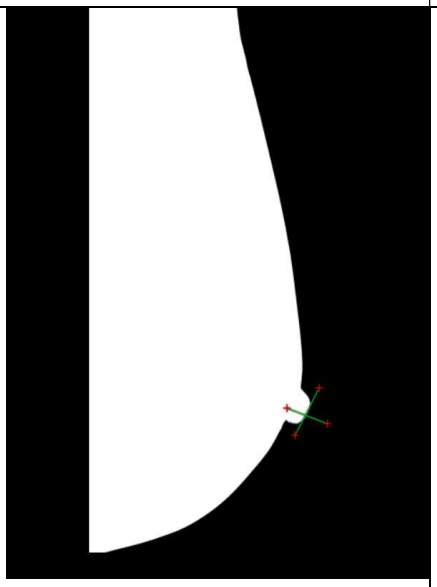

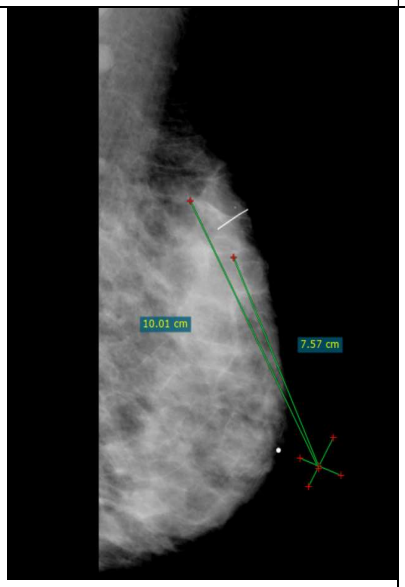

Left	
Surface Depth (mm)	Inner Depth (mm)
MLO	MLO
75.7	100.1
Diameter (mm)	
MLO	
25.5	

T2

3

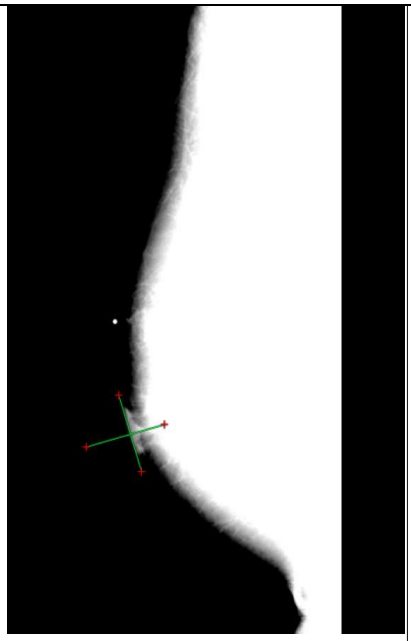

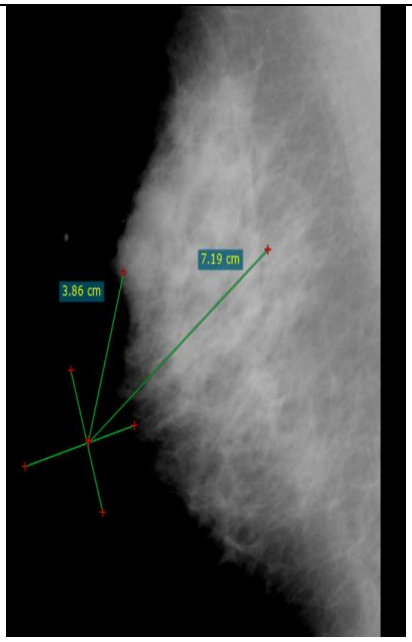

Right	
Surface Depth (mm)	Inner Depth (mm)
MLO	MLO
38.6	71.9
Diameter (mm)	
MLO	
33.3	

4

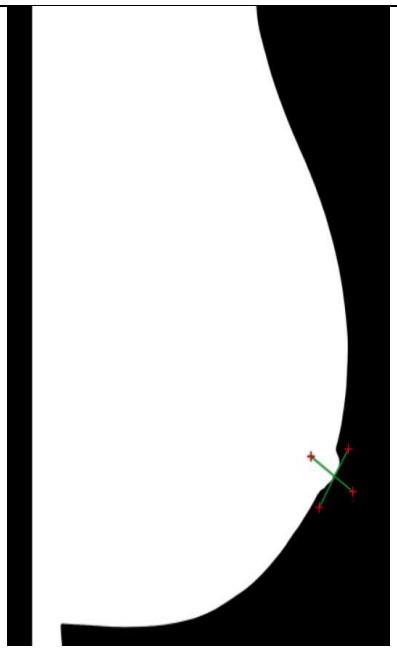

Left	
Surface Depth (mm)	Inner Depth (mm)
MLO	MLO
96.1	120.8
Diameter (mm)	
MLO	
24.7	

T2

5

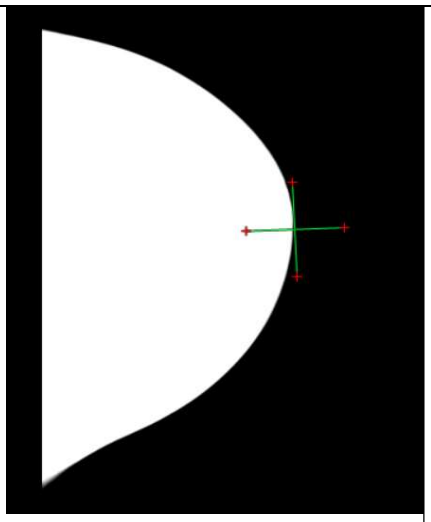

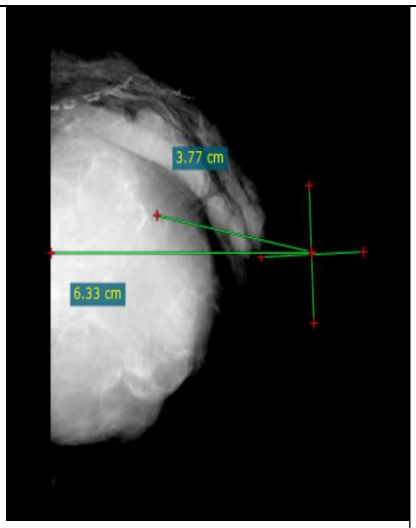

Left	
Surface Depth (mm)	Inner Depth (mm)
CC	CC
37.7	63.3
Diameter (mm)	
CC	
25.6	

6

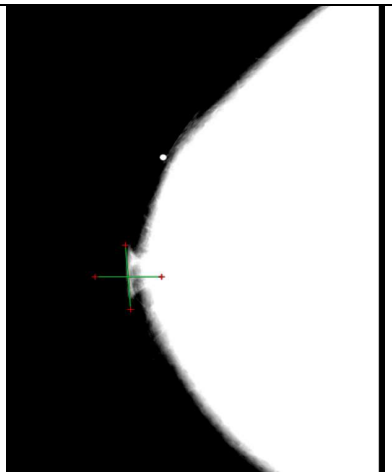

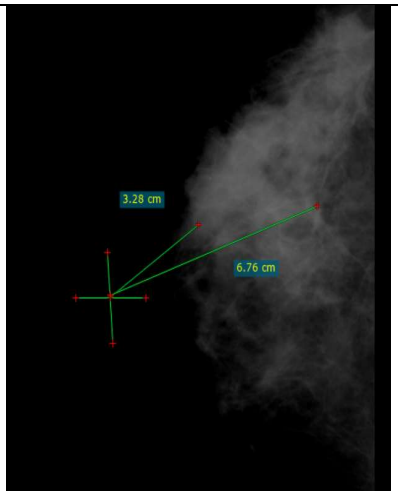

Right	
Surface Depth (mm)	Inner Depth (mm)
CC	CC
32.8	67.6
Diameter (mm)	
CC	
34.8	

T3

1

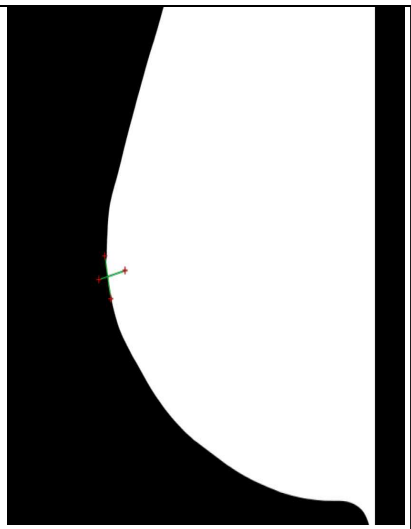

Right	
Surface Depth (mm)	Inner Depth (mm)
MLO	MLO
29.9	87.1
Diameter (mm)	
MLO	
57.2	

2

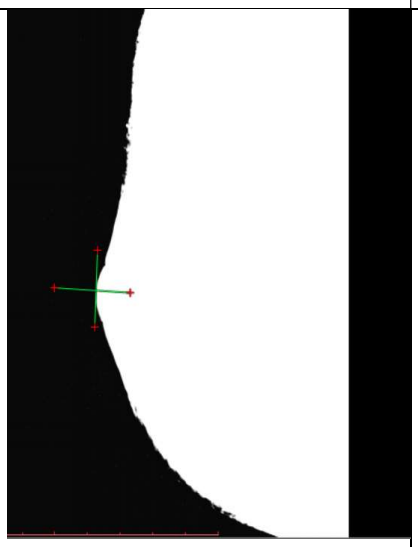

Right	
Surface Depth (mm)	Inner Depth (mm)
MLO	MLO
43.6	96.2
Diameter (mm)	
MLO	
52.6	

T3

3

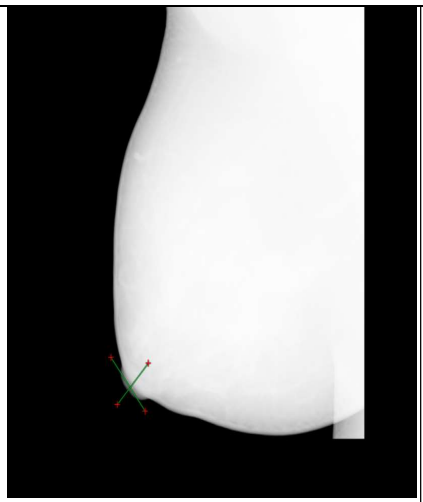

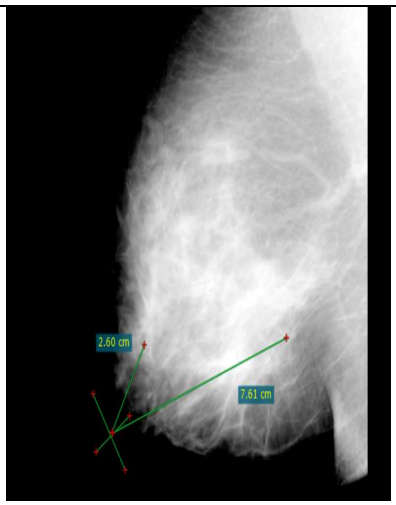

Right	
Surface Depth (mm)	Inner Depth (mm)
MLO	MLO
26	76.1
Diameter (mm)	
MLO	
50.1	

4

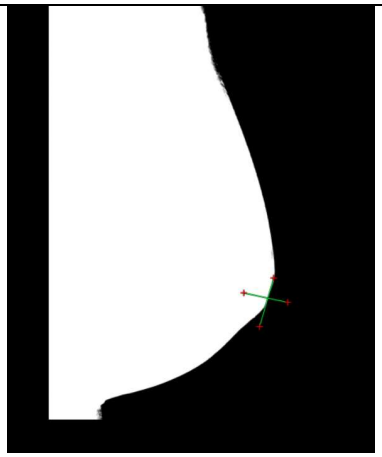

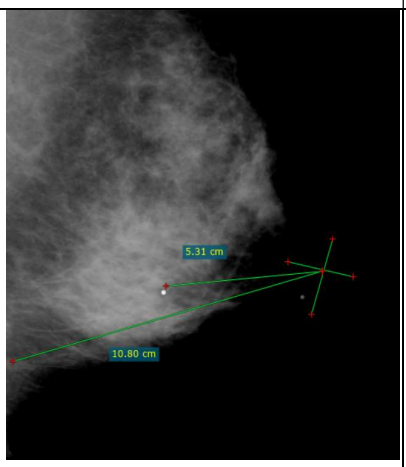

Left	
Surface Depth (mm)	Inner Depth (mm)
MLO	MLO
53.1	108
Diameter (mm)	
MLO	
54.9	

T3			
5	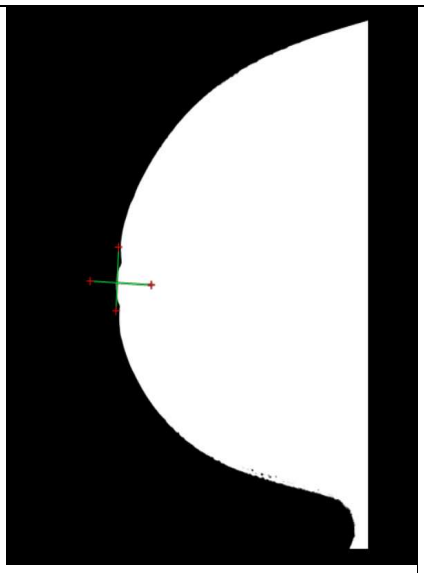	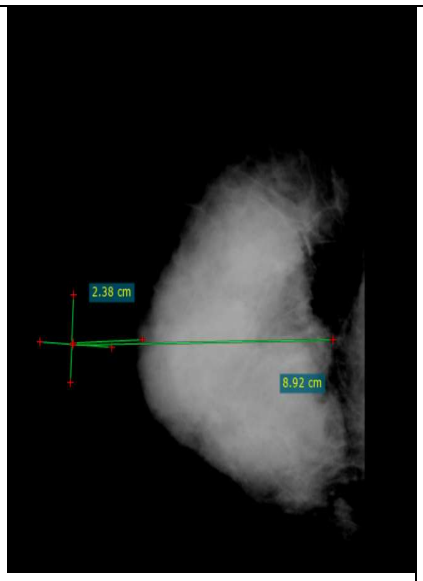	Right Surface Depth (mm) / Inner Depth (mm) CC / CC 23.8 / 89.2 Diameter (mm) CC 65.4

T4 : Cancer spreads from where it starts to another body organ. This stage is called secondary or metastatic cancer.
Will not be investigated because the images are not provided, considering that surgery is implemented for stage 4 cancer

Appendix C: DoE 1b: Selection of input power

915MHz	SAR distribution (2D view)	Results Focus Position Distance(FPD)/ SAR(peak)	SAR distribution (3D view)
T1		Pin=10W	
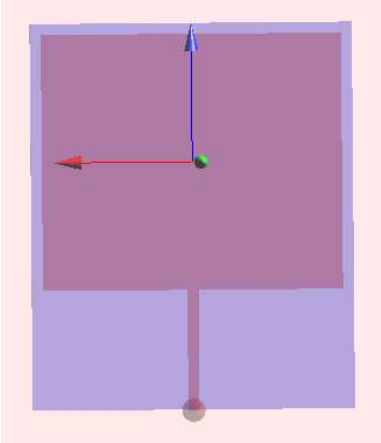	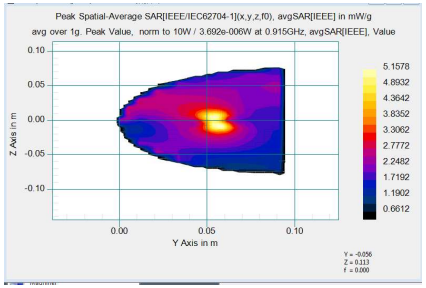	SD: 40mm ID: 66.8mm SAR(peak) = 5.1578mW/g	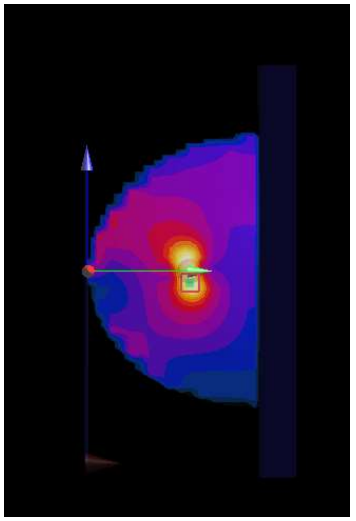

T1		Pin=1W	
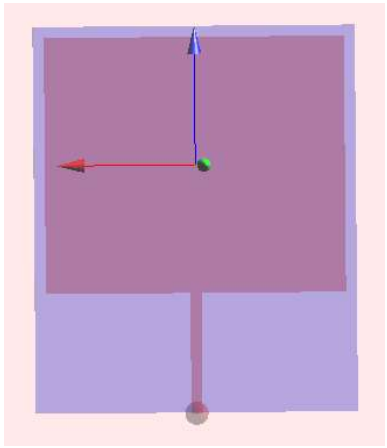	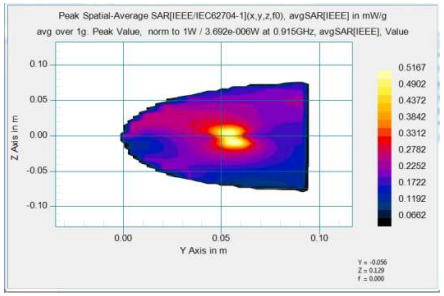	SD:40mm ID:66.8mm SAR(peak) = 0.5167 mW/g	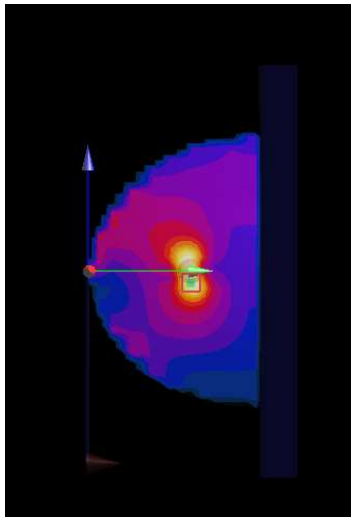

T2		Pin=10W	
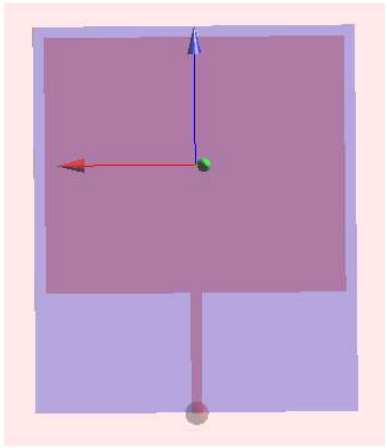	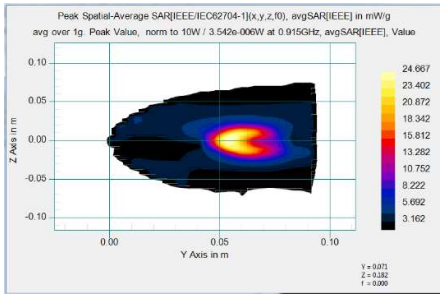	SD:46.5mm ID:71.7mm SAR(peak) = 24.667 mW/g	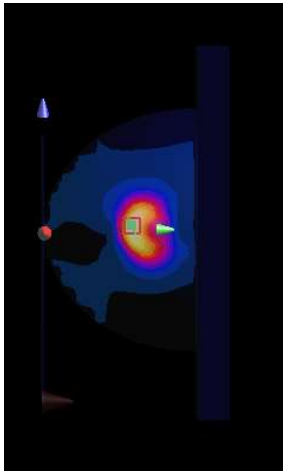

T2		Pin=1W	
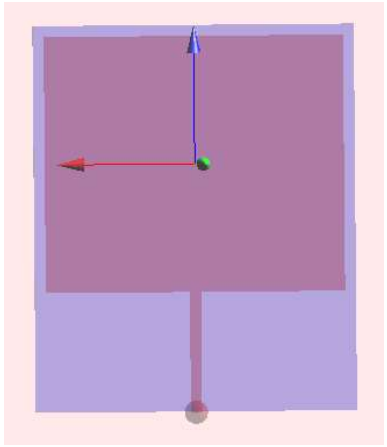	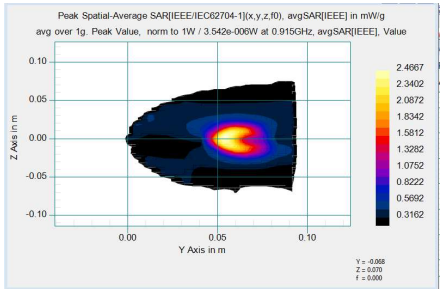	SD: 46.5mm ID:71.7mm SAR(peak) = 2.4667mW/g	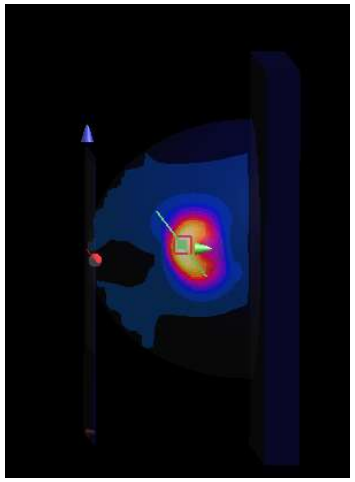

T3		Pin=10W	
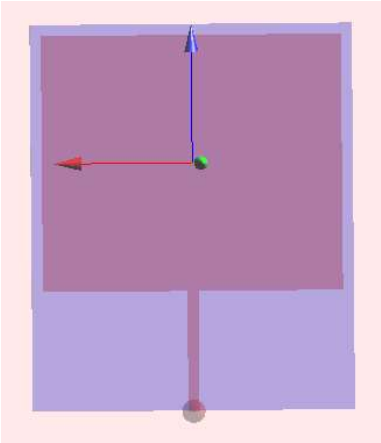	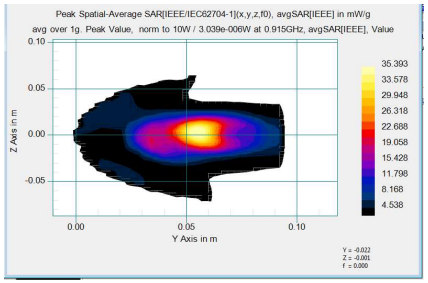	SD:42.6mm ID: 67mm SAR(peak) = 35.393mW/g	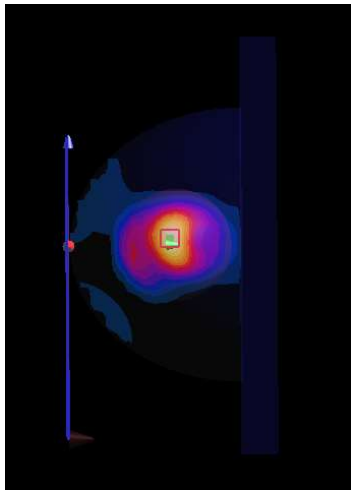

T3		Pin=1W	
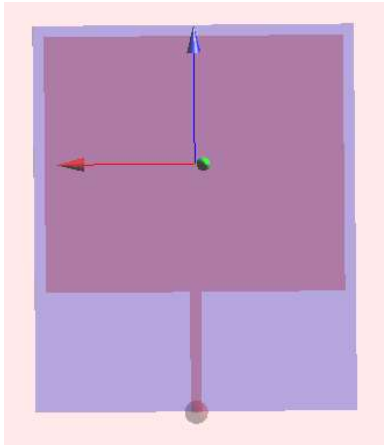	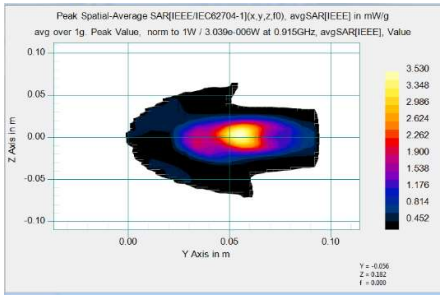	SD:42mm ID: 67.2mm SAR(peak) = 3.530 mW/g	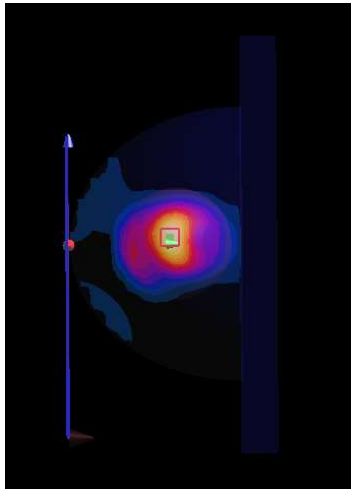

Appendix D: DoE 1c: Selection of SAR average mass

915M	SAR distribution (2D view)	Results Focus Position Distance (FPD)/ SAR(peak)	SAR distribution (3D view)
T1	1g		
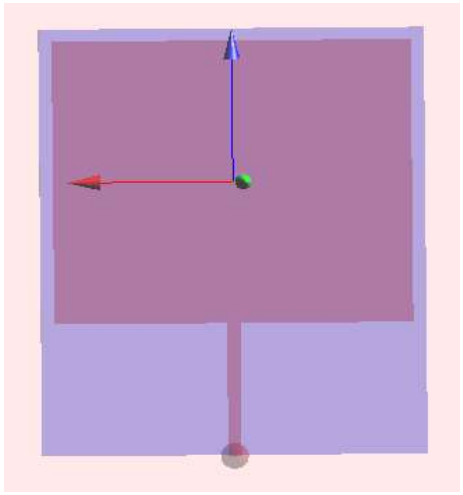	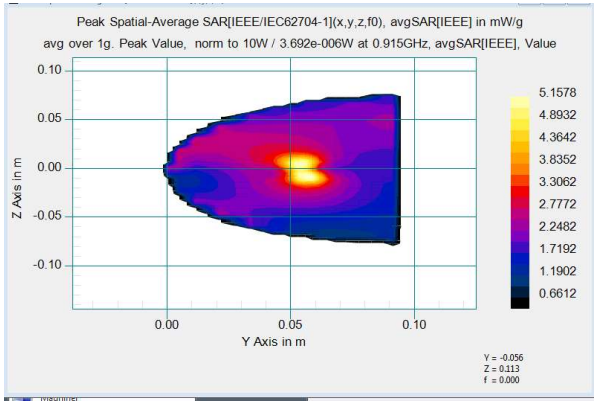	SD:40mm ID: 66.8mm SAR (peak) = 5.1578mW/g	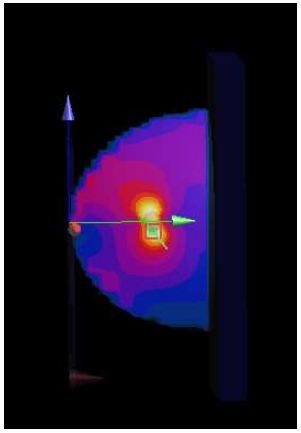

T1	10g		
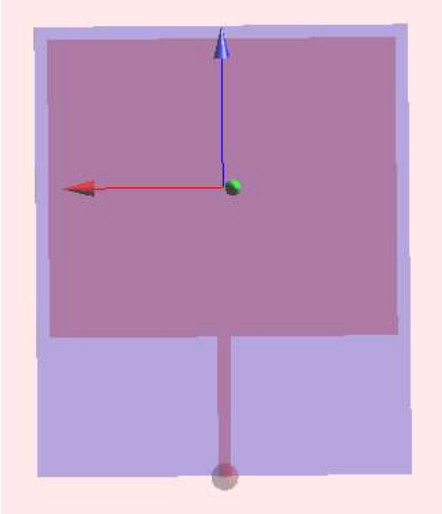	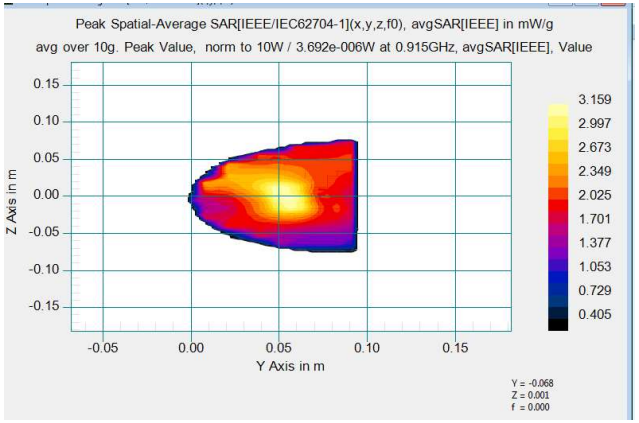	SD:5.4mm ID:91.9mm SAR (peak) = 3.159mW/g	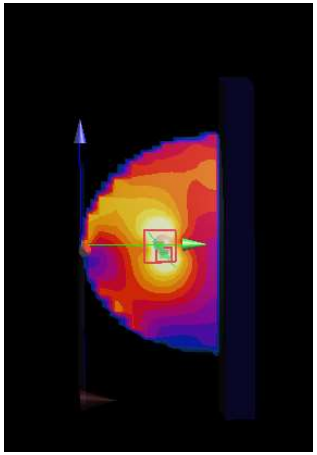

T2	1g		
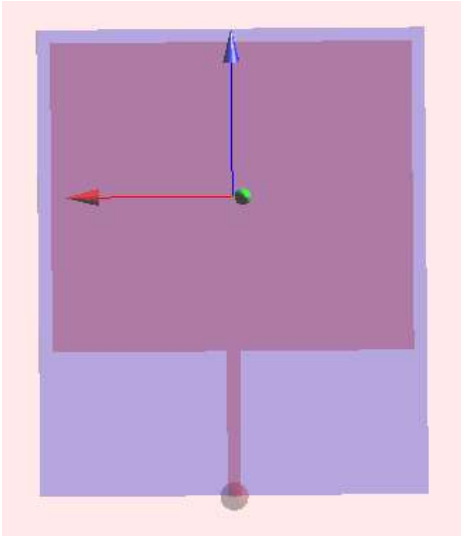	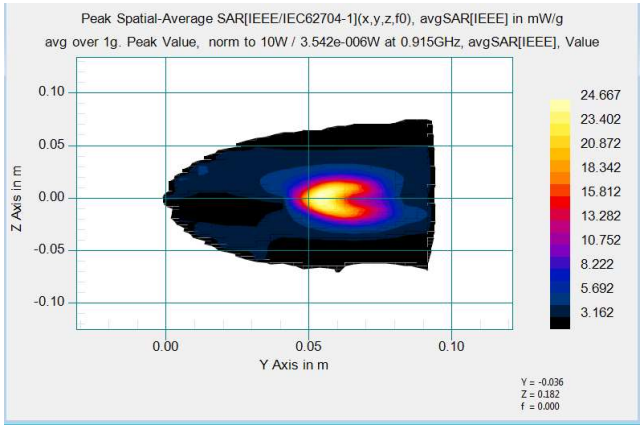	SD:46.5mm ID:71.5mm SAR (peak) = 24.667 mW/g	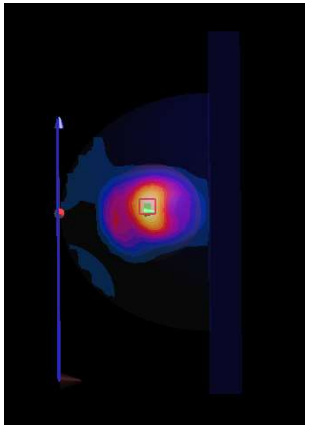

T2	10g		
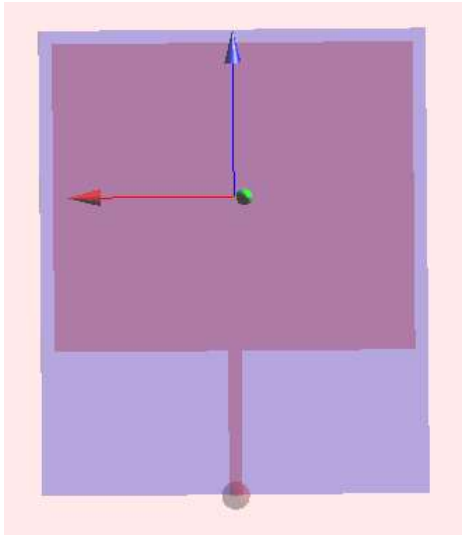	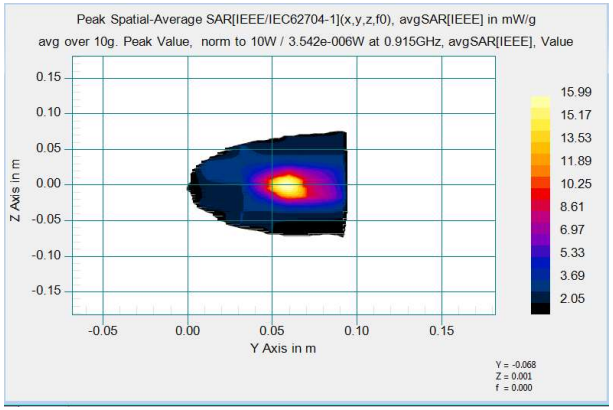	SD:46mm ID: 71mm SAR (peak) = 15.99mW/g	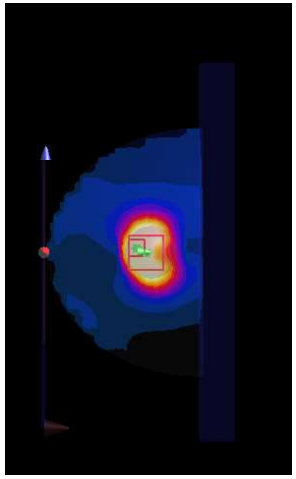

T3	1g		
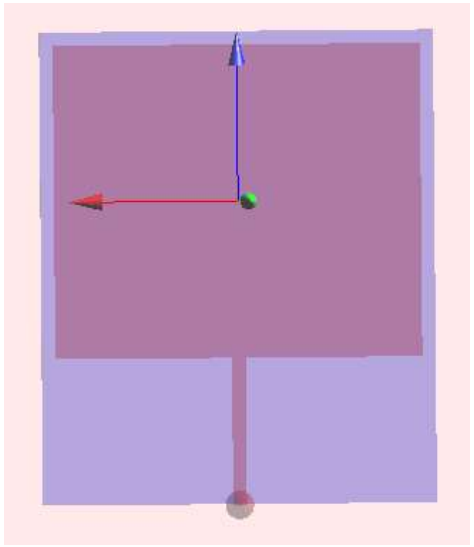	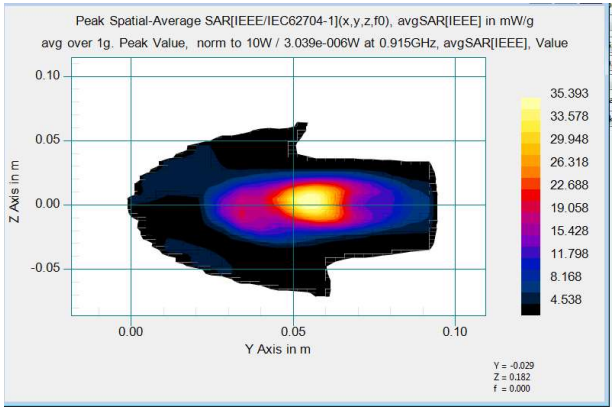	SD:42.6mm ID: 67mm SAR (peak) = 35.393 mW/g	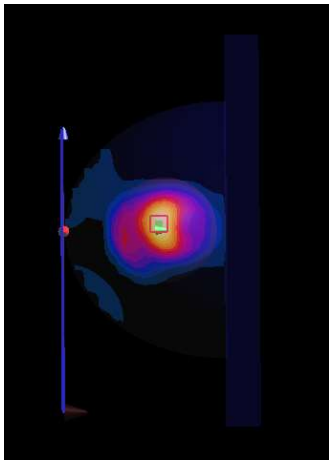

T3	10g		
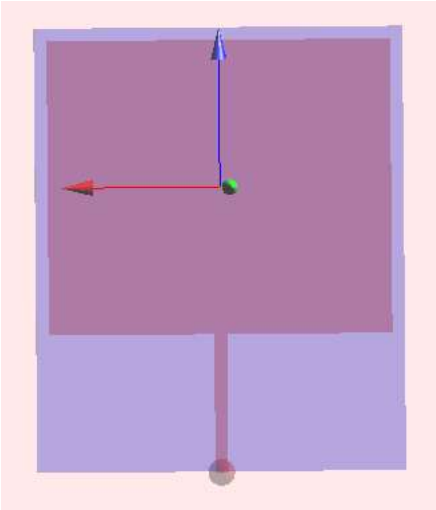	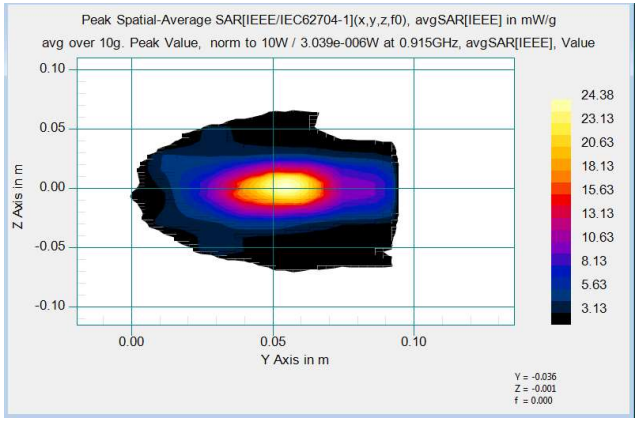	SD:35mm ID:69mm SAR (peak) =24.38mW/g	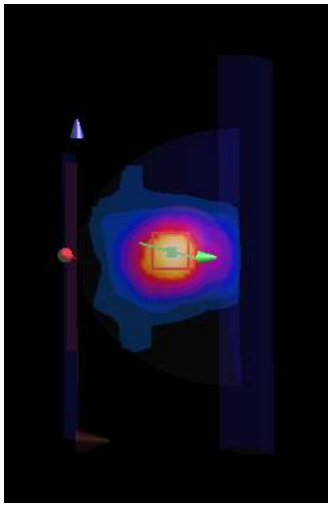

Appendix E: DoE2b- Distance breast phantom to the applicator: T1,T2,T3

Distance mm	T1	T2	T3
0	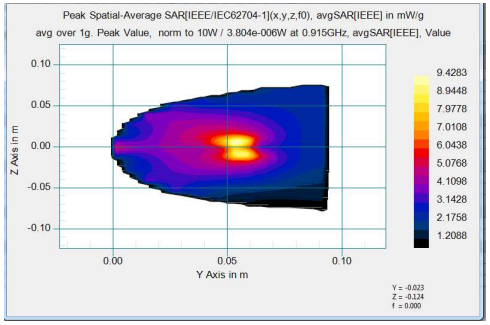	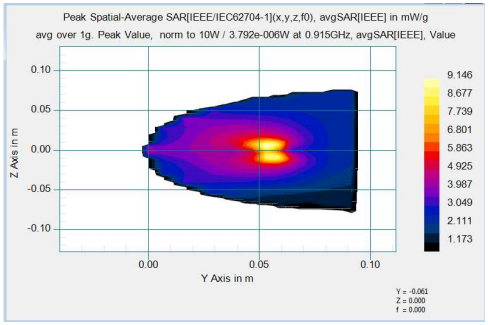	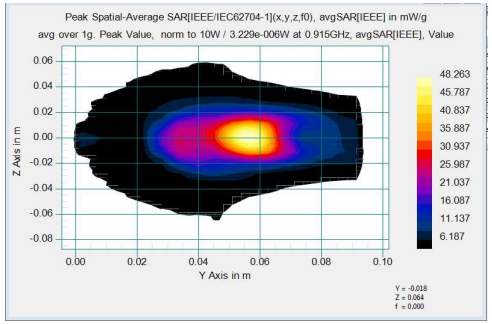
SD-ID	40 -64.5mm	46.6 to 70.5mm	43- 66.6mm
5	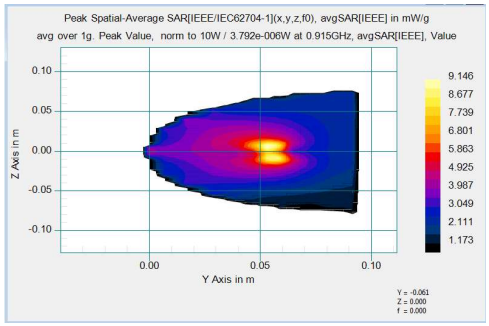	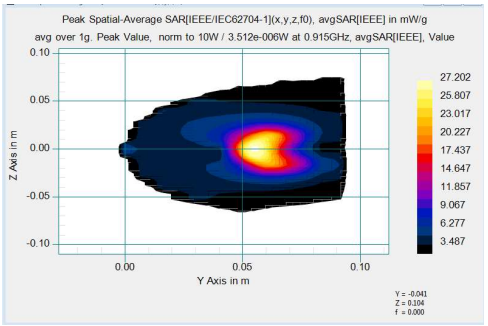	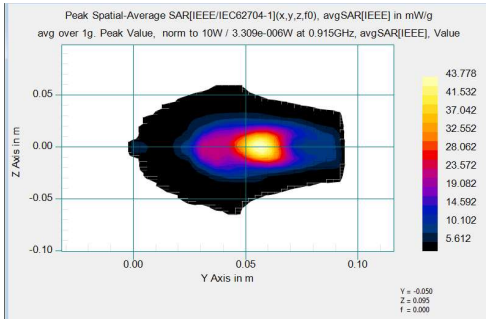
SD-ID	40.1 to 64.4mm	46.6 to 70.5mm	43.8 to 66.7mm

10	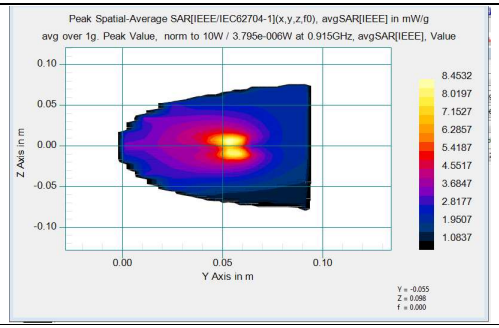	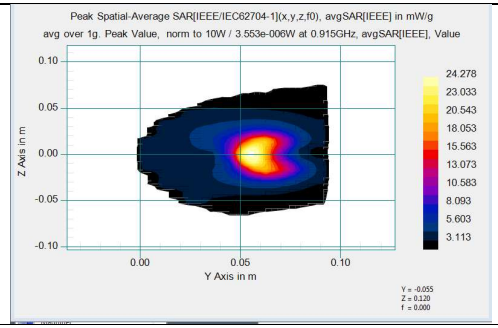	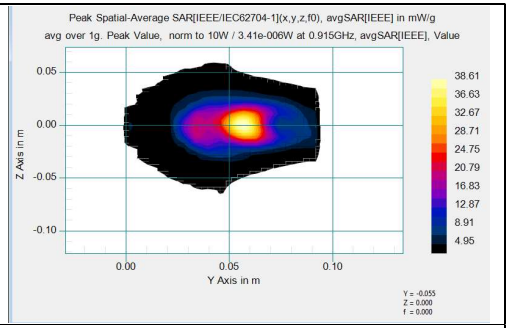
SD-ID	40 to 64.4mm	46.8 -71mm	45 -66.8
15	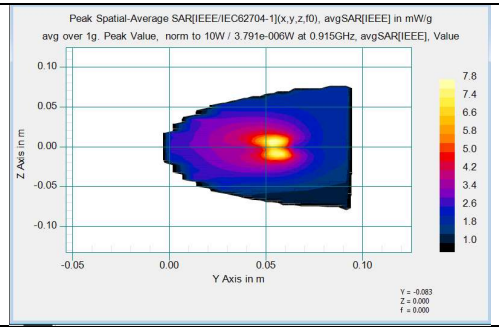	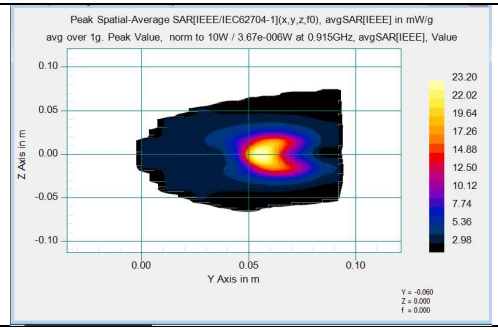	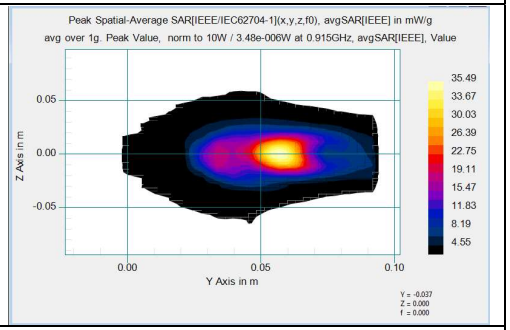
SD-ID	40 to 64.5mm	46.7-71.2mm	46 to 66.6
20	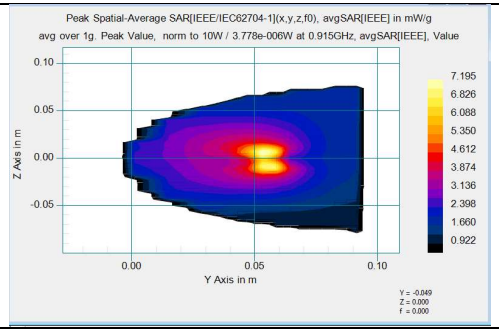	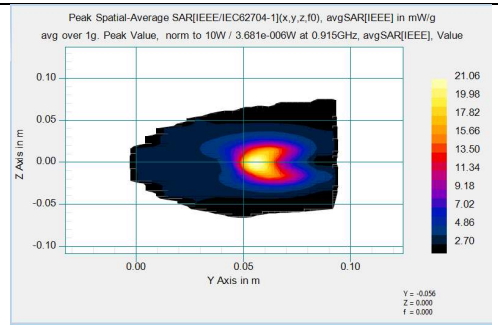	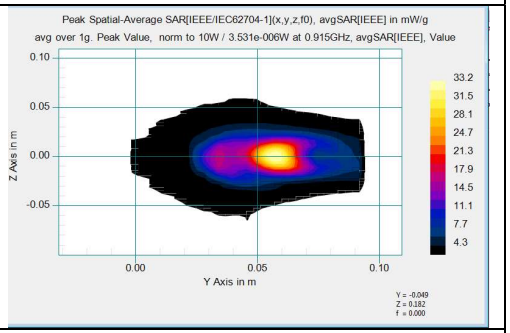
SD-ID	40 to 64.3mm	47-71mm	46.2-66.6mm

Appendix F: DoE4 : Hyperthermia Treatment Time

Tumor Sizes	Without waterbolus	With waterbolus
T1	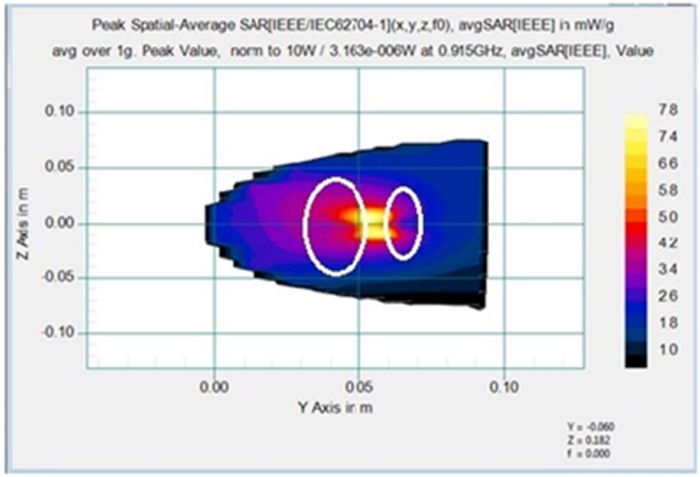	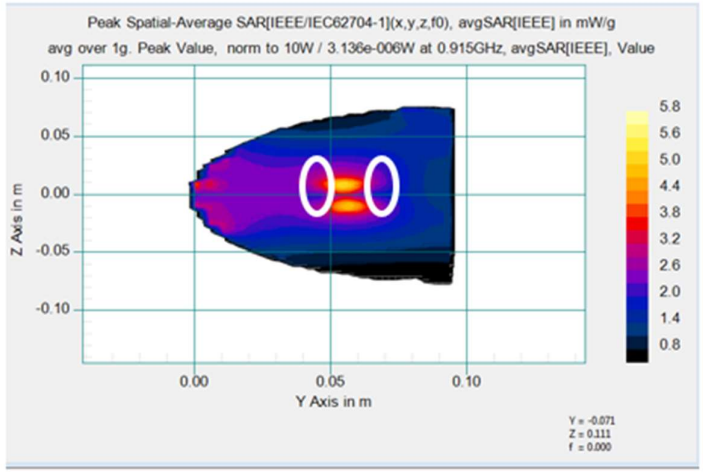
	SD: 40.3mm ID: 64.2mm SAR(peak)=7.8mW/g	SD: 47mm ID:64mm SAR(peak)=5.8mW/g

Tumor Sizes	Without waterbolus	With waterbolus
T2	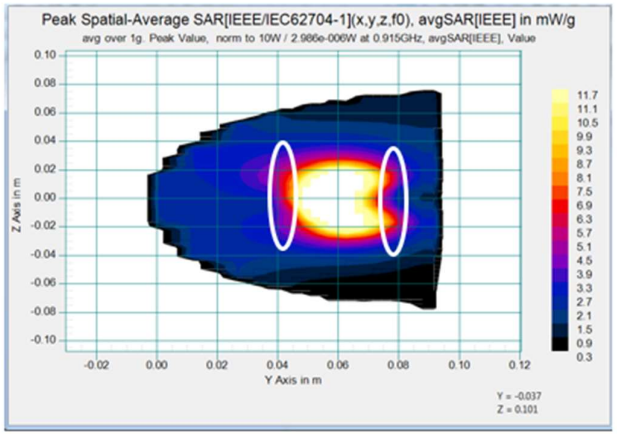	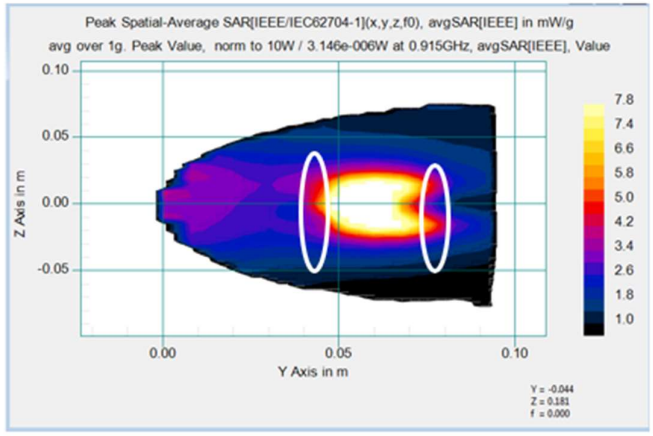
	SD: 40.3mm ID: 64.2mm SAR(peak)=7.8mW/g	SD: 47mm ID:64mm SAR(peak)=5.8mW/g

Tumor Sizes	Without waterbolus	With waterbolus
T3	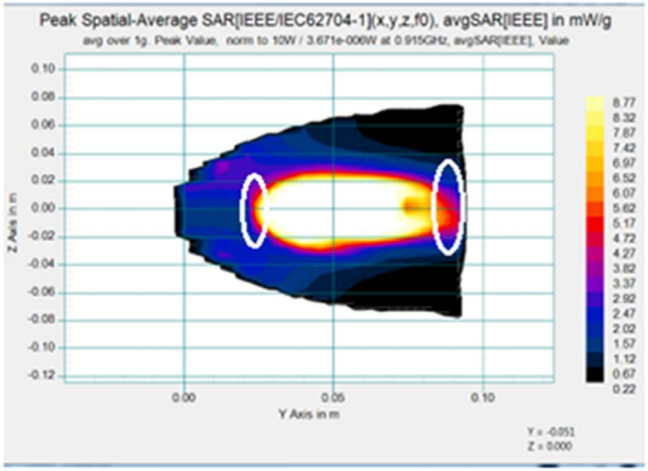	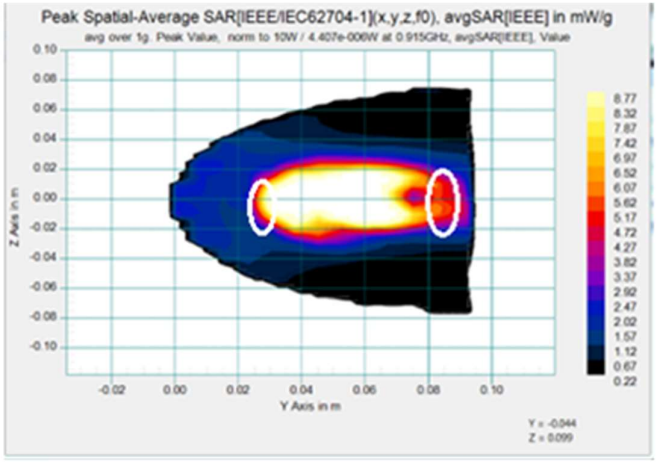
	SD:23.3mm ID: 91mm SAR(peak) =8.77mW/g	SD:25 mm ID: 90mm SAR(peak) = 8.77mW/g

Appendix G: Publication and Awards

Journal

1. An Overview Study of Dual Band Microstrip Antenna for Non-Invasive Hyperthermia Treatment, **Bibi Sarpinah Sheikh Naimullah,** Kasumawati Lias, Norlida Buniyamin and Mazlina Mansor Hassan, International Journal of Advanced Research in Engineering and Technology(IJARET) Volume 11, Issue 8, August 2020 pp738-746

2. A Review on Water Bolus Structure Integration for Non-Invasive Hyperthermia Treatment, Mazlina Mansor Hassan, Kasumawati Lias, Norlida Buniyamin, **Bibi Sarpinah Sheikh Naimullah**, International Journal of Advanced Research in Engineering and Technology (IJARET) Volume 11, Issue 7, July 2020 pp 524-532

3. Specific Absorption Rate distribution evaluation in a different substrate for hyperthermia treatment, **Bibi Sarpinah**, Kasumawati, Norlida Buniyamin, Ahmad Tirmizi and Mazlina, Indonesian Journal of Electrical Engineering and Computer Science, September 2022 pp 1311-13

4. SAR performance of Rectangular Microstrip Antenna for Breast Cancer Hyperthermia with different period of treatment procedure, Mazlina, Kasumawati, Norlida Buniyamin, **Bibi Sarpinah**, Journal of Physics, Conference Series, 2021, vol 2071, issue 1

5. SAR analysis using various substrates of microstrip antenna for breast cancer hyperthermia treatment, Mazlina, Kasumawati, Norlida Buniyamin, Mohd Zulkarnaen, **Bibi Sarpinah** , Dzufi , Journal of physics, Conference Series, 2023 volume 2622, Issue 1.

6. SAR Distribution with Different Water Bolus Shape for Hyperhtemia Breast Cancer Treatment, Mazlina Mansor Hassan, Kasumawati Lias, Norlida Buniyamin, Mohd Zulkarnaen Ahmad Narihan , **Bibi Sarpinah**, Hazrul Mohd Basri, Syah Alam, Journal of Advanced Research in Fluid Mechanics and Thermal Sciences 128, Issue 1(2025) 32-47, Semarak Ilmu

7. Heat Transfer Distribution for Breast Cancer Hyperthermia Treatment with Rectangular Micostrip and Water Bolus, Mazlina Mansor Hassan, Kasumawati Lias, Norlida Buniyamin, Mohd Zulkarnaen Ahmad Narihan , **Bibi Sarpinah,** Journal of Advanced Research in Numerical Heat Transfer, vol 37. No1: October (2025)

8. SAR Performance for Breast Cancer Hyperthemia Treatment using 2.45GHz and 0.915 GHz Circular Non-Invasive Microstrip Patch Antenna Integration with Various Shapes of Water Boluses, Mazlina Mansor Hassan, Kasumawati Lias, Norlida Buniyamin, Mohd Zulkarnaen Ahmad Narihan , **Bibi Sarpinah,** Malayisa Journal of Medicine and Health Sciences –Vol 25,pp 108-116 (Nov2025)

9. Evaluating E-slot Microstrip Antenna for Breast Cancer Hyperthermia Treatment, **Bibi Sarpinah**, Kasumawati, Norlida Buniyamin, Ahmad Tirmizi and Mazlina, **Malayisa Journal of Medicine and Health Sciences –Vol 25, pp 126-134(Nov 2025)**

10. Performance of Hypertehrmia Applicator Under ISM frequency for Breast Cancer Treatment, **Bibi Sarpinah Sheikh Naimullah**, Kasumawati Lias, Ahmad Tirmizi Jobli, Mazlina Mansor Hassan, Fatimatul Anis Bakri, **Journal of Advanced Research Design** . Vol 145 Issue 1 2026 pp 1-12 (Oct 2026)

Conference

1. SAR Evaluation Towards Breast Cancer in Hyperthermia Treatment, **Bibi Sarpinah**, Kasumawati, Norlida Buniyamin, Mazlina, Hazrul , Dzufi, 2021 IEEE Symposium of Industrial Electronics & Applications(ISIEA)

2. Specific Absorption Rate and Input Power on 915MHz Microstrip Applicator with Htperthemia Treatment, **Bibi Sarpinah**, Kasumawati, Ahmad, Mazlina,Dzufi, 2023 IEEE 21st Student Conference on Research and Development (SCOReD)

3. Performance of Hyperthemia Applicator under ISM Frequency for Breast Cancer Treatment , **Bibi Sarpinah**, Kasumawati, Ahmad Tirmizi, Mazlina, Fatimatul Anis, Muhd Firdaus, presented : 15th International Engineering Conference(EnCon) 2024, 14-16 Feb 2024, The waterfront Hotel, Kuching

4. Evaluating E slot Microstrip Antenna for Breast Cancer Hyperthermia Treatment, **Bibi Sarpinah**, Kasumawati, Ahmad Tirmizi, Norlida Buniyamin, Mazlina, The 2nd International Conference on Biomedical Engineering & Health Science 2024 (2nd ICBMEHS 2024), 11-12 September 2024

5. SAR Performance for Breast Cancer Hyperthermia Treatment using 2.45GHz and 0.915GHz Circular Non-Invasive Microstrip Antenna Integrated with Various Shapes of Water boluses, Mazlina , Kasumawati,Norlida Buniyamin, **Bibi Sarpinah**, Mohd Zulkarnaen,Dzufi Iszura The 2nd International Conference on Biomedical Engineering & Health Science 2024 (2nd ICBMEHS 2024), 11-12 September 2024

6. Effect of non-invasive applicator to phantom distance on SAR distribution in breast cancer hyperthermia, **Bibi Sarpinah Sheikh Naimullah**, Kasumawati Lias, Norlida Buniyamin, Ahmad Tirmizi Jobli, Mazlina Mansor Hassan, 2025 IEEE 8th International Conference on Electrical, Electronics and System Engineering (ICEESE)

7. SAR Optimization with water bolus height variation and rectangular microstrip antenna for non-invasive breast cancer hyperthermia, Mazlina Mansor Hassan, Kasumawati Lias, Norlida Buniyamin, Mohamad Zulkarnaen Ahmad Narihan, **Bibi Sarpinah Sheikh Naimullah**,2025 IEEE 8th International Conference on Electrical, Electronics and System Engineering (ICEESE)